CRITICALITY SAFETY ANALYSIS OF THE DESIGN OF SPENT FUEL CASK, ITS MANIPULATION AND PLACEMENT IN A LONG-TERM STORAGE

Mosebetsi J Leotlela

A thesis submitted to the Faculty of Science, University of the Witwatersrand, Johannesburg in fulfilment of the requirements for the degree of Doctor of Philosophy. Johannesburg, 2015

DECLARATION

I, the undersigned, hereby declare that the work contained in this thesis is my own original work. It is being submitted for the degree of Doctor of Philosophy in the University of the Witwatersrand, Johannesburg. It has not previously, in its entirety or in part, been submitted for any degree or examination in any other University.

……..

MJ Leotlela

……..day of May…….2016

ABSTRACT

Spent nuclear fuel storage is gradually becoming a nightmare for nuclear reactors which were commissioned in the 1980s. This leaves the nuclear facility management with the dilemma of having to choose between pursuing the cask storage option to relieve the demand pressure on the spent fuel pool, or to opt for the more radical but unpopular option of shutting down the reactor compromising the energy supply, and South Africa is no exception. In a bid to minimise the risk of reactor shut down**,** the Nuclear Analysis Section (NAS) of Eskom launched the present study of investigating the design requirements of spent fuel casks suitable for the storage and transportation of spent fuel assemblies that have an initial enrichment of up to 5 wt% and much higher burnup of between 50 and 60 GWD/MTU.

The aim of the present study is to investigate the suitability of the existing casks for use in 5 wt% enriched fuel, given that they are licensed for a maximum enrichment of 3.5 wt%. As a result of the huge number of casks required, there is potentially a risk of shortage of cask storage space and, therefore, it was prudent that the study also investigates the most optimum storage array that will maximise the storage space, while keeping the effective neutron multiplication factor (k_{eff}) below the internationally recommended value of 0.95 [IAEA, 2014]. As such, it is also necessary to identify parameters which have the greatest effect on the neutron multiplication factor. These include determining the effect of changes in moderator and fuel temperature on the neutron multiplication factor and also what the effect of an increase in the concentration in ^{10}B of the boral plate will have on the neutron multiplication factor.

Keywords:

Rim effect, Burnup credit, Sensitivity and Uncertainty, Dancoff factor, Misloading, water ingress, End effect, axial profile, spent fuel storage, neutron absorber inserts, impact of storage matrix the k_{eff}, neutron absorber inserts.

Dedication

Dedicated to my family; Liz my wife and my two sons Kenneth and Thabo.

To my brothers and my sister who provided me with the initial opportunity to obtain a tertiary education.

To John Beer, my all-time friend, who dedicated all his working life to maintaining the Tandem and Walton Cockcroft accelerators at the Schonland Research Centre for Nuclear Sciences so that postgraduate students "can finish their studies and go and earn a living".

To all my guardian angels from whom I learnt very early in my life that being born into a poor family, having parents with little or no primary education, walking 20 kilometres to school and back barefooted on an empty stomach, living in a squatter camp, being a security guard (albeit for a short period of time), living under the apartheid regime where black people were treated like second-class citizens should not define who you are, or what you will become. These should instead be motivation to succeed and not the justification to fail. Sadly, for many people who lived under the same conditions, these were the cause of failure and not the motivation to succeed. In life you can choose to be a victim (or a victor) and blame all your problems (social/financial/academic) on your poor upbringing, poverty, affirmative action, apartheid or any other forms of injustice you were subjected to; but that will not change the situation you find yourself in. It is only when you roll up your sleeves and start doing something about it that your situation will change. Remember, the world does not owe you (or anyone for that matter) anything; you cannot expect to have anything unless you have worked for it. Nothing will become yours without you having earned it. The world does not revolve around you! Whatever you need in life and from the world, you must work for it. You must roll up your sleeves and be prepared to commit a fair amount of energy and effort, and only then will the situation change. When you do so, remember that the Earth cannot be recycled; do what you can to improve your wellbeing but remember to leave it just as you found it for the betterment of all humanity and the next generations to come. Sitting back and blaming the past but doing nothing to improve your situation will only make matters worse not only for yourself but for everybody, especially your children and your grandchildren!

Acknowledgements

It has been a great honour and privilege for me to have been mentored and guided by Mr. Mueller of Oak Ridge National Laboratory, for whom I have great respect. First as a person who, even though he has so much knowledge in the field of nuclear criticality safety analysis and SCALE code, is still down to mother earth and very humble. Secondly for his ability to disseminate knowledge so that even the novice of novices in the application of SCALE code and Nuclear Criticality Safety Analysis can understand and are able to stand up and be counted as proud and eloquent users of SCALE; that is something to be celebrated and honoured. He has been a source of inspiration and strength, a fountain of knowledge and indeed a great influence in my life in the past 4 years or so since I started my studies.

In all cases where I requested assistance from *scalehelp*, he would respond to the request and make a follow-up on the matter to find out if I understood the explanation. He has been a true inspiration, a guardian angel and a true role model of what a true Teacher is.

There are too many instances where he went out of his way to get me the help I needed, which if I took time to name each one of them it would take too long, but the one that really stands out is the *batchfile* request where he took time off from his family vacation and responded to my request. This is one moment I will never forget in my life and really want to thank the family for their understanding. The other one relates to the "*shell command*" which I needed to create the *sysin2* file for use in TSUNAMI-3 sensitivity and uncertainty. The entire sensitivity and uncertainty analysis depended on this sysin2file coming right before I could proceed to the next stage. Without his generous time and kindness this would have taken me a long time.

Some of the SCALE6.0 modules which I learnt from him in spite of being miles away are STARBUCS and TSUNAMI-3 which are used for Burnup Credit Analysis and Sensitivity and Uncertainty analysis respectively. Thank you so much Mr. Mueller!

There are many great scientists behind the *scalehelp* button who are too many to be mentioned in this thesis but all played their role in helping me get here. Some of the great Scientists who deserved to be mentioned and credited for their generosity are Dr. Bradley Rearden and Mr. Ian Gauld who kindly gave me permission to copy the graphs in NUREG/CR 6700 for use in my thesis.

I am also highly indebted to the kindness and generosity of: Professor Ivo Petr, my Supervisor; Mrs Christina Thinane, the secretary for the Head of School of Physics and my sister, my dear friend Lorraine "Maloloza" Ndala and my absolute all-time favourite for her endless support and encouragement in my studies and for her wise word "*you can't give up now, you're almost done, you must just carry on and finish it* "; to Itumeleng Kungoane for her advice: "*Mara le wena ntate o rata gonna o ntse o ithogakisa ka mothaka o, it's not like you can't do it on your own! The more o mmotsisa, is the more you inflate his ego"* Thank you Itu, that was so empowering and uplifting! To Tshepo Olifant and Morongwa Ngoepe-Ndou, my 'children' for their love and respect, Professor David Mycock, the chairman of the graduate committee and also the Assistant Dean Postgraduate School of Animal, Plant & Environmental Sciences Faculty of Science who played the "fireman's" role, extinguishing all "fires" whenever and wherever there are flare-ups! Abafana bami be Giant Resonance, uDr. Maxwell Jingo, Dr. Oscar Kureba no Dr.Iyabo Usman. *The next round is on me guys, this time in my Nkandla!!!*

Also, to Eskom management for providing all the necessary support for this research but most specifically to Mr Hans Lensink in whose department this project was started and continued to support it until to the end, to Dr Isaac Malgas, Mr Sadika Touffie and Mr. Mervin Theron who in spite of it belonging to another group, they continued to support it financially and otherwise and finally Dr. Eugene Taviv who initiated this research project and continued to have interest in it in spite of being retired. As my industrial supervisor, we published a number of papers together in various international journals. To Mrs Annatjie Mogaladi and Mr. Nkosinathi Khumalo for their respective assistance with flow chart drawings and 3D drawings and Madams Jenny De Wet <jen.dewet@yahoo.com> and Alexa Barnby (barnbak@unisa.ac.za alexabarnby@gmail.com) for their excellent editorial work. Last but by no means the least and probably the most important corporate sponsor I received for this project, EPRI for providing me access to CAFTA computer code (student version) for use in my studies. Your generosity and kindness is greatly appreciated guys!!

TABLE OF CONTENTS

LIST OF FIGURES

LIST OF TABLES

APPENDICES

CHAPTER 1

1. INTRODUCTION

For many years prior to the advent of Nuclear Criticality Safety Analysis, criticality-induced accidents were often underestimated, resulting in disasters [Mayne, 1955; Knief, 2000]. Quite often the Criticality Safety Analysis aspect of the entire nuclear safety regime was not thorough (often lumped together with conventional safety), due to lack of high pedigree rigorous computer codes and powerful computers. As a result, large quantities of highly reactive material were often stored in relatively small areas, ignoring the geometry and material density aspect of criticality, thus resulting in reactivity-induced accidents [O'Dell, 1974].

Considering that the South African Government is considering installing additional nuclear reactors in its energy mix [DoE, 2011], it is expected that they will in all probability, be different from the present generation-II Pressurised Water Reactor (PWR) presently run at Koeberg. This suggests that there is a strong possibility that the fuel assemblies, burnup, enrichment etc. might be different from what is currently used in the Koeberg reactor. This raises questions on the safety of storing different spent fuels with different enrichment and burnup, and different designs of spent fuel casks.

As a result of the potential change in configuration of the fuel elements, there is a need to intensify the effectiveness of criticality safety analysis in all our spent fuel management. Additionally, the fact that the burn-up and the fuel enrichment levels might be different, indicates that the Vaalputs Spent Fuel Storage Facility will most probably contain Spent Nuclear Fuels (SNFs) from different reactors with different burn-up and enrichment levels, thus increasing the risk of criticality accidents. It is thus important that Criticality Safety Analysis of the envisaged permanent storage facility takes into account the complexity of the problem in order to prevent a nuclear reaction from being supercritical. Supercriticality may be defined by first describing neutron multiplication factor denoted, by k_{eff} or simply k, as a relationship between the neutron populations of one generation to the neutron population of the generation before. This is represented mathematically by [JJ Duderstadt, 1976; Lewis, 2008]:

$$k \equiv \frac{\text{number of neutrons in one generation}}{\text{number of neutrons in the preceding generation}}, \tag{1.1}$$

alternatively,

$$k \equiv \frac{\text{neutron production rate}}{\text{neutron loss rate}}. \tag{1.2}$$

Therefore, depending on the value of k, three criticality states in a multiplying nuclear system may exist [Lewis, 2008; Lamarsh, 2002; JJ Duderstadt, 1976]:

$k < 1$ the reaction is *subcritical.* (1.3)

$k = 1$ the reaction is *critical* (1.4)

$k > 1$ the reaction is *supercritical* (1.5)

Supercriticality implies that neutron production rate is higher than the neutron loss, therefore k > 1. Nuclear criticality will be described in detail in Section 2.4.1 of this thesis.

1.1 Spent fuel management

The responsibility regarding authorisation of transportation and storage of spent fuel resorts under the National Nuclear Regulator which regulates activities regarding management of spent fuel. Judging from the fact that the National Nuclear Regulator (NNR) has developed a number of Regulatory Documents: Requirement Document or Position Papers, but (as of 8/8/2015), none of them addresses nuclear criticality safety (refer to http://www.nnr.co.za/regulatory-documents/). However, based on its membership of the International Atomic Energy Agency (IAEA), it is accepted that the same top limit of k_{eff} = 0.95 recommended by the IAEA will also be applicable to the NNR [IAEA, 2014]. Therefore based on the IAEA recommendations, it is a regulatory requirement that the licensee demonstrates beyond any reasonable doubt that the design and the materials, out of which the Spent Nuclear Fuel (SNF) casks and fuel assemblies are made, as well as how they are stored or transported, will not render the system unsafe. As such, the design, material composition, transportation and storage of SNF casks have to meet the Criticality Safety requirements of the NNR so as to prevent inadvertent nuclear excursion.

1.2 Status of spent fuel pools

Most Generation-II nuclear power reactors that were commissioned 20 years ago have accumulated a significant amount of spent fuel in their spent fuel pools (SFP), as a result are running out of storage space. This is a huge risk to the security of energy supply of the country and the economy because if no alternative storage space is found, it might lead to the nuclear installation being shut down. This is even more important if one takes into consideration that the Integrated Resource Plan 2010-2030, [IRP2010-2030; DoE, 2011], the Government's official strategy for ensuring security of electricity supply, is aiming at increasing the fraction of nuclear energy in the energy mix of projected energy by a total of 9.600 GW [DoE, 2011]. This point towards an increase in thermal nuclear power reactors, and subsequently in an increase in the rate at which spent fuel assemblies are generated.

Because of this, the Nuclear Analyses Section (NAS) launched a Criticality Nuclear Safety project aimed at investigating options which could be of immediate solution to the spent fuel storage problem while long-term solutions are being investigated. The objectives of this project are:

- Given the fact that the current stock of Castor X/28 casks, (the design specification Castor X/28 casks are summarised in APPENDIX 1 [Thomas, 1992] are only licensed to a maximum enrichment of 3.5%, how feasible would it be to use them in higher enrichments, e.g. 5%.
- Determine whether there is a significant difference in criticality of casks containing fuel assemblies from Areva and the casks containing fuel assemblies from Westinghouse.
- Determine the effect of burnup credit on the capacity of storage facility.
- Determine the storage pattern/array of the Castor X/28F casks that will be used to ensure optimal use of storage space of the storage facility while keeping the k_{eff} of the system below 0.95 as reasonably achievable.
- Perform sensitivity and uncertainty analysis of the system with the view of determining the parameter which has the greatest effect on the k_{eff} of the system.

When the fuel is irradiated in a nuclear reactor, there are two important processes which take place simultaneously; the depletion process which largely accounts for decay (hence depletion) of the original fissile material (the fuel) and at the same time results in the process of increasing the yield of decay or activation products. These are further classified as fission products, light element or actinides, depending on their mode of origin and atomic mass. From the point of view of cask design, radioactive isotopes may lead to a high risk of radiation exposure to members of the public if radiation protection measures are not adequate. In addition, the criticality process which is as a result of an increase in the effective neutron multiplication factor (k_{eff}),which if not controlled, can lead to an increase the risk of inadvertent nuclear excursion as the neutron multiplication factor increases during cask transportation and storage. The other equally important design feature of the cask which needs to be accorded a similar amount of attention is the heat load the cask is designed to withstand when the fuel assemblies are loaded into the casks. Therefore, the casks must be designed to prevent accidents by minimising these risks.

In order to standardise the safety of casks, the International Atomic Energy Agency has subsequently produced a technical document which lists design features which every spent fuel cask must comply with before it can be declared and licensed as safe for use. Hence, the casks, irrespective of the materials they are made of or the supplier, have to meet the following safety design features [IAEA, 2006];

- **Nuclear Criticality Safety**, whose primary goal is prevention or termination of inadvertent nuclear chain reaction in non-reactor environments [Knief, 2000].
- **Shielding**, which is a very important radiological safety consideration given that the fuel assembly which has been irradiated is very radioactive, emitting all types of radiations which may produce various types of radiation, γ and α are particularly damaging to biological tissue. Thus, from a radiological protection point view, it is the most important safety feature.

- **Thermal Safety**, a design feature of the cask which is aimed at ensuring that the casks will be able to withstand heat, whether it is decay heat or heat from a burning building, it must not disintegrate as a result of either of these possibilities.
- **The containment/structural integrity** aspects of cask design have two roles, firstly containment or prevention of escape of radionuclides from the fuel assembly into the atmosphere where they can pose a health risk to members of the public and

to radiation workers and, secondly to ensure that the structural integrity of the cask is maintained under a series of perceived accident conditions.

The structure of this thesis is as follows

CHAPTER 2: THEORETICAL BASIS OF THE RESEARCH: This chapter will describe the theoretical basis behind the project as well as describing the drawings and the design data such as material composition that will be used in the analysis. It will also describe the relationship between nuclear criticality (and the factors influencing the effective neutron multiplication factor of a fissile system) and the material degradation of various components. Crystal structure transformation which is a basis of material degradation due to irradiation of the material and/or exposure to high temperatures will be described in detail.

CHAPTER 3: MODELLING TECHNIQUES: This provides a description of different modelling techniques which are used in the thesis, different modelling scenario considered. The results of these will be described in all subsequent chapters, which are listed below and their respective themes.

CHAPTER 4: STORAGE OF SPENT FUEL. This chapter will describe the analyses and results of various storage arrays with a view of showing that for a given fissile system, there is a relationship between the storage matrices of spent fuel casks and the resulting effective neutron multiplication factor

CHAPTER 5: ABNORMAL OPERATING CONDITION. In the abnormal operating condition, I will be describing two unusual events which the criticality specialist will have to be cautious about. This includes water ingress where the effects of water ingress in vertical and horizontal casks will be studied and finally fuel assembly misload.

CHAPTER 6: BURNUP CREDIT: The objective of this chapter is to assess how the k_{eff} of the system is affected by the presence of various nuclides sets in the system. It will also evaluate the effect of out-of-the-reactor cooling period affects the k_{eff}

CHAPTER 7: PERTURBATION AND VARIATIONAL ANALYSIS OF A CRITICAL SYSTEM: This chapter presents a study of the *sensitivity and uncertainty* of a number of important parameters of fresh fuel such as fuel and moderator temperatures.

CHAPTER 8: CONCLUSION AND RECOMMENDATIONS: A summary of the important findings of the research are presented from which conclusions and recommendations are made.

The key issues of this research project are spread across the entire thesis addressing various aspects of Nuclear Criticality Safety Analyses of casks. For the purpose of neatness and to be systematic they are divided into three areas, each culminating in a publication in an international journal. Starting with the last publication whose title was SENSITIVITY ANALYSIS OF PARAMETERS IMPORTANT TO NUCLEAR CRITICALITY SAFETY OF CASTOR X/28F SPENT NUCLEAR FUEL and Published in Kerntehnik Journal in Germany. The focus of this research was to perform of Sensitivity and Uncertainty Analysis of k_{eff} of the fissile system which culminated in the derivation of the sensitivity coefficients of the neutron multiplication factor (k_{eff}) to a number of parameters of importance to nuclear criticality safety of castor X/28F spent fuel cask. Two techniques were used; Direct Perturbation and TSUNAMI-3D computer program, both of which are based on linear perturbation theory. The parameters that were assessed to evaluate the sensitivity of k_{eff} include:

1. the concentration of ^{10}B,
2. moderator and fuel temperatures,
3. moderator density, and
4. fuel burnup.

The results of this study have recently been published in the German Journal *Kerntechnik* 80 (2015) 5[Leotlela, *et al.*, 2015] and the reader is referred to Chapter 7 for more information. The second area relates to evaluating and quantifying the impact of fuel assembly misload on the neutron multiplication factor. The results of that study were published in *vol. 4, issue 1* (pp.5-10) of 2015 of the *International Nuclear Safety Journal* with the article: EFFECTS OF THE LOCATION OF A MISLOADED FUEL ASSEMBLY ON THE NEUTRON MULTIPLICATION FACTOR OF CASTOR X/28 F SPENT FUEL CASK. The reader is referred to Chapter 5 for the detailed discussion [Leotlela, *et al.*, 2015]. The third theme, relates to an investigation of an optimum spent fuel storage array that can be used to increase the capacity of spent fuel storage facility while keeping the k_{eff} of the system as far below 0.95 as reasonable possible. The results of that study, referenced in Chapter 4, were published under the title THE EFFECTS OF

STORAGE PATTERNS ON THE NEUTRON MULTIPLICATION FACTOR OF SPENT NUCLEAR FUEL CASKS, in *vol. 1 issue 1* (pp. 7-15) of 2012 of the *International Nuclear Safety Journal* in 2012 [Leotlela, *et al.*, 2012].

The fourth area relates to ranking of aluminium composite material for use as neutron absorber inserts in spent fuel pools, (for detail see section 4.4). The results of this study are published under the title: RANKING OF ALUMINIUM COMPOSITE MATERIALS FOR USE AS NEUTRON ABSORBER INSERTS IN SPENT FUEL POOLS in vol. 4 issue 3 (pages 24-38) in the *International Nuclear Safety Journal* in 2015 [Leotlela, *et al.*, 2015].

CHAPTER 2

2.1 Crystal structure transformations during the irradiation period

During the depletion process, the fuel assembly is subjected to two important factors that lead to the degradation of its material: high temperature and exposure to neutron radiation. Which of these have a greater effect depends on the component of the fuel assembly and the intensity of either. One of the changes that occur is amorphisation.

Amorphisation is the transformation in crystal structure of a material as a result of an increase in temperature, presence of impurity or exposure to radiation. Several investigations have been conducted to determine whether irradiation can induce the transformation of amorphous phases. According to Was when the material is irradiated, amorphisation takes place if there is a significant decrease in energy between the quasi-state and amorphous state [Was, 2007]. As a result, there are a number of minima where energy loss between the two states is momentarily at equilibrium. Given sufficient time, further decrease in internal energy will occur and another minimum is reached until it has reached its equilibrium position where there is no further decrease in internal energy and the crystal structure becomes the permanent crystal lattice of that material [Was, 2007]. This transformation can either be thermally induced or radiation induced.

2.1.1 Thermally induced crystal structure transformation

Several analogies have been proposed to describe the crystalline-to-amorphous (C→A) transformation; the most successful one has been by drawing a parallel between transformations and melting, mainly because of the similarity of the two processes. Some of the similarities include, among others, the fact that amorphisations occur in a heterogeneous manner that follows first order nucleation and growth process characteristics of melting. Because of this, C→A is considered to be a kind of melting transformation. In 1999, Okomota *et al* [Was, 2007] presented a solid state physics paper in which the role of irradiation in amorphisation was critically reviewed [Was, 2007].

This argument was largely based on quantum physics phenomena in which it is accepted that normally, the atoms of a material will be under a constant state of vibration and the

rate of vibration increases with temperatures. According to Okomota's report, melting or crystallisation will only occur when the root-mean-square (*rms*) of thermal displacement $\left\langle \delta_{\text{vib}}^2 \right\rangle^{1/2}$ of atoms from their equilibrium position becomes large enough to encroach on their nearest neighbour's or when the vibration amplitude is about 50% of the interatomic spacing. Thus, transformation will occur when the vibration amplitude reaches the critical value equal to a fraction $\left\langle \delta_{\text{vib}}^2 \right\rangle^{1\backslash 2} / r_{\text{nn}}$ of the nearest neighbours spacing, r_{m}. Using the Debye harmonic model of crystal lattice, the mean square thermal displacement for a perfect crystal at a temperature T above the Debye temperature,Θ_0, is defined by [Was, 2007]:

$$\left\langle \delta_{\text{vib}}^2 \right\rangle^{1/2} = \frac{36\pi^2\hbar^2 T}{Mk\Theta_0^2} \tag{2.1}$$

where $\hbar$ is Planck's constant k is Boltzmann's constant and M is the atomic mass of the nuclide. Since transformation will only occur when $\left\langle \delta_{\text{vib}}^2 \right\rangle$ reaches some critical value, then from the above equation, the transformation temperature, which is the temperature at which crystal transformation will occur is [Was, 2007]:

$$T_{\text{m}}^0 = \frac{Mk\Theta_0^2}{36\pi^2\hbar^2}\left\langle \delta_{\text{crit}}^2 \right\rangle \tag{2.2}$$

.

Because the total displacement is due to thermal vibration $\left\langle \delta_{\text{vib}}^2 \right\rangle$ as well as static vibration, which is due to defects such point-defects and dislocations (size mismatch between solute and solvent atoms in solid solutions); the Lindemann crystal structure transformation criterion becomes [Was, 2007]:

$$\left\langle \delta_{\text{crit}}^2 \right\rangle = \left\langle \delta_{\text{stat}}^2 \right\rangle + \left\langle \delta_{\text{vib}}^2 \right\rangle \tag{2.3}$$

where $\left\langle \delta_{\text{crit}}^2 \right\rangle$ is a constant.

This criterion implies that the crystal can undergo transformation by either being heated to the melting point where $\left\langle \delta_{\text{crit}}^2 \right\rangle = \left\langle \delta_{\text{vib}}^2 \right\rangle$ or by increasing the amount of static disorder $\left\langle \delta_{\text{stat}}^2 \right\rangle$ in a crystal until the free energy of the crystal is equal to that of a liquid. As the temperature increases, the damage level increases too, but the crystal transformation

temperature[1] of the defective crystal does not. This implies increasing the temperature of the crystal after it has already reached $\left\langle \delta_{\text{vib}}^2 \right\rangle$ will not result in further transformation but can only damage the material. There is thus an inverse relationship between the level of damage of crystal lattice and transformation temperature. The state of maximum damage is reached when $\left\langle \delta_{\text{crit}}^2 \right\rangle = \left\langle \delta_{\text{vib}}^2 \right\rangle$ or when $T_{\text{m}}^{\text{d}} = 0$. Here $T_{\text{m}}^{\text{d}} = 0$, is the theoretical upper limit for damage accumulation in a defective crystal [Was, 2007]. By substituting Eqn.(2.1) into Eqn. (2.3), this can be re-written as:

$$\left\langle \delta_{\text{crit}}^2 \right\rangle = \left\langle \delta_{\text{stat}}^2 \right\rangle + \frac{36\pi^2\hbar^2 T_m^d}{Mk\Theta_0^2} \tag{2.4}$$

from which the theoretical temperature upper limit T_{m}^{d} is found to be

$$T_{\text{m}}^{\text{d}} = \frac{Mk\Theta_0^2}{36\pi^2\hbar^2}\left\langle \delta_{\text{crit}}^2 \right\rangle \tag{2.5}$$

and the Debye temperature of defective crystal Θ_{d} is given as:

$$\Theta_{\text{m}}^{\text{d}} = \Theta_0^2\left(1 - \frac{\left\langle \delta_{\text{stat}}^2 \right\rangle}{\left\langle \delta_{\text{crit}}^2 \right\rangle}\right) \tag{2.6}$$

In addition to changes which occur at a micro-scale level, there are those which occur at the macro-scale level some of which are linear and others volumetric expansion corresponding to changes in density.

On a macroscopic scale, damage might mean change in linear or volumetric expansion which may either be permanent or temporary depending on whether the material will resume its original length or volume when the thermal strain is removed.

Numerous studies have been conducted with a view to determining the linear and volumetric expansion of UO_2 as a result of irradiation and it has been found that in the

[1]Crystal structure transformation temperature is the temperature required to initiate or sustain transformations. It is the point where the free energy curve intersects that of a super cooled liquid.

temperature range $273\ \text{K} \leq T \leq 923\ \text{K}$, the instantaneous linear thermal expansion coefficient (α) is given by Iqbal, *et al.*, 2006; and Saegusa, *et al.*, 2007 as:

$$\alpha_{\text{p}} = 9.828\text{x}10^{-6} - 6.930\text{x}10^{-10}T + 1.330\text{x}10^{-12}T^2 - 1.757\text{x}10^{-17}T^3\,, \tag{2.7}$$

while for the temperature $923\ \text{K} \leq T \leq 3120\ \text{K}$, α is given by [Iqbal, *et al.*, 2006; Saegusa, *et al.*, 2007]:

$$\alpha_{\text{p}} = 1.1833\text{x}10^{-5} - 5.013\text{x}10^{-9}T + 3.756\text{x}10^{-12}T^2 - 6.125\text{x}10^{-17}T^3\,, \tag{2.8}$$

Here subscript p in (α_{p}) refers to the cubic polynomial and the fractional change in linear thermal expansion of a material/metal with the length L is given by [Giancoli, 1988]:

$$\frac{\Delta L}{L_{273}} = \frac{L - L_{273}}{L_{273}} \tag{2.9}$$

while the relationship between fractional change in density and the fractional change in volume is given by

$$\frac{\Delta\rho}{\rho_0} = \frac{\dfrac{-\Delta V}{V_0}}{\left(1 + \dfrac{\Delta V}{V_0}\right)}. \tag{2.10}$$

It is generally acceptable to quote the coefficient for volumetric expansion as [Giancoli, 1988]:

$$\beta = 3\alpha_{\text{p}}\,, \tag{2.11}$$

since the error introduced will be small (~1%) for many applications. However, in order for the calculations to be accurate it is very important that the accurate coefficient of thermal expansion is reflected and has been found to be [Giancoli, 1988]:

$$\beta = 3\alpha_{\text{p}} + 3\Delta T\alpha_{\text{p}}^2 + \Delta T^2\alpha_{\text{p}}^3 \tag{2.12}$$

and the relationship between α and temperature T(K) is illustrated in Figure 2.1. The stress $\sigma = Force(F)/Area(A)$ induced as a result of the thermal expansion of the UO_2 in the fuel cladding is enormous which eventually could lead to deformation and cracking of the fuel rod. The stress is given by [Saegusa, *et al.*, 2007; Iqbal, *et al.*, 2006]:

$$\sigma = \frac{F}{A} = E\frac{\Delta L}{L_{273}}, \tag{2.13}$$

where E is the Young's modulus which for UO_2 is given by [Jackson, 2004; Iqbal, *et al.*; 2006, Saegusa, *et al.*, 2007]:

$$E = E^0 - CT\exp\left(-T_c/T\right), \tag{2.13}$$

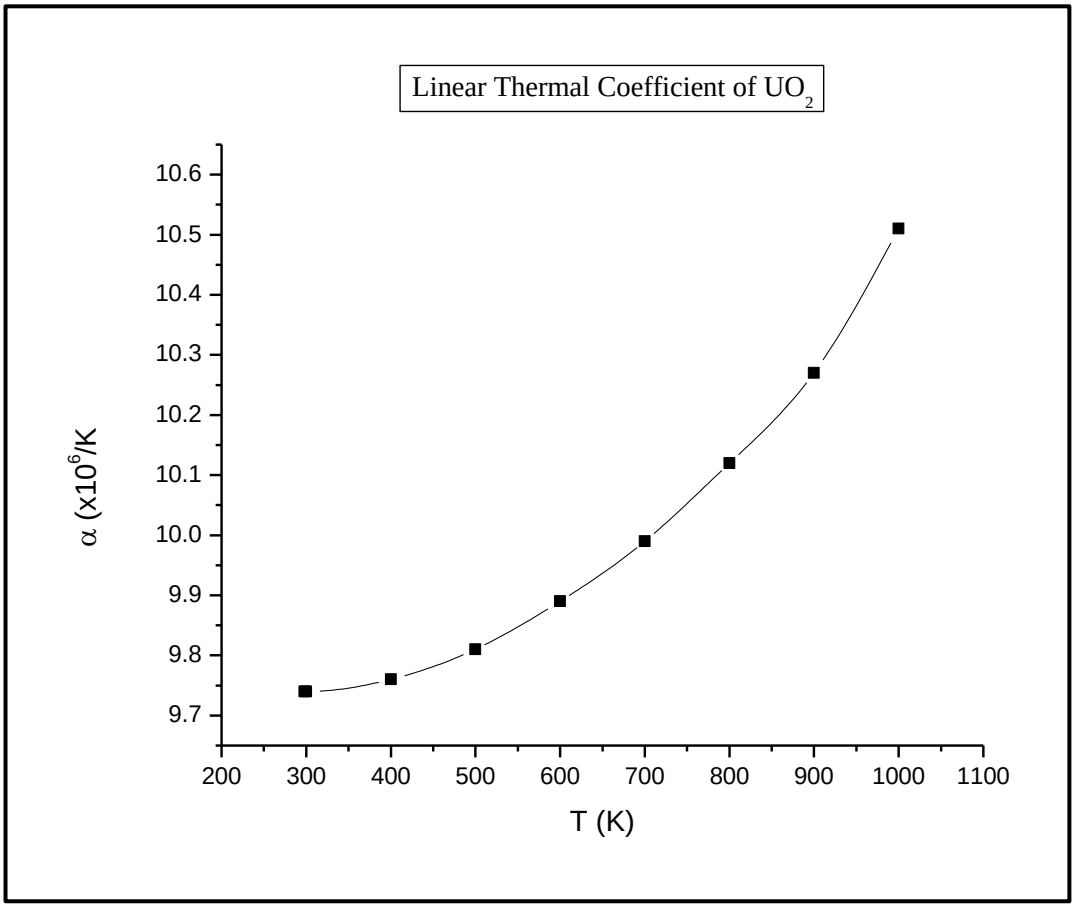

Figure 2.1: Coefficient for linear thermal expansion of UO_2 (Present study).

and E^0 and C are constant equal to 22.7×10^4 N/mm^2 and 20.42 N/mm^2 K respectively and T_c is a characteristic temperature corresponding to one-half of Debye temperature, i.e. 135 K.

2.1.2. Radiation induced crystal structure transformation

In earlier sections reference was made to the fact that sufficient thermal energy was critical for the C→A transformation to proceed to completion. If there is not enough energy, disorder may only be partial and thus transformation may only be partial, resulting in the original crystal structure only being elevated to an excited state and not proceeding to complete the transformation process to a new structure. This alludes to the fact that there is a minimum temperature below which transformation will not occur; therefore, it is only if this temperature is exceeded that transformation can occur. Several studies have been conducted to determine the validity of this claim, which amongst others include that conducted by Dubinko [Was, 2007] and all concur with this finding, confirming that there is a cut-off temperature at which amorphisation occurs.

This model indicates that the rate of change in crystal structure may be indicated by the long range parameter *S*. This consists of two competing processes; a disordering term due to radiation and re-ordering term due to thermal energy and is illustrated mathematically as follows [Was, 2007]:

$$\frac{dS}{dt} = -\varepsilon K_0 S + \nu \exp\left(\frac{-U}{kT}\right)\left[\begin{array}{l} C_A\left(1-C_A\right)\left(1-S\right)^2 - \exp\left(\frac{-V}{kT}\right) \\ \left(S + C_A\left(1-C_A\right)\left(1-S\right)^2\right) \end{array}\right] \tag{2.14}$$

where U is the energy barrier between atoms A and B (A-B) pair interchange, ε is ordering efficiency[2], K_0 is the defect production rate, C_A is concentration of A atoms, k is Boltzmann's constant, T is temperature and V is the ordering energy defined by

$$V = V_{AB} - \frac{\left(V_{AA} + V_{BB}\right)}{2} \tag{2.15}$$

Here, V_{AB}, V_{AA} and V_{BB} are bond energies for a A-B, A-A and B-B pairs, and

[2]Disordering efficiency is the ratio of replacement to displacement of atoms where transformation occurs as a result of A replacing B, it is of the order of 10-100 under neutron irradiation.

$$S = \frac{f_{A\alpha} - X_{\mathrm{A}}}{1 - X_{\mathrm{A}}} \tag{2.16}$$

where $f_{\mathrm{A}\alpha}$ is the probability of atom A being in the α lattice site, and X_{A} is the atomic fraction of atom A. If S = 1, the polymorph is completely ordered and when S = 0, the polymorph is completely disordered [Was, 2007].

From this it is clear that the type of bonds holding two atoms together play a significant role in the transformation process, without this knowledge, it becomes difficult to determine the activation energy. The cut-off temperature T_{C} referred to is the temperature at which amorphisation is initiated where disorder is driven by irradiation and is given by [Was, 2007]:

$$T_{\mathrm{C}} = U\left[k \ln\left(\frac{\nu C_{\mathrm{A}}\left(1 - C_{\mathrm{A}}\right)\left(1 - S_0\right)^2}{\varepsilon K_0 S_0}\right)\right]^{-1}. \tag{2.17}$$

It should be noted that T_{C} depends on the displacement rate and also on the number of replacements per displacements, to account for this ε is included in the equation. Hence the temperature at which amorphisation will occur depends on the irradiating material i.e. the charge and the mass of projectile and the dose rate. Okamoto *et al* describes the main kinetic features of irradiation-induced amorphisation as follows [Weber, *et al.*, 1996; Was, 2007]:

- For a specified particle and dose rate, there is a temperature at which the two competing processes of damage production and recovery just balance; below that temperature, damage production dominates recovery and the crystal can be completely amorphised.
- Amorphisation occurs homogeneously at low temperatures far from the critical dose rate and temperature. Heterogeneous amorphisation occurs near the cut-off temperature.
- For fixed dose rate, $T_{(\mathrm{c\text{-}a})}$ increases with particle mass.

- $T_{(c\text{-}a)}$ is the kinetic parameter that depends on the irradiation variables such as dose rate. Higher dose rates shifts $T_{(c\text{-}a)}$ to higher values.
- There is a temperature, $T_{(c\text{-}a)}$ above which amorphisation is impossible.
- $T_{(c\text{-}a)}$ depends on the target temperature but not irradiation variables.
- Between $T_{(c\text{-}a)}$ and $T_{(th)}$ (where $T_{(th)}$ is the thermal re-crystallisation temperature) irradiation can induce the A→C transformation and the degree and rate of transformation is dose-dependent [Weber, *et al.*, 1996 ;Was, 2007].

Thus, disordering, as indicated in the previous section, is an important factor in crystal structure transformation and can either take place at higher temperature or at low temperature where their thermal displacement has reached the critical values.

2.1.2.1 Radiation damage to UO_2 nuclear fuel and the effect of fission rate in crystal structure transformation

The objective of this section of the research project is to demonstrate that there is a strong correlation between burnup and material degradation resulting from irradiation; there must, therefore, be a similar correlation between k_{eff} and crystal structure transformation of the fuel caused by irradiation.

As stated in Section 2.1, the fuel undergoes several crystalline structural changes during its lifecycle. There have been a number of studies performed to understand what crystal structure transformation means physically, which culminated in the phase diagram Figure 2.2. One of the important changes that UO_2 fuel undergoes is dimensional change caused by transition in crystallographic structure.

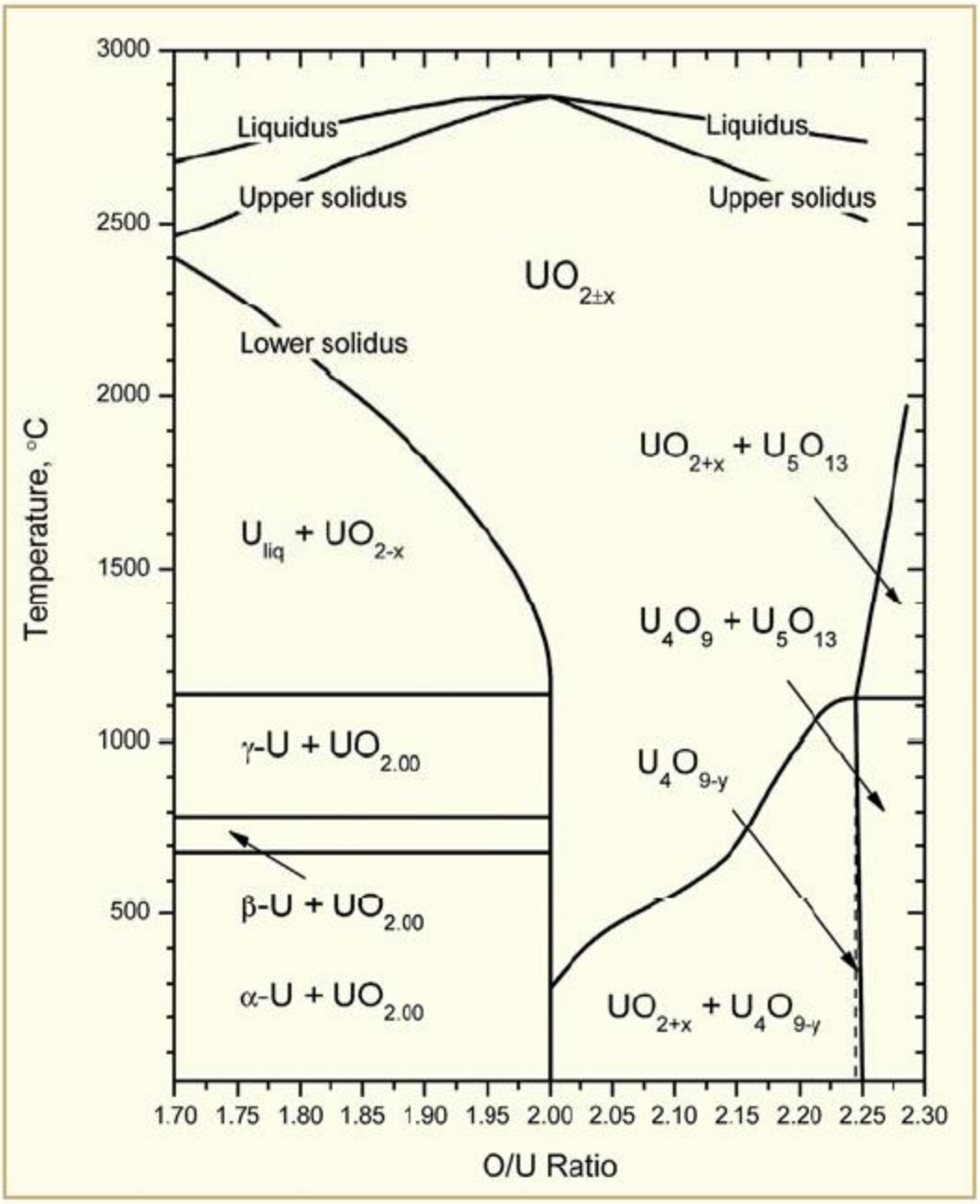

Figure 2.2: Phase diagram of uranium-oxygen system [Patterson, *et al.*, 2010]

According to Matzke [Matzke, 1992], when UO_2 is subjected to high thermal energy, it will undergo the following phase transformation at their respective temperature:

- orthorhombic (α-phase) to tetragonal (β-phase) at (T = 665 ºC),
- β-phase to the body centred cubic (BCC) γ-phase at (T = 770 ºC)

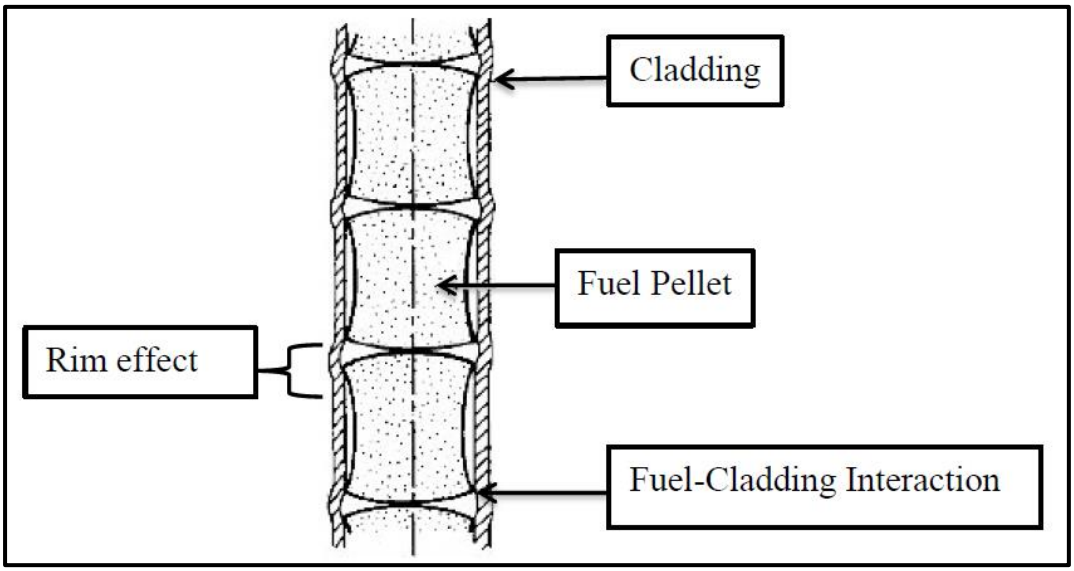

Figure 2.3: Rim effect in UO_2 fuel [Hayes, 2010]

The primary cause of radiation-induced dimensional change in UO_2 fuel is an accumulation of fission products in the fuel matrix which according to Matzke is non-uniform but rather more prominent at the peripheral "*rim*" region of the fuel pellet, as shown in Figure 2.3 [Hayes, 2010], than in the middle of the axial length of the fuel pellet.

Matzke has been able to demonstrate experimentally that formation of the "*rim*" begins at burnups above 40 GWD/MTU and its thickness ranges typically from 100 to 200 μm, making this region much more porous than any other region of the fuel pellet [Turos, *et al.*, 1992; Matzke, 1992].

According to Matzke the reason for the formation of the "rim" in the periphery is because burnup at the periphery is much higher than in the central region by a factor of up to 2.5. This is due to the formation of fissile ^{239}Pu by resonance neutron capture of ^{238}U, which results in a gradient in ^{239}Pu concentration which decreases exponentially towards the centre of the fuel pellet [Matzke, 1992; Matzke, *et al.*, 1997]. As a result of this there is grain subdivision known as the polygonisation process [Matzke, 1992; Matzke, 1996; Matzke, *et al.*, 1997] which converts the original grains of UO_2 that formed during the sintering process into 10^4 to 10^5 new small ones.

These consequently lead to higher fission gas release, low thermal conductivities and changed mechanical properties [Matzke, 1992; Matzke, *et al.*, 1997; Matzke, 1996]. As a result of higher burnup caused by an increase in ^{239}Pu, there is a structural change in that area or rim, which leads to:

i. A phase change from crystalline to amorphous (c-a phase transformation) known as metamictization in materials containing high concentrations of U and Th, which happen to be actinides which decay by α-emission.

ii. A phase change from single crystalline to polycrystalline phase.

iii. Amorphisation occurred in (anisotropic) non-cubic oxides.

Uraniun-238 (^{238}U) is particularly important in the formation of the rim region and not so much ^{235}U because ^{238}U has six strong resonances for (n,γ) cross-sections. These occur at 6.67, 20.90, 36.80, 66.15, 102.47 and 116.85 eV, and therefore, any neutron group falling in any of these energy ranges can be captured. The resonance capture responsible for the formation of the rim is dominated by the first three resonances i.e. 6.67, 20.90 and 36.80 eV but mainly 6.67 eV. This is because at higher neutron energies such as 66.15, 102.47 and 116.85 eV, attenuation by scattering becomes more dominant than neutron capture in contributing to the total resonance interaction rate [Matzke, 1992; Matzke, 1996 Matzke, *et al.*, 1997]. Thus because of these ^{238}U resonances, the surface of the fuel pellet becomes enriched with ^{239}Np which then undergoes a β-decay to ^{239}Pu with the two half-lives 23.45 min and 2.356 d of ^{239}U and ^{239}Np respectively shows that there will be a build-up of ^{239}Np from ^{239}U because the half-life of ^{239}U is much shorter than that of ^{239}Np hence the high enrichment in ^{239}Np:

$$\begin{aligned} &{}^{238}_{92}U \xrightarrow{(n,\gamma)} {}^{239}_{92}U \\ &{}^{239}_{92}U \xrightarrow{t_{1/2}=23.45\text{min}} {}^{239}_{93}Np + \beta^- + \bar{\nu} \\ &{}^{239}_{93}Np \xrightarrow{t_{1/2}=2.356d} {}^{239}_{94}Pu + \beta^- + \bar{\nu} \end{aligned} \quad . \qquad (2.18)$$

Given that ^{239}Pu decays by α- and β$^-$decay, the α-particles will cause a significant amount of radiation damage compared to β$^-$, which also contributes to the formation of the "rim" effect.

According to Matzke [Matzke, 1992], the term "*rim*" effect describes three observations;

1) An increase in ^{239}Pu and burnup along the *rim* region, leading to;

2) (a) a porous zone along the periphery of the fuel pellet, and (b) a large reduction in grain size on the periphery.

3) A decrease in the content of fission xenon within the UO_2 grains as measured with electron microprobe analysis.

Although the rim is thin (in the order of about 100 to 200 μm), it corresponds to 4% to 8% of the fuel volume which is situated near the fuel surface. As a result of its location near the surface, it becomes important for the following points [Matzke, 1992]:

1. As a result of low thermal conductivity in the rim, the fuel temperature may be increased to temperatures higher than in other regions, and because an increase in fuel temperature has a negative effect in the k_{eff} of the system (due to Doppler Broadening which will be discussed in detail in sections 2-4), the result is a lower k_{eff} on the rim with respect to the centre of the fuel pellet,

2. If the spent fuel is going to be stored in a repository, research indicates that in the event of any ingress of ground water into the repository and into the fuel, the water will first interact with the ^{239}Pu-rich, high burnup, large porosity, radiation-damaged rim region for leaching before it reaches the remainder of the rest of the UO_2.

There are other possible alternatives to grain subdivision which result in accumulation of fission products in the fuel matrix. One such reason is over-pressurisation of fission gas bubbles as a result of the difference in volumetric expansion of the fuel and the cladding. The fuel has a much higher volumetric expansion compared to that of the fuel cladding, therefore, when subject to the same temperature the fuel will expand to a greater volume exerting an enormous amount of force on the fuel cladding, which if it does not fail, will result in much finer grain structure of the fuel.

Other alternatives may be due to either a nucleation[3] process or growth in fission gas bubbles which leads to gaseous swelling which increases with temperature and radiation exposure. The accumulation of solid fission products also leads to swelling due to a lower density of fission products and their decay products relative to the uranium atoms from which they originated. The accumulation of fission products results in volumetric expansion of the fuel which exerts severe stress on the cladding material thus critically affecting its performance and causing premature failure.

[3] A type of crystal structure growth mechanism which results from the formation of small droplets or as a result of the presence of impurities in the solution during the crystallisation process.

The accumulation of fission products combined with the radiation damage of the fuel creates intrinsic or vacancy type defects which influence the migration of fission product through the grain boundaries of the fuel pellet. Studies of material properties of UO_2 indicate that under normal conditions UO_2 adopts the face-centred-cubic (FCC) fluoride structure with oxygen occupying the corners of the cube [Hayes, 2010]. However, the stoichiometry of fuel at hand plays a very important role in its physical properties as well as its crystal structure since it determines how the defect processes takes place. This is because the presence of oxygen atoms as interstitials and the number of vacancies are controlled by the UO_2 stoichiometry, which in turn determines the number of vacancies needed in migration and defect formation processes [Matzke, 1996; Matzke, 1992].

In 1994 Rest [Rest, *et al.*, 1994] reported that while studying the effect of irradiation in uranium silicide (U_3Si_2) and uranium dioxide (UO_2) it was observed that at low-temperature, swelling of irradiated U_3Si_2 and UO_2 fuels was caused by the growth of fission-gas bubbles whose size is strongly affected by fission rate. It was further noted that "subdivision" of the original grains was observed in high-burnup UO_2, and the periphery region of the light-water reactor (LWR) fuel pellets revealed that there was an increasingly porous microstructure which increased with burnup [Matzke, 1992; Matzke, 1992; Matzke, 1996; Matzke,1997, *et al.*,].

Detailed inspection of the "*rim effect*" under an electron microscope reveals that there are extremely fine-grained structures which according to Matzke are formed by subdivision of the original fuel grains. If, after irradiation, the sample is allowed sufficient time to cool down under natural cooling, these smaller particles will aggregate to larger ones and form a much coarser structure [Matzke, 1996].

Post irradiation examination of UO_2 samples irradiated to high burnup conducted by Rest *et a*l, confirmed Matzke's results that grain subdivision occurred in high burnup. Changes in fuel volume also indicated that the swelling rate of the material changes from 0.16 to 0.5% ΔV per 10^{26} fissions/m^3 in the burnup range of 1.7-3.6x10^{27} fissions/m^3 [Rest, *et al.*, 1994].

After numerous experiments Rest was able to draw a conclusion that "*grain subdivision is induced when the energy per nucleus is high enough that creation of grain boundary surface is offset by creation of strain-free volume, a resultant net decrease in the free energy of material*" [Rest, *et al.*, 1994]. Subsequent to this, they were able to derive a

mathematical equation that showed that there was a correlation between fission density (FDX) and grain subdivision which is given by [Rest, *et al.*, 1994]:

$$\mathrm{FDX} = \frac{E_{\mathrm{sf}}\, f\Omega\left(c_{\mathrm{i}} + 7\omega_3^{v}/12\omega_0^{i}\right)\omega_0^{i}}{28\pi r_{\mathrm{sm}} kT c_1 D_{v1}\omega_4^{v} c_V}\ , \tag{2.19}$$

where

f = (BK) = $2\mathrm{x}10^{20}$ fissions $\mathrm{m}^{-3}\mathrm{s}^{-1}$ is a fission rate, (B is the conversion factor and K is the damage rate in units of displacements per atom per second (dpa/s) and,

$$E_{\mathrm{sf}} = E_{\mathrm{S}} + E_{\mathrm{f}}\ , \tag{2.20}$$

E_s = stored energy

E_f = the formation energy of a viable nucleus.

c_i = concentration of interstitials

c_v = concentrations of vacancies

$\omega_3^{v}$and ω_4^{v} are jump frequencies of vacancies away from and toward nearest-neighbour nuclei of solute atom.

ω_0^{v} and ω_0^{i} are the jump frequencies of vacancies and interstitials, respectively, unperturbed by the presence of a solute atom.

Ω = atomic volume

r_{sm} = annihilation radius of a nucleus/vacancy-solute pair.

k = Boltzmann constant

T = Absolute temperature

D_{v1} = the diffusivity of the vacancy-solute pair and consists of thermal and radiation enhanced components given by [Likhanskii, *et al.*, 2005; Rest, *et al.*, 1994]:

$$D_{v1} = \xi_{v1} a^2 \nu_v e^{\varepsilon_{v1}} + D_{\mathrm{red}}\,, \tag{2.21}$$

where a is a lattice parameter, ν_v is the vibration frequency factor of vacancies, ε_{v1} is the migration energy for a vacancy-solute pair, ξ_{v1} is the pre-exponential factor that accounts for the deviations from diffusion in a pure solvent, D_{red} is the radiation enhanced component of D_{v1} which is given by [Turos, *et al.*, 1992; Matzke, 1996; Rest, *et al.*, 1994]:

$$D_{red} = D_v c_v + D_i c_i, \tag{2.22}$$

where, D_v and D_i are random walk diffusion coefficient of vacancies and interstitial defined by

$$D_V = \xi a^2 \omega_0^v, \tag{2.23}$$

$$D_i = \frac{2}{3} \xi a^2 \omega_0^i, \tag{2.24}$$

where,

$$\omega_0^v = \nu_v e^{-\varepsilon_V / kT}, \tag{2.25}$$

$$\omega_0^i = \nu_i e^{-\varepsilon_v / kT}, \tag{2.26}$$

where ε_v and ε_i, are the migration energies for vacancy and interstitials and ν_v, and ν_i are vibration frequencies factors for vacancy and interstitials respectively [Rest, *et al.*, 1994]. At relatively low temperatures and high fission rates Eqn (2.22) becomes:

$$D_{red} \rightarrow \chi_1 e^{-\varepsilon_v / 2kT} \sqrt{f}, \tag{2.27}$$

and

$$\chi_1 = \left(\frac{\xi a^2 \nu_v \Omega}{\pi r_{iv} B} \right)^{1/2} \tag{2.28}$$

At high temperatures and low fission rates Eqn (2.22) becomes:

$$D_{red} \rightarrow \chi_2 f, \tag{2.29}$$

and

$$\chi_2 = \frac{\Omega}{2\pi s_V r_{SV} B} \tag{2.30}$$

The values used by Rest in his calculations are summarised in Table 2.1. In the body centred cubic (BCC) structure the diffusion mechanism is dominantly interstitial in nature with the diffusion coefficient, D_i, given by [Rest, *et al.*, 1994]:

$$D_i = 7 \times 10^{-1} e^{(-22000/T)}. \tag{2.31}$$

Table 2.1: Values of various properties used by Rest *et al.* in UO_2 calculations [Rest, *et al.*, 1994]

Property	**Value**
ν_v	$5x10^{13}$ s^{-1}
ε_v	2.4 eV
ε_{vi}	2.8 eV
χ_2	$2x10^{-39}$ m^5
B	$6x10^{23} m^{-3}$ s^{-1}
E_{sf}	0.62 eV
c_1	$1x10^{-8}$
r_{iv}	$2x10^{-10}$ m
r_{sm}	$3x10^{-10}$ m
ξ_{v1}	0.01
ξ	0.1
a	$3.4x10^{-10}$ m

$$D_v = 1\times10^{-7} e^{(-27800/T)} + 10^{-40}\dot{F}\,, \tag{2.32}$$

where T (°C) is the fuel temperature. In the face centred cubic (FCC) on the other hand the diffusion is largely by vacancy mechanism for which the diffusion coefficient is given by [Likhanskii, *et al.*, 2005]:

$$D_v = a_0^2 w \tag{2.33}$$

After researching on the stability of spatial distribution of crystal structure defects in irradiated high burnup UO_2 Likhanskii and Zborovskii further quantified the Orlander equation to give [Likhanskii, *et al.*, 2005]:

where $\dot{F}$ is the fission rate equal to $1x10^{19}$ fission/m^3s in light water reactors and T (°C) is the fuel temperature [Likhanskii, *et al.*, 2005; Rest, *et al.*, 1994].

From Figure 2.4 it is observed that up to 500 ºC both D_v and D_i are independent of temperature. However, above 500 ºC, there is a rapid increase in D_i as the temperature increases.

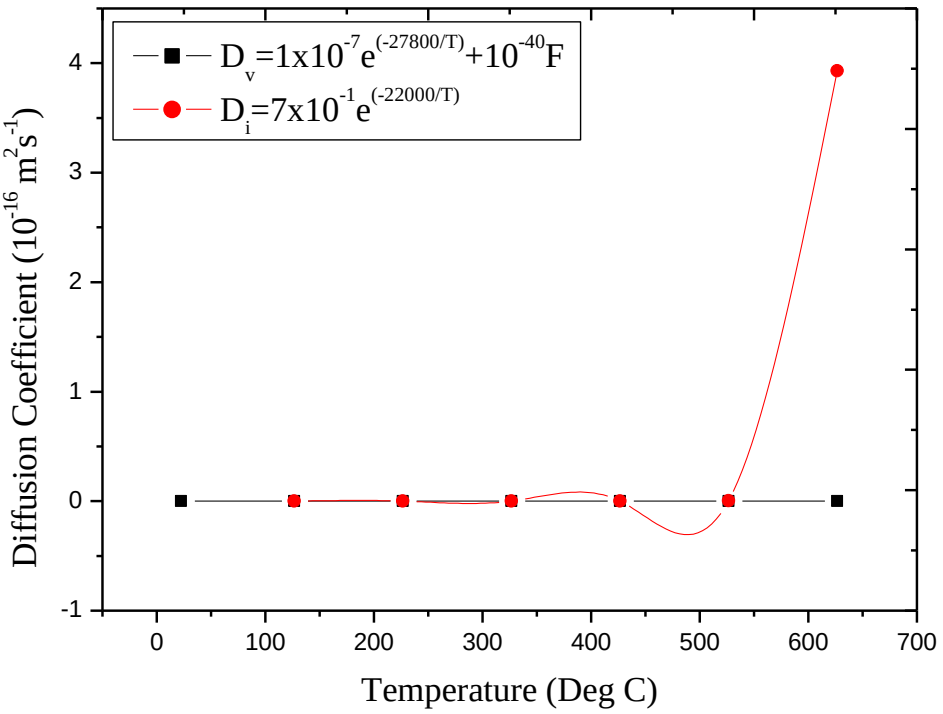

Figure 2.4: Diffusion Coefficient of UO_2 as a function of Temperature (Present study).

This may be ascribed to changes in crystal structure of UO_2 associated with an increase in temperature. If one studies the change D_i together with the phase diagram of UO_2 depicted in Figure 2.2, one will note that between 50 ºC and 300 ºC the fuel composition with a ratio of O/U=2 i.e. UO_2 will largely be made up of α-U +UO_2 in equilibrium with UO_{2+x} +U_4O_{9-y}, each of which has its physical properties, including the diffusion coefficient. However, at 300 ºC the same fuel material will now consist of a solid solution made up of three materials in equilibrium with one another, namely; α-U +UO_2, UO_{2+x} +U_4O_{9-y} and $UO_{2\pm x}$ (refer to Figure 2.2). If the temperature is increased even further to about 670 ºC, the fuel composition will now be made of α-U +UO_2, β-U +UO_2 and $UO_{2\pm x}$. Therefore, because of these changes in crystal structure as the temperature increases the diffusion coefficient of D_i will also change accordingly, and that is the reason why D_i in Figure 2.4 behaves as it does.

Hence, the rate at which neutrons are transported, but more specifically the rate at which they diffuse[4] through the fuel and subsequently result in the reaction between neutrons and ^{235}U atoms, depends on the diffusion coefficient of the neutron in that crystal structure. Looking at D_i (m^2/s) and D_v (m^2/s), it shows that the coefficient for diffusion by an interstitial mechanism is larger than that by vacancy diffusion. This implies that neutron transport in the BCC will be at a much higher rate than is the case with FCC which many neutron transport codes including SCALE and MCNP do not take into consideration. This has further been confirmed by Griesmeyer who cited D_{i0} and D_{v0} as $7.12x10^3$ cm^2/s and $1.0x10^{-3}$ cm^2/s respectively [Griesmeyer, *et al.*, 1978; Veshchnov, *et al.*, 2009].

Thus, assuming that all neutrons will be in the thermal range, it is expected that BCC material will result in a higher k_{eff} than would be the case in FCC.

2.1.3 Free Energy in Radiation Induced Amorphisation

Apart from disordering, one of the most important factors that drives amorphisation is Gibbs free energy released when two or more chemical elements react chemically and release energy in an exothermic reaction, which also applies to nuclear reactions. However, in nuclear technology these processes never occur in isolation of one another; each contributes a certain fraction to the entire requirement for transformation, and which of them dominates depends on the solute-solvent system, dose of solute and temperatures. Motta *et al,* [Was, 2007] summarised the criteria for amorphisation driven by free energy

[4] Neutron diffusion is but one form or mode of neutron transport.

as follows: the free energy change upon irradiation, ΔG_{irr} must as a minimum be equal to or greater than that for the C →A transformation ΔG_{ac} in order for the transformation to occur. This relationship is summarised mathematically as follows;

$$\Delta G_{\text{irr}} \geq \Delta G_{\text{ac}} \tag{2.34}$$

Where ΔG_{irr} includes all the defects created by irradiation and can be written as the sum of terms representing chemical disordering, ΔG_{dis} and all other defects ΔG_{def}. The relationship between these three components may be defined as: [Was, 2007]:

$$\Delta G_{\text{irr}} = \Delta G_{\text{def}} + \Delta G_{\text{dis}} = \sum_j \left(C_j E_j - T\Delta S_j \right) + NV - T\Delta S_{\text{dis}} \tag{2.35}$$

where C_j is the concentration defect j, E_j is the formation energy, V is the ordering energy and ΔS_j and ΔS_{dis} are the configuration entropy changes due to point defects and anti-site defects, respectively, and N is the number of lattice sites per mole. The concentration of defects is given by the defect balance equation defined as [Was, 2007]:

$$\begin{aligned} \frac{dC_{\text{V}}}{dt} &= K_0 - K_{iv} C_i C_{\text{v}} - K_{\text{vs}} C_{\text{v}} C_{\text{s}} \\ \frac{dC_{\text{i}}}{dt} &= K_0 - K_{\text{iv}} C_{\text{i}} C_{\text{v}} - K_{\text{is}} C_{\text{i}} C_{\text{s}} \end{aligned} \tag{2.36}$$

where

C_v = vacancy concentration

C_i = interstitial concentration

K_0 = The effective point defect production rate

K_{iv} = vacancy-interstitial recombination rate coefficient

K_{vs} = vacancy-sink reaction rate coefficient

K_{is} = interstitial-sink reaction rate coefficient

and

$$K_{iv} = 4\pi r_{iv} D_i$$
$$K_{is} = 4\pi r_{is} D_i \quad , \tag{2.37}$$
$$K_{vs} = 4\pi r_{vs} D_v$$

where r_{iv}, r_{vs} and r_{is} are interaction radii for the reaction between the species given by the subscripts i.e. (i, v for interstitial and vacancy, respectively) and represent the radii of surfaces such that if crossed by the defect, it is annihilated; D_i and D_v interstitial and vacancy diffusion coefficients respectively.

2.2 Nuclear Reactions

In order to be able to discuss nuclear reactions, one must start by describing the space within which nuclear reactions take place. When two or more nuclear particles interact, there are a number of possibilities of what can happen in that reaction depending on the cross-section, particle flux, kinetic energy, nuclide-reaction pair, sensitivity coefficient of the nuclide-reaction pair, mass and velocities of the incident particles which consequently determine the nature of the final particle(s).

These factors also determine the rate at which the reaction proceeds and for a reactor core are initiated by neutron flux being related to one another by [Lamarsh, 2002]

$$R = \phi N \sigma, \tag{2.38}$$

where,

R = reaction rate (reactions/sec)

ϕ = neutron flux (neutrons/cm^2-sec

N = atom density (atom/cm^3)

σ = microscopic cross-section (cm^3)

Because of the number of possible interaction modes, the reaction rate will depend on the macroscopic cross-section ($\Sigma = N\sigma$) used in the calculation, and in reactor physics the nuclear reaction of interest is normally a fission reaction. However nuclear fission is not the only nuclear reaction that takes place in fissile system, some of the most common reactions observed include: *inelastic scattering*, *elastic scattering*, (n,n'), (n,2n), capture, (n,γ), (n,p), (n,d), (n,t) and (n,α). As will be seen in section 5.2.2.2, Figure. 5.7 the highest

fission density is in the centre of the cask and decreases gradually as one progresses to the periphery [Leotlela, *et al.*, 2015]

The reactions which are of importance in nuclear reactor analysis involve interactions between neutrons and nuclide and are [Duderstadt, *et al.*, 2010; Lewis, 2008]:

- nuclear fission (*n, fission*), which may generally be represented by the following nuclear reaction;

  $${}^{1}_{0}\mathrm{n}+{}^{A_1}_{Z_1}\mathrm{X}\rightarrow {}^{A_2}_{Z_2}\mathrm{X}+{}^{A_3}_{Z_3}\mathrm{X}+\text{neutron(s)} + 200\text{MeV}$$

- radiative capture (n,γ), generally represented by

  $${}^{1}_{0}n+{}^{A}_{Z}\mathrm{X}\rightarrow\left({}^{A+1}_{Z}\mathrm{X}\right)^{*}\rightarrow {}^{A+1}_{Z}\mathrm{X}+\gamma$$

- scattering (n, n) or (n, n')

$${}^{1}_{0}\mathrm{n}+{}^{A}_{Z}\mathrm{X}\rightarrow {}^{1}_{0}\mathrm{n}+{}^{A}_{Z}\mathrm{X}\ \text{(elastic scattering (n,n))}$$

$${}^{1}_{0}\mathrm{n}+{}^{A}_{Z}\mathrm{X}\rightarrow {}^{1}_{0}\mathrm{n}+{}^{A}_{Z}\mathrm{X}^{*}\ \text{(inelastic scattering (n,n'))}$$

$${}^{1}_{0}\mathrm{n}+{}^{A}_{Z}\mathrm{X}\rightarrow {}^{1}_{0}\mathrm{n}+{}^{A}_{Z}\mathrm{X}+\gamma\ \text{(inelastic scattering (n,n',}\gamma\text{))}$$

Some of the inelastic scattering reactions of interest in reactor physics from the fission and neutron irradiation point of view are neutron-producing reactions like (n, $2n$), (n, $3n$) and (γ, n) .

These are only a few reactions that are of importance to nuclear criticality analysis that will take place in the reactor vessel but there are many other possibilities.

2.3 DOPPLER BROADENING

Doppler broadening can best be understood by studying the quantum mechanics of UO_2 in which it is understood that the particles of a crystal are in a continuous state of vibration, vibrating like a wave where the frequency and the amplitude of vibrations are greatly influenced by the temperature. As a result of the bonding of atoms of a crystal lattice, the displacement of one or more atoms from their equilibrium positions will give rise to a set of vibration waves propagating through the lattice. According to Kittel, there is a minimum amount of energy needed to induce a certain frequency of vibration; which alludes to the quantized nature of vibration [Kittel, 1987]. Furthermore, all lattice vibrations of normal mode types have a well-defined wavelength and frequency of

vibration, which although in classical mechanics they are viewed as wave-like phenomena in nature, in quantum mechanics they are believed to possess certain particle-like properties known as phonons [Kittel, 1987], which is in agreement with the dual nature of matter.

Thus Doppler Broadening in this context refers to change in cross-section as a result of thermal motion of atoms of a crystal structure brought about by the increase in temperature [Borgonovi, *et al.*, 1969; Kadotani, 1970]. As a result of the differences in the two schools of thought i.e. Wave-versus Particle nature of matter, a two-tier approach has been developed to try and explain Doppler broadening [Borgonovi, *et al.*, 1969; Butland, 1974; Kadotani, 1970];

i. The first one was Free Gas Model which was originally introduced by Lamb,
ii. The second one is the Effective Temperature model developed by Nelkin and Parks.

2.3.1 The Free Gas Model

This model uses an analogy of free gas targets in which it is believed that the atoms of a crystalline material are in a constant state of motion as a result of non-zero temperature of the material. The energy distribution of target nuclei assumes an isotropic Maxwellian distribution. As the temperature increases there is a corresponding increase in vibrational and rotational frequency of the atoms of the material and thus an increase in the spacing or distance among different atoms of the material. As a result of this vibration, it is very difficult to pinpoint with absolute certainty where each atom will be at any given time, and the degree of uncertainty increases with energy of the atoms, which is consistent with the - *Heisenberg uncertainty principle* [Merzbacher, 1998].

The same applies to the cross-sections of a nuclide since the uncertainty or probability of a particular projectile-nuclide interaction is a function of relative velocities between the neutron and the target nuclide. Hence in a Maxwellian "sea" of targets, the mono-energetic neutrons can only "see" targets of a certain energy spectrum relative to its own; and this phenomenon is known as Doppler Broadening [Kadotani, 1970].

Doppler Broadening is very important parameter in nuclear criticality safety since depending on the moderator or fuel temperature; the k_{eff} of the system can either increase or decrease as a result of vibration of atoms. Underpinning this is the fact that temperature

change plays a major role on the kinematics of neutron collision which tends to be "thermalized" to energies consistent to material temperature. This is particularly important since the neutron can either gain or lose energy in discrete amounts or quanta and that modifies the double differential cross-section (thermal inelastic scatter) of the material thus affecting the reactivity of the material.

This model has been very successful in a wide variety of applications, particularly in reactor physics [Kadotani, 1970; Borgonovi, *et al.*, 1969; ANL, 1963].

2.3.2 The Effective Temperature Model

This model was first developed by Nelkin and Parks who argued that if either the binding energy among crystalline atoms is 'weak' or the nuclear recoil energy is large, the effect of crystalline binding energy can be given to a good approximation by assuming that the nuclei behave like a free gas, only if an effective temperature $\overline{T}$ is used, and the relationship between the nuclear kinetic energy and the effective temperature is given by $E = \frac{3}{2} k\overline{T}$ where k is Boltzmann constant [Butland, 1974].

It has been found that at higher temperatures these models, (i.e. effective temperature and free gas models) approach one another, it does not matter which one uses, they will yield the same answer [Butland, 1974; Kadotani, 1970; Borgonovi, *et al.*, 1969]. Thus if **v** is the velocity of an incident neutron and **u** is the thermal velocity of a target nucleus, then velocity of the neutron relative to that of a target nucleus is **v**-**u** and the relative energy with respect to u/v is given by

$$E' = \frac{\mu}{2}(\mathrm{v\text{-}u})^2 \simeq E - \sqrt{2\mu E \mathrm{u}} \tag{2.39}$$

Where E is the incident neutron energy, u is the nucleus' velocity projection in the direction of neutron flux. Assuming that the target is in a gaseous phase, then from the kinetic theory of gases, the number of nuclei with the given component u is described by the Maxwellian distribution

$$W(\mathrm{u})\mathrm{du} = \frac{\mathrm{m_A}}{2\pi T} e^{-\frac{\mathrm{m_A u^2}}{2T}} \mathrm{du}, \tag{2.40}$$

Where $\mathrm{m_A}$ is the mass of a target nucleus and T is temperature.

The corresponding relative energy distribution is given by [Butland, 1974; Kadotani, 1970]:

$$W(E,E')dE' = \frac{1}{\sqrt{\pi}} e^{-\frac{(E'-E)^2}{\Delta^2}} \frac{dE'}{\Delta}, \tag{2.41}$$

where $\Delta = 2\sqrt{\mu ET/m_A}$ is the Doppler width, and the averaged thermal-motion cross-section is given by [Butland, 1974; Kadotani, 1970]:

$$\overline{\sigma(E)} = \int dE' W\left(E,E'\right)\sigma\left(E'\right). \tag{2.42}$$

Thus the effective temperature will result in higher frequency of vibration, and consequently to the increase in Doppler Broadening effect. Since the Doppler width is inversely proportional to the atomic mass of the target nuclide, the Doppler width is higher for smaller nuclides [Borgonovi, *et al.*, 1969; Kadotani, 1970].

2.3.3 Temperature-Dependence of cross-section

According to studies conducted by Borgonovi and Kadotani, the radiation capture and total cross-sections in the resonance range are given as [Borgonovi, *et al.*, 1969; Kadotani, 1970]:

$$\sigma_\gamma(E) = \frac{\Gamma_\gamma}{\Gamma}\frac{\sigma_0}{1+\mathrm{x}^2}, \tag{2.43}$$

$$\sigma_t(E) = \sigma_p + \frac{\cos 2\zeta_0 - \mathrm{x}\sin 2\zeta_0}{1+\mathrm{x}^2}, \tag{2.44}$$

respectively, where $\mathrm{x} = 2(\mathrm{E}-\mathrm{E}_\lambda)/\Gamma$ is the energy deviation from the resonance value in total width units and $\sigma_0 = \frac{4\pi}{k^2} g(j)\frac{\gamma_n}{\Gamma}$ is the total cross-section for the resonance energy without potential scattering [Butland, 1974].

Thus the radiation capture and total cross-sections averaged over thermal motion are described by [Borgonovi, *et al.*, 1969; Kadotani, 1970]:

$$\overline{\sigma_\gamma\left(E\right)} = \frac{\Gamma_\gamma}{\Gamma}\left(\frac{\Gamma}{\Delta},\mathrm{x}\right)\sigma_0, \tag{2.45}$$

$$\overline{\sigma_t(E)} = \sigma_p + \left\{ \psi\left(\frac{\Gamma}{\Delta}, \mathrm{x}\right)\cos 2\zeta_0 - \mathrm{x}\left(\frac{\Gamma}{\Delta}, \mathrm{x}\right)\sin 2\zeta_0 \right\}\sigma, \tag{2.46}$$

respectively where,

$$\psi\left(\frac{\Gamma}{\Delta}, \mathrm{x}\right) = \frac{1}{2\sqrt{\pi}}\frac{\Gamma}{\Delta}\int_{-\infty}^{\infty} d\mathrm{x}' \frac{e^{-\frac{\Gamma^2}{4\Delta^2}\left(\mathrm{x}-\mathrm{x}'\right)^2}}{1+\mathrm{x}'^2}, \tag{2.47}$$

and

$$\mathrm{X}\left(\frac{\Gamma}{\Delta}, \mathrm{x}\right) = \frac{1}{2\sqrt{\pi}}\frac{\Gamma}{\Delta}\int_{-\infty}^{\infty} d\mathrm{x}'\mathrm{x}' \frac{e^{-\frac{\Gamma^2}{4\Delta^2}\left(\mathrm{x}-\mathrm{x}'\right)^2}}{1+\mathrm{x}'^2}, \tag{2.48}$$

The function $\psi\left(\frac{\Gamma}{\Delta}, \mathrm{x}\right)$ defines the thermal motion modification of the line shape for the resonance capture and resonance elastic scattering, while $\mathrm{X}\left(\frac{\Gamma}{\Delta}, \mathrm{x}\right)$ defines the interference term in the averaged total cross-section (potential and resonance elastic scattering interference). For the resonance energy,

$$\psi\left(\frac{\Gamma}{\Delta}, 0\right) = \frac{\sqrt{\pi}}{2}\frac{\Gamma}{\Delta}e^{\frac{\Gamma^2}{4\Delta^2}}\left(1 - \frac{2}{\sqrt{\pi}}\int_0^{\Gamma/2\Delta} dy \times \mathrm{e}^{-y^2}\right) \tag{2.49}$$

the function $\psi\left(\frac{\Gamma}{\Delta}, \mathrm{x}\right)$ has been shown to satisfy the condition

$$\int_{-\infty}^{\infty} d\mathrm{x}\, \mathrm{X}\left(\frac{\Gamma}{\Delta}, \mathrm{x}\right) = 0, \tag{2.50}$$

and the function $\mathrm{X}\left(\frac{\Gamma}{\Delta}, \mathrm{x}\right)$ satisfies

$$\int_{-\infty}^{\infty} d\mathrm{x}\, \mathrm{X}\left(\frac{\Gamma}{\Delta}, \mathrm{x}\right) = 0. \tag{2.51}$$

If the natural line is much larger than the Doppler width Δ, then

$$\psi\left(\frac{\Gamma}{\Delta}, \mathrm{x}\right) = \frac{1}{1+\mathrm{x}^2}, \Gamma >> \Delta \tag{2.52}$$

which implies that the line shape is not modified and the averaged cross-section equation, Eqn (2.56) produces a non-thermal cross-section. However, if the natural width is closer to or less than the Doppler width, then the resonance cross-section and the line-shapes are changed to new values. Finally, if $\Gamma << \Delta$ one obtains an expression for the function in the off-resonance range [Borgonovi, *et al.*, 1969; Butland, 1974].

2.3.4 Doppler broadening of UO_2 nuclear fuels

Doppler Broadening has been investigated by a number of scientists to determine the effect of temperature on the broadening of resonances of uranium bound in UO_2. One of these is Schenter who used it specifically in the calculation of temperature dependence on criticality for the Argonne National Laboratory (ANL) critical assembly ZPR—III47 [Butland, 1974; Borgonovi, *et al.*, 1969]. The results showed that although the binding effect of U in UO_2 decreased with an increase in temperature, the magnitude of the decrease depended on whether one was looking at the binding effect of; a) U in UO_2, b) O in UO_2, or c) the average binding energy of an atom in UO_2. It has been established that calculations using averaged binding effects result in values which are significantly higher than the binding effects of U in UO_2 or O in UO_2. The binding effects on U in UO_2 were found to be even smaller than those of O in UO_2.

Other scholars who investigated Doppler Broadening of UO_2 included Jarvis and Thorson who used Bose-Einstein statistics to develop the relationship between the thermodynamic temperature T(K) and effective temperature $\overline{\mathrm{T}}$ of the phonon frequency spectrum $\rho(\beta')$, which is given by [Borgonovi, *et al.*, 1969; Butland, 1974]:

$$\overline{T} = \frac{T}{2}\int_0^\infty \rho\left(\beta'\right)\beta' \coth\left(\beta'/2\right)d\beta', \tag{2.53}$$

where

$$\int_0^\infty \rho\left(\beta'\right)d\beta' = 1 \tag{2.54}$$

This was based on the assumption that nuclear vibrations are described by a set of harmonic oscillators, and using phonon frequency spectra developed by Thorson and Jarvis, Hutchinson and Schofield derived the *effective* temperature of U and O in UO_2 as

$$\overline{T}_U = T\left(1+3110T^{-2}\right)K, \tag{2.55}$$

and

$$\overline{T}_o = T\left(1+27000T^{-2}\right)K \tag{2.56}$$

This has been a significant development in nuclear criticality safety analysis as will be seen in later sections where Doppler broadened cross-sections are discussed [Borgonovi, *et al.*, 1969; Butland, 1974; Kadotani, 1970].

2.3.4.1 Doppler broadening of absorption cross-section

The Doppler broadening of neutron absorption cross-section ($\sigma_{n,\gamma}$) as a function of energy E and the Doppler width, Δ, was first derived by Bethe and Placzek using the free gas model and was found to be [Borgonovi, *et al.*, 1969; Butland, 1974; Kadotani, 1970]:

$$\sigma_{n,\gamma}(\Delta,E) = (\pi\Delta)^{-1/2}\int_0^\infty dE'\sigma_{n,\gamma}\left(E'\right)e^{-\left(E'-E\right)^2/\Delta^2}, \tag{2.57}$$

where E is the kinetic energy of the neutron in the laboratory system, $\sigma_{n,\gamma}\left(E'\right)$ is an unbroadened neutron resonance absorption cross-section, and Δ is the Doppler constant given by:

$$\Delta = 2\left(kTE\,\mathrm{m/M}\right)^{1/2} \tag{2.58}$$

where, k is the Boltzmann's constant, T is the temperature of the gas, m and M are masses of the neutron and target respectively. According to Lamb the Doppler Broadening equation, is only applicable to crystalline targets if T in Eqn (2.69) is replaced with the effective temperature given by:

$$\overline{T} = \overline{\varepsilon}/k, \tag{2.59}$$

where $\bar{\varepsilon}$ is the average energy per vibrational degree of freedom of a crystal. Even then, T can only be replaced with $\bar{T}$ on condition that the following weak-binding condition is satisfied:

$$\frac{1}{2}\Gamma + \left(E\bar{\varepsilon}\,\mathrm{m/M}\right)^{1/2} \gg \Theta, \tag{2.60}$$

where

Γ = natural width of resonance,

Θ = Debye temperature of the crystal in energy units

Doppler broadening of the cross section is caused by an increase in temperature of the fuel temperature. To that effect Doppler broadening of 6.67 eV resonance scattering cross-section of ^{238}U at four different temperatures is shown in Figure 2.6. From this it is observed that as the temperature increases the height of the peak decreases and becomes flatter (broadens out) to cover a much wider area than has been the case at lower temperature (un-broadened peak). As a result of the importance of Doppler broadening in the nuclide cross-section, a number of specialised computer codes have been developed to specifically calculate the Doppler broadening caused by thermal vibration of atoms. One of these is NJOY which used the Sigma1 method first developed by Cullen to evaluate Doppler broadening of absorption cross-section of ENDF/B[5] [Cullen, 1979; Seidel, *et al.*, 1989]. Other codes which are not as specialised as NJOY use an approximate form of Doppler Broadening equation defined as [Duderstadt, *et al.*, 2010]:

$$\bar{\sigma}_\gamma\left(E,T\right) = \sigma_0 \frac{\Gamma}{\Gamma_\mathrm{D}}\left(\frac{E_0}{E}\right)^{1/2} \frac{\sqrt{\pi}}{2} e^{\left[\frac{-\left(E-E_0\right)^2}{\Gamma_\mathrm{D}^2}\right]} \tag{2.61}$$

$$\text{where } \Gamma_\mathrm{D} = \left(\frac{4E_0 kT}{\mathrm{A}}\right)^{1/2}, \tag{2.62}$$

k = the Boltzman constant = 1.380662x10^{-23} J/K,

T = Temperature (K),

[5] ENDF/B = Evaluated Nuclear Data file version B

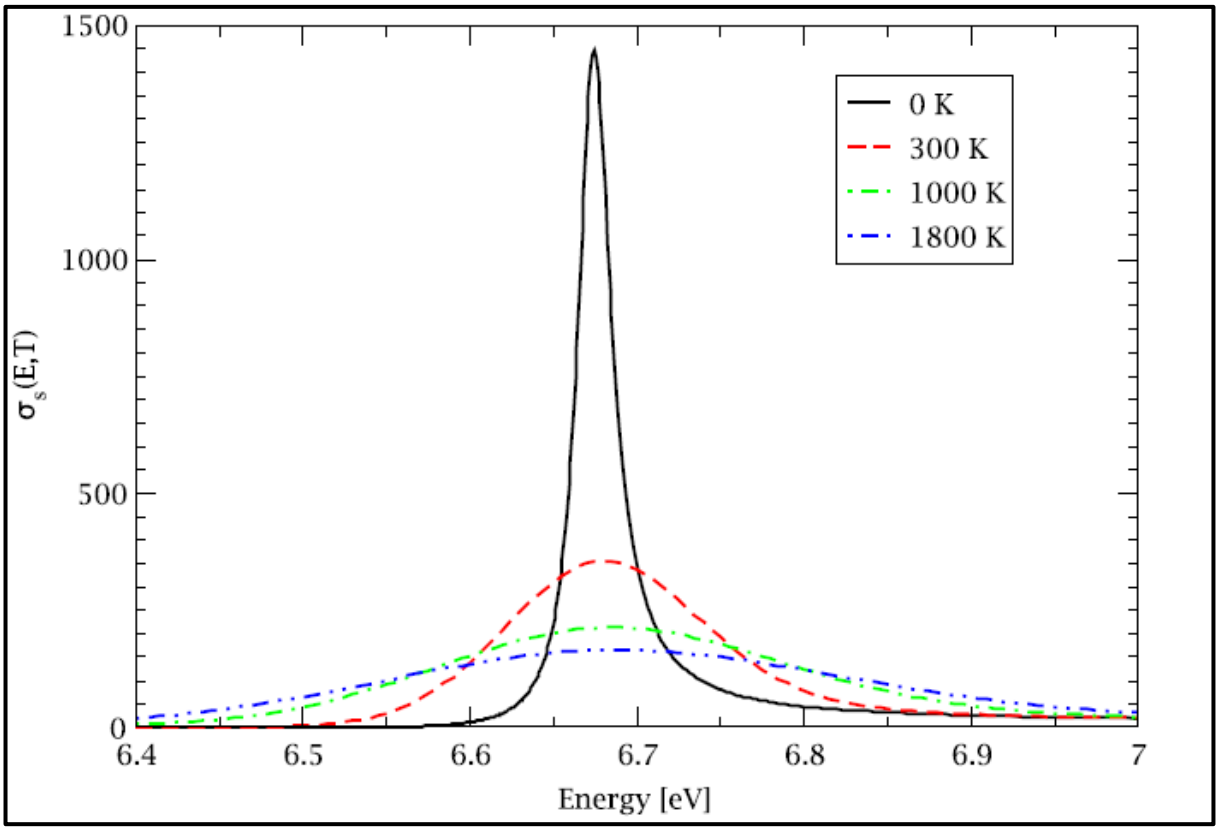

Figure 2.5: Doppler Broadening of 6.67 eV resonance scattering cross-section of ^{238}U [Becker, 2010].

A = Atomic mass of nuclide in question.

E_0 = Maximum energy of a neutron = 10 MeV; and this is the most common Doppler broadening model used by many neutron transport computer codes.

Therefore, because the reactor generates so much decay heat when it is in operation, the fuel temperature increases quite significantly, resulting in broadening of the cross-section and a more effective neutron absorption at the resonance peak and consequently a decrease in k_{eff}.

2.4 NUCLEAR CRITICALITY PROCESSES.

The second process which takes place in a nuclear vessel (which may be the reactor core, the spent fuel cask or even a spent fuel pool), is nuclear criticality which is as a result of an increase in neutron multiplication factor. As Knief [Knief, 2000] pointed out this can lead to inadvertent nuclear excursion if not properly controlled. After the fuel assemblies have been taken out of the reactor core and transferred into the spent fuel pool, irradiation and thermal exposure have decreased quite-considerably except for decay heat and

spontaneous fission/decay which will continue for a long time albeit at a much slower pace [Knief, 2000].

Before going into the modelling process, how it was done and what the results were, it is mandatory that this is preceded by the theoretical bases underlying the phenomena observed. A neutron undergoes a number of histories[6] in its short life in a reactor vessel. Some of these neutrons may be absorbed by the fuel as radiative capture rather than fission, some may be absorbed by other material which may not be fuel and some may leak out of the system. Hence for a nuclear chain reaction to be sustainable, at least one or more neutrons produced in the fission process must survive these competitive processes to produce another fission event. For criticality, it is almost imperative that one first explains the six factor formula and shows how each factor relates to the multiplication factor [Knief, 2000].

2.4.1 The Effective Neutron Multiplication Factor

The relationship between the neutron population of one generation versus the neutron population of the generation before it is often described by using effective neutron multiplication factor denoted by k_{eff} or simply k and has been used as a measure of whether the reaction will be critical or not. This is represented mathematically by Eqn (1.1) [JJ Duderstadt, 1976; Lewis, 2008].

There are a number of factors which determined the neutron multiplication factor and the relationship of these factors to k is described by the six factor formula which is discussed in detail in many reactor analysis text books but is described here as a background theory to support the arguments.

There are a number of factors which determined the neutron multiplication factor and the relationship of these factors to k is described by the six factor formula as shown in Eqn (2.74) [Lamarsh, 2002; Lewis, 2008]:

$$k = \varepsilon p f \eta P_{FNL} P_{TNL} \tag{2.63}$$

[6] The complete random walk of a Monte Carlo particle (including all progeny) from its birth in the source to its death, include scattering, absorption, capture, escape, decay.

where P_{FNL} and P_{TNL} refer to the probability that fast neutrons will not leak out (fast non-leakage) and the probability that thermal neutrons will not leak out (thermal non leakage) respectively.

Thus the neutron multiplication factor is a factor which is used to indicate whether the system is critical or subcritical and the system can go either way depending on the magnitude of any of the six factors. How each one of them will affect *k* is described in detail in the next section.

2.4.1.1 The Fast Fission Factor

This is the first process that neutrons that have just been born will undergo. It is a fission process caused by neutrons in the fast energy range and results in the net increase in the fast neutron population. Since the cross-section for fast fission for ^{235}U or ^{238}U is small, only a small number of fast neutrons cause fission. The fast fission factor is expressed mathematically [Duderstadt, *et al.*, 2010; Lewis, 2008; Lamarsh, 2002]:

$$\varepsilon = \frac{\text{Number of fast neutrons production by all fission}}{\text{Number of fast neutrons produced by thermal fission}}$$

The value of ε is affected by the arrangement and concentration of the fuel and moderator. In a homogeneous system the fuel atoms are surrounded by the moderator, ε has a value of 1.00, while in a heterogeneous system where all fuel atoms are packed separately from the moderator such as in fuel pellets. Thus in a heterogeneous system neutrons emitted from the fission of one fuel atom have a very good chance of passing near another fuel atom and be absorbed or captured before slowing down significantly to cause fission. The value of ε for such an arrangement is about 1.03 and is not easily affected by temperature, pressure, enrichment or neutron poison. In essence the choice of ε is made at the design phase by choosing either the homogeneous or heterogeneous system [Lamarsh, 2002; Lewis, 2008].

2.4.1.2 Resonance escape probability

The number of neutrons will continue to increase as a result of fast fission factor and continue to diffuse through the reactor core or spent fuel cask. As they move along the system, they collide with nuclei of fuel, moderator or other materials loosing part of their energy during the collision and subsequently slowing down. While they are slowing down, they pass through the resonance region of many actinides but most importantly of ^{238}U whose resonance ranges from 6 eV to 200 MeV, and there is a large probability that they

may be captured. The probability that a neutron will not be absorbed by a resonance peak is known as resonance escape probability and is given by [Lamarsh, 2002; Lewis, 2008]:

$$\mathrm{p} = \frac{\text{number of neutrons that reach thermal energy}}{\text{number of fast neutrons that start to slow down}}$$

The value of resonance escape probability is influenced largely by the fuel-moderator arrangement, i.e. whether the system is homogeneous or heterogeneous and the amount of enrichment used (^{235}U or ^{239}Pu). To undergo resonance absorption, the neutron must pass as close to ^{238}U as possible while slowing down. This condition is easily met in the heterogeneous system since the neutron does its slowing down in the fuel region. Thus the neutron has a high probability of being absorbed; hence its escape probability is low. In a homogeneous mixture the neutron slows down in a moderator where there is no ^{238}U and it cannot be absorbed, hence its escape probability is high.

In water-moderated, low enrichment systems, raising the temperature of the fuel will increase the resonance absorption in ^{238}U as a result of Doppler Broadening, which implies a decrease in resonance escape probability. As water temperature increases, water density decreases. The decrease in water density allows more resonance energy neutrons to enter the fuel and be absorbed [Lamarsh, 2002; Lewis, 2008].

2.4.1.3 Thermal Utilisation Factor

After the neutrons have been thermalized, they continue to diffuse throughout the system and as a result may be absorbed by any material of the system. The thermal utilisation factor refers to how effectively neutrons are absorbed by the fuel or colloquially how well they are utilised within the system. Since the some of the neutrons will be absorbed by other materials of the system other than the fuel, the value of f will always be less than one (f < 1). It is defined as:

$$f = \frac{\text{number of thermal neutrons absorbed in the nuclei of the fuel}}{\text{number ofthermal neutrons absorbed in all reactor materials}}$$

It may be described mathematically as

$$f = \frac{\sum_a^{\mathrm{U}} \Phi^{\mathrm{U}} \mathrm{V}^{\mathrm{U}}}{\sum_a^{\mathrm{U}} \Phi^{\mathrm{U}} \mathrm{V}^{\mathrm{U}} \sum_a^{\mathrm{m}} \Phi^{\mathrm{m}} \mathrm{V}^{\mathrm{m}} + \sum_a^{\mathrm{p}} \Phi^{\mathrm{p}} \mathrm{V}^{\mathrm{p}}}, \tag{2.64}$$

where

a = absorption

U = uranium

m = moderator

p = poison

Φ = flux

V = volume

Again here there will be a distinction between heterogeneous system and the homogeneous system. In the heterogeneous system as is the case with A PWR such as the Koeberg reactor, the flux in the fuel region will be different from that of the moderator region primarily because of the absorption rate of the fuel.

This is further compounded by the fact that the volume of the fuel, moderator and poison will also be different in the two regions [Lamarsh, 2002; Lewis, 2008].

In a homogeneous system, the neutron flux seen by the fuel, moderator and poison will be the same and also because they are spread throughout the system, all occupy the same volume. Thus for the homogeneous system, Eqn (2.75) may be approximated as

$$f = \frac{\sum_a^{\mathrm{U}}}{\sum_a^{\mathrm{U}} + \sum_a^{\mathrm{m}} + \sum_a^{\mathrm{p}}} \tag{2.65}$$

The thermal utilisation factor will vary with temperature since the absorption varies with temperature.

In a heterogeneous water-moderated system, when the fuel temperature increases the water moderator expands forcing a significant amount of them out of the core. This means that the atom density of the fuel will be reduced and subsequently reducing the probability of a neutron being absorbed. This will then result in the increase in the thermal utilisation factor as the temperature increases because the neutrons have a much better chance of reacting with the fuel. As a result of this, the temperature coefficient of the thermal utilisation factor is positive [Duderstadt, *et al.*, 2010; Lamarsh, 2002; Lewis, 2008].

2.4.1.4 Reproduction Factor

Not all neutrons absorbed by the fuel result in fission; some are absorbed and only lead to an increase in internal energy of the fuel while others actually do cause fission. The reproduction factor is therefore, a factor that relates the relationship between fast neutrons produced as a ratio of thermal neutrons absorbed and is defined as:

$$\eta = \frac{\text{number of fast neutrons produced by thermal fission}}{\text{number ofthermal neutrons absorbed in the fuel}}$$

The effectiveness of thermal neutrons in the production of fast neutron can be determined from the product of fission reaction rate $\sum_f^{\mathrm{U}} \Phi^{\mathrm{U}}$ and the average number of neutrons produced per fission (ν). This may be summarised mathematically by:

$$\eta = \frac{\Sigma_f^{\mathrm{U}}\ \Phi^{\mathrm{U}}\nu}{\Sigma_a^{\mathrm{U}}\ \Phi^{\mathrm{U}}} \tag{2.66}$$

In a case like the PWR such as the Koeberg reactor fuel where the fuel contains both ^{235}U and ^{238}U, the reproductive factor is calculated by:

$$\eta = \frac{\mathrm{N}^{235\mathrm{U}}\sigma_f^{235\mathrm{U}}\nu^{235\mathrm{U}}}{\mathrm{N}^{235\mathrm{U}}\sigma_a^{235\mathrm{U}} + \mathrm{N}^{238\mathrm{U}}\sigma_a^{238\mathrm{U}}}, \tag{2.67}$$

where N is atom density of the respective nuclides [Lamarsh, 2002; Lewis, 2008].

2.4.1.5 Fast Non-Leakage Probability

In an ideal system which is infinitely large there would be no leakage of neutrons because regardless of where they went, they would still be inside the vessel. However, in practice the reactor core and the spent fuel cask have a finite size and as such neutrons do leak out of the system. The fast non leakage probability describes the relationship between fast neutrons that do not leak to those produced by all fission. The relationship is represented mathematically as [Lamarsh, 2002; Lewis, 2008],

$$\mathrm{L}_f = \frac{\text{number of fast neutrons that do not leak from the reactor}}{\text{number of thermal neutrons produced by all fission}}$$

2.4.1.6 Thermal Non-Leakage Probability

Not only fast neutrons leak out of the system, thermal neutron too do leak out. The number of thermal neutrons that do not leak out of the system in relation to the number of neutrons that are thermalized is defined be the thermal non-leakage probability which is defined by

$$L_t = \frac{\text{number of thermal neutrons that do not leak from the reactor}}{\text{number of neutrons that reach thermal energies}}$$

These factors are affected by temperature differently when studied in isolation. However when considered collectively, they produce a new factor known as the total non-leakage probability given by L_T which describes the fraction of all neutrons; thermal and fast neutrons, that do not leak out of the system. In a heterogeneous water-cooled, water-moderated system, both L_t and L_f are affected by the coolant temperature as follows; when the coolant temperature increases it expands and as a result its density decreases. This implies two things; a decrease in atom density needed for collision and the expansion of the path they have to travel. The neutrons thus have a much longer path to travel to slow down in which there is very little collision. This increases the probability of leakage and consequently decreases the non-leakage probability. The temperature coefficient for non-leakage probability is thus negative since as the temperature increases the non-leakage probabilities decrease [Lamarsh, 2002; Lewis, 2008].

Thus the neutron multiplication factor is a factor which is used to indicate whether the system is critical or subcritical and the system can go either way depending on the magnitude of any of the six factors. How each one of them will affect *k* is described in detail in the next section.

2.5 Neutron Transport

The success of nuclear criticality safety analysis depends largely on the understanding of how neutrons are transported from one region to another and how they interact with matter. Notwithstanding the difficulty of not being able to describe the mechanism of transport of neutron, how they interact with matter, or their energy content Boltzmann derived a most important equation; the Boltzmann transport equation which provides a mathematical relationship among all factors needed to transport neutrons from one region to another. The Boltzmann transport equation is based on the kinetic theory of gasses

which was derived earlier and expanded by introducing the neutron balance concept which is summarised by the following relation [Stacey, 2001; Lamarsh, 2002; Duderstadt, *et al.*, 2010; Chochran, *et al.*, 1999]:

$$(\text{the rate of change in neutron density}) = (\text{sources} - \text{losses})$$

What this relation means is that in a closed system, the number of neutrons leaving must always be the same as those entering it, i.e. there must be a balance between the two processes. The above relation is summarised mathematically in terms of the angular neutron flux $\phi\left(r,E,\hat{\Omega},t\right)$ by [Chochran, *et al.*, 1999; Duderstadt, *et al.*, 2010]:

$$\begin{aligned}&\frac{1}{v}\frac{\partial\phi(r,E,\hat{\Omega})}{\partial t}+\nabla\left[\hat{\Omega}\phi(r,E,\hat{\Omega},t)\right]+\sum_t(E)\phi(r,E,\hat{\Omega})\\&=\int_{E'}dE'\int_{\Omega'}d\hat{\Omega}'\sum_S\left(E'\to E,\hat{\Omega}'\to\hat{\Omega}\right)\phi\left(r,E',\hat{\Omega}',t\right)\\&+S\left(r,E,\hat{\Omega},t\right)\end{aligned} \tag{2.68}$$

where,

$\sum_t(E)$ = the total macroscopic cross-section of the neutron energy with energy E,

$\sum_s(E'\to E,\ \hat{\Omega}'\to\hat{\Omega}$ = differential scattering cross-section (per unit energy E', per unit solid angle Ω',

and

$\phi\left(r,E,\hat{\Omega},t\right)dEd\hat{\Omega}$ = the number of neutrons per square centimetre per second at point r, at time t, with energy between E and $E+dE$, moving in a direction $\hat{\Omega}$ inside a solid angle $d\hat{\Omega}$. The source term is defined by [Chochran, *et al.*, 1999; Duderstadt, *et al.*, 2010]:

$$S\left(r,E,\hat{\Omega},t\right)=S_{\text{ext}}+\chi(E)\int dE'\int d\hat{\Omega}'v(E')\sum_f(E')\phi\left(r,E,\hat{\Omega}',t\right) \tag{2.69}$$

where,

$S_{ext}=f\left(r,E,\hat{\Omega},t\right)$ = a given non-fission external source.

v(E) = the number of neutrons per fission caused by a neutron with energy E.

χ(E)dE = neutron fission per spectrum = fraction of fission neutron with energy between E and $E + dE$.

There are a number of approximations of Boltzmann transport equations each leading to a solution of an equation of a completely different mode of neutron transport. The Diffusion Approximations being just one of many which is derived from the transport equation by dropping the $\hat{\Omega}$ variable which is a unit vector that describes the direction of motion of the neutron. Diffusion, as will be seen later, plays a very significant role in the design of the cask and selection of the storage pattern to ensure that the selected storage array results in the k_{eff} which is as far below 0.95 as possible. What is also important to note is that the UO_2 will change its crystal structure as a result of irradiation, and because of this the rate of diffusion of neutrons will change depending on the diffusion coefficient of that crystal structure in question. This is particularly so for higher burnup since this will result in a higher fission rate and consequently in the increase in the fission product density. According to Matzke, the diffusion coefficient increases with increase in Oxygen-to-Metal ratio O/M, thus any factor that will change the stoichiometry of UO_2 to UO_{2+x} where $x > 0$ will have a net effect of increasing the diffusion coefficient of that material [Matzke, 1996; Matzke, 1992]

The other important neutron transport variation which results from dropping time factor *t*, results in a solution that represents a steady-state. Using the one group diffusion theory the neutron balance can be written as

$$\frac{\partial \mathbf{n}}{\partial \mathbf{t}} = \frac{\mathbf{neutron\ produced}}{\mathbf{unit\ volume.time}} - \frac{\mathbf{Neutrons\ lost\ by}\ \text{absorption}}{\mathbf{unit\ volume.time}} - \frac{\mathbf{neutrons\ lost\ by}\ \text{leakage}}{\mathbf{unit\ volume.time}}. \tag{2.70}$$

In a steady state system that is just critical, the neutron balance requirement is only met if [Duderstadt, *et al.*, 2010; Lewis, 2008]:

$$\text{Neutron losses} = \text{Neutron gains}$$

From this the diffusion equation can then be written as:

$$\frac{\partial n}{\partial t} = 0 = S - \Sigma_a \phi + D\nabla^2 \phi, \tag{2.71}$$

where

ϕ = the neutron flux (n.cm^{-2}.sec).

Σ_a = macroscopic absorption

D = diffusion coefficient.

S = source term

The diffusion coefficient is a function of the macroscopic scattering cross-section Σ_s and the relationship between the two is given by [Duderstadt, *et al.*, 2010; Lewis, 2008]:

$$D = \frac{1}{3\Sigma_s}. \tag{2.73}$$

Given that the macroscopic transport cross-section is given by

$$\Sigma tr = \Sigma_s\left(1-\overline{\mu_0}\right), \tag{2.74}$$

where $\overline{\mu_0}$ is the average cosine of the scattering angle in the laboratory system, then according to Stacey and Duderstadt D may be written as [Duderstadt, *et al.*, 2010]:

$$D = \frac{1}{3\left\{\Sigma_a + \Sigma_s\left(1-\overline{\mu_0}\right)\right\}}. \tag{2.75}$$

Substituting Eqn (2.84) into Eqn (2.85) yields Eqn (2.86).

$$D = \frac{1}{3\{\Sigma a + \Sigma \mathrm{tr}\ \}}. \tag{2.76}$$

However, since the transport mean free path (λ_{tr}) is related to the transport cross-section by

$$\lambda_{tr} = \frac{1}{\Sigma \mathrm{tr}}, \tag{2.77}$$

and assuming that Σ_a is very small relative to Σ_s, Eqn (2.86) can then be written as

$$D = \frac{1}{3\Sigma_{\mathrm{tr}}}. \tag{2.78}$$

Substitution of Eqn (2.86) into Eqn (2.87), will yield

$$D = \frac{\lambda_{\mathrm{tr}}}{3} \tag{2.79}$$

From this one can see that there is a linear relationship between the diffusion coefficient and transport mean free path.

Therefore, the diffusion coefficient of a particle (e.g. neutron) through a given material is paramount to the criticality of a system. This is particularly so if one has to compare different cladding materials for their effect in the criticality nuclear safety. The material with the highest diffusion rate will tend to allow more neutrons to pass though cladding and reach the fuel, but it is material that will be able to slow the neutrons down to thermal energy range and has a high diffusion coefficient that will ultimately determine the criticality of the system.

2.5.1 Neutron Diffusion Theories.

Generally neutrons in a reactor vessel like a reactor core or the cask have a wide ranging energy spectrum which may vary from eV to MeV, with the cross-section also varying accordingly. Trying to treat them the same has proven to be impossible because in spite of being in the same vessel at the same time they have different energies and interact with different matter differently. As a result of this a number of theories were developed each one breaking them into smaller discrete energy groups and studying how elements of each group behave.

2.5.1.1 One-group Theory

The One-group theory purports all neutrons in a reactor vessel as though they all have the same energy and all travelled the same distance and interacted with matter in the same way. This soon proved to be a problem to advocates of the one-group theory since they soon discovered that trying to express all neutrons in the reactor vessel as having the same energy, presented them with too many problems since the theory could not explain some of the nuclear phenomena which were observed. It is thus impossible to expect the one-group theory to be accurate in describing the energy of neutrons in a system given that they are in a continuous state of motion and there are always new ones being born at a higher energy while some are moderated to thermal energy range [Duderstadt, *et al.*, 2010].

Most importantly, it is critical to take note that since their cross-sections are energy dependent, there will therefore be nuclear reactions which can only take part at a certain energy range and cannot take place outside that range which the one group theory fails to explain. Similarly, there are nuclides which can only participate in certain nuclear reactions and not in others because of the energy-dependence of their cross-section. It is therefore, important that the particle (neutron) energy spectrum is divided into a number of discrete energy groups each being characterised by its boundaries, and the characteristics of nuclear reactions uniquely belonging in that energy group identified [Duderstadt, *et al.*, 2010; Chochran, *et al.*, 1999]. As a result of ineffectiveness of the one group theory in that regard the energy range was divided into even smaller discrete groups and resulted in two-, three- or even four group theory which will be studied in detail in the next section.

2.5.1.2 Two-Group Theory

The two-group model was developed as a result of the inability of the one-group theory to provide an explanation of nuclear phenomena taking place in reactor vessel. It portrays the neutron energy of the system to be divided into two groups. Because of this, there was quite an improvement from the one-group theory since it allowed one to study nuclear reactions belonging to either of the two groups separately. Studying nuclear reactions using this model gave much better results with minor changes on the energy-averaged cross-section compared to the one-group theory [Chochran, *et al.*, 1999; Duderstadt, *et al.*, 2010; Stacey, 2001].

2.5.1.3 Multi-group Theory

The Multigroup energy model has been found to yield the most accurate cell calculation results compared to the one-group, two-group or the semi-two group model. This because the neutron energy spectrum is divided into a number of discrete sub-groups indicated in Figure 2.6 and the reaction mechanism of each nuclear reaction is studied in only that particular energy group where it yields reliable results. Therefore, because of reliability, reproducibility and accuracy of its results it finds application in a much wider scope in reactor physics than the less discretized groups i.e. one- and two-group theory.

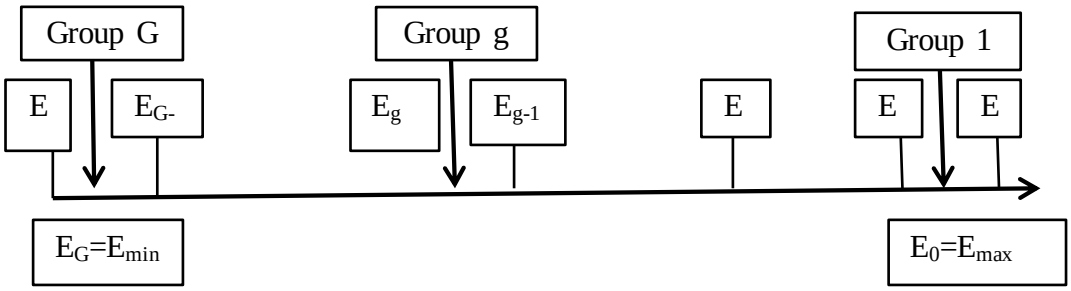

Figure 2.6: Neutron Energy Numbering System [Duderstadt, *et al.*, 2010]

Subsequently, the multigroup energy equation was derived, which is based on the assumption that the entire energy spectrum is divided into G groups with *g*'th group having E_g and E_{g-1} as its boundaries. The properties of each variable in that group e.g. cross-sections, particle energies, sensitivity are thus assumed to be the same and this assumption is applied in all calculations involving neutron transport [Duderstadt, *et al.*, 2010; Stacey, 2001].

Thus whenever one studies a particular nuclear reaction, one has to always take their energy, and thereby the energy group into account. This determines the cross-section of the nuclide and hence the probability of whether the reaction in question will take place or not.

The calculation of the eigenvalue, *k* and the source term referred to earlier are thus based on the multigroup group theory rather than on one- or two group-theory, because it is imperative that the calculated eigenvalue of the system is as accurate as can be found to avoid the system going super-critical [Duderstadt, *et al.*, 2010].

2.6 PERTURBATION OF A SYSTEM AND THE SEARCH FOR THE APPROPRIATE EIGENVALUE

In criticality safety analysis it is often necessary to calculate the effect of a perturbation (i.e. minor change) of material (composition, temperature or density) or geometry of the vessel will have on the neutron multiplication factor (k[7]) of the system. If the perturbation is sufficiently small and sensitivity of *k* is insignificant (i.e. less than one standard deviation) one does not have to repeat the original criticality calculation, but instead can use the perturbation theory to express the corresponding neutron multiplication factor in

[7]The concepts k_{eff}, k and eigenvalue mean the same thing, except that the eigenvalue is more suitable when used in an operational sense where the eigenvalue can be manipulated by adjusting certain reactor controls, while the other two k and k_{eff} are more suitable in computer modelling. In this study they will be used interchangeably

terms of the fluxes of the unperturbed core [Duderstadt, *et al.*, 2010; Chochran, *et al.*, 1999].

This however is not always the case since, as Stacey argued [Stacey, 2001], in real life, the value of k is seldom based on a steady state system where there is an immediate balance between in-coming and outgoing neutrons. In real life, the system is rather more dynamic than steady, and in a dynamic system there is a continuous change in material composition, material density, macroscopic cross-section or density of material. In such a system, these will always affect the value of k whenever they change. To maintain the value of k at a particular point, the number of neutrons or material compositions is regularly changed such that a required constant value of k is maintained. To enable us to manipulate the neutron transport equation better, Eqn (2.79) is rewritten in operator notation as [Rearden, 2004; Rearden, *et al.*, 2008]:

$$M^{\circ}\phi = \frac{1}{k}F^{\circ}\phi, \tag{2.80}$$

and

$M^{\circ} \equiv -\nabla.D(r)\nabla^{\circ} + \Sigma_a(r)^{\circ}$ is the destruction operator (leakage plus absorption)

$F^{\circ} \equiv \nu\Sigma_f(r)^{\circ}$ is the production operator (fission)

Since the source term, S, on the right hand side (RHS) of Eqn (2.90) is unknown (as can be seen from its absence from the equation), the process of determining it starts by [Chochran, *et al.*, 1999]:

1. guessing an initial estimate value of the fission source and k:

$$S(r) = S^{\circ}(r) \qquad k = k^{\circ}, \tag{2.81}$$

2. next the flux $\phi^{(1)}$ resulting from the new source is calculated

$$M^{(1)} \equiv -\nabla.D\nabla\phi^{(1)} + \Sigma_a\phi^{(1)} = \frac{1}{k^{\circ}}S^{(\circ)}, \tag{2.82}$$

3. Now a new fission source term is calculated using the fluxes just obtained

$$S^{(1)} = F\phi^{(1)} = \nu\Sigma_f\phi^{(1)} \tag{2.83}$$

This is taken as the new fission source term which can be used to calculate a new flux $\phi^{(2)}$ etc. as long as a new and improved estimate of *k* is made. In general, this implies that a new and improved fission source term $S^{(n+1)}$ can be calculated iteratively from the previous one $S^{(n)}$ by solving [Chochran, *et al.*, 1999]:

$$M\phi^{(n+1)} = \frac{1}{k^{(n)}}S^n, \tag{2. 84}$$

and then computing

$$S^{(n+1)} = F\phi^{(n+1)}. \tag{2.85}$$

After the *nth* iteration a test for convergence is performed as follows:

$$\left|\frac{S^{(n)} - S^{(n-1)}}{S^n}\right| < \varepsilon_S, \tag{2.86}$$

and

$$\left|\frac{k^{(n)} - k^{(n-1)}}{k^{(n)}}\right| \varepsilon_k, \tag{2.87}$$

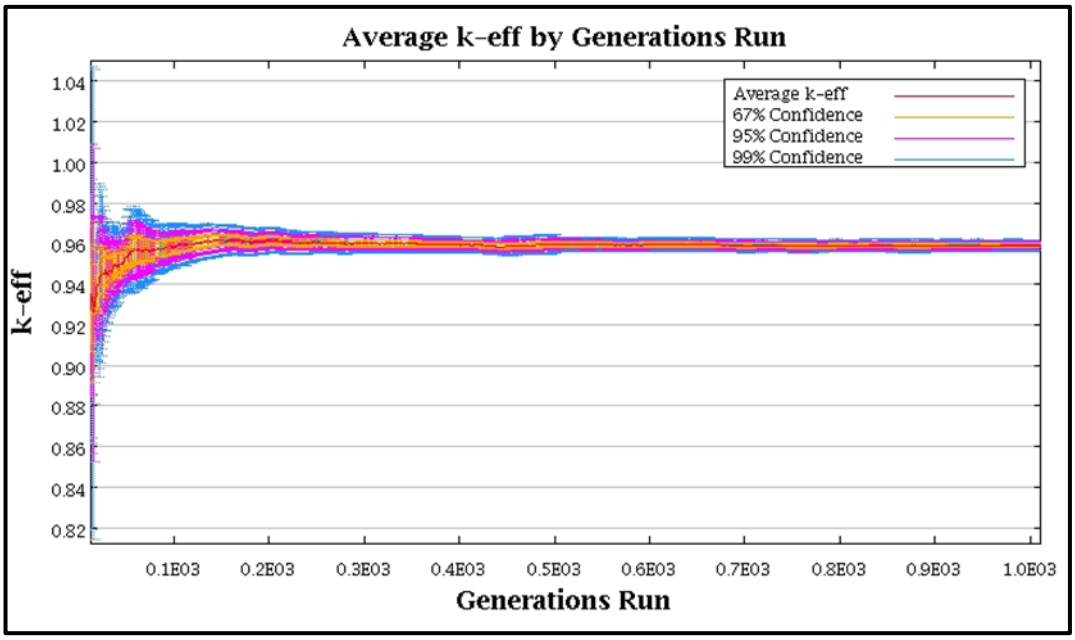

Figure 2.7: Convergence of an iteration of eigenvalue to a system's average eigenvalue (Present study).

where the values of the convergence criteria of ε_s and ε_k range from $1x10^{-5}$ to $1x10^{-3}$. If that convergence criterion is met as shown in Figure 2.8, then calculation is completed, if not the process starts all over again until it is met [Chochran, *et al.*, 1999].

To ensure convergence, in this thesis a high number of neutron generations (between 1000 and 10000 and the same number of neutrons per generation) were used and the eigenvalue converged to 99% confidence level of the systems k_{eff}.

2.7 RANKING OF NUCLIDES IMPORTANT TO CRITICALITY SAFETY

As stated in the previous sections nuclides of interest to Criticality Nuclear Safety may generally be divided into the following groups:

- Actinides
- Fission products
- Light elements

Actinides and Fission Products have been studied quite extensively as indicated in the previous section. Light elements on the other hand have generally been found to make no significant impact in criticality and as such are by far and large ignored except for ^{18}O which although it has a small cross-section, is included in the analysis because of its huge fraction in water rather than for its cross-section. Even in Actinides and Fission Products,

not every nuclide in those groups is important to criticality safety analysis. A study was launched in the USA to determine which nuclides in the either group is more important than the others [Gauld, *et al.*, 2000].

2.7.1 Rankings of Actinides.

According to Gauld, the criterion for expressing the importance of each nuclide is based on the fractional contribution of each nuclide to the total neutron absorption rate for a given enrichment and cooling period [Gauld, *et al.*, 2000]. For high enrichment and burnup (5 wt% and 60 GWD/t respectively) the relative total actinide absorption in PWR has been found to be 82%. Based on this the individual fractional contributions is calculated as a fraction of the total. In the criticality rankings that were performed by I Gauld, in 2000, he classified the actinides into three groups in accordance to their fractional contribution to the total absorption as shown in Figure 2.9. These were [Gauld, *et al.*, 2000]:

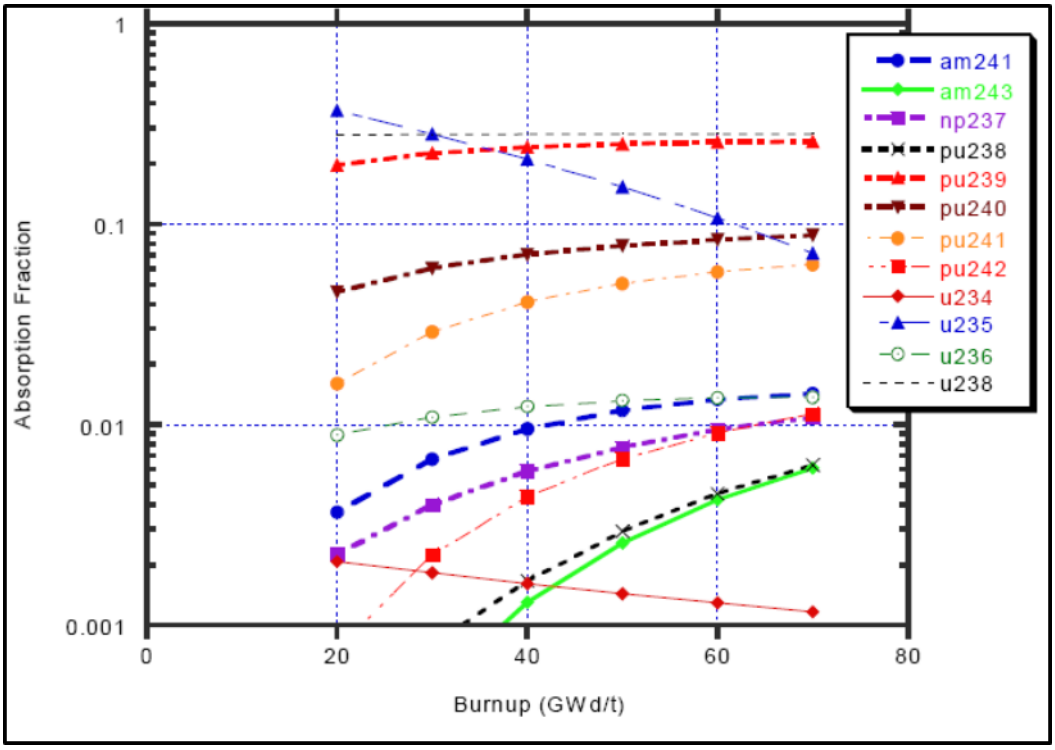

Figure 2.8: Fraction of total neutron absorption from actinides for 5 wt% and 5 years cooling [Gauld, *et al.*, 2000] with permission from BT Rearden and IC Gauld

1) Dominant actinide absorbers (absorption fraction > 0.1), which consisted of:

   a) ^{238}U whose absorption fraction remained constant at about 0.28 as burnup increases.

   b) ^{239}Pu whose fraction increased up to about 50 GWd/t and then levelled out.

   c) ^{235}U whose absorption fraction decreased rapidly with burnup as it is depleted by fission.

2) Moderately absorbing actinides (0.01 < absorption fraction < 0.1) included;

   ^{240}Pu, ^{241}Am, ^{236}U and ^{241}Pu. All these were found to be increasing quite rapidly in importance up to about 40 GWd/t and from there the increase was less rapid up to 70 GWd/t.

3) Least absorbing (< 0.01 absorption fraction): Except for ^{234}U whose importance decreases with burnup, the importance of other members of this group increases fairly rapidly across all burnup ranges regardless of the cooling time used. These include: ^{238}Pu, ^{243}Am, ^{242}Am and ^{237}Np.

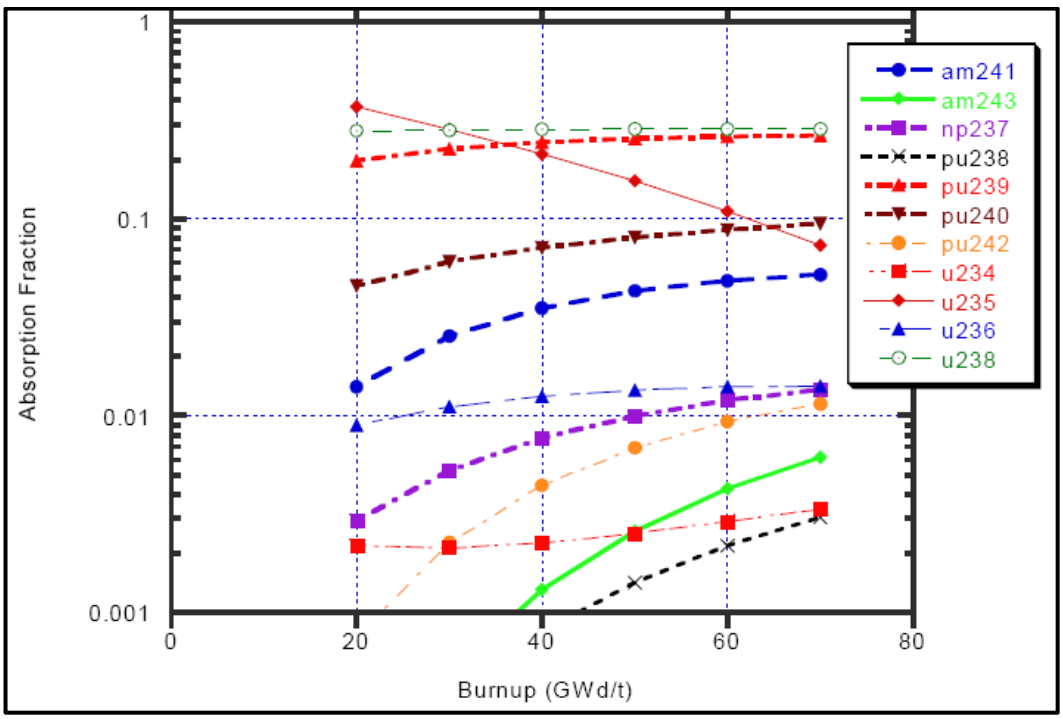

Figure 2.9 Fraction of total neutron absorption from actinides for 5 wt% and 100 years cooling [Gauld, *et al.*, 2000] with permission from BT Rearden and IC Gauld

As a result of variations in isotopic inventory caused by enrichment, burnup and cooling time, the analysis was done on 5 wt% enrichment across all of burnup ranges and at 5 year and 100 year cooling time. Their respective graphs are in Figure 2.9 and Figure 2.10 respectively. It is interesting to note that the total actinide absorption in the PWR has been found to be higher than that in the Boiling Water Reactor (BWR) fuel assembly, being 82.3% and 80.7% respectively [Gauld, *et al.*, 2000].

According to Gauld, this could be due to the difference in structural material per fuel assembly mass, which results in greater neutron absorption by structural material, hence a higher absorption in PWR.

2.7.2 Rankings of Fission Products

Apart from the actinides which have just been discussed, fission product also must be accounted for in burnup credits. During the ranking of this group of nuclides, ORNL found that they only account for between 6% and 15% of the total absorption taking place in the PWR [Gauld, *et al.*, 2000]. It was also observed that with the exception of ^{149}Sm and ^{147}Sm which have a steady increase in importance, all others show quite a rapid increase across all burnup ranges. Following this ranking, the following nuclides were found to be of great importance in nuclear criticality [Gauld, *et al.*, 2000];

- ^{103}Rh, ^{143}Nd, ^{149}Sm, ^{133}Cs, ^{131}Xe, ^{99}Tc, ^{152}Sm, ^{153}Eu, ^{155}Gd, ^{151}Sm,^{145}Nd,^{109}Gd,^{95}Mo,^{150}Sm, ^{154}Eu, ^{147}Sm, ^{101}Ru,^{155}Eu, ^{105}Pd.

A graphical representation of the importance of fission products at 5-year cooling and 100-year cooling are indicated in Figure 2.11 and Figure 2.12 respectively. It is observed that the nuclide that shows the most rapid increase is ^{155}Gd, primarily because it is stable and its predecessor ^{155}Eu has a only a half-life of 4.75 years. There is therefore, a continual supply of ^{155}Gd from the decay of ^{155}Eu whereas it is not being depleted by any form. Another nuclide which has shown a similar rapid increase as ^{155}Gd does is ^{153}Eu. The only difference between these two nuclides is that the order of half-lives between the parent and the daughter is reversed. In the second case, ^{153}Eu which is stable is the precursor of ^{153}Gd with a half-life of 241.6 days.

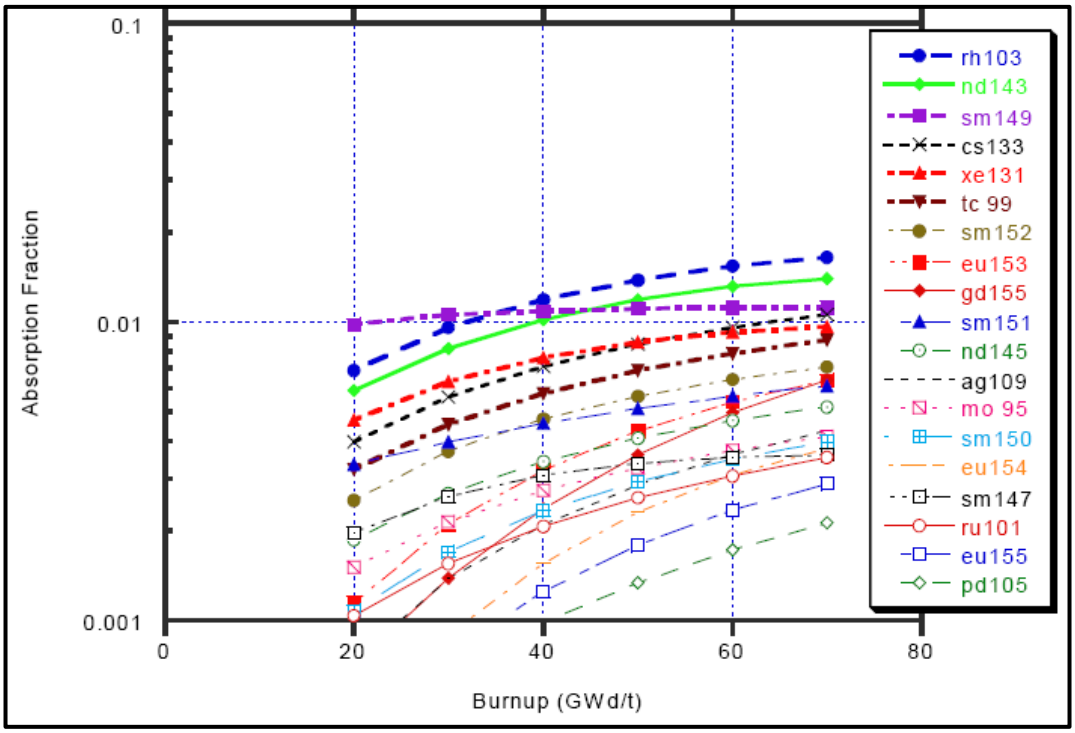

Figure 2.10 Fraction of total neutron absorption from Fission Products for 5 wt% and 5 years cooling [Gauld, *et al.*, 2000] with permission from BT Rearden and IC Gauld.

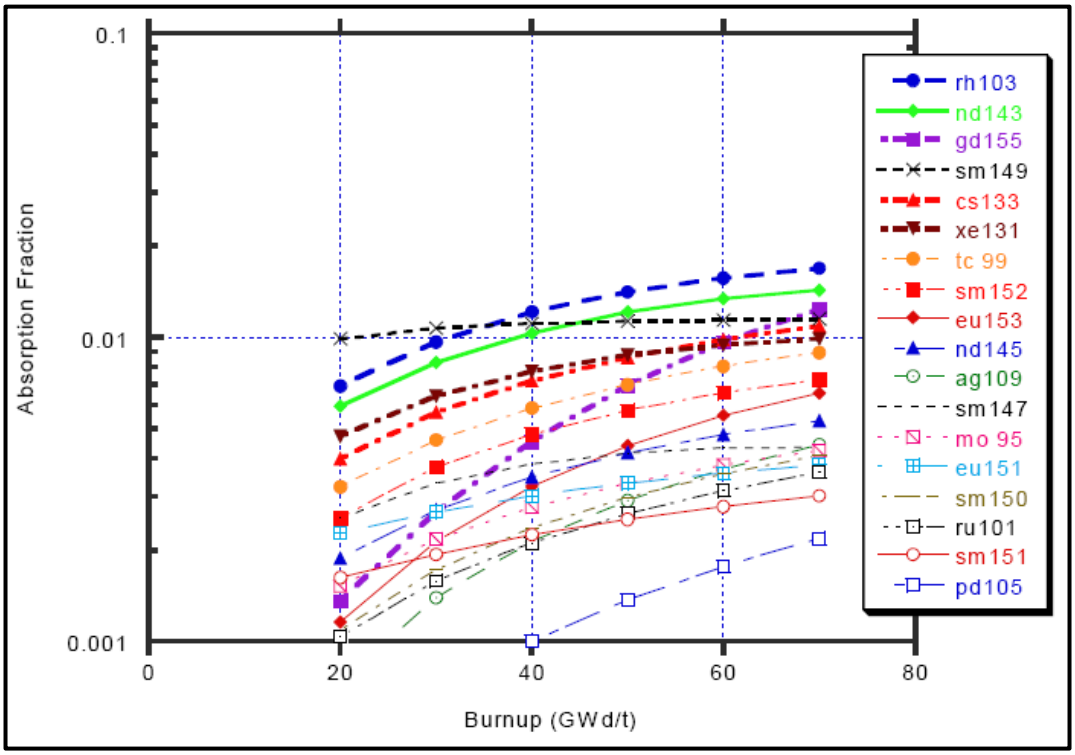

Figure 2.11: Fraction of total neutron absorption from Fission Products for 5 wt% and 100 years cooling [Gauld, *et al.*, 2000] with permission from BT Rearden and IC Gauld.

Thus, the rate of decay of ^{153}Eu is not fast enough to generate ^{153}Gd at a reasonable rate; as a result the importance of ^{153}Gd is affected negatively because there isn't enough of it to contribute to fractional absorption.

As a result of the huge neutron absorption cross-section fission products have, they are rarely studied on their own when it comes to burnup credits. As such they are always used in conjunction with major actinides so that major actinides can complement whatever neutrons have been lost to absorption by fission products.

CHAPTER 3

3. MODELLING TECHNIQUES

3.1 Introduction

Generally, there are two main methods for simulating and modelling neutron transport and interaction of neutrons with matter in the reactor core (or neutronics as often called) and these are deterministic methods and Monte Carlo Methods [Dupree, *et al.*, 2002; Landau, *et al.*, 2005].

According to Landau [Landau, *et al.*, 2005], the deterministic technique approaches the solution of the Boltzmann Transport Equation (BTE) using numerical approximations throughout the system that is being modelled. As such the results obtained are approximations and are therefore, less accurate compared to their Monte Carlo counterparts [Dupree, *et al.*, 2002; Landau, *et al.*, 2005]. The Monte Carlo (or stochastic) methods, on the other hand, model the nuclear system almost exactly and use statistical approximations to solve the Boltzmann Transport Equation of the system being modelled. As a result, the calculations are much more accurate and reliable compared to their deterministic counterparts in spite of the lengthy period of time it takes to complete a given task [Dupree, *et al.*, 2002; Landau, *et al.*, 2005]. However, both techniques have profound benefits in numerical analyses; the deterministic methods are fast for one-dimensional systems while Monte Carlo methods are slow but give a more reliable answer.

Modelling in this thesis will largely use Monte Carlo Techniques using various modules of SCALE 6.1.3; for nuclear criticality safety analysis and sensitivity analysis *and* uncertainty analysis with direct perturbation techniques KENO VI, a module of SCALE [Bowman, *et al.*, 2005] will be used to determine the neutron multiplication factor (k_{eff}). For Sensitivity and Uncertainty analysis where the goal is to determine the sensitivity coefficient of all nuclear reactions that may possibly take place in the fissile system, the TSUNAMI-3 code [Mueller, *et al.*, 2005b] will be used. However, where necessary, deterministic techniques are employed such as in the case of determining the source term.

3.2 Research Methodology

The present study was performed by modelling criticality from either *fresh fuel* (un-irradiated fuel) or *spent fuel* using the SCALE (standardized computer analysis for licensing evaluation) computer code that uses Monte Carlo techniques to calculate the neutron transport of the system [Gauld, *et a*l., 2004; Bowman, *et al*., 2005; Hollenbach, *et al*., 2009].

SCALE computer code consists of a number of analytical sequences, referred to as *functional modules,* which actually perform the analysis. They are automated by other modules of SCALE known as *control modules,* to perform data processing and analysis to the required accuracy and level of detail of a high pedigree and rigorous computer code. SCALE is designed as a modular structure, each type of analysis requiring that a specific control module be used. For example, for criticality safety analyses where no burnup credit is taken into account, the KENO-VI module of SCALE is used whereas for Burnup Credit Analyses and Sensitivity and Uncertainty analyses STARBUC and TSUNAMI-3D are used.

The analyst prepares an input file based on the engineering parameters of the system to be modelled. The SCALE control modules, then uses this input data to generate additional parameters and creates an input for the functional modules, which are necessary to derive the results being sought.

Since it is a regulatory requirement that all licensing analytical software undergoes a verification and validation (V&V) process, it is worth mentioning that both SCALE6.0 and SCALE6.1, as used in this thesis, have undergone an extensive and rigorous V&V process as part of the Oak Ridge National Laboratory Development programme [Broadhead, 1996].

The '*fresh fuel'* analyses assume that fuel has never been irradiated, i.e. it is being irradiated for the first time, which implies that other nuclides present in the reactor core are ignored. The fresh fuel assumption plays a very important role in Nuclear Criticality Safety Analysis in a sense that if the fuel is analysed as '*fresh fuel', there is usually a certain degree of conservatism built into the calculations which often results in an over-estimation of, for example, the distance between neighbouring spent fuel assemblies or absorber thickness needed to prevent criticality (thus a better safety margin).* If however,

burn-up credit were taken into account, this could have resulted in more fuel assemblies per cask, fewer transportation trips and a lower risk of accidents during transportation. Therefore, one could achieve the same criticality value by either reducing the distance between fuel assemblies or by keeping the distance constant and increasing the thickness of boral plate [Parks, *et al.*, 2006].

Burn-up credit (BUC), on the other hand, assumes that the fuel has been in the reactor for some time and thus a number of nuclides have been generated, some of which have a very high neutron absorption cross-section and high sensitivity coefficients thus have a high propensity of reducing criticality, a phenomenon known as burn-up credit [Parks, *et al.*, 2006; Pesic, *et al.*, 1997]. Thus, application of burn-up credits often results in the saving of storage space by removing over-conservatism associated with analysing spent fuel as fresh fuel. This allow for more spent fuel to be stored in a smaller space compared to that of fresh fuel, while at the same time complying with sub-criticality requirement of safe storage of the fuel [Cousinou, *et al.*, 2001; Withee, *et al.*, 2000].

3.2.1 Fresh Fuel

Most nuclear regulators are generally not very keen to licence any spent fuel storage facility that takes burnup credits into account as the basis of their safety analysis. They would rather have calculations performed on the basis that the fuel is fresh because *fresh fuel* assumptions do not take credit for the high absorption cross-section for neutrons of nuclides concerned. Such nuclides include ^{155}Gd, ^{147}Sm, ^{150}Sm, ^{151}Sm, ^{152}Sm, and ^{133}Cs which because of their high neutron absorption cross section will through absorption, capture etc. remove some neutrons from further participation in the fission process, thereby making the system less reactive and safer than without them, [Radulescu, *et al.*, 2006; Parks, *et al.*, 2006]. As a result of this, burnup credits often allow the licensee to store more fuel assemblies in a storage space which would never have been allowed under fresh fuel assumptions. Although it is scientifically correct and safe to do so, it is a safety risk the nuclear regulator is not prepared to take. As such, 'fresh fuel' *analyses result in a large safety margin and thus preferable to nuclear regulators while burnup credits analyses on the other hand have less safety margin and hence are more economical, providing the nuclear operator with more storage space and hence are preferable to the nuclear operator*.

The important factors which fresh fuel assumptions take into consideration when calculating criticality are initial enrichment of the fuel, fuel temperature, moderator temperature and fuel and moderator densities and their respective compositions. These have a direct bearing on the criticality of the system and on the choice of the materials from which the cask is made and the number of fuel assemblies that can be stored in the cask [Gauld, *et al.*, 2004; Radulescu, *et al.*, 2006]. In this work a number of different combinations of temperature, moderator density, flooding with freshwater or with seawater simulations were run to determine the effect of varying these factors on k_{eff}.

3.2.2 Spent Fuel

When a fuel assembly is irradiated in the core, the amount of nuclear fuel (^{235}U and ^{238}U) will decrease with *time* and *increase in burnup*, and because of this there will be a corresponding decrease in k_{eff} of the system because of the build-up of nuclides with parasitic absorption of neutrons. These include among others fission products which have a high absorption cross-section and as a result will reduce the amount of neutrons participating in the fission process and thus result in the decrease in k_{eff}

Not only do fission products have a high absorption cross-section, according to Mueller, [Mueller, *et al.*, 2005a] their sensitivity coefficient is also marginally higher than those of Major Actinides which implies that they will have a much greater effect on the Δk_{eff} than the Major Actinides. This is further exacerbated by the fact that in some cases where fission products have a lower sensitivity, their predecessors, will compensate for the shortfall by their own high sensitivity coefficients.

The build-up of fission products such as; ^{243}Am, ^{237}Np, ^{133}Cs, ^{143}Nd, ^{151}Sm, ^{155}Gd, ^{99}Tc, ^{145}Nd, ^{147}Sm, ^{150}Sm, ^{151}Sm, ^{152}Sm ^{151}Eu and ^{153}Eu are particularly important since they have a high neutron absorption cross-section, and as a result will decrease reactivity by absorbing neutrons in the system thus reducing the amount of neutrons that are available to participate in the fission process [Parks, *et al.*, 2006; Pesic, *et al.*, 1997]. According to Chochran [Chochran, *et al.*, 1999], the effective yield of fission product *i*, from actinide *a*, is a function of the independent yield Y, neutron flux ϕ and the number of atoms $N_a(t)$ of fissile actinide *a* (which in this case can primarily be either ^{235}U, ^{239}Pu or ^{241}Pu) at the time *t* of irradiation. The relationships of these factors are summarised mathematically by

$$\alpha_{\mathrm{i}} = \sum_{a} \sum_{\mathrm{k}=1}^{\mathrm{N}} \sigma_{a,\mathrm{k}}^{\mathrm{F}} \phi_{\mathrm{k}} \mathrm{N}_{a}(t) \mathrm{Y}_{a,\mathrm{k}}^{\mathrm{i}}, \tag{3.0}$$

where

$\sigma_{a,\mathrm{k}}^{\mathrm{F}}$ = is the effective group averaged fission cross-section of actinide *a* in the k^{th} neutron group of N group. For this research 238 neutron groups were used.

ϕ_{k} = is the neutron flux in the k^{th} neutron group

$\mathrm{N}_{a}(\mathrm{t})$ = the number of atoms of fissile actinide *a* at the time *t* of irradiation

$\mathrm{Y}_{a,\mathrm{k}}^{\mathrm{i}}$ = the independent yield of fission product *i.*

These nuclides play a significant role in criticality safety and have to be accounted for in burnup credit calculation since their presence in a vessel can lead to either an increase or decrease in criticality. However, because there are so many of them, their importance in criticality has to be ranked and only those which prove to be important need be taken into account in criticality analysis. Since ranking has already been done, it will not be repeated in this thesis but will use already available data published in various publications. One such publication which has been referenced quite extensively in nuclide ranking because of the level of depth and the scope of nuclides it covered is NUREG/CR-6700 ORNL/TM-2000/284 [Gauld, *et al.*, 2000]. In this publication the importance of nuclides is ranked according to their impact in criticality, shielding and radiation protection. In addition to the gradual increase in nuclide which were initially not part of the fuel, there is also a gradual decrease in the amount of the initial fuel due to the depletion process, and the criteria of how they are ranked is described in the next section [Gauld, *et al.*, 2000].

3.3 Fuel depletion

Fuel depletion is one of the nuclear processes that take place in the reactor core where the original amount of fuel, ^{235}U and ^{238}U undergo nuclear reactions (fission, capture, or absorption) with neutrons. As a result the fuel is slowly depleted because of transmutation and/or decay which converts it into other nuclides like decay or fission products. Some of the nuclides that result from these reactions are fissile such as ^{239}Pu, ^{240}Pu, ^{241}Pu and ^{242}Pu

etc. resulting in a positive reactivity in the core which if not accounted for in a criticality safety analysis can result in a nuclear excursion. The build-up of actinides and fission products as a function of burnup is indicated in APPENDIX 5 and APPENDIX 6 respectively and their respective importance in burnup credit analysis will be discussed in detail in the respective section dedicated to this topic. After the fuel assemblies have been in the reactor core for approximately 18 months, most of the fuel i.e. ^{235}U and ^{238}U will be depleted, and is offloaded and replaced by the new ones. According to Stacey, depletion is when "*the fuel left in the assemblies can no longer produce enough power to the electricity grid, the fuel assembly is said to be spent and must be replaced with new fuel assemblies*" [Stacey, 2001]. The time at which the fuel must be offloaded is known as the End-Of-Cycle (EOC) time, and according to Stacey this is defined as "*the time at which the reactor can no longer be maintained critical with the control rods withdrawn as fully as allowed by safety consideration"* [Duderstadt, *et al.*, 2010; Stacey, 2001].

Thus, the End-Of-Cycle time (t_{EOC}) is defined mathematically as [Stacey, 2001]:

$$t_{\mathrm{EOC}} = \left\{ \begin{array}{l} \dfrac{\eta\rho_{\mathrm{ex}}(1+\alpha)-(\gamma^{\mathrm{Te}}+\gamma^{\mathrm{Xe}})\phi(0)\sigma_a^X/\lambda^X-\gamma^{\mathrm{Nd}}}{\left[(\eta-1)(1+\alpha)\sigma_a^F-\gamma^{\mathrm{Nd}}\sigma_a^F+\gamma_{fp'}\right]\phi(0)}, \phi(t) \ll \dfrac{\lambda^X}{\sigma_a^X} \\ \\ \dfrac{\eta\rho_{\mathrm{ex}}(1+\alpha)-\left(\gamma e^{\mathrm{Te}}+\gamma^{\mathrm{Xe}}+\gamma^{\mathrm{Nd}}\right)}{\left[(\eta-1)(1+\alpha)\sigma_a^F-\left(\gamma^{\mathrm{Te}}+\gamma^{\mathrm{Xe}}+\gamma^{\mathrm{Nd}}\right)\sigma_a^F+\gamma_{\mathrm{fp}'}\sigma_{\mathrm{fp}'}\right]\phi(0)}, \phi(t) \gg \dfrac{\lambda^X}{\sigma_a^X} \end{array} \right\} \quad (3.1)$$

where,

α = the capture-to-fission ratio of the fuel, and

σ_a^F= microscopic absorption cross-section for the fuel,

γ_{fp}= fission yield of other fission products which accumulates over time

σ_{fp}= the microscopic cross-section of other fission products.

ϕ = The quantity $\gamma_{fp}\sigma_{fp}$ ranges from 40 to 50 barns per fission, and

$$\rho_{\mathrm{ex}} \equiv \frac{k_\infty(0)-1}{k_\infty(0)}, \quad (3.2)$$

is the excess reactivity at the beginning-of-cycle (BOC) without xenon, samarium, fission products or control cross-section.

From Eqn (3.1) it is clear that the t_{EOC} is indirectly proportional to the power or flux level. Hence given that the fuel density is about 10^{22} nuclei/cm^3 compared to the neutron flux density of about 10^{14} n/cm^{2}s it takes a few months before an appreciable fuel depletion is noticed. That is one of the reasons why the fuel outage only takes place once every 18 months [Garland, 2005].

The nuclides cited above are only a few of a large number of nuclides produced in the core and to keep track of every reaction they all undergo may be cumbersome without a computer programme. As a result, computer codes such as SCALE and MCNP have been developed to address this very problem and have among many other modules a module which is specifically designed for the calculation of fuel depletion in a reactor core. The general equation for the calculation of depletion of nuclides in a core is thus given by [Chochran, *et al.*, 1999]:

$$\frac{dN_i}{dt} = \sum_{j=1}^{M} l_{ij}\lambda_j N_j + \phi \sum_{k=1}^{M} f_{ik}\sigma_k N_k - \left(\lambda_i + \phi\sigma_i + r_i - c_i\right) N_i + F_i \,|\, i = 1, M, \quad , \tag{3.3}$$

where,

N_i = atom density of nuclide i,

M = number of nuclides,

l_{ij} = fraction of decays of nuclide j, leading to formation of nuclide i

λ_i = radioactive decay constant of nuclide i

ϕ = neutron flux, position and energy averaged,

f_{ik} = Fraction of neutron absorption by nuclide k, leading to the formation of nuclide i.

σ_k = average neutron absorption cross-section of nuclide k,

r_i = continuous removal rate of nuclide i, from the system,

c_i = continuous feed rate of nuclide i,

F_i = production rate of nuclide i directly from fission,

$\sum_j^M l_{ij}\,\lambda_j N_j$ = production of species i as a result of the decay of all the nuclides present,

$\phi \sum_{k=1}^{M} f_{ik}\,\sigma_k N_k$ = production of species i as a result of neutron capture by all nuclides present,

$\lambda_i N_i$ = loss of nuclide i through its own decay,

$\phi\sigma_{\,i} N_i$ = loss of nuclide i as a result of neutron capture,

$F_i = Y_i \sum_j^i \phi$ = production rate of nuclide i, directly from fission, and

Y_i = fission yield of nuclide i.

There are a number of detectors in the core which measures the degree of depletion of the fuel. In addition to that, they also provide in-core physics data such as assembly power, maximum power, assembly burnup, boron fraction etc. from various fuel assemblies which is then used to plot flux maps. Assuming that they are 100% efficient, and that the amount of thermal power produced by each assembly depends on its fuel and poison content as well as its location with respect to the core, the power produced by any assembly j is thus defined by [Duderstadt, *et al.*, 2010]:

$$P_j = \int_{V_j} q(r)dV = E_{\mathrm{f}} \sum_{g=1}^{G} \overline{\sum fgj}\,1\overline{\phi_{gj}} V_{\mathrm{j}}, \tag{3.4}$$

where

P_j = power produced by assembly j,

$q(r)$ = power density (W/cm^3),

E_{f} = energy per fission,

$\overline{\sum_{fgj}}\,1$ = average (group) macroscopic fission cross-section,

$\bar{\phi}_{gj}$ = average flux by group and

V_j = volume of assembly j

The average power per assembly is given by [Lamarsh, 2002]:

$$\bar{P} = \frac{P}{N} \tag{3.5}$$

$$\bar{P} = \frac{E_f \sum_{j=1}^{N} \overline{\Sigma f_{gj}} \overline{\phi_{gj}} V}{N}, \tag{3.6}$$

N is the number of fuel assemblies in the core, and in the case of Koeberg $N = 157$.

Each fuel assembly is 17×17 array consisting of:

- 264 fuel rods,
- 24 guide thimbles and.
- 1 instrumentation tube.

The fuel rods are in turn composed of fuel pellets which contain enriched uranium dioxide (UO_2) stacked in cold pressed cladding materials which may either be Zircaloy as is the case with AFA-3G or Zirlo as is the case with (374RFA) Westinghouse Fuel. There are two types of zirconium alloys (zircaloys) commonly used as cladding material of nuclear fuels, zircaloy-2 and zircaloy-4.

Each of these materials is characterised by unique physical properties such as corrosion resistance, compressive and tensile strength. The choice of the alloys has to meet the criticality as well as material strength requirements of the cladding material. The distribution of fuel assemblies in the Koeberg reactor is as per Table 3.1, and the chemical compositions of cladding materials referred to above are summarised in Table 3.2 [Chochran, *et al.*, 1999]. Therefore, knowing the thermal power to which each fuel assembly has been exposed and the duration of exposure, provides valuable information about the burnup of the fuel assembly which is an important factor in deciding whether the fuel assemblies have been depleted or whether they still need to be put back in the core for another irradiation cycle. The quantitative indication of whether the fuel assemblies have been depleted or not is based on the concentration of isotopes that are known as *burnup markers*, which consist of ^{134}Cs, ^{137}Cs, ^{154}Eu and ^{95}Zr.

Experimental analysis conducted by Tsao [Tsao, *et al.*, 1993] and Caruso [Caruso, *et al.*, 2006] using destructive and non-destructive gamma spectroscopic measurement of activities of ^{134}Cs, ^{137}Cs, ^{154}Eu and ^{95}Zr showed that $^{134}Cs/^{137}Cs$ and $^{134}Cs/^{154}Eu$ *changed*

as burnup of each fuel assembly changed and that these ratios were a function of the *location of the fuel assembly in the core and also of the location of the fuel pin in the fuel rod*. The study further indicated that, $^{134}Cs/^{137}Cs$ is only accurate for burnups less than 50 GWD/t [Tsao, *et al*., 1993] and as the burnup increases beyond 50 GWD/t, the $^{134}Cs/^{154}Eu$ becomes much more reliable [Caruso, *et al*., 2006].

Table 3.1: Distribution of fuel assemblies in the core

Core region	**Number of fuel assemblies**	**Mass of Uranium (Tons)**
1	53	24.46
2	52	24
3	52	24
Total	**157**	**72.46**

Table 3.2: Chemical Composition of cladding material

Element	**Thermal Neutron Absorption Cross-sections (Barns)**	**Zircaloy-2 (wt%)**	**Zircaloy-4 (wt%)**	**Zirlo (wt%)**
Tin (Sn)	0.63	1.20-1.70	1.20-1.70	1.0
Iron (Fe)	2.6	0.07-0.20	0.18-0.24	0.2
Chromium (Cr)	3.1	0.05-0.15	0.07-0.13	N/A
Nickel (Ni)	4.8	0.03-0.08	0.007 (max)	N/A
Fe+Cr+Ni		0.18-0.38	0.28-0.37	N/A
Niobium (Nb)	1.10	N/A	N/A	1
Zirconium (Zr)	0.18	The balance	The balance	The balance

Equation **(**3.6**)** also provides valuable information on the amount of decay heat and the level of radioactivity released per fuel assembly at the end of the fuel cycle. It has also been confirmed that when decay heat (Watts) is plotted as a function of decay period, the largest contributor in decay heat of all isotopes in the core will be fission products, followed by actinides and finally light elements. However, if the same plot is made against burnup, (i.e. Watts versus burnup) the largest contributor will be actinides followed by fission products.

Before the fuel assemblies are transferred from the reactor core into the spent fuel pool, a decay heat load calculation is performed to determine whether the total amount of decay heat released from all spent fuel assemblies in the core is within the acceptable range of 10-12 MW.

This takes into consideration the number of fuel assemblies in the spent fuel pool and their residual decay heat which in past outages has averaged to 1.4 kW per fuel assembly. Then, in accordance with the design specification of Castor X/28, the fuel assemblies will be stored in the spent fuel pool for 10 years before being transferred into the casks. The casks will then be shipped to the Interim Spent Fuel Storage Facility (ISFSF). Depending on the National Spent Fuel Management Policy, they might then be shipped to Long Term Storage or Spent Fuel Reprocessing Facility.

The reload pattern is governed by the optimal balance between production (economic) and safety related factors, which includes the physics need to prevent or reduce neutron escape and to keep the neutron flux map as flat as possible. As a result, there are many different ways in which the core is loaded, which can be either IN-OUT, OUT-IN or MIXED, loading pattern, depending on the position and distribution of fresh assemblies in core.

3.3.1 OUT-IN vz IN-OUT Core-loading Pattern

In the early days of many generation II PWR such as the Koeberg reactor when the enrichment was still about 1.8 wt%, many nuclear operators used the OUT-IN loading pattern where fresh fuel (1^{st} cycle) was loaded in the periphery of the core and the most burnt (cycle 3) in the centre [Duderstadt, *et al.*, 1976; Lamarsh, 2002] shown in Figure 3.1. It was found to be uneconomical to continue with this as the fission density was concentrated on the periphery of the core and a lot of neutrons escaped the core leading to low fission rate and consequently low efficiency. It was also found that the internal

structures, system and components (SSC) of the reactor pressure vessel (RPV) experienced a significantly high level of radiation damage because of interaction of high energy neutrons with the SSCs. As a result of this the SSCs that are closest to the fuel such as the *core barrel* and *thermal shield* often result in premature failure or aging due to radiation induced corrosion. Since every reactor is designed with the neutron dose limit in mind, the IAEA has compiled the flux and fluence design limits for some of the PWR in the market which shouldn't be exceeded. If the limits listed in Table 3.3 are exceeded, there is a risk of premature component failure (IAEA, 2009).

To prevent this, taking into consideration that the enrichment and burnup have since been increased and will most likely reach the enrichment of 5% and the burnup of 50 GWD/MTU, the loading pattern has since been changed to IN-OUT shown in Figure. 3.2.

One of the disadvantages of these two strategies is that they concentrate fission density in one region of the reactor vessel which results in an uneven neutron flux, with the highest neutron flux concentrating in the higher enrichment fuel and the lowest flux in the depleted fuel or low enrichment fuel. This strategy, makes it mandatory that the vessel must be divided into three regions and every fuel assembly must at least be in the core for three cycles (one cycle being approximately 18 months), spending one cycle in each region.

Given that there are three burnup groups or regions in the core, in the IN-OUT loading pattern the region with the highest power density is in the centre, the second lowest in the middle and the region with the lowest power being in the periphery. Hence, in line with the IN-OUT principle, the fresh fuel batch (1^{st} cycle batch) is loaded in the centre of the core while the most burnt (3^{rd} cycle) batch is loaded in the periphery. The second cycle batch will be halfway between batches 1 and 3 and will advance to take the position of batch 3 when it is finally unloaded. One of the most important benefits of this strategy is that it minimizes the escape of neutrons which are needed in the fuel burnup process and it is also less damaging to the reactor pressure vessel [Was, 2007].

Table 3.3: Design neutron flux/fluence limit for PWRs

Reactor type	Flux	Lifetime fluence[8]
	($n.m^{-2}.s^{-1}$) (E>1 MeV)	(n/m^2) (E>1 MeV)
VVER-440 core weld	$1.2x10^{15}$	$1.1x10^{24}$
VVER-440 maximum	$1.5x10^{15}$	$1.6x10^{24}$
VVER-1000	$3\text{-}4x10^{14}$	$3.7x10^{23}$
PWR(W)	$4x10^{14}$	$4x10^{23}$
PWR	$1.2x10^{14}$	$1.2x10^{23}$

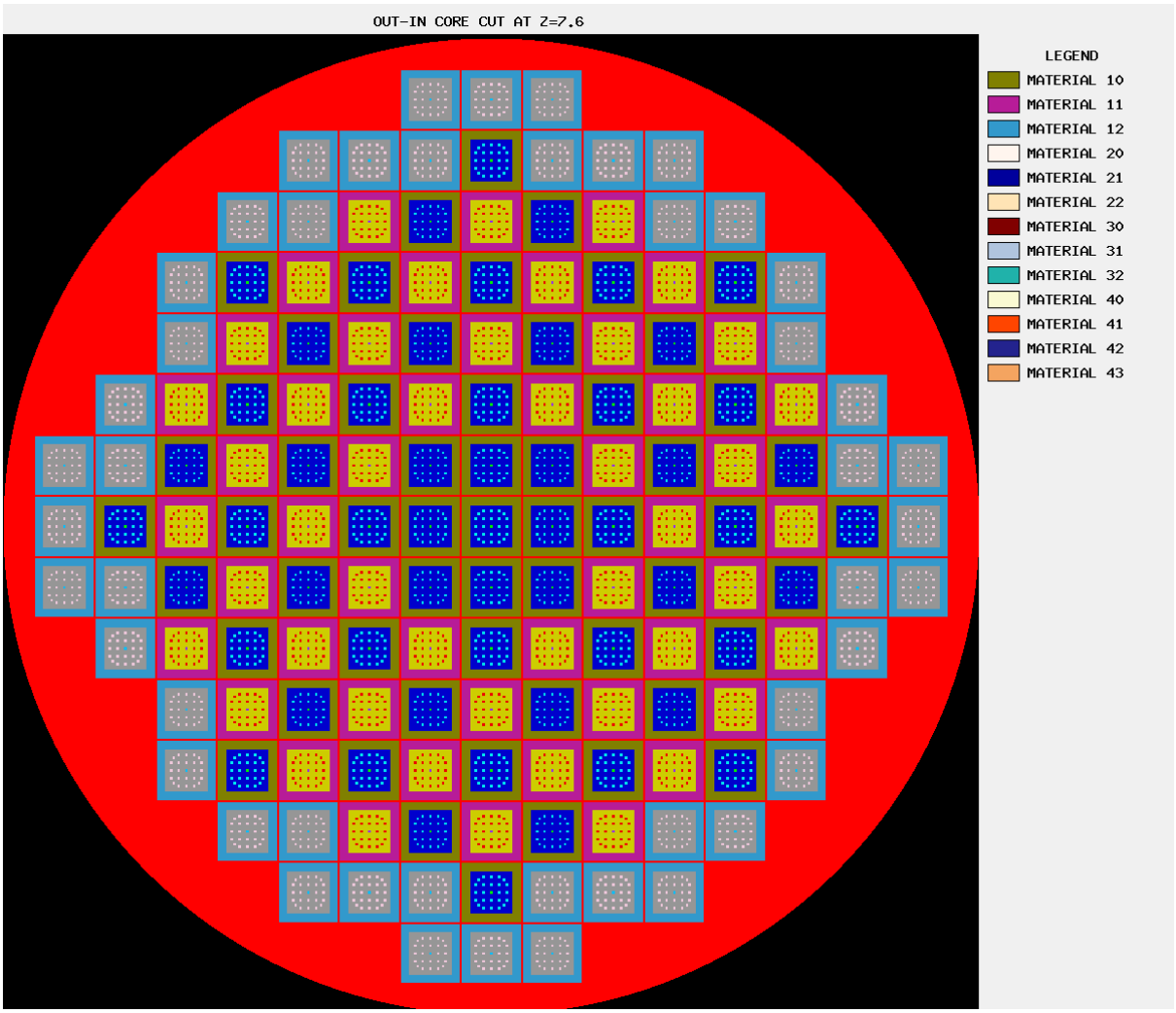

Figure 3.1: OUT-IN Fuel loading pattern[9]

[8] Design lifetime for VVERs is 30-40 calendar years and PWRs operate for 32 EFPY

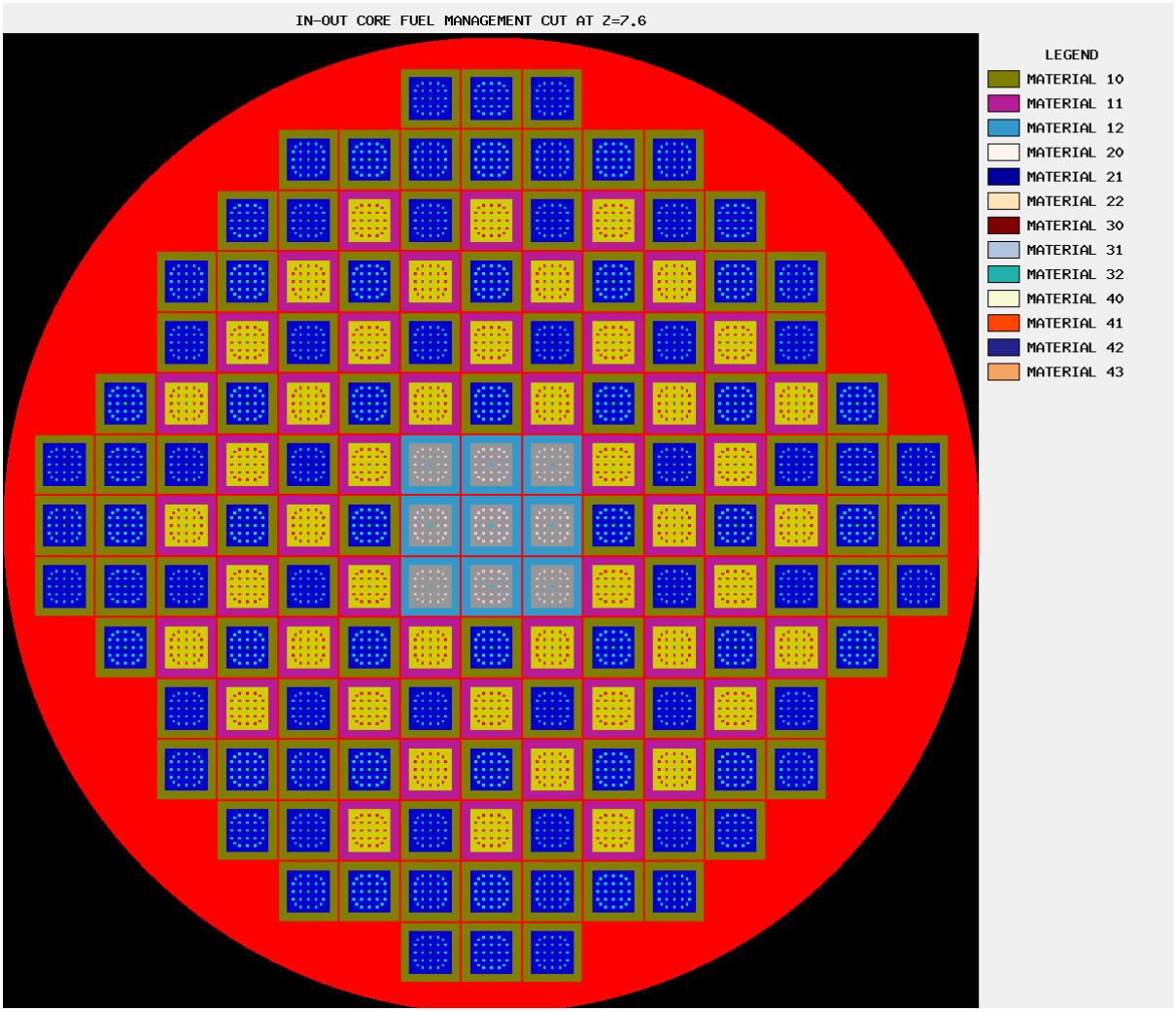

Figure 3.2: IN-OUT Fuel loading pattern

3.3.2 MIXED core-loading pattern

To minimize uneven distribution of the flux and to prevent material degradation of systems, structure and components (SSCs) of the vessel, a third loading pattern was developed called MIXED or SCATTER core loading pattern, where the fuel assemblies of different enrichment levels or burnups are distributed randomly throughout the reactor core as shown in Figure 3.3. According to Duderstadt although the fuel assemblies are distributed randomly throughout the core, it is still found that they do not experience the same burnup at it was anticipated [Duderstadt, *et al.*, 1976]. Those in the centre of the

[9] Material numbers 40, 41 and 42 in all three figures illustrating the reactor core, refer to fuel assemblies with 1.8, 2.4 and 3.1 wt% enrichment levels respectively.

core have a much higher burnup because of the high neutron flux compared to those on the periphery, even though to a lesser extent compared to IN-OUT and OUT-IN fuel loading patterns.

The *axial and radial profile* has been found to be common to all three loading patterns but much more pronounced in the IN-OUT and OUT-IN loading patterns. As a result of this, irrespective of location of the fuel assembly in the core and what loading pattern is chosen they will be exposed to uneven distribution of the flux both radially and axially, which will result in a phenomenon known as *End-Effect*. When the above simulations are executed, it also observed that they had yielded different k_{eff} values as indicated in Table 3.4.

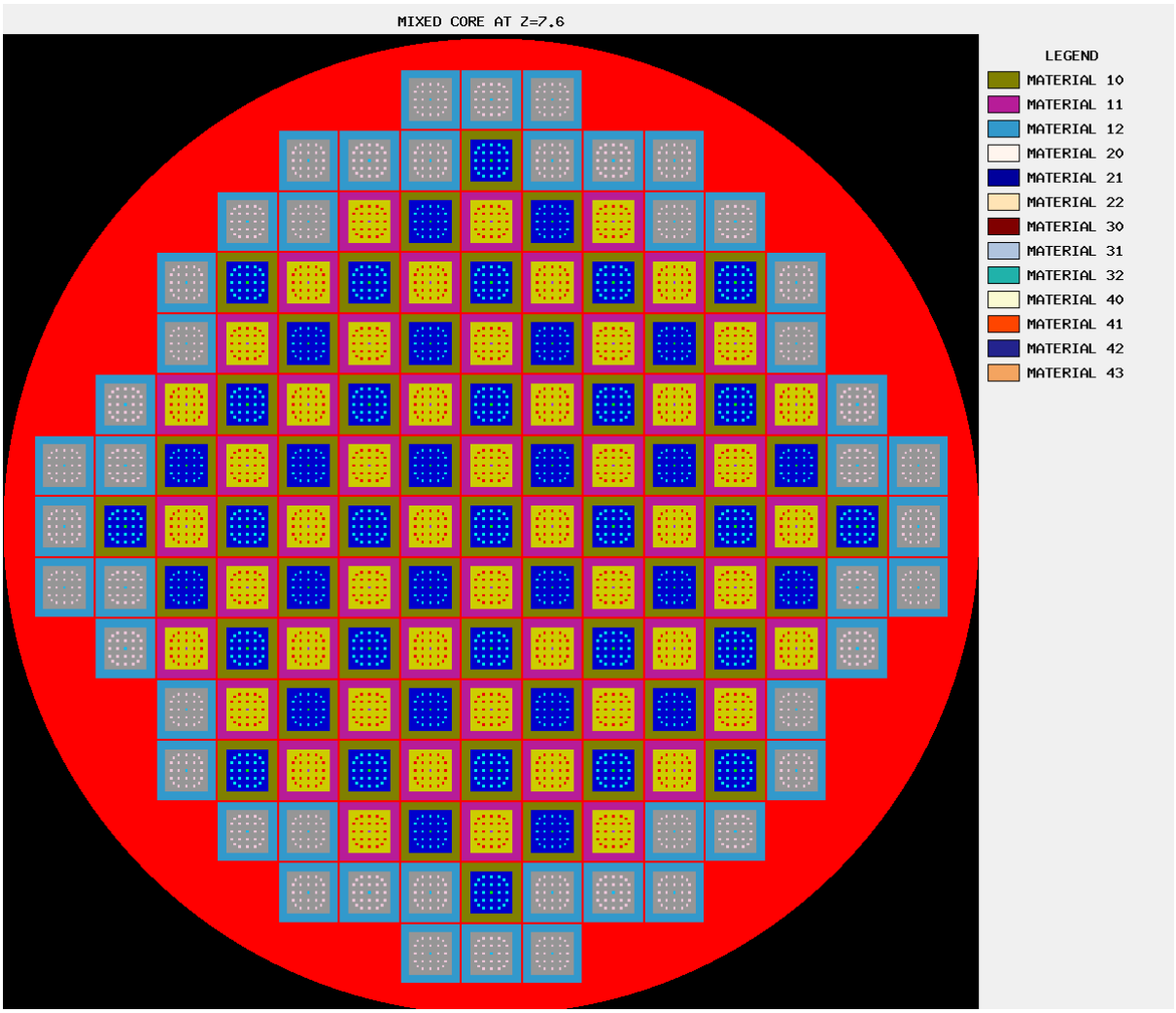

Figure 3.3: Mixed core loading pattern

Table:3.4: Impact of loading pattern on the k_{eff} of the system

	Core loading pattern		
	IN-OUT	OUT-IN	MIXED
k_{eff}	0.90190	0.91757	0.89133

3.3.3 Structure of the Fuel assembly

There are many designs of fuel assemblies but each cask design has to be according to the dimensions of the fuel assembly it is meant to store or transport, taking into account the initial enrichment level of the fuel and the burnup the fuel assembly has been exposed to. The casks in question are specifically designed for a fuel assembly which ranges from 3867.1 mm to 4063.37 mm in height and are of 17×17 array type.

Table 3.5: Main parameters of fuel assemblies under study

Parameter	**Westinghouse (374RFA)**	**Framatome (AFA-3G)**
Number of Fuel rods/assembly	264	264
Assembly Pitch (mm)	215	215
Array Size	17X17	17X17
Number of Instrumentation Tubes	1	1
Number of Guide Thimbles	24	24
Fuel rod pitch (mm)	12.60	12.60
Cladding outer diameter (mm)	9.50	9.50
Cladding inner diameter (mm)	8.36	8.36
Active height (mm)	3657.1	3657.6
Overall Assembly Height (mm)	4063.37	3867.1
Pellet Diameter (mm)	8.19	8.192
Pellet Height (mm)	13.46	13.46
Pellet density (g/cm^3)	10.96	10.96

The details of the fuel assemblies under investigation are sourced from two different manufactures; Westinghouse (USA) and Areva (France) and are summarised in Table 3.5. The primary criterion for the selection of the material out of which the fuel assembly is made is that it should be able to withstand the harsh environment to which it will be exposed. They must therefore have very good resistance to high radiation and high temperature.

3.3.3.1 Fuel assembly lattice

The nuclear fuel assembly under study is a 17×17 array type with dimensions of 200 mm × 200 mm × 3657.6 mm[10] made up of 24 guide thimbles, 1 instrumentation tube and 264 fuel rods indicated in Figure 3.4.

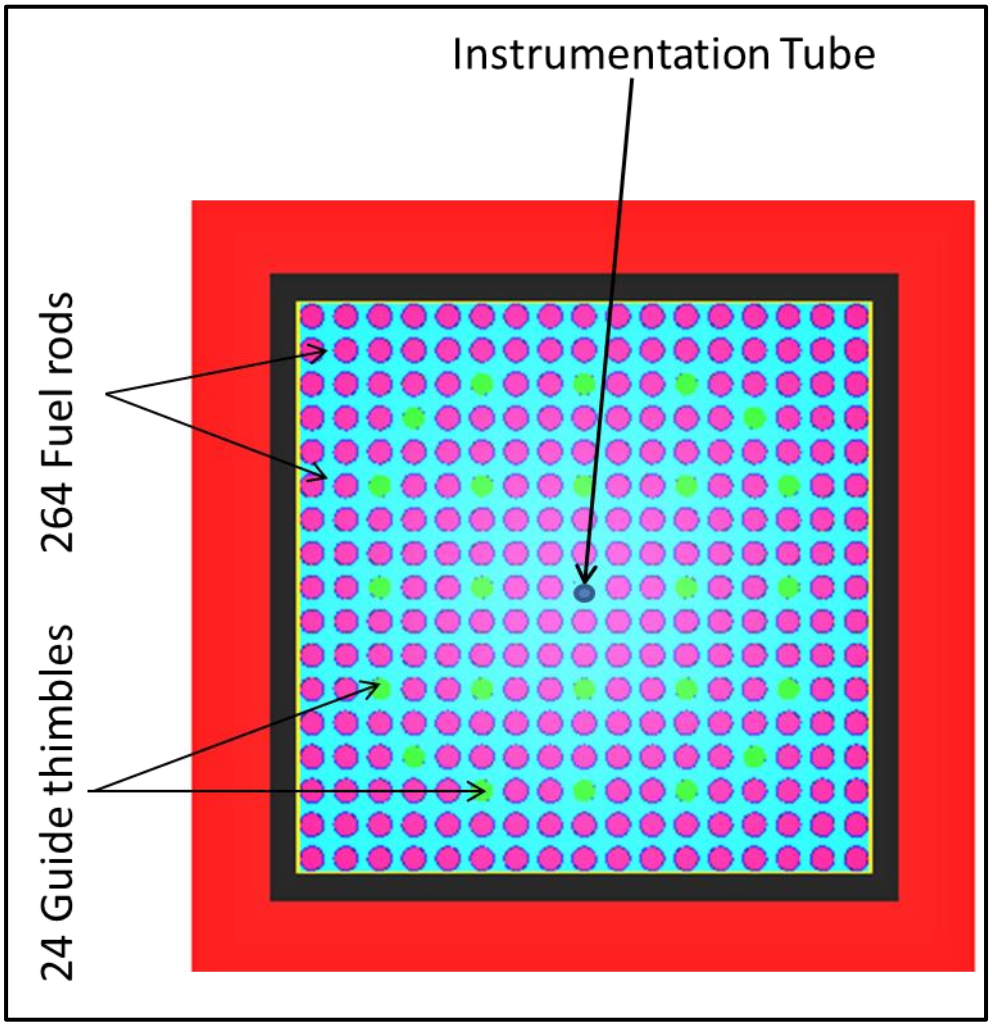

Figure 3.4: cross-section view of the 17 × 17 fuel assembly as modelled in this study [Leotlela, *et al.*, 2015].

[10] The total length of a fuel rod is 386.71 cm and the active fuel length is 365.76 cm.

The fuel rods are in turn made up of fuel pellets which are 13.46 mm in length as shown in Figure. 3.5.

Given that the active fuel length of the rod is 3657.6 mm, there are 3657.6 mm/13.46 mm = 271.73 fuel pellets stacked inside the fuel rod. Furthermore, since there are 264 fuel rods per fuel assembly each containing 271.73 fuel pellets, the number of fuel pellets per fuel assembly = 264 fuel rods per fuel assembly x 271.73 fuel pellets per fuel rod = 71 738 fuel pellets per fuel assembly.

Not all fuel pellets mentioned above have the same enrichment levels. In practice, fuel pellets from 50 cm upwards and those occupying the bottom 50 cm of the fuel assembly have lower enrichment than the middle ones to prevent the *End-Effect* which will be discussed in detail in section 4.3.3. However, in this study all fuel assemblies are modelled as containing uniform enrichment as it is conservative. Furthermore, because of the amount of material density of oxygen in the fuel and moderator, the calculation has to take it into account as well. Thus the fraction of U in UO_2 can be calculated from

$$\mathrm{U\%} = \frac{\mathrm{M_U}}{\mathrm{M_U + 2 \times M_O}} \times 100\%. \qquad 3.7$$

where,

M_U = Relative atomic mass of uranium=238.02891 amu[11]

M_O = Relative atomic mass of oxygen = 15.9994 amu

Thus, the fraction of U in UO_2 $\frac{238.02891}{238.2891+2(15.9994)} \times 100\%$ = 88.14981% of the fuel mass and O = 11.85019%.

Since the average mass of the *fuel* in the fuel assembly = 465 kg, therefore the mass of U in UO_2 may be calculated as follows:

$$\begin{aligned} M_U &= \%U_{\text{in } UO_2} \times M_{\text{total fuel mass}} \\ M_U &= 88.14981\% \times 465 \text{ kg} \\ \Rightarrow M_U &= 409.8966165 \text{ kg} \end{aligned} \qquad 3.8$$

[11] Atomic mass unit

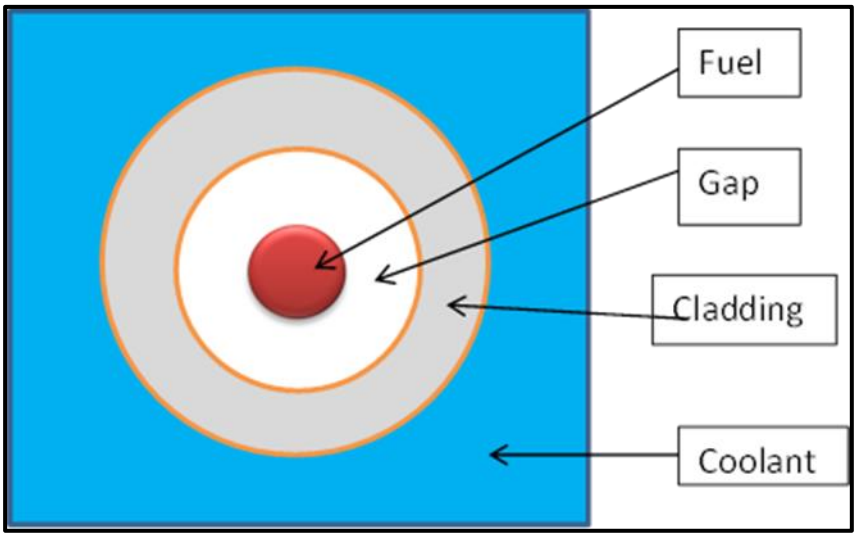

Figure 3.5: Fuel assembly lattice (Present study).

Thus, the amount of ^{235}U in the fuel assembly required to generate power for the entire fuel cycle in a fuel that is 3.5% enriched is $3.5\% \times 409.8966\ \text{kg} = 14.34638\ \text{kg}$. Given that at any one time there are 157 fuel assemblies in the core, thus the total mass of ^{235}U in the core $=14.34638 \times 157 = 2252.382\ kg$, which is a very small amount of fuel compared to what fossil fuel i.e. coal power stations burn for the same duration. In an unevenly enriched fuel assembly the largest part of the fuel is in the middle of the fuel assembly.

3.3.4 Structure of Castor X/28F Spent fuel Cask

Castor 28/X F is a high capacity dry spent fuel cask manufactured by Gesselschaft für Nuklear-Behalter mBH (GNB) in Germany. It is designed to for 28 fuel assemblies which have had a 10 year decay period (as indicated by 28 and the suffix X which is Roman numeral for 10) to allow for the reactivity and decay heat to decay to a level acceptable to be stored in the casks. Before then, the fuel assemblies are kept in a spent fuel pool filled with water. Because of the stringent nuclear safety requirements the design of the cask has to comply with, the selection of material from which they are manufactured must meet all the design requirements listed in section 1.2. The material compositions from which the cask is made are tabulated in APPENDIX 1. Some materials will only serve the one purpose while others will serve more than one. For example, cast iron will provide both mechanical strength and because of the carbon (graphite) content it will also contribute in nuclear criticality safety. Iron and nickel on the other hand will by far and large be for

structural and mechanical safety purposes. The borated steel is specifically designed to increase the neutron absorption capability by increasing the fraction of natural boron in the borated steel composition to 0.9% of the entire material composition of borated steel .The polyethylene rods are by far and large responsible for neutron shielding and will be studied in great detail in sections 3.3.4.2 and 7.7.1.4. Therefore, the general design criteria of the spent fuel cask are that it should be able to meet all licensing requirements of its own (i.e. exporting) country, before making an attempt to license it in the importing country. The importing country must still perform its own safety analysis to the satisfaction of the nuclear regulator [IAEA, 2006; IAEA, 2007].

3.3.4.1 Arrangement of fuel assemblies in the cask

The 28 fuel assemblies (FAs) inside the CASTOR X/28 cask are arranged in such a manner that 12 fuels assemblies form the inner source surrounded by stainless steel, the air-gap and the outer source consisting of 16 fuel FAs evenly distributed around the circumference of the cask as indicated in Figure. 3.6.

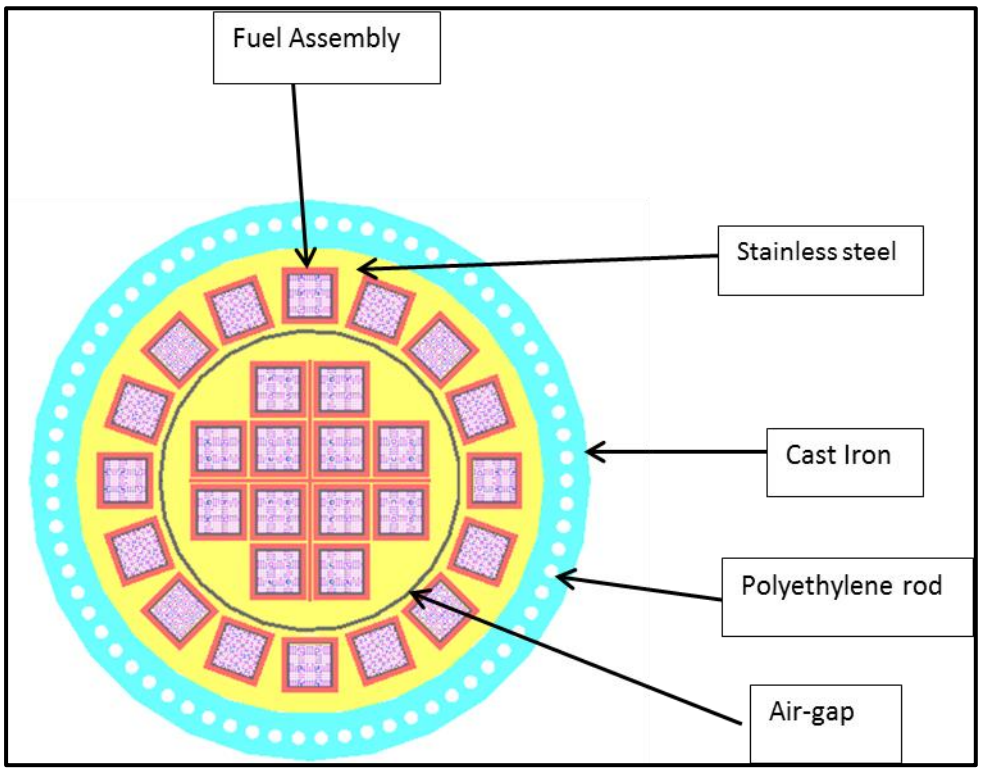

Figure 3.6 : Cross-Section of a CASTOR X/28 spent fuel cask as modelled in this study (Present Study)

If 360° of the circumference of the cask is divided by 16 FAs the result is the angle between two adjacent FAs in degrees, which is equal to:

$$\theta° = \frac{360°}{16\,fuel\,assemblies} = 22.5°/fuel\ assembly, \tag{3.9}$$

and

$$\theta = \frac{22.5°X\pi}{180°} = 0.393\ Radians/fuel\ assembly \tag{3.10}$$

To understand the location of the each fuel assembly on the outer source or periphery of the cask, one has to draw a triangle with the x-axis drawn from the centre of the cask (C) to the middle of fuel assembly (B) at 45 degrees to the cask. From this point draw the y-axis by drawing another line to the middle of the fuel assembly (A) just above it. If points C and A are joined, one will obtain the triangle shown in Figure 3.7 where the line $\overline{AC}$ is the hypotenuse (R). From basic geometry, the relationship of the distances *R* between C and A and the distance *X* between C and B and the distance Y between A and B is given by Eqn (3.11). The actual lengths of the X and Y vectors which are the coordinates of each of the 16 FAs on the circumference of the cask are calculated from Eqn (3.11) given that *R* = 94.9 cm.

$$\begin{matrix} X = R\cos\theta \\ Y = R\sin\theta \end{matrix}, \quad \text{where } 0 < \theta < 2\pi \tag{3.11}$$

The *z*-plane of fuel assemblies formed a tangent of circle described by radius *R* = 94.9 cm. In order to have all outer source fuel assemblies at an angle indicated in Figure 3.6, the azimuthal angle β in SCALE, was varied from -45° to 45° depending on the coordinates obtained. Thus, the co-ordinates of each of the 16 outer fuel assemblies are given in APPENDIX 2.

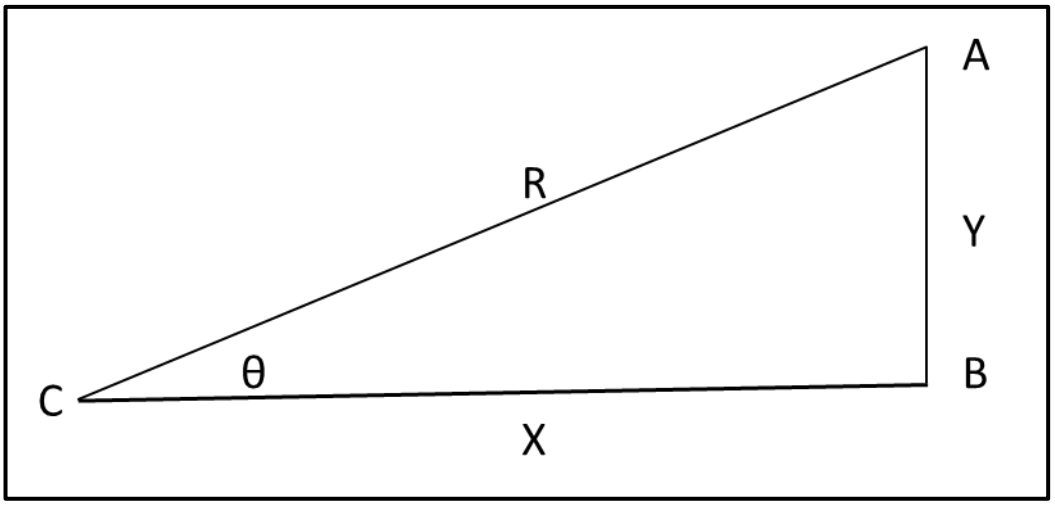

Figure 3.7: Co-ordinates of the fuel assemblies in the CASTOR X/28 cask (Present study)

3.3.4.2 Polyethylene rods

There are 70 polyethylene rods that are of 7 cm in diameter and 370 cm in length placed in a 141.7 cm radius from the centre of the cask. The rationale for the inclusion of the polyethylene in the design is to increase the effectiveness of neutron shielding. This is because polyethylene has a very high concentration of carbon and hydrogen which are light elements and are known to be exceptionally good in scattering material. The calculation of the location of the polyethylene rods was based on the fact that the distance R, from the centre of the cask to that of the polyethylene rod is 141.7 cm(i.e. R = 141.7 cm) and the angular separation between the polyethylene rods is calculated by dividing 360° by the number of polyethylene rods as follows:

$$\theta = \frac{360^{\circ}}{70} = 5.1429^{\circ} \quad . \tag{3.12}$$

The lengths of X and Y are calculated from Eqn (3.11) taking into account that R = 141.7 cm and θ is in radians [Hahn, 2007].

CHAPTER 4

4 STORAGE OF SPENT FUEL

4.1 Introduction

Spent fuel storage has been a subject of major concern since the advent of nuclear technology [Dowson, 1962]. The main concern is not only radiation exposure of members of the public but also due to the potential risk of inadvertent nuclear explosion if stored without due regard to potential coupling/interference between neutrons from one fuel assembly to another adjacent fuel assembly. Coupling is largely dependent on the separation gap between various rows of casks and generally on the type of the storage array selected and also on the enrichment levels of fuel assemblies. This was further raised by Mayne [Mayne, 1955] who indicated that if the spacing among different casks is not adequate and the enrichment is higher than the array allows, there could potentially be a criticality incident [Mayne, 1955]. Subsequently he developed a technique that estimated the level of criticality associated with a storage array. In this thesis, a storage array of 4 and 30 casks in different arrays will be investigated where only major actinides are taken into account.

4.2 Cask Storage Matrices

To assess the adequacy of the separation gap among adjacent casks, KENO-VI and STARBUCS modules of SCALE computer code were used for fresh fuel and spent fuel respectively. The purpose of this entire exercise was to obtain the most optimum storage configuration of spent fuel casks in a given storage room that will conserve the storage space and still not compromise nuclear safety, i.e. staying as far below the regulatory limit of the neutron multiplication factor as possible [Leotlela, *et al.*, 2012]. Since the dimensions of the cask storage building are: $(L \times B \times H)$ 60 m × 23.5 m × 8.97 m with a 48.5 cm thick concrete slab below ground surface, the centre of the cask was shifted to z = -180.2 cm. When the thickness of the slab is taken into account it is found that $+z_{slab}$ = -400 cm and $-z_{slab}$ = -448.5 [Leotlela, *et al.*, 2012].

Table 4.1: Coordinates of the four vertical casks in their storage building

D (cm)	100		150		200		250		300		350		400		450		500	
x-y co-ordinates	x	y	x	y	x	y	x	y	x	y	x	y	x	y	x	y	x	y
	-388	0	-438	0	-488	0	-538	0	-588	0	-638	0	-688	0	-738	0	-788	0
	0	0	0	0	0	0	0	0	0	0	0	0	0	0	0	0	0	0
	388	0	438	0	488	0	538	0	588	0	638	0	688	0	738	0	788	0
	776	0	876	0	976	0	1076	0	1176	0	1276	0	1376	0	1476	0	1576	0

Also, because the radius of the cask is 144.3 cm, to make a 100 cm gap between adjacent casks, a 100 cm was added to the radius resulting in the distances and their corresponding x-y co-ordinates are summarised in Table 4.1[Leotlela, *et al.*, 2012]. The project was divided into two main categories; fresh fuel and spent fuel, which was further divided into two subgroups; thirty casks and four casks.

The 30 casks were further subdivided into 2×15 and 3×10 arrays whereas the 4 casks were subdivided into 1×4 and 2×2 array [Leotlela, *et al.*, 2012]. The four and thirty casks will be discussed in detail in section 4.2.2 and 4.2.3 respectively.

4.2.1 'Fresh Fuel' Approach

It is generally acceptable to analyse spent fuel as '*fresh fuel*' because it yields the most conservative results, which envelop those obtained when burnup credit is taken into account (EPRI, 2008; Gauld, 2003; Wagner *et al.*, 2003). Fresh fuel is generally highly reactive owing to the absence of nuclides with parasitic absorption [Parks *et al.*, 2006]. Such fuel assemblies are treated differently from those which have already been used, or spent fuel as they are generally referred to.

Given that there are already four full casks in the low level waste and that even more may be acquired to ease the demand in the spent fuel pool, it is expected that there might be a need

for a larger storage space for spent fuel casks in the near future. It is expected that eventually about 30 casks will have to be acquired for all the spent fuel in the spent fuel pool; hence, it is imperative that a suitable cask storage array be found that will primarily store as many casks as possible without compromising nuclear criticality safety in any way. It is important to note that, as recommended by US Nuclear Regulatory Commission in NUREG-1536 (USNRC, 2010), the casks are partially filled with water to enable them to reach higher k_{eff} values.

4.2.2 Four Casks

In this section, the study investigated the most suitable and optimum storage array that can be used to store four casks without wasting storage space, while also complying with regulatory requirements. The two storage arrays that were investigated were the linear array and the square array.

4.2.2.1 Vertical Linear Storage Array

In the first scenario, the four casks under study were arranged in a 1×4 linear array where all the casks were at the same height above ground level (refer to Figure 4.1). In the second scenario, the height of the alternate casks in the traditional linear matrix was lifted by 20 centimetres to ensure that the reactive ends of the casks, as a result of the end effect, were misaligned, as shown in Figure 4.2.

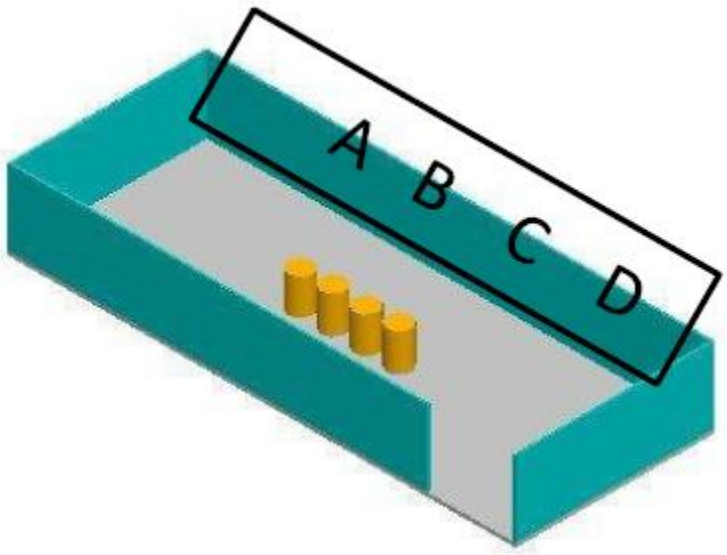

Figure 4.1: Isometric view of cask storage room with four casks in a traditional vertical array

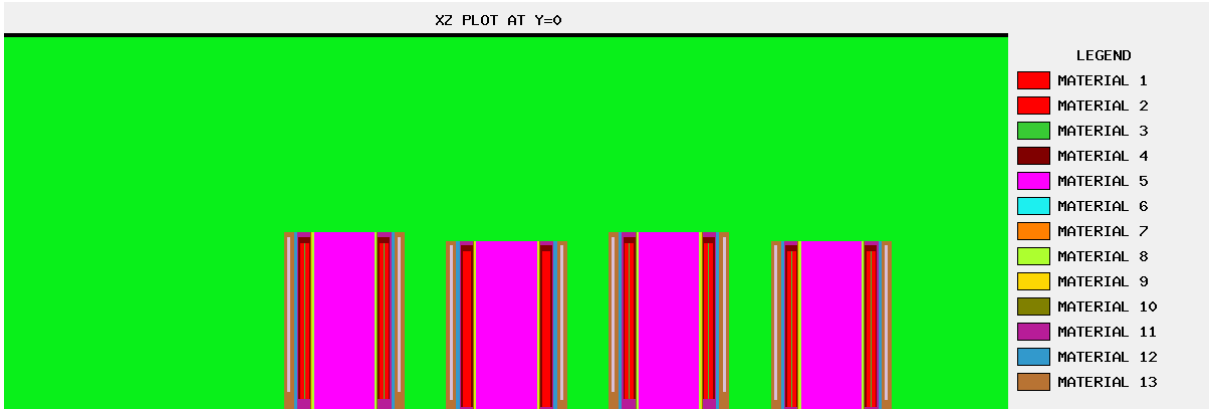

Figure 4.2: Sectional view of a 1X4 staggered linear matrix

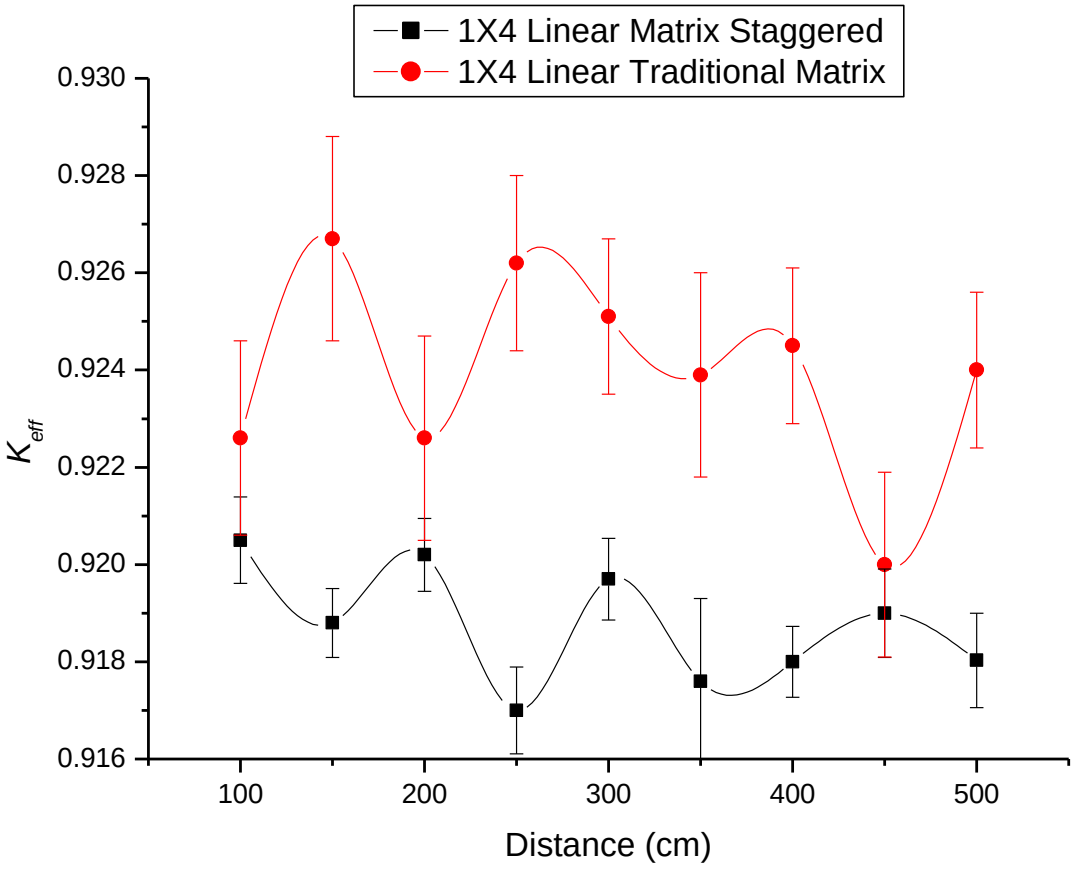

Figure 4.3: Comparison of traditional and staggered 1X4 linear storage matrix (Present study).

The two configurations were compared on the basis of the k_{eff} of the system as shown in Figure 4.3. It is observed that the *staggered/misaligned* storage array results in lower k_{eff} compared to the *traditional* 1X4 linear matrix. This is due to the fact that the reactive top and

bottom ends of adjacent casks are misaligned and when the casks stand next to each other the reactive end of one cask fits in the non-reactive middle part of its adjacent partner. As a result, the misaligned casks result in a lower fission rate than in traditional 1 X 4 array, where the reactive ends are aligned. The results of this analysis are consistent with those reported by the *Transportation issues and resolutions – compilation of laboratory work packages* [McConnel, 2012]. Using the analogy of misalignment of fuel assemblies in the cask, McConnel believes that the behaviour of the graphs may be ascribed to the fact that spacers are used inside the casks to keep the fuel assemblies properly aligned. If the spacers fail, it is possible that the fuel assemblies might shift and end up in the region of the cask where there is no neutron absorber to separate them, thus becoming misaligned. This would result in an increase in k_{eff}, as a result of an increase in "communication" between adjacent fuel assemblies [McConnel, 2012]. Similarly, looking at the cross-section in Figure 5.13, it is noted that there are gaps between the fuel assemblies on the periphery of the cask. It is therefore possible that in some configurations two adjacent casks may be able to "communicate" owing to the alignment of the regions that do not have neutron absorbers. This consequently results in higher k_{eff}, although those configurations where the alignment is such that neutrons are adequately absorbed between fuel assemblies might result in lower k_{eff}, which is the reason why there is this sine wavelike graph in Figure 4.5.

4.2.2.2 Horizontal Linear Storage Array

Subsequent to the analysis of the vertical casks, the study proceeded to analyse the horizontal casks with a view to determining what the effect of storing casks in the horizontal position would be on the k_{eff}. The z-axes of the casks were altered by 90°. The coordinates and the locations of four casks in the cask storage building are summarised in Table 4.2 and Figure 4.4 respectively. The results were compared with those of the traditional 1 X 4 matrix and are indicated in Figure 4.5. It is observed from the results that vertical casks are more reactive when they are farther apart than their horizontal counterparts, and vice versa. This may be due to backscattering from the walls and the fact that neutrons from the vertical casks can reach much higher areas of the wall than those from horizontal casks.

Table 4.2: Coordinates of the four casks in a horizontal position

1X4 Horizontal Positions																		
D (cm)	100		150		200		250		300		350		400		450		500	
x-y co-ordinates	x	y	x	y	x	y	x	y	x	y	x	y	x	y	x	y	x	y
	-388	0	-438	0	-488	0	-538	0	-588	0	-638	0	-688	0	-738	0	-788	0
	0	0	0	0	0	0	0	0	0	0	0	0	0	0	0	0	0	0
	388	0	438	0	488	0	538	0	588	0	638	0	688	0	738	0	788	0
	776	0	826	0	876	0	926	0	976	0	1026	0	1076	0	1126	0	1176	0

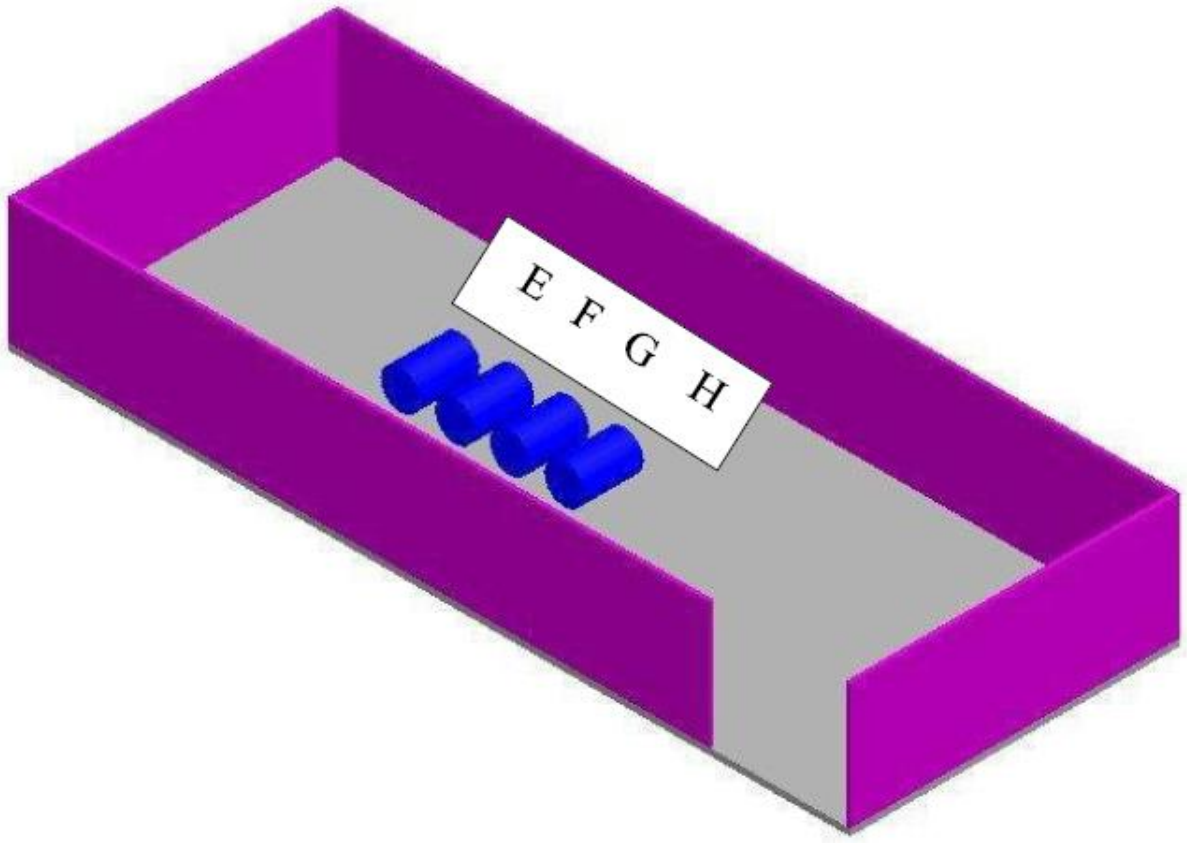

Figure 4.4: Top view of casks in a horizontal orientation

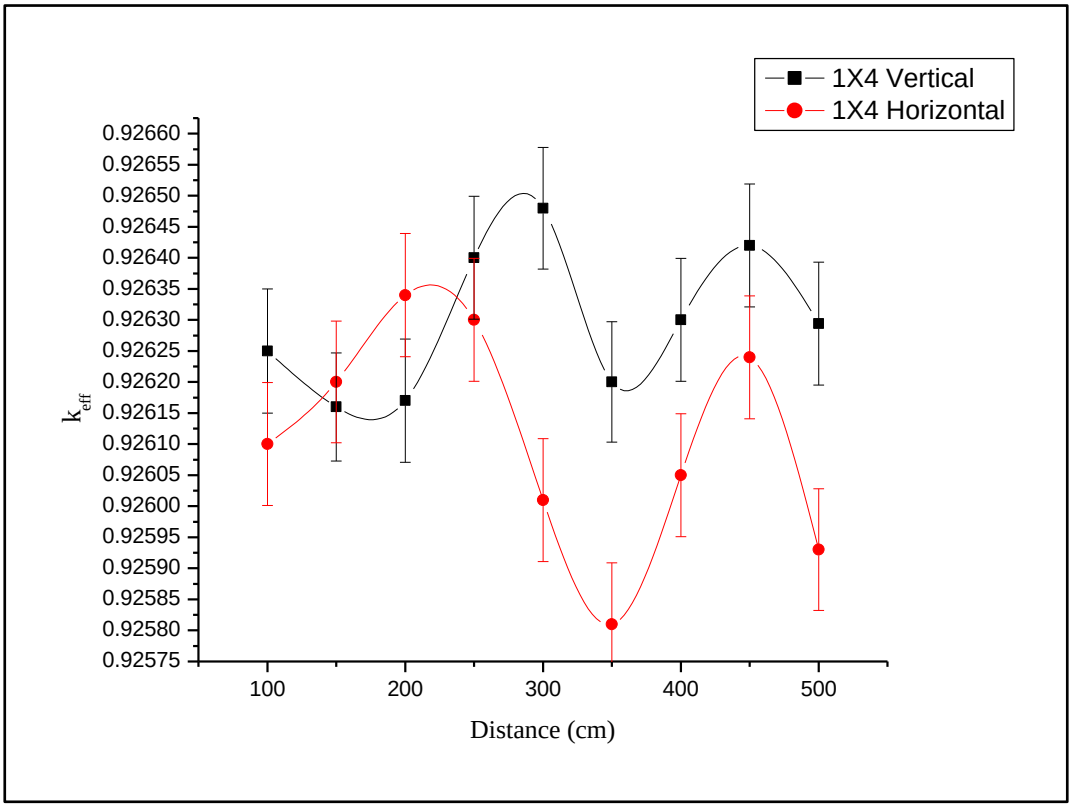

Figure 4.5: Comparison of the k_{eff} of casks in a vertical and a horizontal position (Leotlela *et al.*, 2012)

Since the casks are partially filled with water, when they are placed horizontally there will be some fuel assemblies that will be above the water level, thus little or no moderation will take place. However, this is not the case with the vertical casks since as long as there is some water in the cask that covers a certain portion of the active region of the fuel assembly, all fuel assemblies will have the same region covered by water. As a result, there will be higher neutron density in the thermal region of the vertical cask than the horizontal cask. Consequently, the k_{eff} in the horizontal casks is lower than in the vertical casks.

4.2.2.3 Vertical Square Storage Array

The storage array was later changed to 2×2 square array, as indicated in Figure 4.6 to determine how the k_{eff} of this system compared to that of the 1×4 traditional linear array.

In the 2×2 square array, the gap between adjacent casks was increased by 50 cm in every subsequent run. The k_{eff} was then compared to that of the traditional linear array (Leotlela *et*

al., 2012). The general trend indicated by the linear fit in Figure 4.8 suggests that there is a slight increase in the k_{eff} of the 2×2 array as the distance between adjacent casks increases, whereas there is a decrease in k_{eff} for the 1×4 array over the same distance. The difference in the two trends is due to the amount of shielding each cask provides for one another combined with backscattering. To understand the interference and the interaction of neutron flux from one source with another, it is better to have the above figure in 2D, as in Figure 4.7. It should be noted from Figure 4.7 that no single cask can take credit for shielding the others. In contrast, in the linear array the two casks between the outer casks are shielded from any external source by the outer two casks.

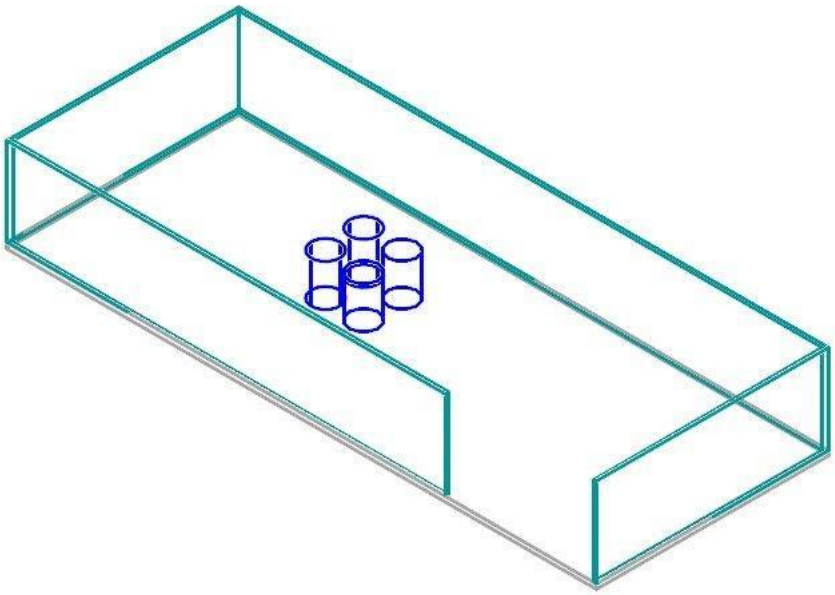

Figure 4.6: 2 X 2 square array in isometric view

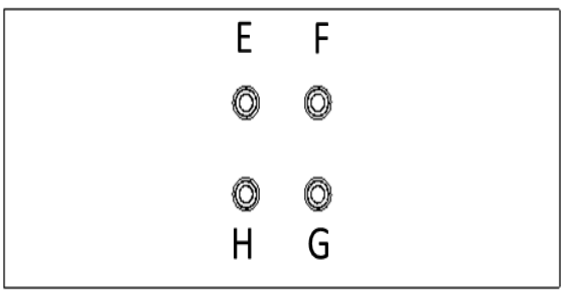

Figure 4.7: Top view of four casks in a **2 × 2** Matrix (Leotlela *et al.*, 2012)

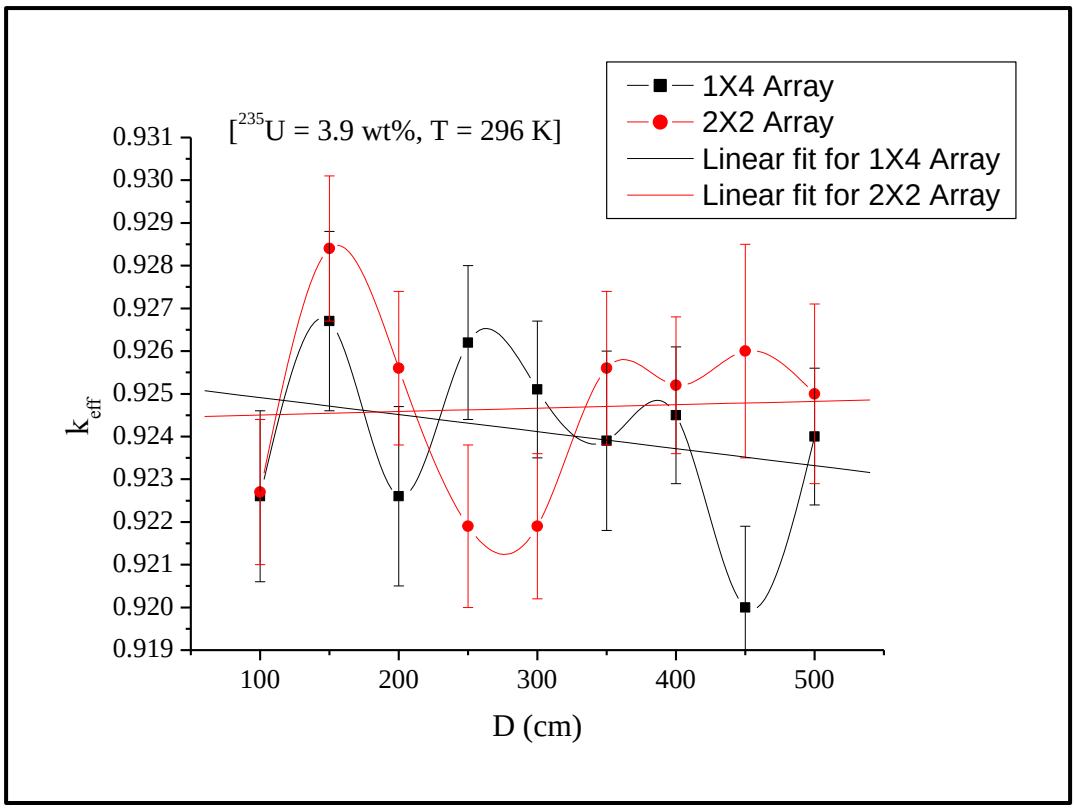

Figure 4.8: Comparison of reactivity between 1 × 4 array and 2 × 2 array (Leotlela *et al.*, 2012).

In addition, because of the different arrangement of the two arrays, the *Dancoff factor* of the two will differ (refer to Sect 4.3.1 for detail). As a result, the 1 × 4 array tends to experience a much more rapid decrease in k_{eff} with an increase in distance compared to the 2 × 2 array. Secondly, backscattering from the wall and other casks will tend to decrease the neutron energy to thermal range, thereby resulting in an increase in k_{eff} with an accompanying increase in the separation gap rather than a decrease, as is the case with a 2×2 array. It will also be noted that the casks in a 2×2 array are surrounded by air which has very low density and low attenuation coefficient compared to that of the cast iron which shields the inner two casks of the 1 × 4 array. Therefore, because of the difference in the density and attenuation coefficient, it is expected that the decrease in k_{eff} in a 1 × 4 array will be as rapid as that of a 2×2 array. For a detailed description of the effect of these factors the reader is referred to section 4.3.

4.2.3 Thirty Casks

Given that most generation II (GEN II) reactors have a lifespan of about 60 years, with an outage frequency of between 18 to 24 months, it is expected that an additional 30 casks will be needed. Thus, this calculation was based on the projected additional 30 casks that might be needed. The original plan was to model the storage of 33 casks. However, it became evident after a few runs that the dimensions of the storage room would not allow an adequate separation gap between adjacent casks. Consequently, this was abandoned and the project continued by basing all calculations on the 30 casks. Furthermore, because of the limitations of the size of the building, the distance between adjacent casks was changed along the y-axis only. Two different storage arrays were investigated, and various configurations of 2×15 and 3×10 were studied and compared on the basis of the neutron multiplication factor.

4.2.3.1 2X15 Array

In the 2×15 array analysis, two possible options were investigated: the traditional 2×15 array where all the casks in the adjacent rows were on the same x-coordinates as in Figure 4.9 [Leotlela *et al.*, 2012]. The distance between the rows in the two arrays were the same and only differed in terms of their spatial position. In the second 2×15 array, the x-coordinates of the cask in the two rows were misaligned as indicated in Figure 4.10. The results in Figure 4.11 indicate that the k_{eff} in the misaligned array is lower than in the traditional 2×15 array by an average Δk of 0.0050. Since the distance between the two rows was the same in both arrays, the difference in the k_{eff} may be ascribed to the change in the *Dancoff factor* that takes place when an array is changed.

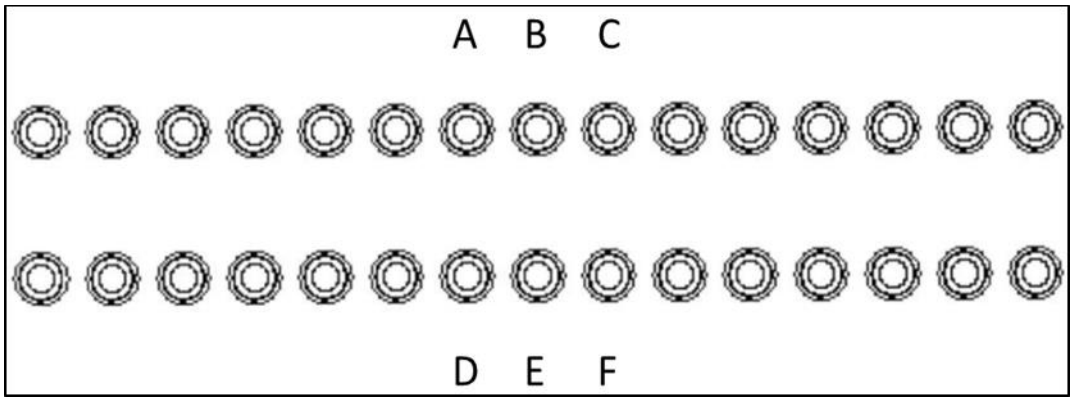

Figure 4.9: Top view of the traditional 2X15 storage matrix (Leotlela *et al.*, 2012)

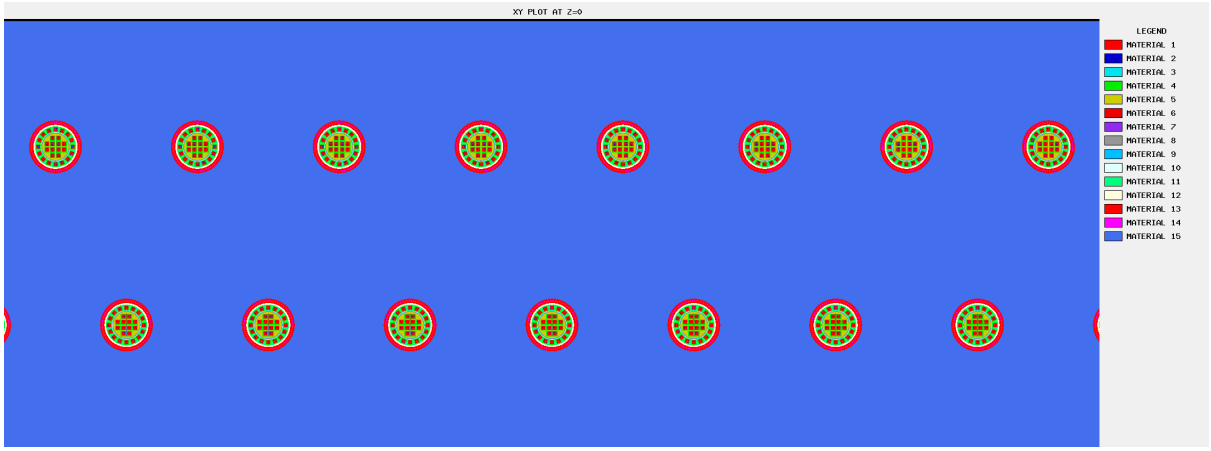

Figure 4.10: Misaligned 2 X 15 array

The end-effect consequently becomes less effective as the distance between the adjacent casks increases.

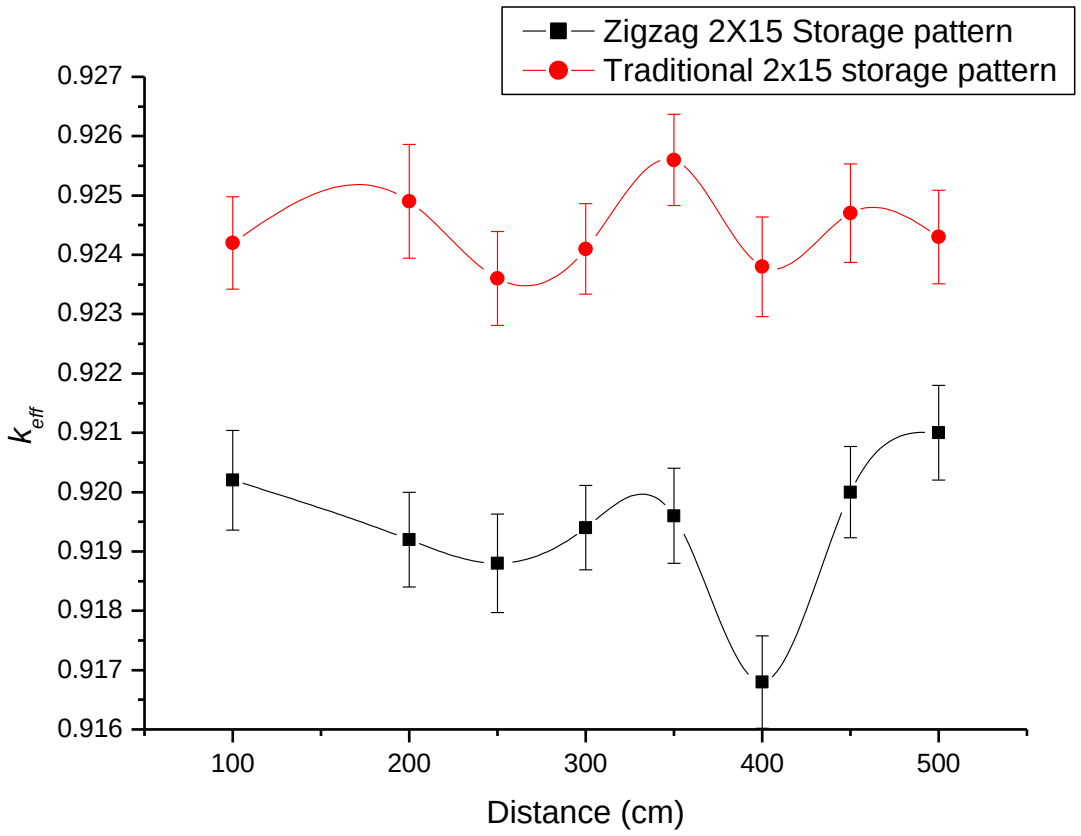

Figure 4.11: Traditional 2 X 15 vs misaligned 2 X 15 array (Present study)

4.2.3.2 3×10 Array

In the second part of the study of 30 casks, the impact of changing the orientation of the casks from vertical to horizontal was studied to determine the effect on the neutron multiplication factor. The basis for this was that water ingress affected the vertical and horizontal casks differently, particularly when the fuel assemblies had uniform enrichment. When there is water ingress in a horizontal cask, it is possible that some fuel assemblies may be above the water level while others may be submerged. However, regardless of the water level in the cask, in the horizontal cask the two highly reactive ends will be submerged in water at the same time, whereas in the vertical array the two vertical ends will be below the water level at different times.

This may potentially have a significant effect on the k_{eff} of the system, depending on the number of fuel assemblies covered with water, and ultimately on the storage capacity of the spent fuel storage facility.

4.2.3.2.1 Vertical Orientation

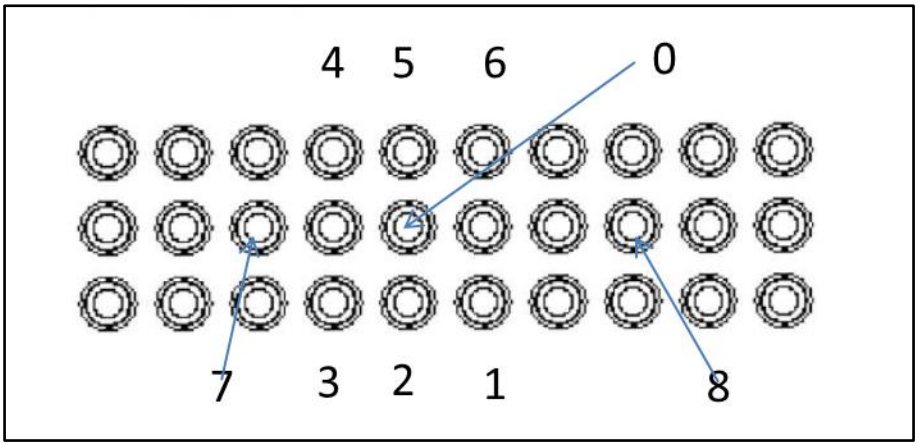

Figure 4.12: Traditional 3 X 10 storage array in vertical orientation

In the vertical orientation, two options were analysed; the first one was the *traditional* 3 X 10 array indicated in Figure 4.12, where all the casks in the three rows were positioned at the same level with respect to the ground surface.

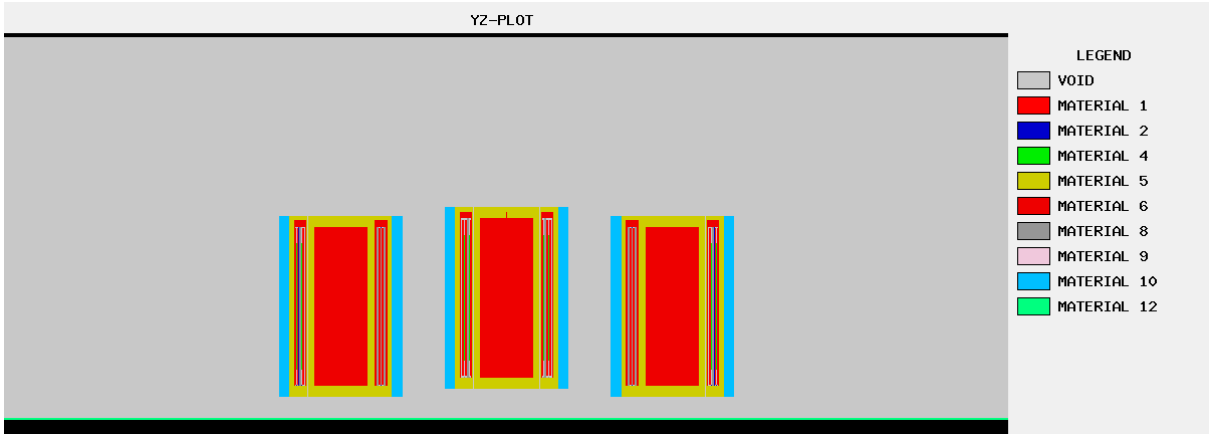

Figure 4.13: Misaligned 3 X 10 storage array with the middle row elevated by 20 cm.

The second option was a 3 X 10 array in which the casks in the middle row were elevated by 20 cm to ensure that the neutron flux peak due to the end-effect was misaligned as in Figure 4.13.

4.2.3.2.2 Horizontal Orientation

Following the insight obtained on the effect of elevating one of the adjacent casks on the k_{eff}, it was imperative to determine what the combined effect of changing the orientation of the vertical cask to horizontal and increasing the height of the middle row by 20 cm, as in Figure 4.14, would be on the k_{eff}. The results were subsequently compared to those of the traditional 3 X 10 array in a vertical orientation, as was shown in Figure 4.12.

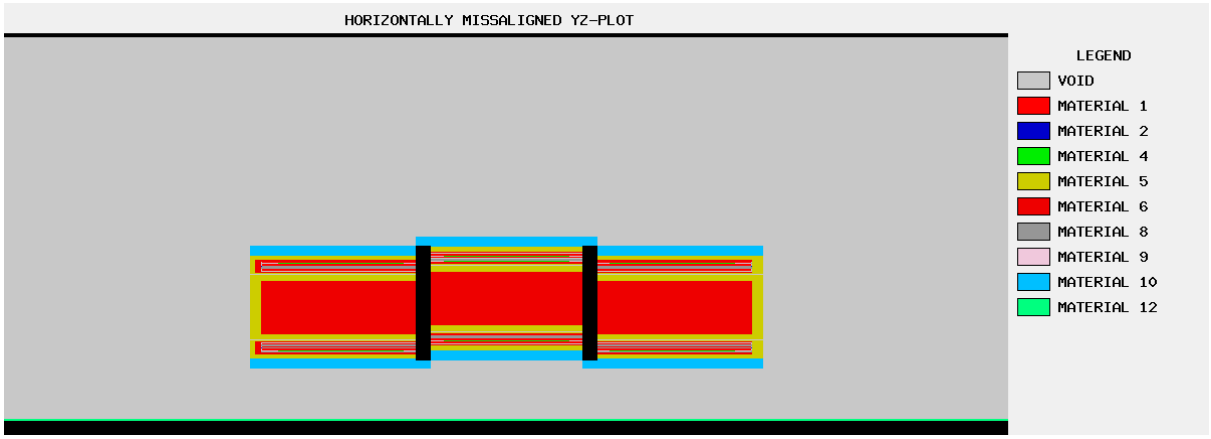

Figure 4.14: 3 X 10 storage array in a horizontal orientation with the middle row elevated by 20 cm.

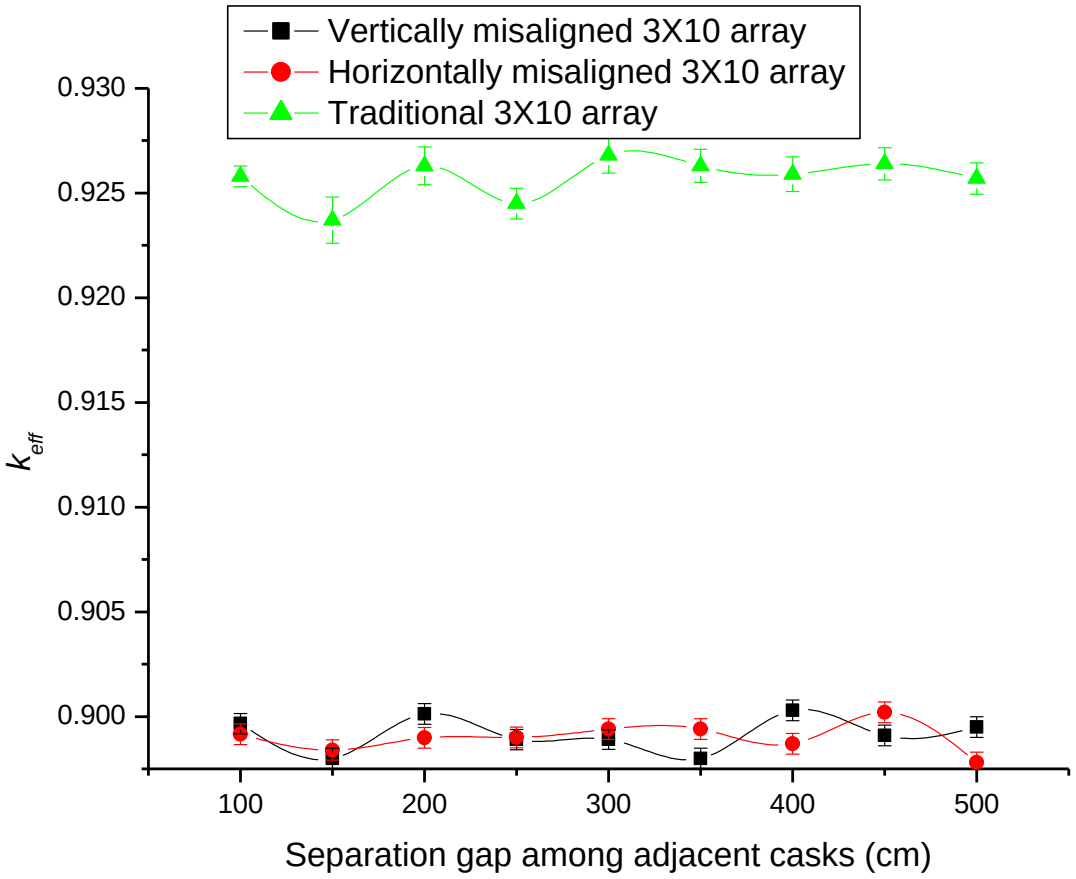

Figure 4.15: Comparison of various orientations of 3 X 10 arrays (Present study).

The results in Figure 4.15 indicate that casks in misaligned 3×10 storage arrays, irrespective of whether they are horizontal or vertical, result in much lower k_{eff} than those in a traditional 3×10 vertical orientation. Since the gaps between the rows of the two arrays were kept constant, the difference in k_{eff} will be as a result of the misalignment of the two reactive ends of the adjacent casks, thus resulting in a decrease in the k_{eff}. When vertical and horizontal casks are compared, it is observed that there is no significant difference in the neutron multiplication factor of the two arrays; the sine wave-like variation in k_{eff} from one position to the next is as a result of stochastic variation in the number of neutrons in the thermal energy range. When the casks in a traditional 3×10 vertical orientation were compared to the traditional 2×15 vertical orientation, it was observed that as the gap between adjacent rows was increased, there was a corresponding decrease in k_{eff} in both arrays.

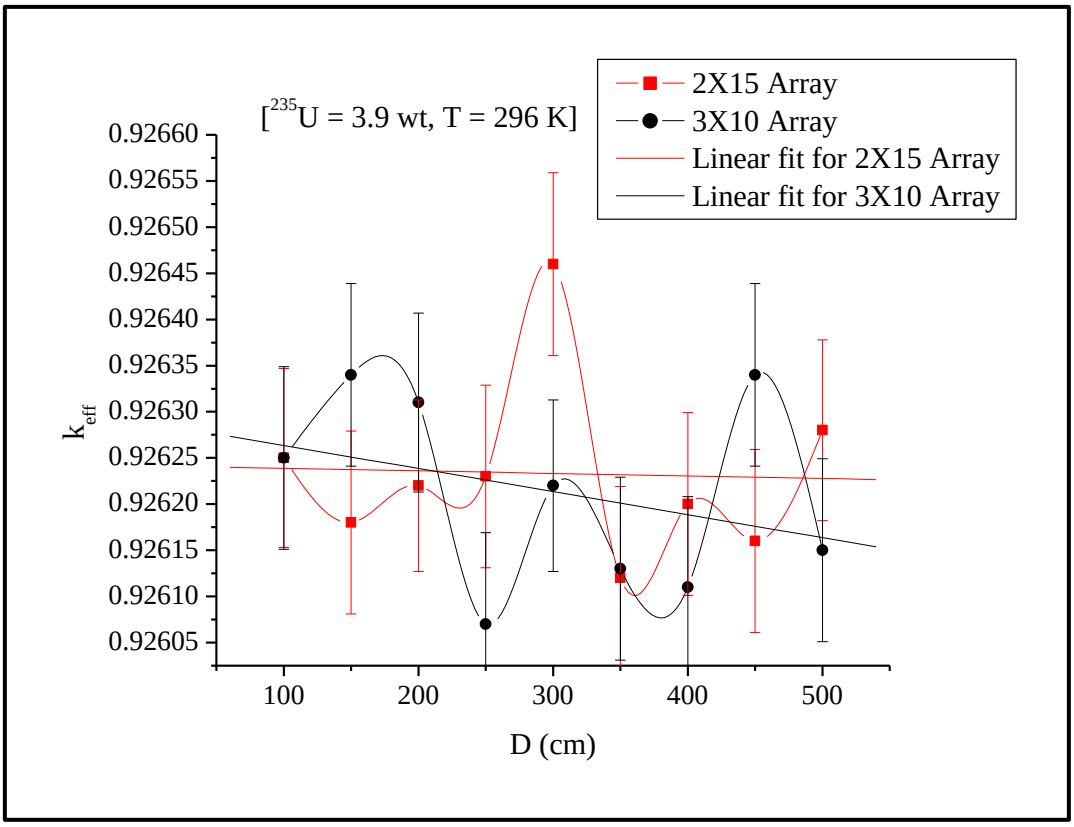

Figure 4.16: 2×15 vz **3×10** storage array (Leotlela *et al.*, 2012)

However, the decrease was much more rapid in the 3×10 array than was the case with a 2×15 array, as indicated in Figure 4.16. One of the factors that play a major role in the behaviour of the k_{eff} relative to the position of the cask in the matrix is the Dancoff factor, which is described in detail in sections 4.3.2.1 and 4.3.2.2.

Considering Figure 4.12, the probability that a neutron born in cask 0 will be absorbed before reaching any one of the neighbouring casks, i.e. 1, 2, 3, 4, 5 and 6 is much higher than that of casks 7 and 8. Cask 8 is completely shadowed from 0 by the two casks between itself and 0, and thus has the lowest probability of interacting with neutron from 0.

In Figure 4.9, on the other hand, there is no shielding between A and D, B and E or C and F. Therefore, because of the absence of additional shielding, a neutron has a much higher probability of interacting with the outer rows in the array than is the case in the 3×10 array. As a result, there is a much more rapid decrease in k_{eff} with distance in 3×10 than is the case with the 2×15 array (Leotlela *et al.*, 2012).

4.3 Storage of used fuel.

In the previous section the '*fresh fuel*' technique was used, which assumes that the fuel is being irradiated for the first time and does not take into account any fission or decay products since it is assumed that they are not there. In spent fuel (or *used fuel* as it is often called) analysis, however, it is acknowledge that the fuel has been irradiated for quite some time and as a result has generated a number of fission products with parasitic absorption which must be accounted for in the analysis. This approach is known as *burnup credit* analysis and will be described in detail in chapter 6.

4.3.1 Taking credit for burnup in spent fuel storage

In burnup credit analysis, there are three sets of nuclides of importance to nuclear criticality namely: *Major actinides only*, *Major actinides + Minor Fission Products* and *Major Actinides + Principal Fission Products*, the elements of which will be discussed in detail in chapter 6.

Of these three, only the major actinides set has been accepted as a set of nuclides for which credit can be taken for burnup. For this reason the next section will focus on major actinides only.

In this study the two traditional arrays of 2×15 and 3×10 analysed in the fresh fuel technique were simulated at two different burnup levels, 20 GWD/MTU and 40 GWD/MTU, which included major actinides nuclide sets in their input file. The objective was to determine how taking credit for burnup would influence the storage array. The results in Figure 4.17 show that the degree of burnup has a much greater effect in the reduction of the k_{eff} than the type of array. It is also observed that when burnup credit is taken into account, the type of array has insignificant value for the k_{eff}. This proves that although the choice of the storage array can make a meaningful contribution to increasing the capacity of the storage facility, this is more relevant to fresh fuel than used fuel. In spent fuel, burnup credit is by far the most effective means to achieve this goal.

According to Chochran, the yield of various nuclides as a result of an increase in burnup is given by (Chochran et al., 1999):

$$y_i^n = \frac{\sum_{g=1}^{G} \sum_m y_{i,g}^{n,m} N_m \sigma_{f,g,m} \phi_g}{\sum_{g=1}^{G} \sum_m N_m \sigma_{f,g,m} \phi_g}$$

and

$$y_c^n = \frac{\sum_{g=1}^{G} \sum_m y_{c,g}^{n,m} N_m \sigma_{f,g,m} \phi_g}{\sum_{g=1}^{G} \sum_m N_m \sigma_{f,g,m} \phi_g} \qquad (4.1)$$

where,

y_i^n = independent fission yield of nuclide n

y_c^n = cumulative yield of nuclide n for energy group g

N_m =atomic density of fissile nuclide m

$\sigma_{f,g,m}$ =microscopic fission cross-section of nuclide m for energy g

ϕ_g = neutron flux at energy g.

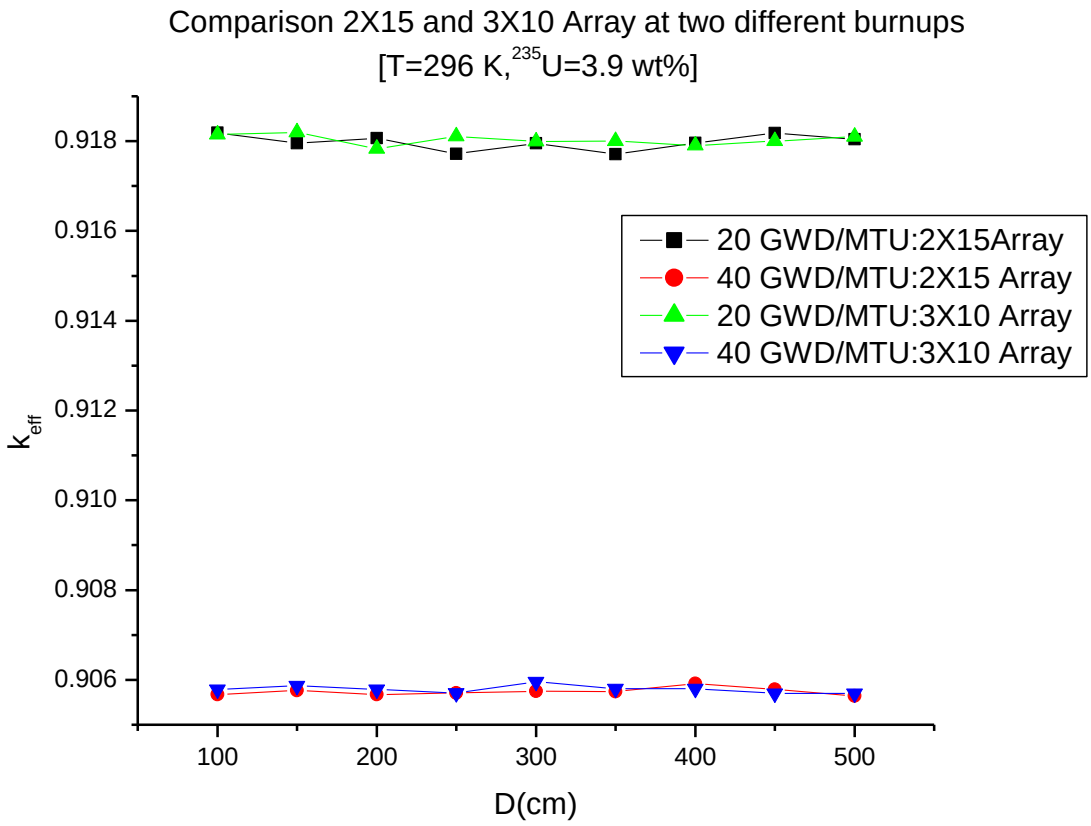

Figure 4.17: Effect of degree of burnup on criticality (Leotlela *et al.*, 2012)

4.3.2 Factors affecting the neutron multiplication factor of spent fuel storage matrices

It has been shown in the previous section that there is a relationship between the separation gap between adjacent casks and the k_{eff} of the system. This section will now provide the scientific explanation and describe a number of factors which influenced the k_{eff} to behave as it did.

4.3.2.1 Spatial self-shielding and the lumping effect

There are a number of factors which must be taken into account in this mode of shielding. Increasing the distance between the source and the detector, or as is the case here increasing the gap between adjacent casks is not the only factor that will serve to decrease the k_{eff}. Other factors in addition to the increase in the separation gap include the macroscopic cross-section

and thickness of the shielding material. The relationship among these factors is found to obey the following mathematical equation [Lamarsh, 2002; Lewis, 2008].

$$I_x = I_0 e^{-N\sigma x} \tag{4.2}$$

where,

I_0 = the initial intensity of the neutron beam with no shielding (or 0 cm thick shield),

I_x = the intensity of the beam after traversing x cm thick shielding material,

N = the number of nuclei of the material (nuclei/cm^3), and

σ = the microscopic cross-section (cm^2/nucleus).

Given that,

$$\Sigma = N\sigma \tag{4.3}$$

where Σ (cm^{-1}) is a macroscopic cross-section.

If Eqn. 4.3 is substituted of into Eqn. 4.2, that can be rewritten as

$$I_x = I_0 e^{-\Sigma x}. \tag{4.4}$$

Also, because,

$$N = \rho \frac{N_0}{A} \tag{4.5}$$

where,

ρ = density of the shielding material (g/cm^3),

N_0 = Avogadro's number = 6.023x10^{23} mol^{-1}, and

A = atomic mass of the material, (g/mol)

If we substitute Eqn. 4.5 into Eqn. 4.3 then Eqn. 4.3 can be written as;

$$\Sigma = \rho \frac{N_0}{A} \sigma \tag{4.6}$$

and substituting Eqn. 4.6 into Eqn. 4.4 , Eqn. 4.2 can be written as

$$I_x = I_0 e^{-\rho \frac{N_0}{A} \sigma x} \tag{4.7}$$

It can be deduced from this that there is an exponential relationship between the number of neutrons crossing the shielding medium and the density or thickness of the shielding. This is one of the fundamental reasons why different storage arrays result in different k_{eff}. For example, in the case of a 2×2 array, the shielding media which occupies the largest volume is air which has a very low density and low absorption cross-section and will therefore result in low scattering or absorption of the neutrons and consequently give rise to higher k_{eff}

The second important factor is the "*lumping effect*" which plays a very significant role in determining the value of the k_{eff} by taking into consideration the type of an array used in spent fuel storage. The type of storage pattern has a great effect on the outcome of the k_{eff} in a sense that it determines which material, fuel or moderator, the neutrons will interact with first when they slow down to thermal energy level. Depending on the type of an array, they may interact with the fuel first and be absorbed before they have their next collision with the moderator. This is because of the lumping effect of fuel [Lamarsh, 2002; Duderstadt, *et al.*, 2010] which implies that the neutrons "see" a group of fuel particles as a lump; and if there is more than one lump in the fuel lattice, the neighbouring lumps tend to shield one another from the view of the neutrons [Duderstadt, *et al.*, 2010; Kulikowska, 2000; Petrie, *et al.*, 2011]. This will result in the reduction of the number of fuel lumps in direct view of neutrons and consequently in lower probability of absorption by the fuel resonances thereby increasing the probability of interacting with the moderator. As a result of this, there will be more neutrons reaching the thermal energy levels and hence a higher k_{eff} than without spatial shielding. Dancoff and Ginsburg derived a formula to calculate the reduction in surface resonance absorption due to the neighbouring absorbers and this reduction is known as the Dancoff-Ginsburg factor, or more commonly the *Dancoff factor* which is defined as [Wei, *et al.*, 2011; Kulikowska, 2000]:

Definition: "*The Inter-volume Dancoff factor is the probability that a neutron escaping from a fuel lump in a finite volume enters another fuel lump in a different finite volume.*" [Kulikowska, 2000]

The Dancoff factor has been found to depend on the material of the lattice, the amount of lumps, the geometry and the size of the lumps [Kulikowska, 2000; Wei, *et al.*, 2011]. As a result the same number of casks, the same size and same shape arranged differently will yield different k_{eff} values. This is the reason why the 2×15 array has a much higher k_{eff} per distance of separation than the 3×10 array.

Therefore, for a neutron travelling from cask A of Figure 4.1 to cask D (and vice versa) in a 1×4 array must successfully pass through two casks B and C without being absorbed by the fuel before it can reach D to cause fission. Thus the two middle casks form a shield between A and D. The factors that play a role in this case are the shielding coefficients of the material participating. These include, iron (Fe), air between the casks. Other factors include the thickness of the two materials, the gap among adjacent casks and density of the shield. [Leotlela, *et al.*, 2012];

In a 2×2 array on the other hand, there is no self-shielding among various casks. The shielding material which covers the largest area is *air* which has a very low density and low shielding coefficient. Also the fact that Figure 4.1 is arranged in series while in Figure 4.7 there is in a square array, the spatial shielding factor plays a much more significant role in the linear array as opposed to the square array. In Figure 4.7 a neutron from E has an equal chance of reaching casks F, G or H without being absorbed, which is in contradiction to what has been observed in Figure 4.1and Figure 4.4. Thus because of higher probability of causing fission in a 2×2 array, Figure 4.7 experiences a much slower decrease in k_{eff} as the gap among adjacent casks increased as shown in Figure 4.8 [Leotlela, *et al.*, 2012].

4.3.2.2 Resonance self-shielding

In addition to spatial shielding which becomes important only in as far as *how* various casks are positioned with respected to one another, (which defines the type of an array), it is also imperative that the resonance self-shielding of various casks from one another is taken into consideration, when designing the storage array of casks.

At higher energies in heavier nuclei, the resonances get so close together that they cannot be given separately. This region is known as the unresolved resonance range, and is characterised by the difficulty in computing simple cross-section versus energy [Lamarsh, 2002] [Duderstadt, *et al.*, 1976]. This is particularly important in the selection of neutron

absorber material and the type of fuel used since each one of them has its own characteristic resonance which will contribute to self-shielding.

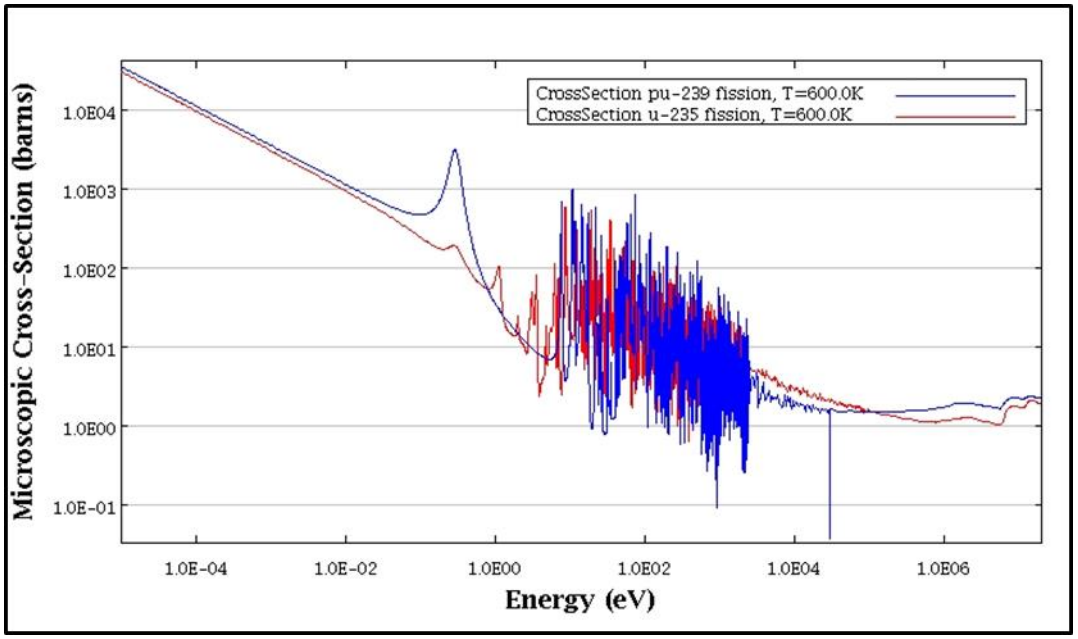

Figure 4.18: Microscopic fission cross-section of ^{235}U and ^{239}Pu at 600 K (Present study)

For example self-shielding in the UO_2 fuel will be different from that of PuO_2 because of the presence of ^{238}U in the UO_2 which has a number of resonance peaks which is not available in PuO_2.

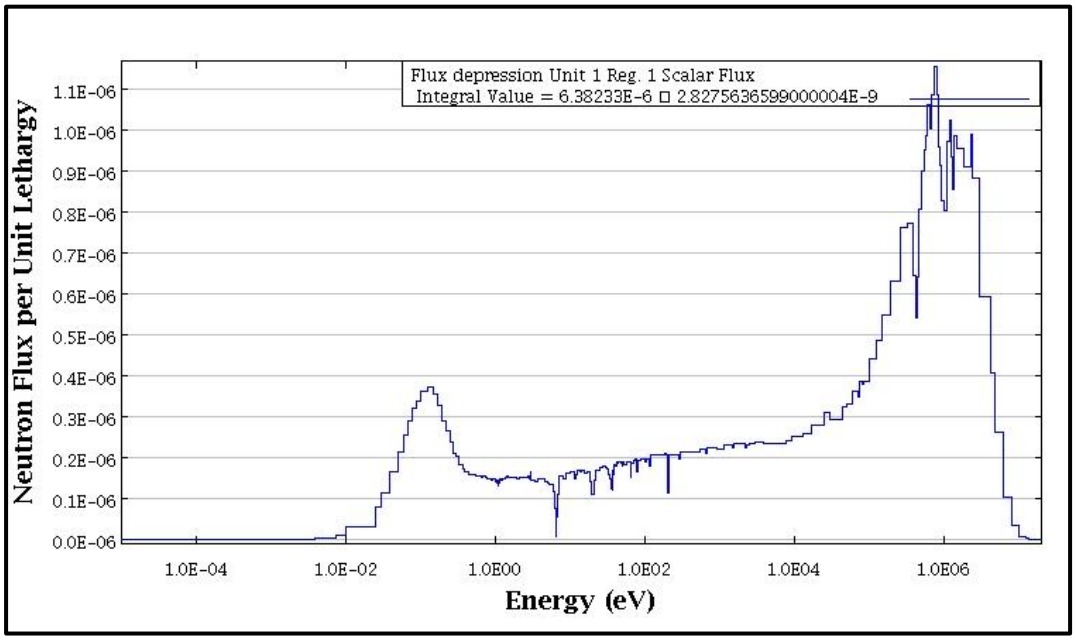

Figure 4.19 : Neutron flux in Unit 1 Region 1(i.e. fuel region) (Present study)

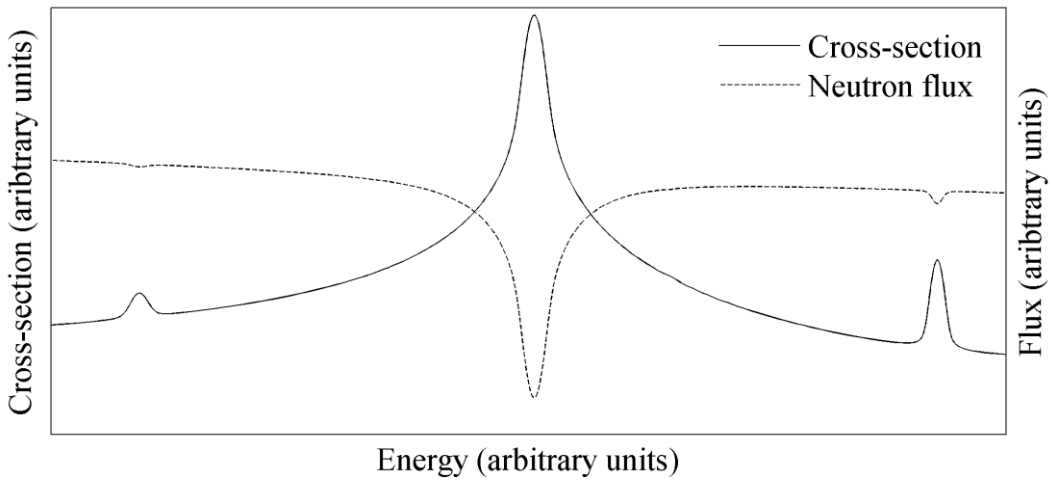

Figure 4.20: Flux depression as a result of high cross section. [Ball, 2012]

Apart from the fuel, selection of the moderator and other material which makes the largest fraction of the material composition will come with their own resonances in the system which will add to the self-shielding of the array.

Therefore, if the material is made up of a nuclide with a wide narrow resonance peak in the resolved resonance range, the microscopic cross-section at the energy range corresponding with the resonance will increase sharply thereby causing a flux depression in that energy range. This phenomenon can be observed in the dip in neutron flux between 1eV and $1x10^4$eV in Figure 4.19 which coincides with resonance region of ^{235}U and ^{239}Pu in the same energy range in Figure 4.18 [Frohner, *et al.*, 2000; Lamarsh, 2002].

When these two spectra are superimposed, they will result in a spectrum such as shown in Figure 4.20 which also shows that the flux will subsequently return to its original level at energies just below the resonance [Duderstadt, *et al.*, 2010]. Alternatively, if a material with high resonance is present in minute quantities in a dilute mixture; its resonance will have very little effect on the neutron flux.

However, if a nuclide with a large resonance is present in large quantities or is pure, its resonance will have a significant effect in the neutron flux, acting as a neutron sink, causing sharp dips in the neutron spectrum corresponding to each resonance [Trkov, 2000].

It is clear from this that the resonance region plays a very crucial role in neutron absorption of the moderator and that of the fuel. As stated earlier, one of the six factors which plays a significant role in determining the k_{eff} of the system is the resonance escape probability which

is defined as *the probability of a neutron to escape the resonance absorption* and is given by [Duderstadt, *et al.*, 2010];

$$p = \exp\left(-\left(\Sigma^{r}\right)_{e} / \xi\Sigma^{s}\right), \tag{4.8}$$

where $\left(\sum^{r}\right)_{e}$ is the effective resonance integral ,ξ is the average logarithmic energy decrement given by [Duderstadt, *et al.*, 2010; Lewis, 2008]:

$$\xi \cong \frac{2}{A + 2/3}, \tag{4.9}$$

where, A is the atomic mass of the nuclide in question, and $\sum^{s}$ is the macroscopic scattering cross-section. In the context of the reactor lattice cell, if a neutron leaves the fuel/cladding interface of its origin it should be able to enter another adjacent fuel/cladding interface without collision.

The *Dancoff factor* therefore, plays a significant role in taking into account how the fuel rods or spent fuel casks are arranged with respect to one another (i.e. the type of an storage array or fuel assembly array type) when the correlation between the type of an array and the k_{eff} is determined. It is for this very same reason that 3×10 has a lower k_{eff} than the 2×15 [Kulikowska, 2000; Wei, *et al.*, 2011].

4.3.2.3 End-effect

When one takes a look at the vertical distribution of neutron flux along the length of the fuel assembly, it is observed that the central region, in the area bordered by 50 cm from the top and 50 cm from the bottom has a much higher burnup than those at the extreme ends; the top-end has an even lower burnup compared to the bottom-end as shown in Figure 4.21 [Parks, *et al.*, 2006; Suyama, *et al.*, 2008]. This is due to the axial profile of the flux caused by uneven distribution of the neutron flux, being higher in the middle of the fuel assembly than at the top and bottom ends.

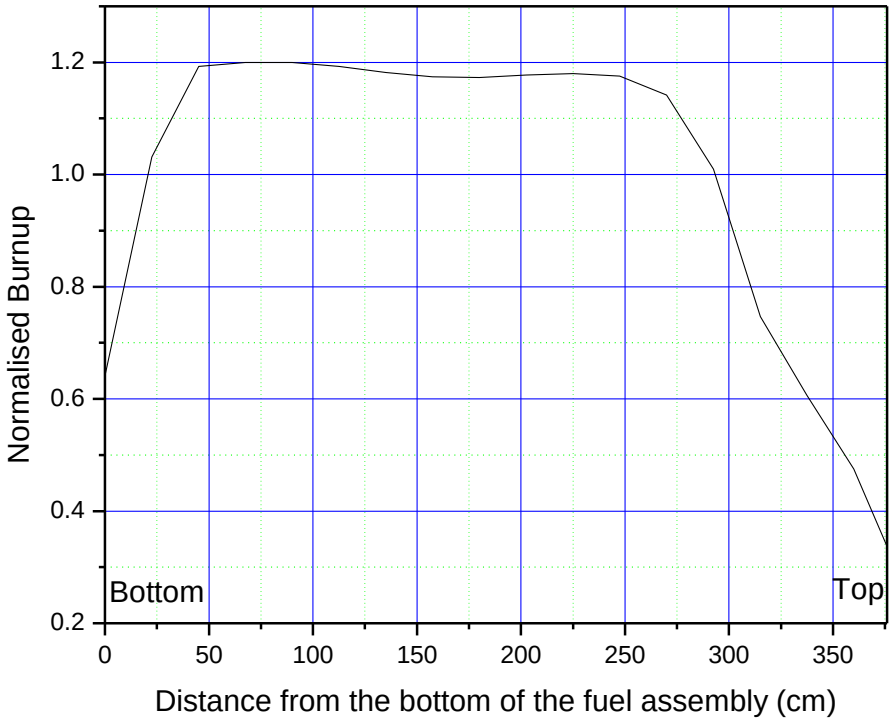

Figure 4.21 Schematic illustration of the End-Effect

Since the top and bottom regions of the fuel assembly are underburned, they are much more reactive than in the middle part, thus limiting the distance of proximity of how close the fuel assemblies or casks can be stacked together without the interference of the neutron flux with fissile nuclides from adjacent ones. This became evident at Figure 4.7, in which there was a peak at 150 cm for the 2×2 array. This may be ascribed to the end-effect which resulted in extreme end regions of the fuel assembly having a higher concentration of under reacted fissile material compared to the middle part of the fuel assembly, thus resulting in the increase in k_{eff} when casks are stacked closer to one another [Parks, *et al.*, 2006; Wagner, 2006].

4.3.2.4 Back-scattering

Back scattering has a profound effect on the storage of fuel assemblies and spent fuel casks. If the building is not big enough, neutrons will be scattered from the walls of the building back to the cask and cause an increase in k_{eff}, and also scattered among the casks into the fuel and cause fission and subsequently higher k_{eff}. As a result of the intricacies associated with the effect of back-scattering on the k_{eff}, it has been studied extensively. One of the scientists

that did an extensive study on the neutron dose rate around casks is Buchillier [Buchillier, *et al.*, 2007].

Buchillier performed neutron measurements at different distances and locations around Castor HAW[12] 20/28 cask. The location and the corresponding distance where measurements were taken are summarised in Table 4.3, and the results in Figure 4.22 through to Figure 4.25. As shown in Figure 4.23, the neutrons were detected as far as 10 m from their cask. Not only were neutrons that far from the casks, it was also established that their energy peaked at $1x10^{-8}$ MeV which is well within the thermal range and can potentially cause fission if they interact with fissile material.

Many scientists ascribed this increase in neutron measurement farther away from their source to back-scattering from wall, air, floor surface and from other casks in the same building [Buchillier, *et al.*, 2007; Kralik, *et al.*, 2002]**.** Therefore, because dose rate measurement differed depending on the location on the casks where measurements were taken, and because neutrons were detected as far as 10 m from their source, it would therefore be recommended that in future measurement be taken at different locations of the cask and also that a 10 m dose rate measurement be performed on all casks.

Table 4.3: Location of radiation measurements around the cask containing spent fuel [Buchillier, *et al.*, 2007]

Location	Angle (degree)	Distance from external surface (m)	Height (m)
1	270	1	1.95
2	180	10	0.86
3	270	1	3.92
4	Centre	On Top	0.47[13]

[12] HAW: High Active Waste
[13] Above top surface

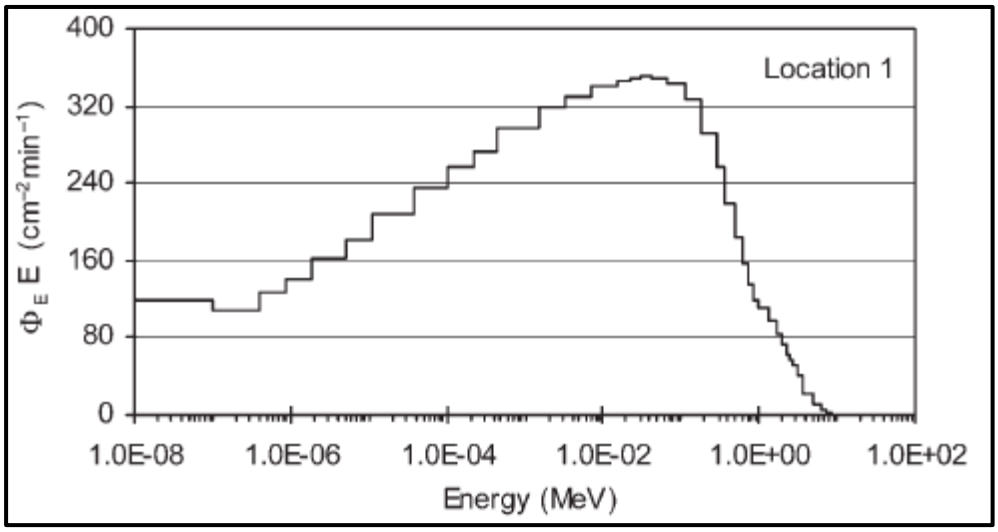

Figure 4.22: Spectrum at location 1 [Buchillier, *et al.*, 2007]

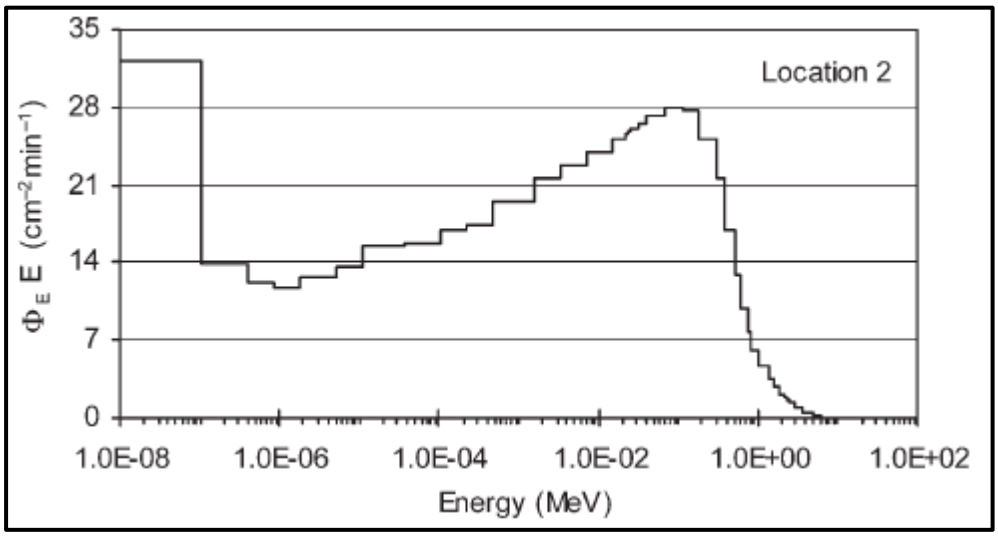

Figure 4.23: Spectrum at location 2 [Buchillier, *et al.*, 2007]

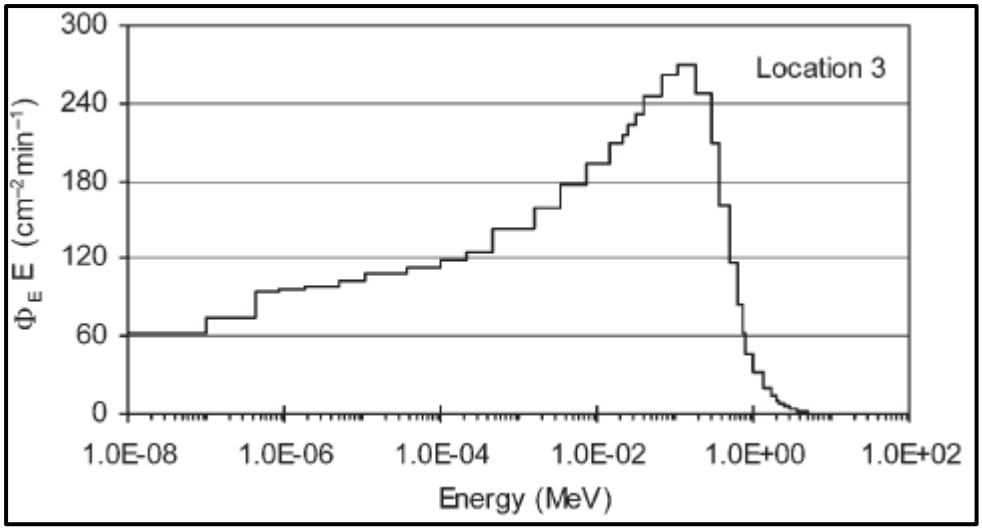

Figure 4.24: Spectrum at location 3 [Buchillier, *et al.*, 2007]

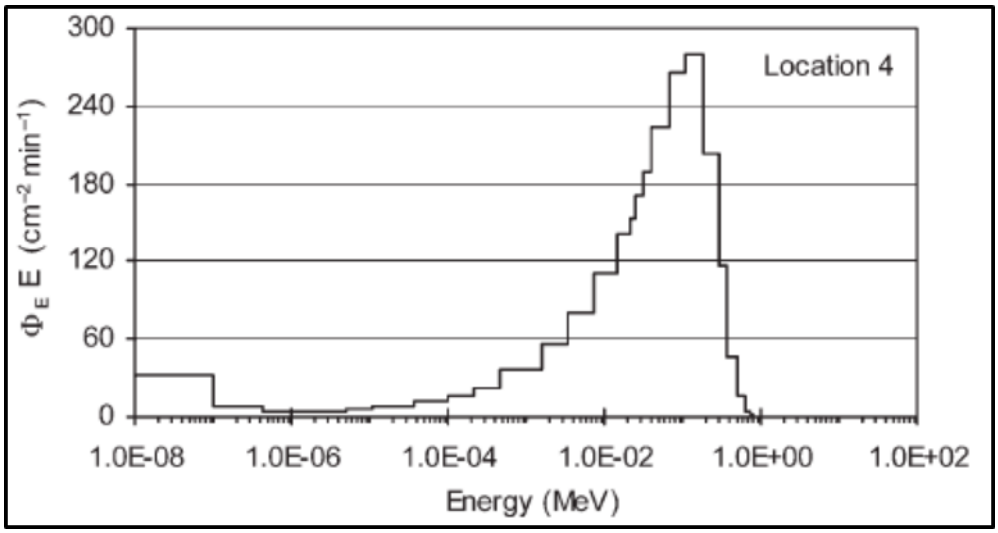

Figure 4.25: Spectrum at location 4 [Buchillier, *et al.*, 2007]

Later, Rimpler [Rimpler, *et al.*, 2010] performed a similar study using TN85 cask and the description of measurement locations are summarised in Table 4.4. The results were later compared to those of Castor HAW 20/28. Comparison of Figure 4.26 and Figure 4.27 show the neutron fluence spectrum of TN85 on its own and when it is compared to Castor HAW respectively [Buchillier, *et al.*, 2007; Rimpler, *et al.*, 2010].

Table 4.4: Description of measurement location in Rimpler's experiment [Rimpler, *et al.*, 2010].

Measuring Position	Distance from cask surface (m)	Height above floor (m)	Axis/Angle (°)
P1	-	0.20[14]	Centre
P2	0.9[15]	0.2[12]	270
M1	0.2	3.30	90
M2	2.00	3.30	90
M3	10.00	1.80	135
M4	20.00	1.80	135
M5	0.25	0.63	90

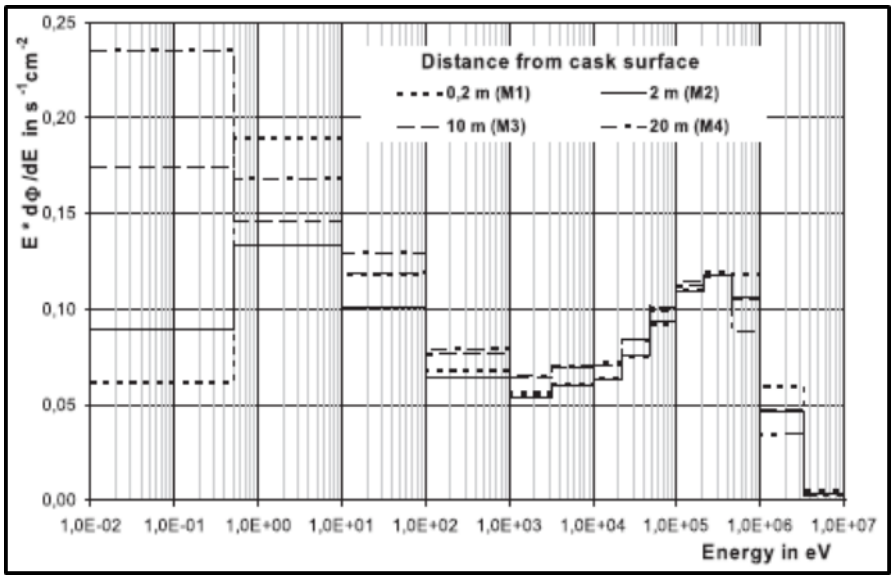

Figure 4.26 Neutron fluence spectra at various locations around TN85 normalized to fluence maximum for fast neutrons.

[14] From top of protective cover
[15] From Top Centre

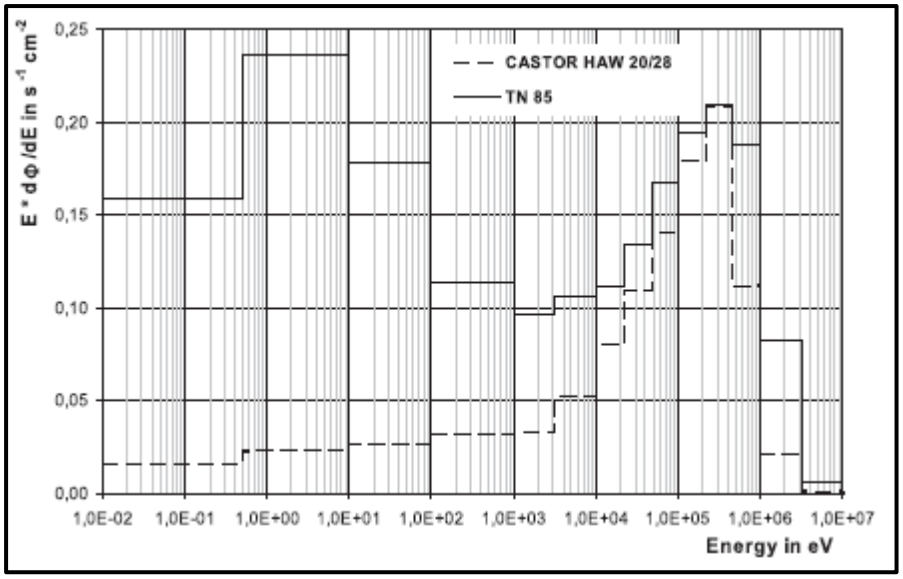

Figure 4.27: Neutron spectra at a distance of 2 m from TN85 and CASTOR HAW 20/28 cask normalized to fluence maximum for fast neutrons.

From this experiment, Rimpler was able to detect neutron fluence as far as 20 m from TN85, which defied the belief that no neutrons can pass through the wall of any cask and cause fission in neighbouring casks, thereby confirming earlier studies by Buchillier [Rimpler, *et al.*, 2010].

This was confirmed by the results of comparison between Castor HAW and TN85 in which it was shown that when measurements are taken from the same distance, CASTOR 20/28 has a much lower rate of neutron escape than TN85 as seen from lower neutron detection level around CASTOR HAW compared to TN85. Looking at Figure 4.26 it is observed that the farther away neutron measurements are taken from the cask, the lower is the energy of neutrons detected. Therefore, the widest gap between adjacent casks in storage is no guarantee that the storage array will not be critical, in some array types it may have an opposite effect as seen in $\mathbf{2 \times 2}$ array. Given that there are 3 or 4 energy groups depending on the energy cut-off point of each group. The upper and lower limits of 3-and 4 energy groups are indicated in Table 4.5 [Duderstadt, *et al.*, 2010]. Therefore, the neutrons detected in Rimpler and Buchillier experiment can be regarded as thermal, epithermal or even fast neutrons.

Table 4.5: Range of energy spectrum

Designation of Energy Group	3 Group Theory	4 Group Theory
Thermal Energy	0.02 eV to 1 eV	0.02 eV to 0.625 eV
Epithermal	1eV to10 keV	0.625 eV to 5.5 keV
		5.5k eV -0.86 MeV
Fast Neutrons	10 keV – 10 MeV	0.86 MeV – 10 MeV

It is evident from this that in the absence of scattering or absorption media neutrons can travel a long distance from their source. What is even of greater concern in nuclear criticality safety analysis is that they can also be in the thermal range, making it quite likely that they may induce fission to fissile material in neighbouring casks [Leotlela, *et al.*, 2012].

4.3.2.5 Statistical uncertainties

As has been shown in various storage arrays e.g. Figure 4.16 there is a huge statistical uncertainty in the k_{eff} of the system as the distance between adjacent casks increases. According to Dean [Dean, *et al.*, 2007], there are many factors which contribute to this and these will be discussed in section 7.4. Some of the main factors include uncertainty in the measurements of the radii or thicknesses of the cladding materials or in the mass of the amount of the fuel loaded in the fuel assembly. This is further compounded by the uncertainty in the spacing among adjacent fuel rods [Dean, *et al.*, 2007].

The compounding effect in modelling process due to biasing and the statistical error/uncertainty in the sensitivity of nuclide cross-section will result in a high uncertainty noted [Dean, *et al.*, 2007].

4.3.2.6 Neutron Importance

The final and possibly the most effective factor making the most significant contribution to variation of k_{eff} with the type of the array is neutron importance, which will be described in detail in section 7.6 of this thesis.

As Lewins once said *"If an independent neutron source S is taken into consideration, it has been established that in a linear system of sources, the behaviour of neutrons and its progeny will not be affected by other neutrons or the independent sources of neutrons, thus the importance equations is independent of the source S. In non-linear systems however, this equation must be modified since the systems properties (fission, scattering, absorption) and therefore, the way in which progeny will propagate in the system will be influenced by the neutron density, fission density and therefore, indirectly by the source"* [Lewins, 1965; Lewins, 1960].

In the context of this project, this implies that when the casks are arranged in a linear array (1×4) the behaviour (fission, scattering, absorption etc.) of the neutrons and its progeny will not be affected by other neutrons from other sources or the independent source of neutrons S and subsequently the k_{eff}. However, if they are in non-linear system such as in a 2×2 array, the independent source has a much greater effect on the behaviour of neutrons and its progeny, since the way in which the progeny propagates is influenced by the neutron density and fission density and therefore, indirectly by the independent source of neutrons. This is the fundamental difference between the results obtained in 1×4 array versus those obtained from 2×2 array.

4.4 Alternative methods of increasing the capacity of spent fuel storage facility

4.4.1 Ranking of aluminium Composite Material for use as Neutron Absorber Inserts

As a result of the continual increase of spent fuel assemblies in the spent fuel pools and the reluctance of many nuclear regulators to take credit for burnup, an alternative method has been developed that will preserve the storage capacity of the spent fuel pool while maintaining the safety margin and thus reduce the demand of the casks. This involves the use of aluminium composite material as neutron absorber inserts [EPRI, 1988].

In this study three types of aluminium composite material were analysed to determine their effectiveness to reduce the k_{eff}, namely; AA1100 UNS, Boral Metal Matrix and ALCAN Metal Matrix. The ALCAN Metal Matrix was further divided into derivatives 15.3% B_4C

and 15.9% B_4C as shown in Table 4.6 [O'Leary, *et al.*, 1996; Lindquist, *et al.*, 1993; Northeast Technology Corp, 2008; EPRI, 1988].

The inserts are designed according to the location/area of the fuel assembly they were going to be located. As such three locations were identified as areas where high neutron densities are likely to occur which will need neutron absorber inserts to reduce fission rate, namely [Leotlela, *et al.*, 2015]:

- The basket design
- The End-effect design,
- The Central Instrumentation tube design

Table 4.6: Chemical composition of aluminium composite material used as neutron absorber inserts (Present study).

Elements	AA100 UNS A91100 Temper O (%)	Boral Metal Matrix Material Spec (%)	ALCAN Metal Matrix Material Spec (%)	ALCAN 15.3% (%)	ALCAN 15.9% (%)
Al	99 min	99 min	99 min	97.214059	97.00698
Si	0.95 max	1.00 max	0.45 max	0.446691	0.461375
Fe					
Cu	0.05-0.20	0.05-0.20	0.05-0.20	0.1293053	0.130131
Mn	0.05 max	0.05 max	0.05 max	0.011755	0.01183
Zn	0.10 max	0.10 max	0.10 max	0.011755	0.01183
Mg			0.05	0.011755	0.01183
Ti			1.00-2.5	2.1746797	2.366024
				100	100
B_4C				15.30	15.90

4.4.1.1 Basket Design

In this design, the composite material formed the basket of the fuel assembly where the fuel assembly would be placed before being transferred into the spent fuel pool. In a case where there is already neutron absorber material used as is the case in re-racking, this design is further classified as either the new inserts were put inside the existing one or outside as indicated in Figure 4.28 and Figure 4.29 respectively [Leotlela, *et al.*, 2015].

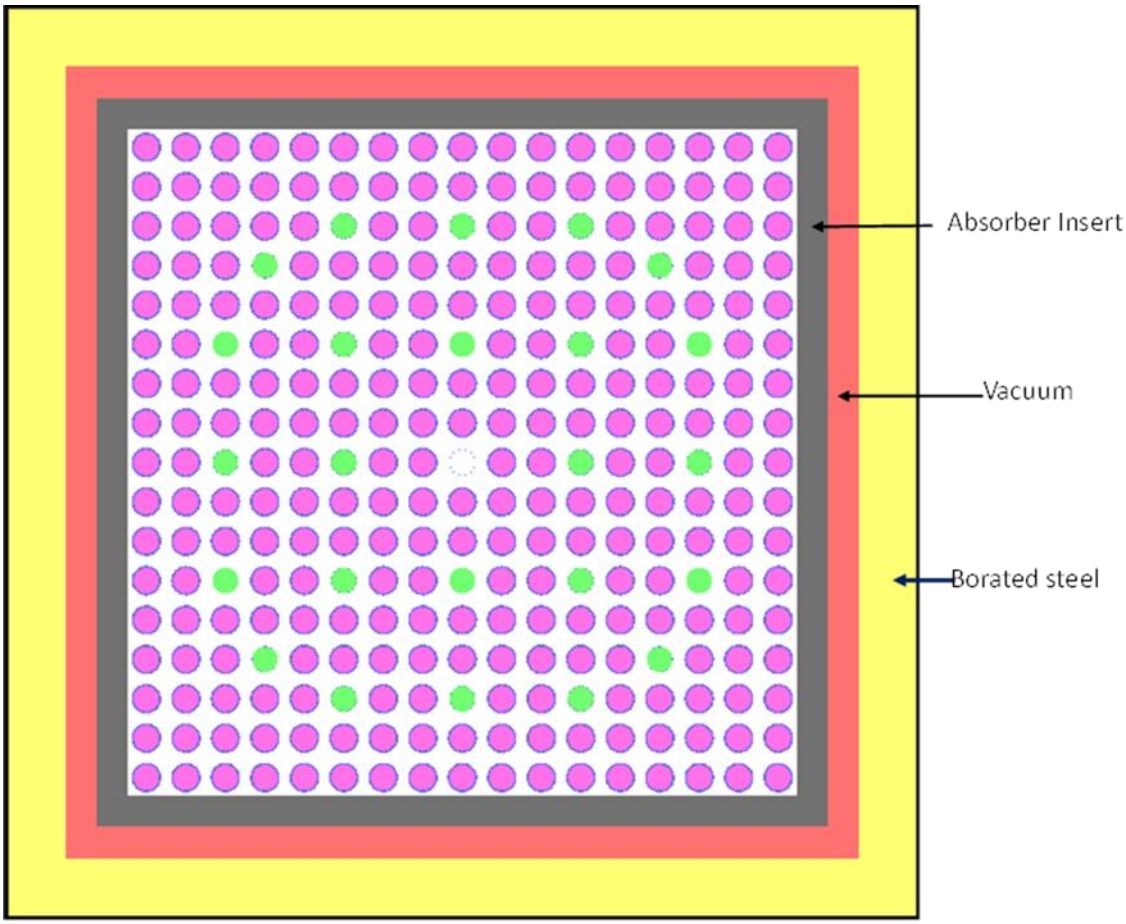

Figure 4.28 Neutron absorber insert inside the fuel assembly flask [Leotlela, *et al.*, 2015].

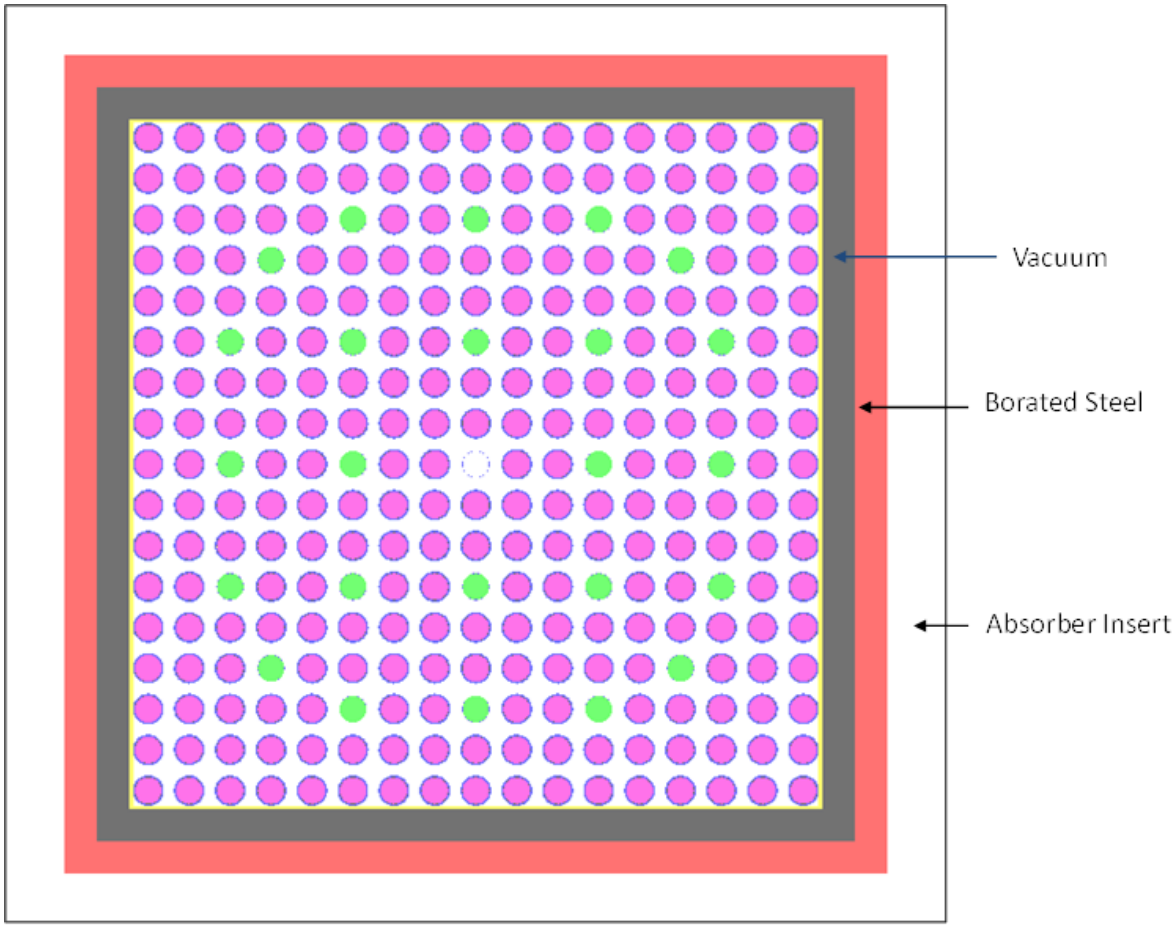

Figure 4.29: Neutron absorber insert outside the fuel assembly flask [Leotlela, *et al.*, 2015].

4.4.1.2 End-Effect Design

In this design, the neutron absorber inserts sleeves were placed at the top and bottom end of the fuel assembly as shown in Figure 4.30, to reduce neutron flux occurring at the ends of the fuel assembly as a result of uneven distribution of neutron flux causing the end-effect phenomena [Leotlela, *et al.*, 2015].. The top sleeve ranged from 76.1 cm to 201.1 cm while the bottom sleeve ranged from -135.81 cm to -185.81 cm. They were then enclosed with the outer region, enveloping all of them, called the global region [Leotlela, *et al.*, 2015]..

The design was further divided into two groups depending on whether region4 of the model was made of water or borated steel and the models were executed As will be shown below, the model with region4 made of water resulted in higher k_{eff} than that of borated steel. It has also been observed that in general this was less effective in reducing the k_{eff} compared to a basket design [Leotlela, *et al.*, 2015].

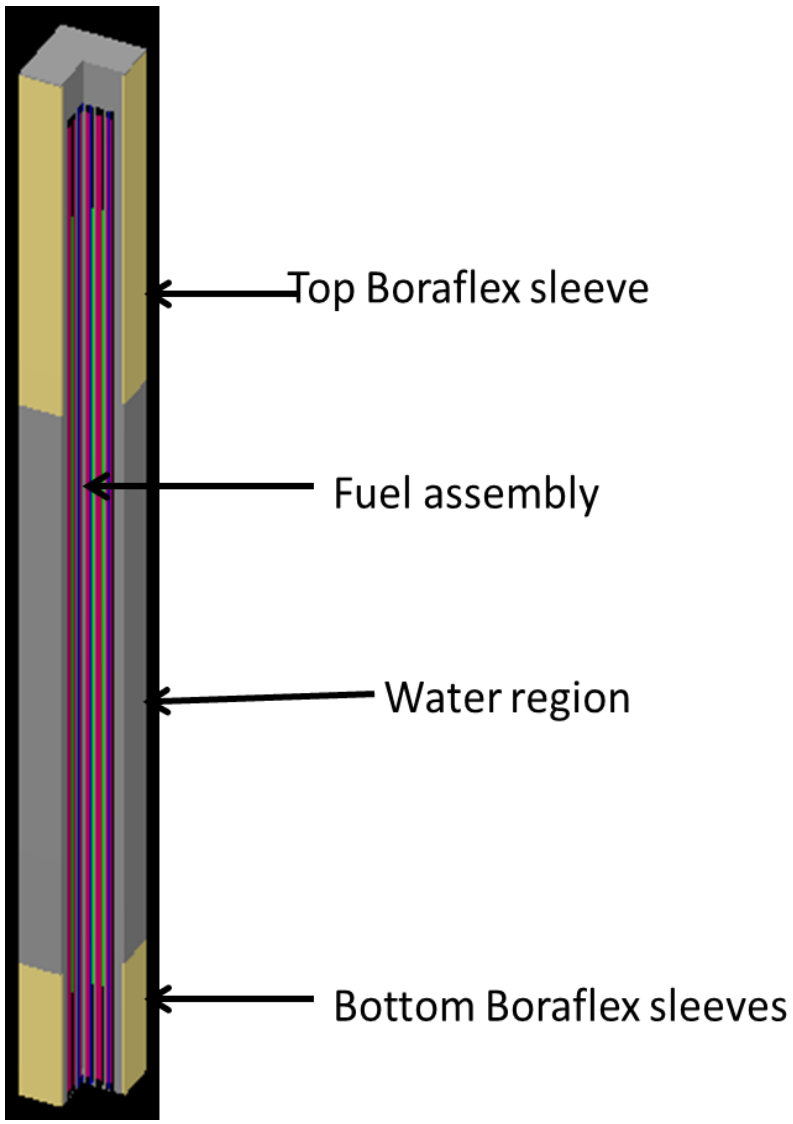

Figure 4.30: Boraflex sleeves at the Top and Bottom end of the Fuel assembly [Leotlela, *et al.*, 2015].

4.4.1.3 The Central Instrumentation Design

In this design two options were assessed: in the first case the neutron absorber inserts was placed inside the instrumentation tube without its own cord as shown in Figure 4.31. In the second case the neutron absorber was covered with the zirc2 cladding material as shown in Figure 4.32 [Leotlela, *et al.*, 2015].

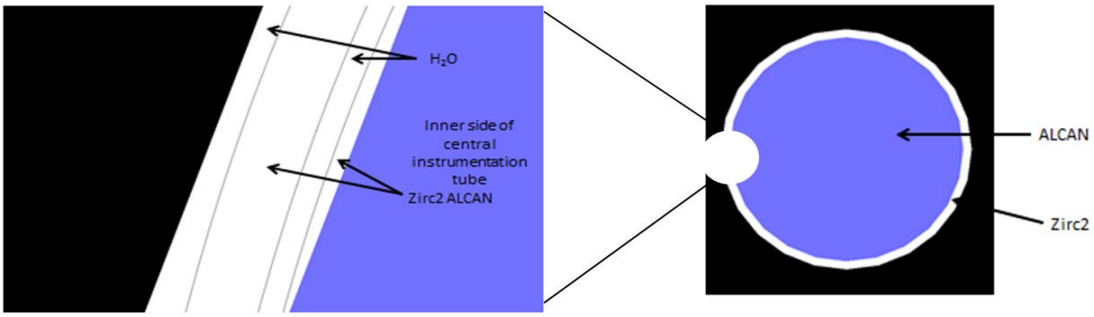

Figure 4.31: Neutron Absorber insert as a cord (without cladding) in the Central Instrumentation Tube [Leotlela, *et al.*, 2015].

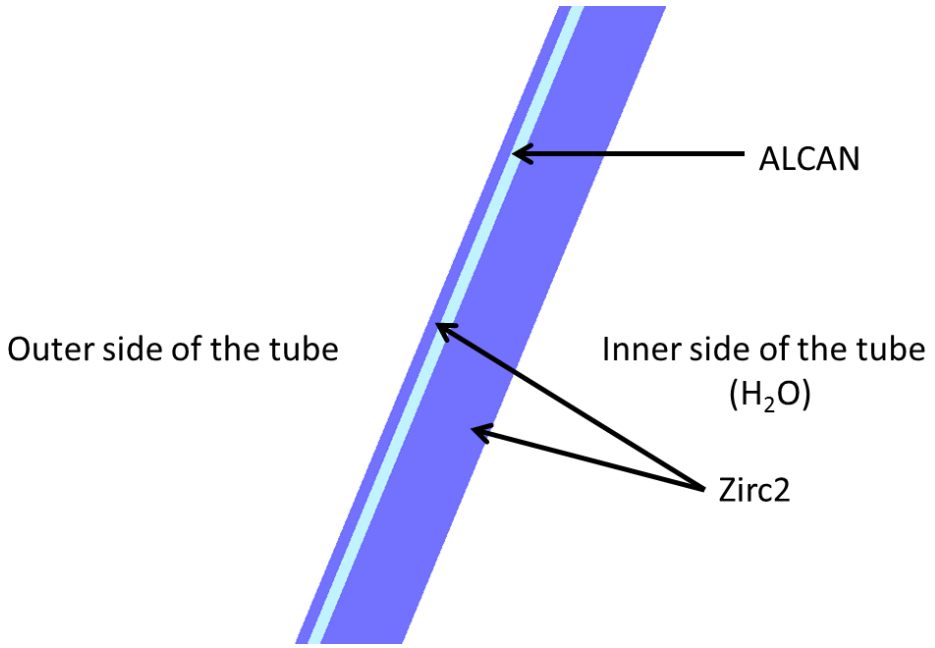

Figure 4.32: Schematic illustration of neutron absorber inserts sandwiched by Zirc2 cladding

The results in APPENDIX 8 [Leotlela, *et al.*, 2015]. indicate that of the three designs, the basket design has the largest effect in reducing the k_{eff} .This varied depending on the location of the neutron absorber used and what the chemical composition of the neutron absorber was

Within the variations of the basket design, it was found that the largest decrease occurred when the borated steel was replaced with boraflex and boraflex was the *innermost* layer as was the case in Figure 4.28. That resulted in the $\%\Delta k/k_{ref}$ varying between 13.6 and 16.69%. The second largest $\%\Delta k/k_{ref}$ was noted when neutron absorber was on the *outside* of the borated steel as shown in Figure 4.29, where it was found that the $\%\Delta k/k_{ref}$ varied from 9.34 and 11.69 [Leotlela, *et al.*, 2015].

The $\%\Delta k/k_{ref}$ in end effect was found to be between 5.41 and 6.1, which occurred when region4 was made-up of borated steel.

The central instrumentation tube design had the least decrease in k_{eff} with $\%\Delta k/k_{ref}$ ranging between 0.27 and 2.02 for the cord design and between 0.188 and 0.55 for the sandwich design [Leotlela, *et al.*, 2015]. Furthermore, the results also showed that inclusion of B_4C in the chemical composition of ALCAN will have a negative effect on k_{eff} of the system, resulting in an increase in k_{eff} instead of decreasing it. This is due to spectral hardening whereby the amount of thermal neutrons required for fission with ^{235}U, reduced to an extent that the flux density is dominated by neutrons in the high energy range [Wagner, *et al.*, 2002]. As a result of this, there is an increase in nuclear reaction between ^{238}U and high energy neutrons.

Table 4.7: Moderating ratio of materials used in the calculations [Leotlela, *et al.*, 2015].

	$\sum_s$	$\sum_a$	ξ	$\frac{\xi\sum_s}{\sum_a}$
	cm^{-1}			
Al	0.08	0.02	0.07	0.40488
Si	0.09	0.01	0.07	0.776525
Fe	0.93	0.22	0.99	4.152691
Cu	0.61	0.03	0.03	0.579138
Mn	0.18	1.04	0.04	0.006248
Zn	0.24	0.07	0.03	0.100067
Mg	0.16	0.00	0.08	4.190167
Ti	0.23	0.33	0.04	0.028319
SUM				**10.23803**
B_4C	1.664	81.00	0.397	0.008156
H_2O	1.47	0.019	0.92	71.17

Table 4.8: Chemical composition of borated steel [Leotlela, *et al.*, 2015].

		$\sum_a$	$\sum_s$	ξ	$\frac{\xi\sum_s}{\sum_a}$
Element	%	absorption	scattering		MR
B	0.9	103	0.346	0.171	0.000574
Si	1	0.008	0.089	0.0698	0.776525
Mn	2	1.04	0.181	0.0359	0.006248
Cr	19	0.255	0.247	0.9872	0.956229
Fe	67.1	0.222	0.933	0.9881	4.152691
Ni	10	0.42	1.6	0.9887	3.766476
SUM					**9.658743**

This will subsequently result in the increase in ^{239}Pu and ^{241}Pu which will then increase fission and consequently an increase in k_{eff}. To understand why there is a difference in $\%\Delta k/k_{ref}$ in different designs of neutron absorber inserts, one will have to take into account the nuclear interaction, whether it is scattering or absorption that occurs inside the fuel assembly [Leotlela, *et al.*, 2015].

Thus if the neutron absorber inserts were to be placed on the inside of the existing re-racking material it is likely to have a significant impact rather than when placed on the outside. The other factor that played the significant role is the chemical composition of the neutron absorber used which is shown in Table 4.6. Since the current neutron absorber is borated steel, it is important that its specific chemical composition is analysed to determine its moderation ratio (MR), defined by [Duderstadt, et al., 2010];

$$MR = \frac{\xi \sum_s}{\sum_a}, \tag{4.10}$$

where,

ξ =Logarithmic energy decrement,

$\sum_s$ =Macroscopic cross-section for scattering, and

$\sum_a$ =Macroscopic cross-section for absorption

Looking at Table 4.7 and Table 4.8 [Leotlela, *et al.*, 2015], it is noted that the moderation ratio for borated steel, neutron absorber inserts and water are respectively 9.658743, 10.23803 and 71.17, which excludes the moderation ratio for B_4C which is 0.008156. For neutron absorber inserts the moderation ratio must be low [Leotlela, *et al.*, 2015]. Therefore to decrease the k_{eff} of the system, the borated steel must be on the inside and the new neutron absorber on the outside which explains why the k_{eff} is lower when the neutron absorber is on the outside. Similarly, when one looks at the moderation ratio of B_4C, one will note that it is the lowest of them all in the table. Therefore inclusion of this in the chemical formula will result in the drastic decrease in the number of thermal neutrons, leaving the population of high energy neutrons much higher. As a result of this there will be an increase in the reaction rate between ^{238}U and the high energy neutron leading to an increased yield of ^{239}Pu and ^{241}Pu, which will subsequently result in an increase in k_{eff} instead of decreasing. That is the

reason why ALCAN that contains B_4C has higher k_{eff} as shown in APPENDIX 8 compared to the standard ALCAN with no B_4C [Leotlela, *et al.*, 2015].

CHAPTER 5

5. ABNORMAL OPERATING CONDITION

5.1 Introduction

The CASTOR X/28 cask that is under study is designed to function normally with only dry air or helium, at a pressure of 31 bars (3100 kPa), surrounding the fuel assemblies. However, it must be demonstrated that the cask will remain subcritical under a number of anticipated accident conditions, such as misloading or water ingress due to aging. In noting that most power reactors are literally on the edge of the sea, they could be filled with either fresh water or seawater; as a result it was necessary to model both cases.

5.2 Water ingress scenario

Two approaches were used: in the first instance a '*fresh fuel*' approach was used and, secondly, the spent fuel approach

5.2.1 Water ingress in 'fresh fuel'

5.2.1.1 The neutron multiplication factor as a function of the volume of water in the cask

The objective of this analysis was to determine how the k_{eff} of the system would be affected by a gradual increase in the water level in a cask, and the results on castor x/28F were compared to those MPC-24 which were performed by Bechtel on Behalf of US DOE.

To achieve this, the entire length of the cask and its fuel assemblies were divided into divisions of 10% along the length of the fuel assembly and then gradually filled with fresh water. At every 10% interval, an analysis of k_{eff} was performed in relation with the volume of water in the cask. The results shown in Table 5.1 indicate that there is a sudden increase in k_{eff} as the water level increases from 0 to 10% and thereafter a gradual increase is registered up to 40%. From 40% the k_{eff} then decreases until 60%, and then increases again between 70 and 80%; thereafter it continues to decrease until it is 100% full

Table 5.1: k_{eff} as a function of amount of water in the cask (fresh fuel)

	MJ Leotlela (this study) on Castor X28F using scale6.1		Bechtel on behalf of US DOE On MPC-24 using MCNP	
Water level (%)	k_{eff}	σ(±)	k_{eff}	σ(±)
0	0.1076	0.0004	0.3654	0.0001
10	0.8882	0.0001	-	-
20	0.9190	0.0001	-	-
25	-	-	0.9184	0.0003
30	0.9206	0.0001		
40	0.9207	0.0001		
50	0.9206	0.0001	0.9450	0.0003
60	0.9206	0.0001		
70	0.9208	0.0001		
75	-	-	0.9575	0.0003
80	0.9208	0.0001		
90	0.9208	0.0001		
100	0.9207	0.0001	0.9594	0.0003

The variation in the magnitude of the k_{eff} as the water level increases along the length of the cask is brought about predominantly by two factors:

- End-effect: this accounts for the *increase* in k_{eff} from a water level of 0 to 40%, and the *decrease* from a level of 40 to 60%, and also for the increase from 60 to 80%.
- The length of the fuel rod with respect to the length of the cask: The active length of the fuel rod is 365.76 cm, whereas the length of the cask is 423.6 cm. The 57.84 cm difference is filled with water and there is no fissile material present in that area; hence no fission takes place in that part of the cask. As a result of this there is a decrease in k_{eff} as the water level rises from 90 to 100% (refer to Table 5.1).

5.2.2 Water ingress in used fuel

Having studied water ingress and its effect on the k_{eff} of fresh fuel, it was necessary to determine how spent fuel would respond to a similar incident. This was driven by the need to ascertain how the k_{eff} of spent fuel analysis that takes burnup credit of various nuclide sets

into account would respond to a gradual increase in water levels in the cask. To that effect two scenarios were investigated, the first one focused on the water ingress in a vertical cask, and the second one focused on a horizontal cask.

In both cases, the fuel assemblies under study had a burnup of 20 GWD/MTU and 30 GWD/MTU, in which the *axial profile* was taken into consideration in the calculation. This is particularly important since, if omitted, it could result in the k_{eff} being 3 to 5%Δk non-conservative [Mueller, 2015; J.C.Wagner, *et al.*, 2003]. To that effect the *control* in the input deck was thus modified to read in the same way as the excerpt of the input file in Figure 5.2

read control

arp=w17x17

nax=18

axp= 0.668 1.034 1.15 1.094 1.053 1.048 1.064 1.095 1.121 1.135 1.14 1.138 1.13 1.106 1.049 0.933 0.669 0.373 end

nuc= U-234 0.635 U-235 1.085 U-238 0.992 Pu-238 0.856 Pu-239 1.076 Pu-240 0.945 Pu-241 1.087 Pu-242 0.848 Am-241 0.609 end

end control.

Figure 5.1: Excerpt of the input file of STARBUC showing the control input deck where credit for burnup of actinides is taken.

Furthermore, each of them i.e. the vertical and horizontal casks, included one of the three burnup credit nuclide sets in their input files.

5.2.2.1 Water ingress into a vertical cask

In the vertical cask the same geometry as in the fresh fuel analysis was used, with the cask being divided into discrete parts of 10%. However, instead of using KENO-VI [Bowman, 2008] to calculate the neutron multiplication factor, STARBUCS (Radulescu *et al.*, 2011) was used since it has been specifically developed for burnup credit analysis. Figure 5.2 shows a lengthwise section of the vertical cask showing the water level, fuel assembly and other components of the cask. This must be analysed in conjunction with fig.5.3. It will be observed from that that a cask does not need a lot of water to reach its maximu k_{eff}.

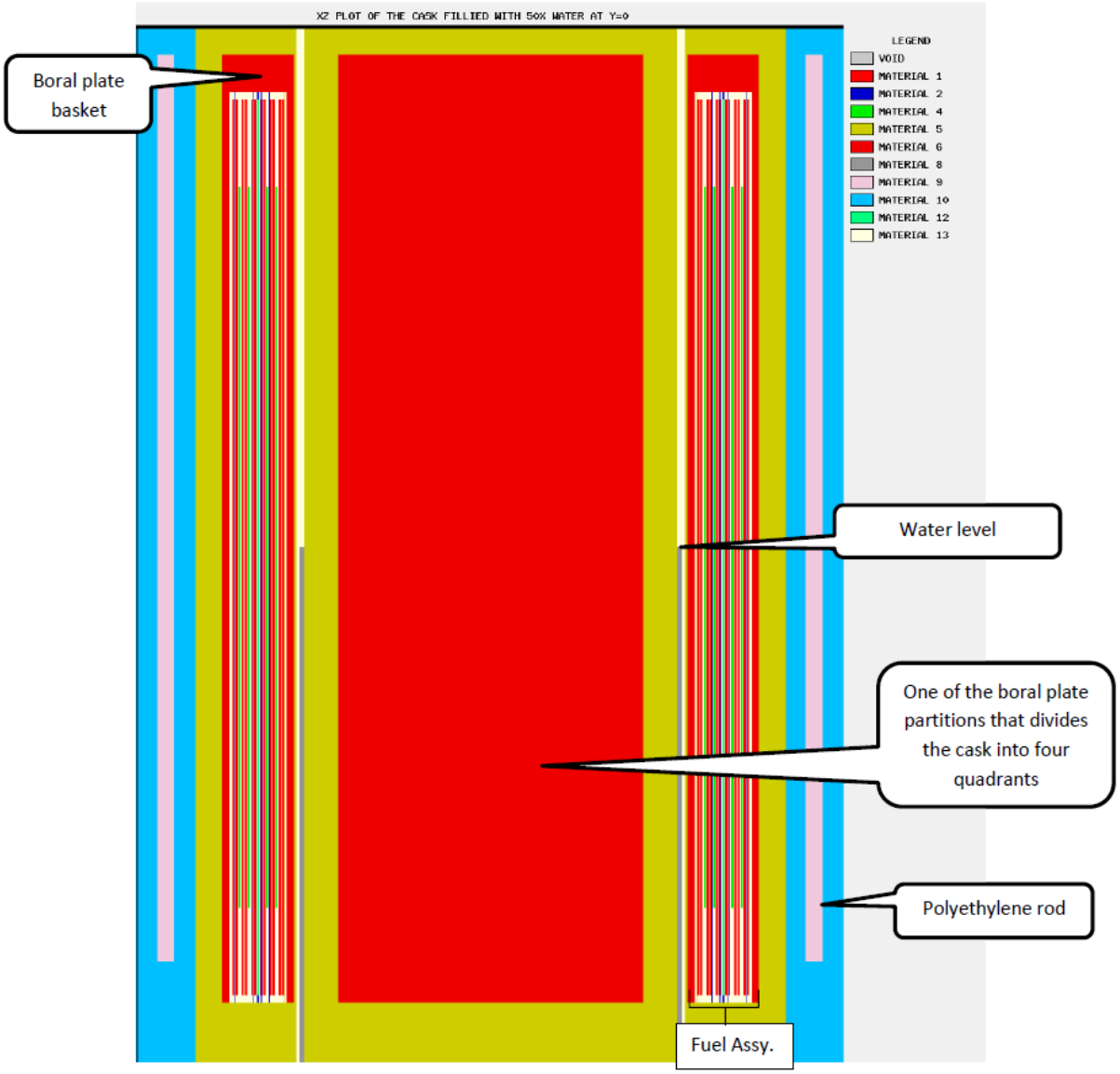

Figure 5.2: XZ View of the vertical cask indicating water level at 50% (Present study)

5.2.2.2 Water ingress into a horizontal cask

In the case of a horizontal cask, because the computer codes used in modelling this do not allow for two geometry regions to intersect, only those areas where it would be possible to insert the plane and divide the cask into smaller sections without intersecting any of the fuel assemblies were divided.

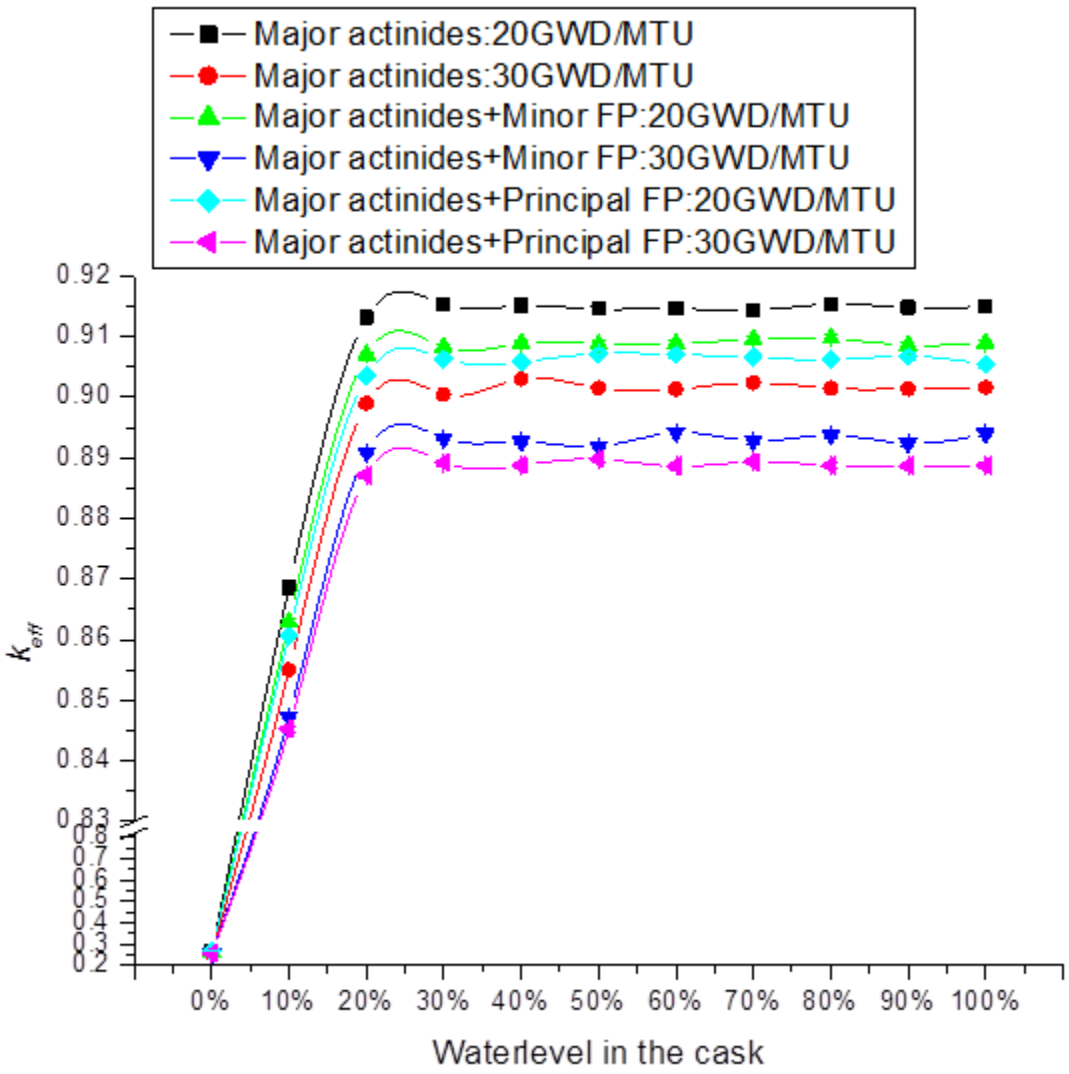

Figure 5.3: Water ingress in a vertical cask (Present Study)

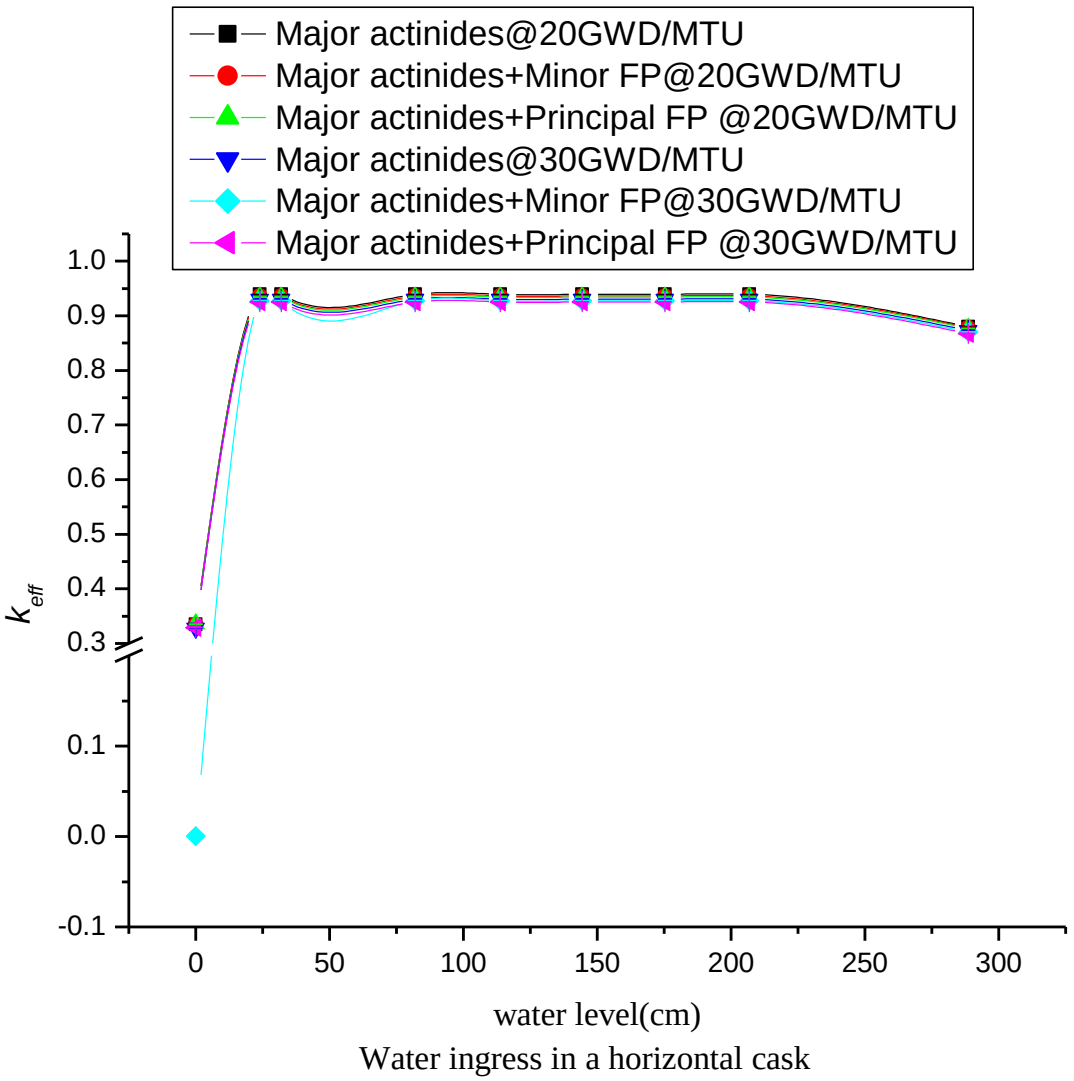

Figure 5.4: water ingress in a horizontal cask (Present study)

As such, a plane was used to divide the cask perpendicular to the Y-axis. The results of the two scenarios are indicated in Figure 5.3 and Figure 5.4 and in both cases the results agree, showing that the most critical amount of water from a nuclear criticality safety point of view is the first few litres (up to 10% of empty space), since this has the greatest effect on the k_{eff} of the system.

From both Figure 5.3 and Figure 5.4, it may be observed that the first 10% of the water level in the cask will increase the k_{eff} of the system from the lowest eigenvalue (k_{eff}) (of 0.21 and 0.34 in vertical and horizontal casks respectively) when filled with air to its highest (0.92 and 0.938 respectively), irrespective of whether the cask is horizontal or vertical. From there

onward, the k_{eff} will stay constant regardless of the amount of water added except when it reaches the midsection of the casks where the k_{eff} decrease. The k_{eff} increases again after the level has passed the midsection. It has also been shown that water ingress in a horizontal cask results in higher k_{eff} than in vertical casks, by an average $\Delta k \approx 0.02$ at any level of water in the cask. However, when the two scenarios are compared at 100% full, the horizontal cask has a lower k_{eff} than the vertical cask. This is due to the fact that all fuel assemblies in the study have uniform enrichment, and therefore the end-effect is much more significant than it would otherwise have been had this not been the case. Secondly, when a horizontal cask experiences water incursion, the water covers all areas (top, middle and bottom) of the fuel assembly at the same time, whereas in the vertical cask the water starts covering the bottom part first, rising through to the middle part and finally the top part. Looking at Figure 5.5, it is noted that the highest fission rate occurs at the top and bottom ends of the cask, and the lowest in the middle of the cask, further confirming the uneven distribution of the neutron flux, which consequenly results in the end-effect phenomenon.

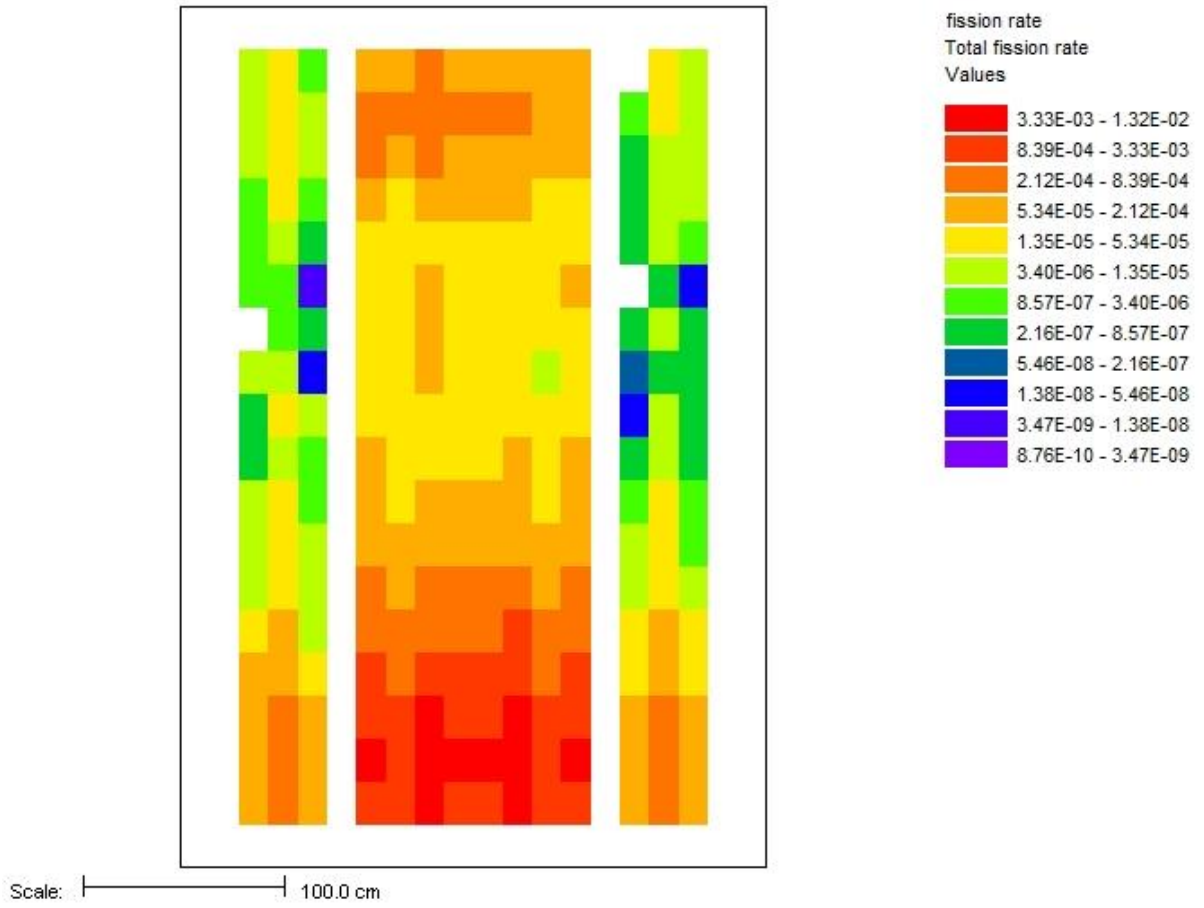

Figure 5.5: Front view of the cask showing fission rate at various regions (Present study)

Since in the horizontal cask there is a reactive part of the fuel assembly (top and bottom part) that is always submerged in water, neutron thermalisation is much higher than in the vertical cask. Also, because ^{10}B is exposed to water, spectral hardening is much more dominant in the horizontal cask, resulting in a higher yield of ^{239}Pu and ^{241}Pu and a decrease in ^{235}U fission [Sanders *et al.*, 2002]. As a result, fission rate is much higher in the horizontal cask than in the vertical one which consequently leads to higher k_{eff} in that cask than in the vertical cask. Furthermore, it is observed from Figure 5.6 that the highest fission rate, and thus the highest fission density, occurs in the centre of the cask and decreases gradually as one moves outwards to the periphery of the cask, as was reported earlier [Leotlela *et al.*, 2015].

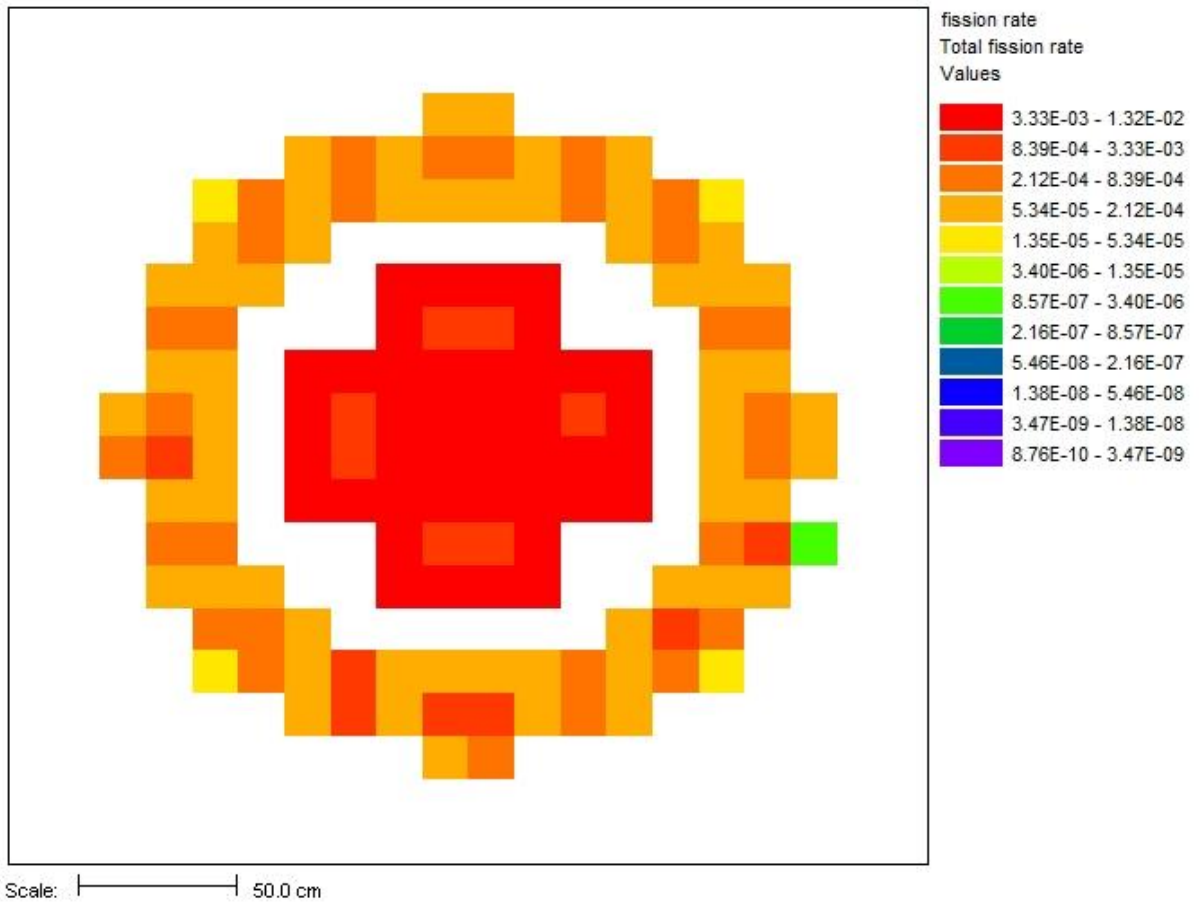

Figure 5.6: Cross-section of the cask (cut at z = -160) showing fission rate at the the two sources (Present Study)

5.3 Cask flooded with water of different chemical compositions

Having determined how the k_{eff} is affected by the gradual increase in water in the cask, the focus was now to determine how water with different chemical composition would affect the neutron multiplication factor of the system. To achieve that, two separate models were run with the cask flooded with freshwater and seawater.

It is assumed that all air-gaps in the cask are filled with water and the pressure kept constant as under normal operating conditions. When reading this, it is advisable to note that this is not about testing the process of how water will get into the casks; the objective is to test what the effect of water ingress will be on the k_{eff} of the system if the fuel assemblies were to get into contact with water, irrespective of how water got into the cask. For the full process of how water will get into the cask, the reader is referred to: http://www.eurosafe-forum.org/userfiles/2_03_Eurosafe2010%203_Kilger%20(GRS).pdf. That is a subject on its own which is outside the scope of this project. From the neutron moderation theory, it is well-known that neutrons are born in the high energy range (MeV) [Duderstadt, *et al.*, 2010]. At such high energy range, it is very unlikely that they will induce fission when interacting with either fissile nuclides (^{235}U, ^{239}Pu and ^{241}Pu) or fertile isotopes (such as ^{238}U). However, it is far more likely that fast neutrons will undergo inelastic scattering with lighter moderator nuclei ($^{1}_{1}H$ and $^{12}_{6}C$) and slow down to the thermal energy range where they have a much higher probability of causing fission. During the slowing down process they may also leak out of the system or continue to diffuse until they are absorbed by either the fuel (^{235}U in this case) or moderator (B_4C-Al_2O_3 in the case of our model). As stated above, two accident scenarios have been investigated:

- flooding with freshwater and
- flooding with seawater.

These scenarios received a priority after the recent earthquake in Japan which led to the closure of the Fukushima Daiichi Nuclear Reactor. Considering that many nuclear power stations are very close to the sea for use in their cooling system, it was prudent that a study was conducted to determine what the effect of freshwater and sea water would be in the k_{eff} of the cask given that under accident conditions the cask can be filled with either of them. This

is particularly important for South Africa as Koeberg is on the edge of Atlantic Ocean and there are a few more nuclear power stations planned to use the same cooling medium. Two scenarios were run, one for the cask with seawater the other for freshwater. The results were compared on the basis of the change in k_{eff}.

5.3.1 Effect of water of different chemical composition on the k_{eff} of a system.

The comparison of the effects of the two media was based on the changes in k_{eff} with an increase in moderator temperature as well as the increase in enrichment in either case.

5.3.1.1 The neutron multiplication factor versus temperature

As shown in Table 5.2, seawater contains significantly more chemical elements than fresh water some of which some have very high cross-section for neutron absorption [Pidwirny, *et al.*, 2006; Duderstadt, *et al.*, 2010]. Chemical elements with significantly high microscopic absorption (σ_a) and scattering (σ_s) cross-sections only found in seawater and not in fresh water are chlorine (Cl) and bromine (Br). High neutron absorption cross-section will reduce the number of neutrons that participate in criticality and thus reduce k_{eff}.

To test the effect of temperature increase on the k_{eff}, the temperature was increased to 900K, which is very close to that recommended by the IAEA (IAEA, 2000). The IAEA requirement for analysis of containers of hazardous nuclear fuel materials like the Castor X/28 cask is that the analysis must include heat up to 800 °C (1073.15K) [IAEA, 2000] [Sprung, *et al.*, 2000; WNTI, 2010]. It will be noted the graph shows a number of changes in slopes which signifies transition in internal phase [Sprung, *et al.*, 2000].

The other physical property that is important, particularly to criticality is the logarithmic energy decrement (ξ) which gives an indication of the *number* of collisions required to slow a high-energy neutron to the thermal energy range, which can be calculated from Eqn (5.1) as follows [Duderstadt, et al., 1976],.

$$\xi = \overline{\ln E_0 - \ln E_{th}} = \ln \frac{E_0}{E_{th}} \qquad 5.1$$

where, E_0 and E_{th} refer to higher and thermal energies respectively.

The number n of collision required to thermalize a neutron from E_0 to E_{th} is given by

$$n = \frac{\ln \frac{E_0}{E_{th}}}{\xi} \qquad 5.2$$

Furthermore, ξ can be calculated as

$$\xi \approx \frac{2}{A + 2/3} \qquad 5.3$$

where A is the atomic mass of the scattering material. It will be noted from this that ($^{1}_{1}H$, $^{12}_{6}C$) always have higher ξ (ξ =1 and 0.158 for $^{1}_{1}H$, and , $^{12}_{6}C$). Stated otherwise, you will need a smaller number of collisions to reach thermal energy if light elements are used.

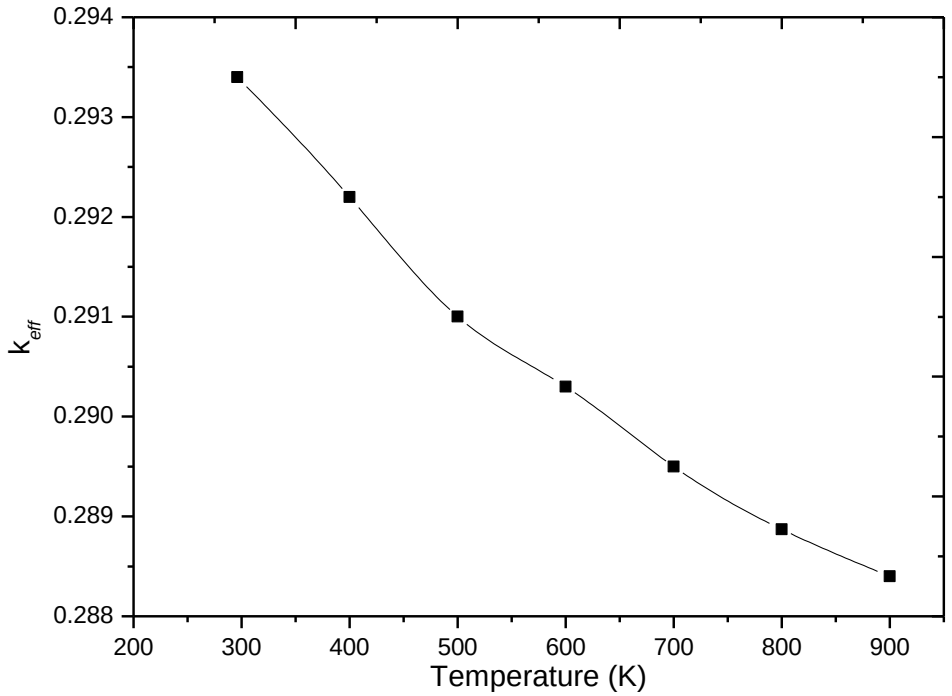

Figure 5.7: Effect of variation in Temperature on the k_{eff} : Dry Air (Present study)

Thus, although seawater contains carbon with $\xi = 0.158$ which should aid in slowing neutrons down to thermal range and thereby improve the chance of fissioning, this is overcome by the collective absorption from all other elements present.

The results in Figure 5.8 indicate that ingress of water regardless of whether it is fresh or seawater, it will result in an increase in k_{eff} relative to that of a dry cask shown in Figure 5.7. However, it is the water that has highest amount chemical impurities that will have the least increase in k_{eff}. Reading the k_{eff} at 296 K in Figure 5.8, it is noted that the k_{eff} of fresh water and seawater are respectively 0.9678, and 0.9369, whereas that of dry cask Figure 5.7 at the same temperature is 0.2934. This implies that the increase in k_{eff} due to fresh water ingress will result in a $\Delta k_{fw} = 0.9678\text{-}0.2934 = 0.6744$ while,Δk_{sw} due seawater will be 0.6435.

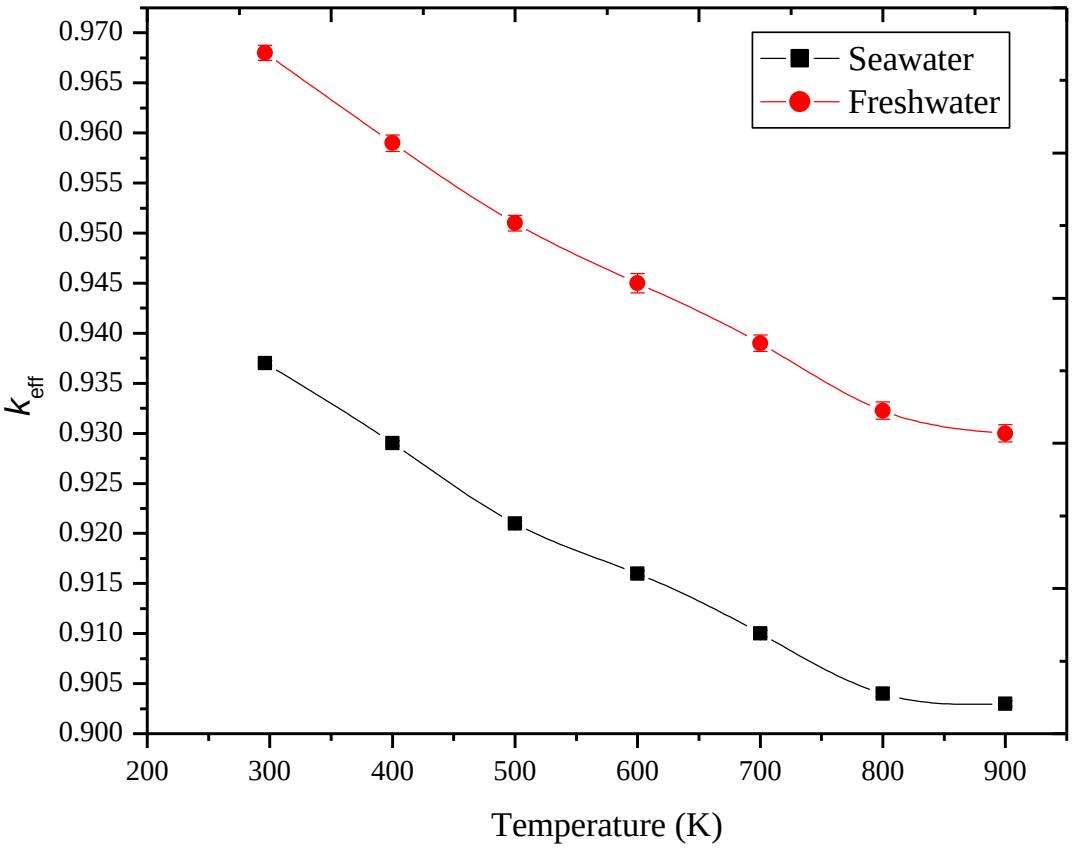

Figure 5.8: k_{eff} as a function of temperature: cask filled with water of three different chemical compositions (^{235}U = 4.4 wt%) [Leotlela, *et al.*, 2015]

Table 5.2: Physical properties of water that are important to nuclear criticality safety analysis (Present study)

Element	Seawater	Freshwater	Density		Cross-section					
Composition			$g.cm^{-3}$		barns			cm^{-1}		
chemical symbol	%			ξ	σ_a	σ_s	σ_t	Σ_a	Σ_s	Σ_t
O	85.85	88.89	0.0014	0.120	20	4.2	24.2	0.0	21	21
H	10.82	11.11	8.9[8]	1.00	0.33	38	38	1.7[16]	0.002	0.002
Cl	1.94	-	0.0032	0.0561	33.8	16	49.8	0.002	80[8]	0.003
Na	1.08	-	0.971	0.0845	0.525	4	4.53	0.013	0.102	0.115
Mg	0.1292	-	1.74	0.0811	0.069	3.6	3.67	0.003	0.155	0.158
S	0.091	-	2.07	0.0612	0.52	1.1	1.6	0.020	0.043	0.063
Ca	0.04	-	1.55	0.0492	0.44	3.0	3.44	0.010	0.070	0.080
K	0.04	-	0.87	0.0504	2.07	1.5	3.57	0.028	0.020	0.048
Br	0.0067	-	3.12	0.0247	6.7	6	12.7	0.157	0.141	0.298
C	0.0028	-	1.60	0.158	0.004	4.8	4.8	32[8]	0.385	0.385

[16] Value has been multiplied by 10^5 to effect a meaningful number

It is important to note that between 800 K and 900 K, water is in equilibrium with steam. Looking at the results presented in Figure 5.9, it is observed that, between 800 K and 900 K, the rate at which the k_{eff} decreases is much slower than earlier, that is, it is beginning to plateau. This may be ascribed to cladding failure, which is caused by either irradiation induced corrosion and/or temperature induced stress [Kononen, 2012]. Therefore, as a result of fuel cladding failure there will be ingress of water. This will result in extra moderation to an otherwise under-moderated system and thus will result in an increase of the k_{eff} as is shown in Figure 5.9. In addition, since the fuel will now be in contact with the moderator, which could be either steam or liquid water, it will be at the same temperature. As it was indicated in section 2.1.2.1, as the temperature increases the fuel undergoes several crystal structure transformations (refer to fig. 2.2). At 655 °C (938 K) the fuel changes from the orthorhombic (α) to the tetragonal (β) phase, and at 770 °C (1043 K) it changes from the β-phase to the γ-phase, which has a BCC structure.

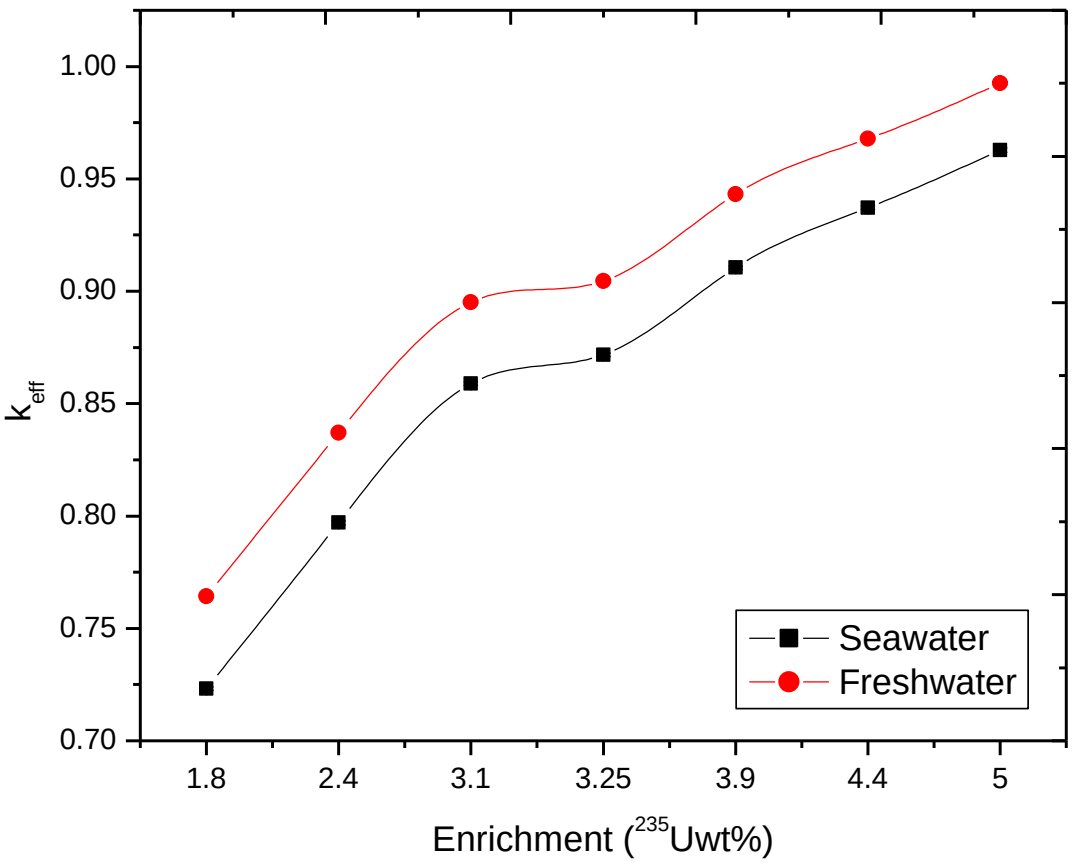

Figure 5.9 : k_{eff} as a function of enrichment: cask filled with water of two different chemical compositions (T = 296 K) (Present study).

Therefore, not only will the increase in temperature affect $k_{eff,}$ as a result of Doppler broadening, but also changes in crystal structure will by themselves have an effect on the k_{eff} as they change the diffusion coefficient (for neutrons) of that material (see fig. 2.4). This is to be expected since seawater contains a significantly higher concentration of salts in the form of chlorides (Cl) and bromides, which have high neutron absorption microscopic cross-section (σ_a).

5.3.1.2 The neutron multiplication factor versus Enrichment

Again for the same reason stated above the results in Figure 5.9 indicate that when two are compared on the basis of k_{eff} versus temperature, the increase in k_{eff} is much slower in seawater compared to freshwater.

5.3.1.3 Effect of increase in moderator density on the neutron multiplication factor.

In case of freshwater ingress, it is imperative to establish how change in moderator density will affect the neutron multiplication factor of the cask. To that effect, three different models were run at three different temperatures: 296 K, 600 K and 900 K with a view of determining what the effect of increase in moderator density would be in criticality. The enrichment on all of them was kept constant at 3.9 wt%. The results in Figure 5.10 show that as the water density increases, the k_{eff} will increase accordingly. In analysing this, it is important to note that the Castor X/28 cask and the PWR reactor core such as that found at Koeberg are heterogeneous systems in which the moderator is separate from the fuel.

The six factors discussed in section 2.4.1 affect a heterogeneous and a homogeneous system differently. The main factors which play role in this are the resonance escape probability and thermal utilisation factor as described in sections 2.4.1.2 and 2.4.1.3 respectively. As described in Section 2.4.1.1, in the heterogeneous system the flux in the fuel region will be different from that of the moderator region primarily because of the absorption rate of the fuel. This is further compounded by the fact that the volume of the fuel, moderator and poison will also be different in the two regions. Therefore, when the fuel temperature increases, the water moderator expands (resulting in a decrease in density) forcing a significant amount of water out of the reactor vessel or the cask whichever vessel is used.

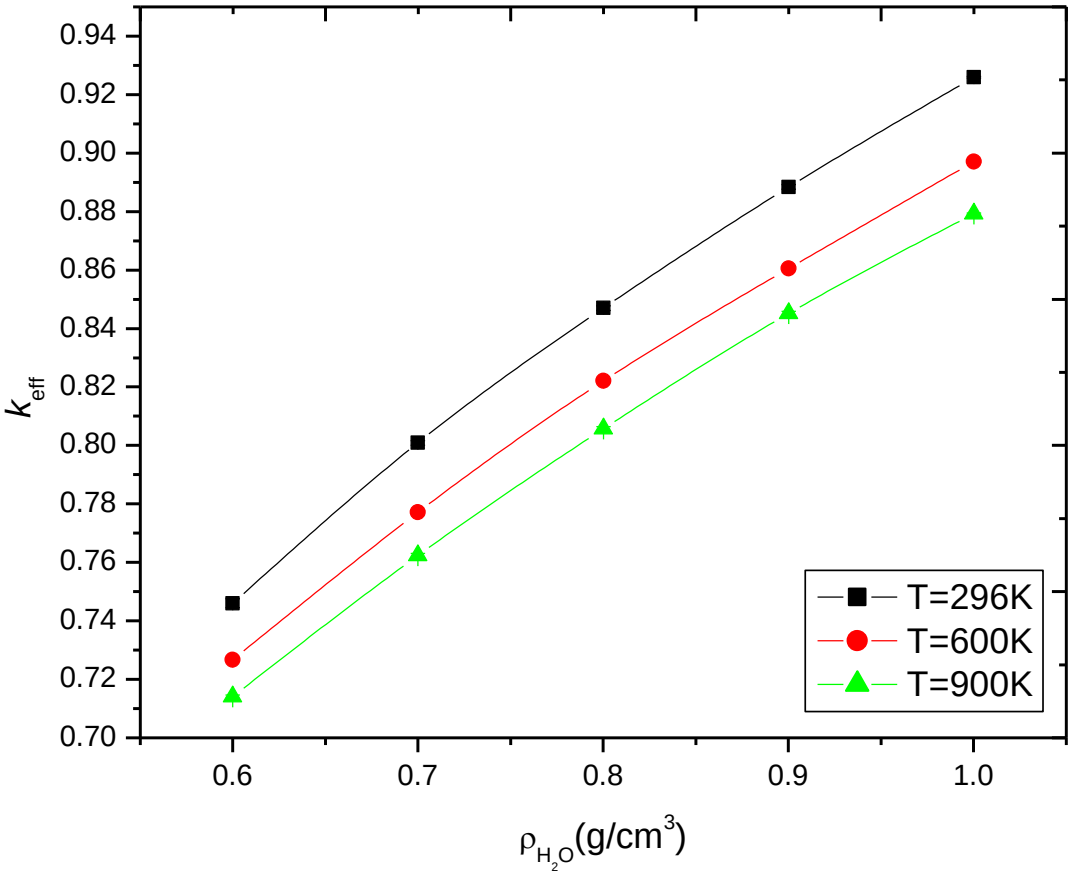

Figure 5.10: Effect of increase in moderator density on criticality [Leotlela, *et al.*, 2015]

This means that the atom density of the fuel will be significantly reduced thereby reducing the probability of a neutron being absorbed by the fuel. This will then result in the increase in the thermal utilisation factor as the temperature increases because the neutrons have a much better chance of reacting with the fuel. As a result of this, the temperature coefficient of the thermal utilisation factor will be positive [Duderstadt, *et al.*, 2010; Lewis, 2008] Secondly, it is a known fact that lighter nuclei (low atomic mass) such as hydrogen are much more effective in slowing down neutrons to thermal energy range compared to heavy nuclei, stated differently lighter nuclei need a fewer number of collisions to thermalize a neutron from 2 $x10^6$ MeV to 1 eV, compared to their heavier atomic mass counterparts [Duderstadt, *et al.*, 2010]. Hence, the higher the density of hydrogen per unit volume, the greater is the probability of scattering from which it can be inferred that the more collisions a neutron encounters with hydrogen, the higher will be the fission rate and subsequently the higher the criticality will be.

5.3.2 Comparison of fuel assemblies from different manufacturers.

If the nuclear reactor operator intends sourcing nuclear fuel from different fuel suppliers, it is imperative that both their physical and chemical properties are thoroughly analysed and a comparative study is performed to prevent any significant difference in any of their physical properties. If there is a difference at all, the significance of the difference must be ascertained and quantified and whether it will not pose any safety risk if they happen to be mixed in the core or cask should also be ascertained.

If there is a significant difference in the coefficient of thermal expansion of the fuel assemblies, there is a risk that they may expand at different rates and entangle one another, creating a huge safety risk when removing them from the core or cask which may result in a nuclear incident.

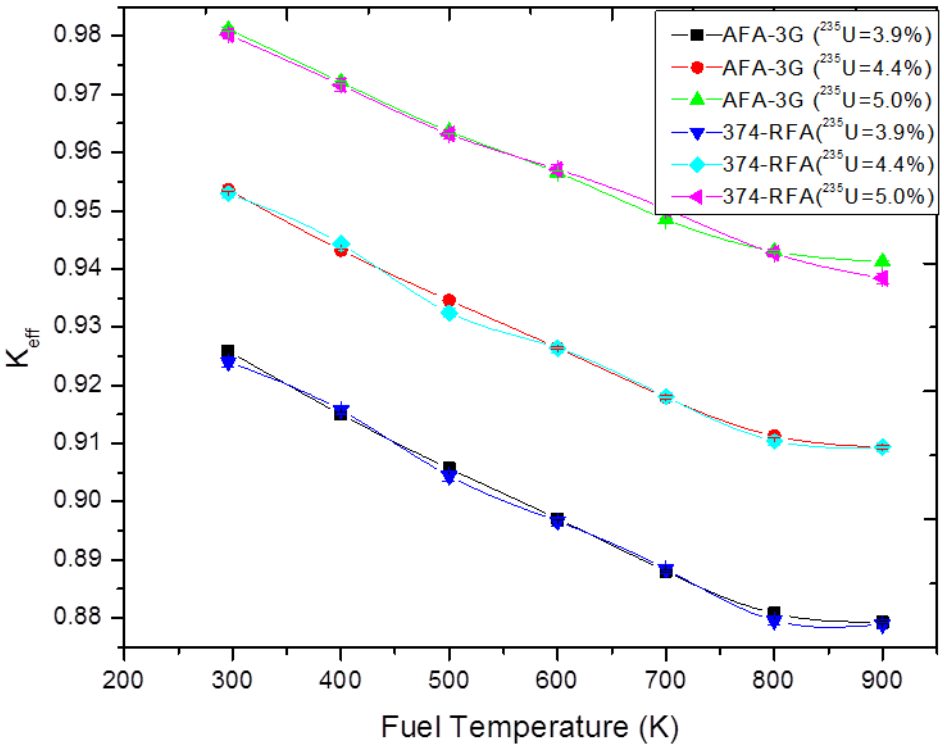

Figure 5.11: Comparison of 374-RFA and AFA-3G Fuel Assemblies (Present study)

That kind of study is a specialised field on its own and falls outside the scope of this thesis. The two fuel assemblies under study were supplied by Westinghouse and AREVA with fuel types 374-RFA and AFA-3G respectively. In this study their comparison was based purely on their nuclear criticality aspects with respect to increased fuel temperature.

The fuel temperature referred to in this research is the effective fuel temperature rather surface temperature T_s or the centreline temperature T_c which is a function of both of them. Their relationship to one another is given by [Radulescu, *et al.*, 2006]:

$$T_{\text{eff}} = T_S + 4/9\left(T_C - T_S\right). \tag{5.4}$$

The results in Figure 5.11 indicate that within the same enrichment levels e.g. 3.9% the change in fuel temperature had the same effect on criticality on both fuel assemblies.

The reason for the decrease in criticality as the temperature increases, is because in water-moderated systems, increasing the fuel temperature will result in an increase the resonance absorption by ^{238}U due to Doppler broadening. This implies that there will be a decrease in resonance escape probability of neutron which will result in a decrease in k_{eff}. Furthermore, as the temperature of water increases, its density decreases allowing more resonance energy neutrons to enter the fuel and be absorbed which contributes to an even further decrease in k_{eff} [Lewis, 2008; Duderstadt, *et al.*, 2010; Lamarsh, 2002].

Also, as expected at a constant temperature and burnup, the k_{eff} increases with an increase in the level of enrichment [Duderstadt, *et al.*, 2010].

This is because an increase in ^{235}U will lead to in an increase in the fission rate and hence the increase in criticality. However, the purpose of this exercise was not to prove the latter, but rather to determine whether Castor X/28F which is only licensed to a maximum enrichment level of 3.5% can be used for higher enrichments.

At the temperature of 296 K both fuel assemblies (refer to Figure 5.11) with an enrichment of 4.4 wt% and 5.0 wt% are already above the recommended regulatory limit of 0.95. This proves that the Castor X/28F cask cannot be used in fuel assemblies with enrichment higher than 3.9 wt%, which is in agreement with the design specification. The main factors which play role in this are the resonance escape probability and thermal utilisation factor as described in sections 2.4.1.2 and 2.4.1.3 respectively.

Table 5.3: Comparison of AFA-3G and 374-RFA

T(K)	k_{eff}					
	3.9 wt%		4.4 wt%		5.0 wt%	
	AFA-3G	374-RFA	AFA-3G	374-RFA	AFA-3G	374-RFA
296	0.9259	0.9240	0.9536	0.9530	0.9812	0.9803
600	0.8971	0.8966	0.9264	0.9264	0.9566	0.9571
900	0.8793	0.8789	0.9093	0.9094	0.9412	0.9384

As described in section 2.4.1.3, in the heterogeneous system the flux in the fuel region will be different from that of the moderator region primarily because of the absorption rate of the fuel. This is further compounded by the fact that the volume of the fuel, moderator and poison will also be different in the two regions.

Therefore, when the fuel temperature increases, the water moderator expands (resulting in a decrease in density) forcing a significant amount of water out of the reactor vessel or the cask whichever vessel is used. This means that the atom density of the fuel will be significantly reduced thereby reducing the probability of a neutron being absorbed by the fuel. This will then result in the increase in the thermal utilisation factor as the temperature increases because the neutrons have a much better chance of reacting with the fuel. As a result of this, the temperature coefficient of the thermal utilisation factor will be positive [Duderstadt, *et al.*, 2010; Lewis, 2008]

Secondly, it is a known fact that lighter nuclei (low atomic mass) such as hydrogen are much more effective in slowing down neutrons to thermal energy range compared to heavy nuclei, stated differently lighter nuclei need a fewer number of collisions to thermalize a neutron from 2 x10^6 MeV to 1 eV, compared to their heavier atomic mass counterparts [Duderstadt, *et al.*, 2010]. Hence, the higher the density of hydrogen per unit volume, the greater is the probability of scattering from which it can be inferred that the more collisions a neutron encounters with hydrogen, the higher will be the fission rate and subsequently the higher the criticality will be.

5.4 Misloading

5.4.1 The risk of misloading spent fuel casks

This section will study the abnormal operating condition of the spent fuel casks as result of misloading which can happen as a result of poor spent fuel management such as inadequate record keeping of assembly power history, enrichment, out-of-reactor cooling period etc.

Misloading of underburned fuel assemblies results in an increase in reactivity. The magnitude of increase depends on several factors but the most common ones are; power history of the fuel assembly, post-irradiation decay period, fuel enrichment, assembly burnup, assembly position in the reactor core and the amount by which assembly is less than the minimum burnup value for loading acceptance, and the latter is the most important factor of all of them [Wagner, 2008].

There are therefore, a number of combinations of misloading that can be evaluated, which may be classified into the following categories [Wagner, 2008];

- Scenario 1: The effect of misload involving underburned fuel, where the degree of under-burn can range from 1% to about 90% underburned.
- Scenario 2: The effect of misloading involving fresh fuel with enrichment (^{235}U) levels varying from 2, 3, 4 or 5 wt%.
- Scenario 3: The effect of misload involving multiple fuel assemblies in the above two scenarios.

The study of the probability of misload falls outside the scope of this research as such no attempt will be made to quantify scenario 1, however where necessary will take credit of applicable probabilistic risk assessment (PRA) results and apply them without deriving them. Some such values which are particularly important in this study are those used in Wagner's [Wagner, 2008] study in which it is estimated that the probability of a single misloading can range between 10^{-3} and 10^{-5} for a large cask. Furthermore, according to Wagner if it is assumed that multiple misloading events in a single cask are independent, then the probability of misloading *n* fuel assemblies can be estimated by raising the probability of a single misloading to the power *n* [Wagner, 2008].

In this thesis scenario 2 in combination with scenario 3 involving reactivity axial burnup will be evaluated. This is primarily because there has already been extensive research about scenario 1 where reactive axial profile is not involved.

5.4.1.1 Application of the loading curve to mitigate the consequences of misload

The misloading events are based on castor X/28 F where there is uniform fuel enrichment throughout fuel rod, hence much more reactive axial profiles and only major actinides nuclide sets were used. When spent fuel are to be loaded into the spent fuel cask, the decision whether they are acceptable or not acceptable for loading is based on the loading curve of the cask (to be discussed in detail in 6.4 a), b), 6.4.1 and 6.4.2. The loading curve may therefore, be described as a representation of the combination of burnup and the initial enrichment that corresponds to the limiting value of the k_{eff} for a given configuration such as a cask or a spent fuel pool. Thus the fuel assembly with insufficient burnup (i.e. with lower burnup than the limiting burnup obtained from the loading curve are not acceptable for loading. Therefore, the further below the limiting burnup value the misloaded cask is; the more critical the situation of exceeding the regulatory limit becomes.

5.4.1.2 Compilation of STARBUCS Misload Input File

If one wants to perform misload calculation involving a fuel assembly of either a lower burnup or fresh fuel into a cask containing high burnup fuel assemblies using SCALE, one will need to have two separate fuel assemblies at two different burnups in the model. However STARBUCS can only use one ARP library in a STARBUCS calculation. Consequently, one cannot put two different fuel assemblies with different power histories and decay period into the same model.

Thus in this thesis a mechanism of working around this STARBUCS limitation was found which involved performing STARBUCS calculations on all fuels as though they were the same. Then the CSAS6 model was copied out of the STARBUCS output file and modified the CSAS6 input file to use as an additional fuel type, including addition of fuel composition for the additional fuel type. This needed an additional fuel rod and fuel assembly model to be created for the misloaded assembly and placing the misload assembly in the array in the cask, finally gave the intended results.

Starting from STARBUCS model which was run for actinides before, the following changes were made as required by STARBUCS to create a Reference input file:

- Changed the mixtures in the unit cell model to use mixtures 1 (fuel) , 2 (Cladding), 3 (Moderator) and 0 or 4 (Gap)

- Then in the same input file, (call it reference input file), the following were added: nax and axp inputs to define the 18 fuel mixtures:

- nax=18 and axp= 0.649 1.044 1.208 1.215 1.214 1.208 1.197 1.189 1.188 1.192 1.195 1.190 1.156 1.022 0.756 0.614 0.481 0.284 end). It is important to note that the axp array added may not be appropriate for other reactor/fuel types.

- Added the shell command at the end of the input file to save the csas6 input created by STARBUCS. The shell command is as follows;

  "=shell copy sysin2 "%RTNDIR%\csas6r0.inp end"

- The model was then executed and produced a new csas6 input file which is saved as csas6r0.inp and shows all nuclides concentration after the Reference input file was run .

- From this (i.e. csas6r0.inp) a new input file (see APPENDIX 7), csas6r1, was created by modifying csas6r0.inp as follows:

  - Added mixtures 21 (92234=0.040 wt%, 92235=2.4 wt%, 92236=0.02 wt%, 92238=97.53 wt%), 22 (Zirc2) and 23 (H_2O) for fresh fuel rod compositions

  - Added a new first lattice cell in the read cell data block for the fresh fuel rod which is as follows: lattice cell square pitch fuelr=0.4096 21 gapr=0.418 0 cladr=0.475 22 hpitch=0.63 23 end

  - Created unit 21 (just above unit 1) to model a single fresh fuel rod

  - Added unit 24 which is a fresh fuel assembly and a copy of unit 4 where array 1 is unit 4 is replaced by array 2 in unit 24.

  - Replaced the first "hole 4" with "hole 24" in unit 5. This replaces one burned fuel assembly with a fresh fuel assembly which is a misloaded fuel.

- Added array 2 in the array data. Array 2 is a copy of array 1 with the fuel rods changed from unit 1 to unit 21.

The misloaded fuel assembly was moved around the cask to find the worst case misload [Leotlela, *et al.*, 2015]. The aim of the analysis was to determine the following;

- How the location of misloaded fuel assemblies will affect the k_{eff} of the system.
- What the effect of multiple fuel assembly misload would be on the k_{eff} of the system.

To determine how the location of misloaded fuel assemblies would affect the k_{eff}, of the system, three cases of single misloaded fuel assemblies at different locations of the casks were investigated.

To determine the effect of multiple fuel assembly misload on the k_{eff} of the system, three different cases were investigated which were categorised as;

- Single FA misload,
- Two FA misload and
- Three FA misload.

Each case was misloaded as per Tables 5.4, 5.5, and 5.6 respectively. The k_{eff} of the three fuel assemblies were then compared with those of a single FA located at location #1 of Table 5.4.

Each case was investigated at different fuel enrichment of the fresh fuel. The results indicate that if the misloaded cask is near the centre of the cask, it will exhibit the highest k_{eff} for enrichments above 2.5 wt%. For enrichments below that, casks further away from the centre will exhibit the highest k_{eff}. The increase in k_{eff} in fuel assemblies near the centre is a function of the number of fuel assemblies that surround the misloaded fuel assembly and the distance between misloaded fuel assembly and those which surround it.

Table 5.4: X-Y Co-ordinates of three cases of single misloaded fuel assemblies [Leotlela, *et al.*, 2015]

Case #	X	Y	Comment
1	16.25	16.25	Inner Source
2	46.95	16.25	Inner Source
3	94.90	0.00	Outer Source

Take for example the misloaded FA in Figure 5.12 located at (16.25; 16.25) and compare it with those at (46.95; 16.25) and (49.9;0) . The FA at (16.25; 16.25) is surrounded by four (4) fuel which are also very close to the misloaded FA compared to the FA at (46.95; 16.25) and (49.9; 0) which are only surrounded by 2 FA. In addition to having fewer neighbouring fuel assemblies the FA at (49.9; 0) its nearest neighbours are further away compared to those of the other two misloaded fuel assemblies [Leotlela, *et al.*, 2015]. Apart from being far from its neighbouring fuel assemblies, the number of neutrons being transported to it is further reduced by the cast iron material that surrounds it, adding to the decrease in k_{eff}.

The fuel assembly with more neighbouring fuel assemblies close-by has a much greater chance of interaction with neutrons from neighbours than if it had fewer and are far apart, hence the difference in k_{eff} [Leotlela, *et al.*, 2015].

Table 5.5: Co-ordinates of two-misloaded fuel assemblies [Leotlela, *et al.*, 2015]

Location #	X	Y
1	16.25	16.25
2	-16.25	16.25

Table 5.6: Co-ordinates of three misloaded fuel assemblies [Leotlela, *et al.*, 2015]

Location #	X	Y
1	16.25	16.25
2	-16.25	-46.95
3	-16.26	16.25

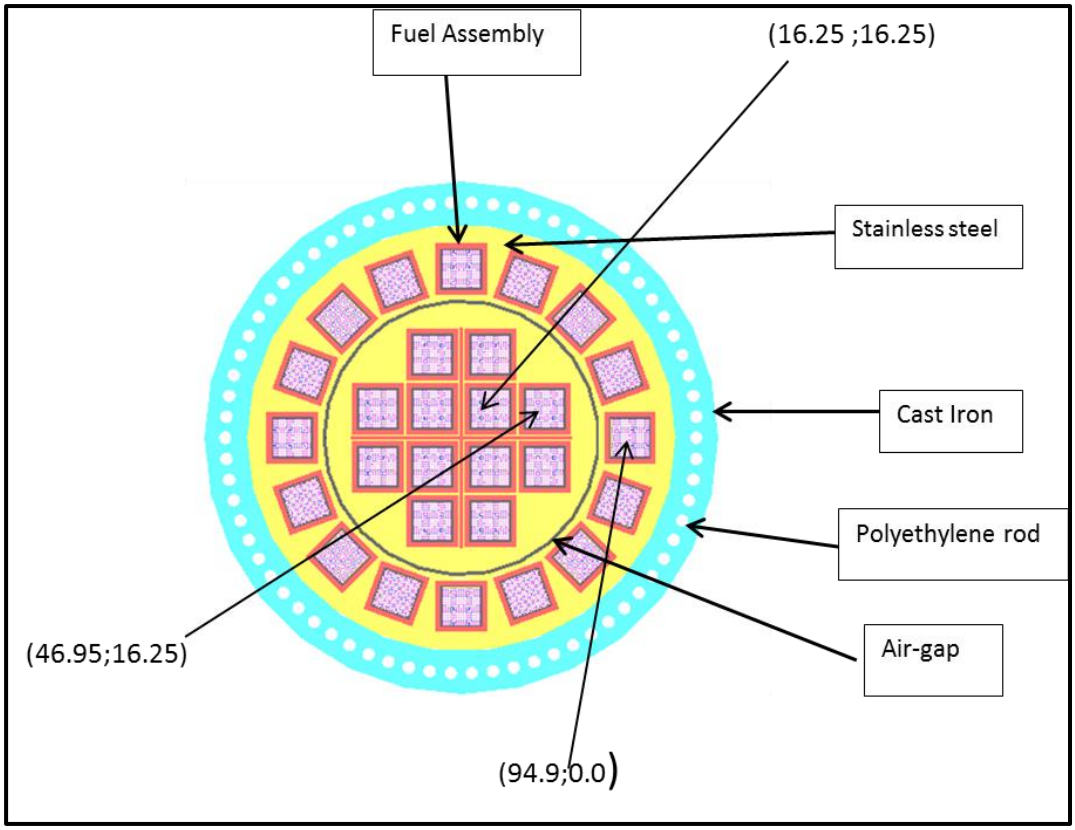

Figure 5.12: Cross-section of the Castor X/28 cask showing misloaded fuel assemblies [Leotlela, *et al.*, 2015].

When there are multiple fuel assembly misloaded, the results indicate that the k_{eff} of the system will increase with an increase in the number of misloaded fuel assemblies. Therefore, as indicated in Figure 5.13 the cask with three misloaded fuel assemblies will have a higher k_{eff} than with two misloaded fuel assemblies which in turn will be higher than that of a single misloaded FA.

However, according to Figure 5.14, that depends on the combination of locations of misloaded fuel assemblies and the number of misloaded fuel assemblies, for example when;

1. two misloaded fuel assemblies both located near the centre of the cask (16.25,16.25) will yield a higher k_{eff} than the same fuel assemblies located in the periphery (94.90,0) [Leotlela, *et al.*, 2015].
2. one of the two misloaded fuel assemblies is located near centre (16.25,16.25) and the other in the periphery (94.90,0.0), the k_{eff} of such a combination will be lower than that of the system where both fuel assemblies are in the centre, i.e. case 1) above [Leotlela, *et al.*, 2015]..

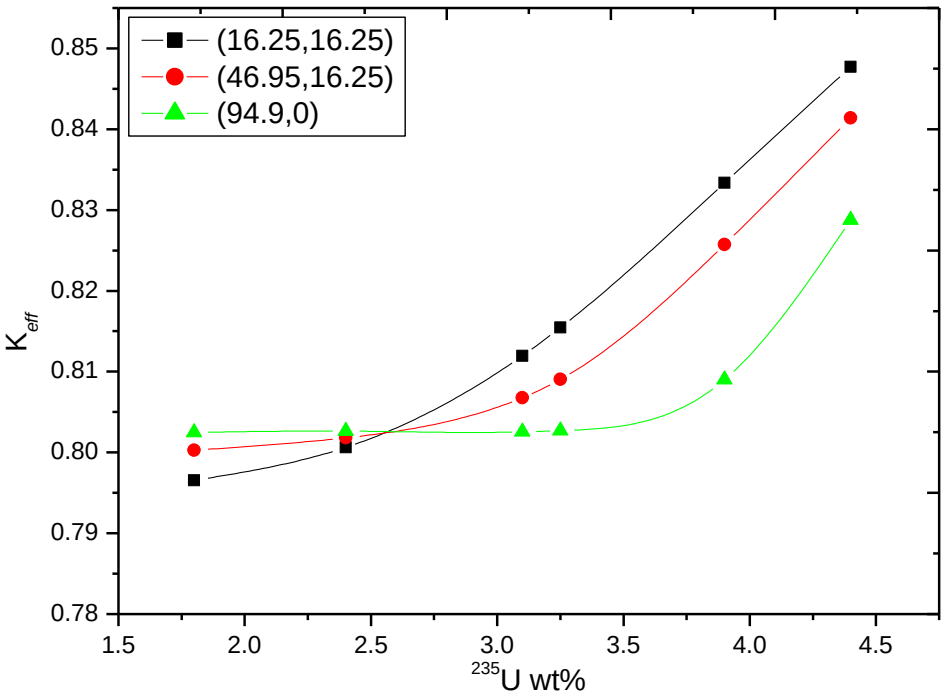

Figure 5.13: Effect of the location of a single misloaded Fuel Assembly on the k_{eff} of the [Leotlela, *et al.*, 2015]

- One of the two is located near the centre of the casks (16.25, 16.25) and the second one in the middle between the centre and the periphery (46.95, 16.25), the k_{eff} will be higher than in case 2) above [Leotlela, *et al.*, 2015]..
- Both misloaded fuel assemblies are in the periphery, they will have the lowest k_{eff} of all combinations [Leotlela, *et al.*, 2015].

For the physics behind the change in k_{eff} with the location and the number of fuel assemblies the reader is referred to the discussion on spatial self-shielding and resonance self-shielding as described in sections 4.3.2.1 and 4.3.2.2 respectively. The other equally important factor is the end-effect in the fuel assemblies given that in this research the fuel assemblies have a uniform enrichment level. Since the initial enrichment fuel assemblies is 2.4 wt%, it implies the top and bottom of the fuel assemblies will stay at about the same enrichment while the centre is depleted because of the build-up of fission products.

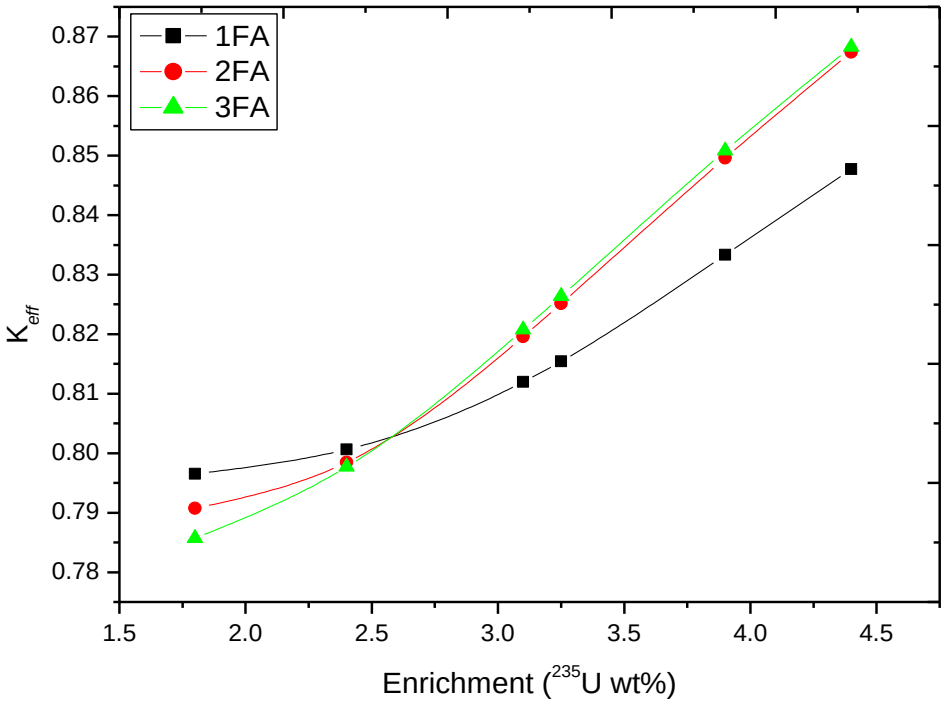

Figure 5.14: Multiple misload where two misloaded FAs are in the centre [Leotlela, *et al.*, 2015]

Therefore, when a fresh fuel is misloaded into the cask, the end-effect will have the greatest contribution to the systems k_{eff}, particularly around 2.4 wt%. As a result of this the graphs (Figure 5.13 and Figure 5.14) in the region around 2.4 wt% are swapped around. The reason for the change in k_{eff} with misloaded fuel assemblies is because the misloaded fuel assemblies are fresh which by definition have not been irradiated and therefore very little fission products with parasitic absorption are produced. Because of the reduced parasitic absorption, there will be an increase in k_{eff}.

5.4.1.3 Probability of misloading the cask

It is not the objective of this project to perform a complete probabilistic risk assessment (PRA) of every event that takes place during the lifespan of the fuel assembly, and that is why no PRA analysis was performed in earlier sections. However, because of the potential consequences associated with misload, its probability calculation has been included in the analysis. The PRA was performed using the computer aided fault tree analysis (CAFTA) code developed by EPRI [EPRI, 2007].

5.4.1.3.1 The importance of a clear and unambiguous operating procedure for the cask loading process

The cask loading process is developed by the fuel engineering department who have the record of what the burnup and decay period of each fuel assembly is in the spent fuel pool, and the expected location in the cask. The process varies from power station to power station, as such a generic loading process was used in this calculation to illustrate how misloading can occur [Knudsen, 2003],

- The appropriate engineering department at the plant will determine which fuel assembly will be loaded into the cask, taking into consideration the design specification of the cask and conformance of fuel assemblies to the design specification. Important factors which determine whether the fuel assembly can be loaded are the burnup, decay period and initial enrichment [Knudsen, 2003].
- A review is performed to verify that the appropriate assembly was selected.
- A fuel move sheet is generated, which is a standard form containing the alphanumeric grid location of the fuel assembly to be loaded, its serial number, final burnup and date on which it was put in the spent fuel pool [Knudsen, 2003].
- A physical inventory using an underwater camera is performed to verify that the serial numbers specified in the sheet are the same as those in fuel assembly.
- Transfer the fuel assembly from the spent fuel pool to the cask. This will consist of verifying that a fuel assembly from the correct grid location of the spent fuel pool is moved to the correct location of the cask.
- Once the cask is fully loaded an independent reviewer (nuclear fuel engineer) will verify that the correct fuel assemblies have been loaded into the cask.

This is summarised in Figure 5.15

The cask loading process described by Figure 5.15 was modelled using an event tree methodology using CAFTA code. An event tree is a systematic process for identifying all possible accidents sequences that can occur as result of an initiating event. A sequence in this context refers to a series of successes and failures of top level events of the event tree. The event tree consists of top level events that are systems or activities relied upon to bring about the desired outcome. The up-branch indicates a *success* while the down-branch indicates the *failure* of the top event.

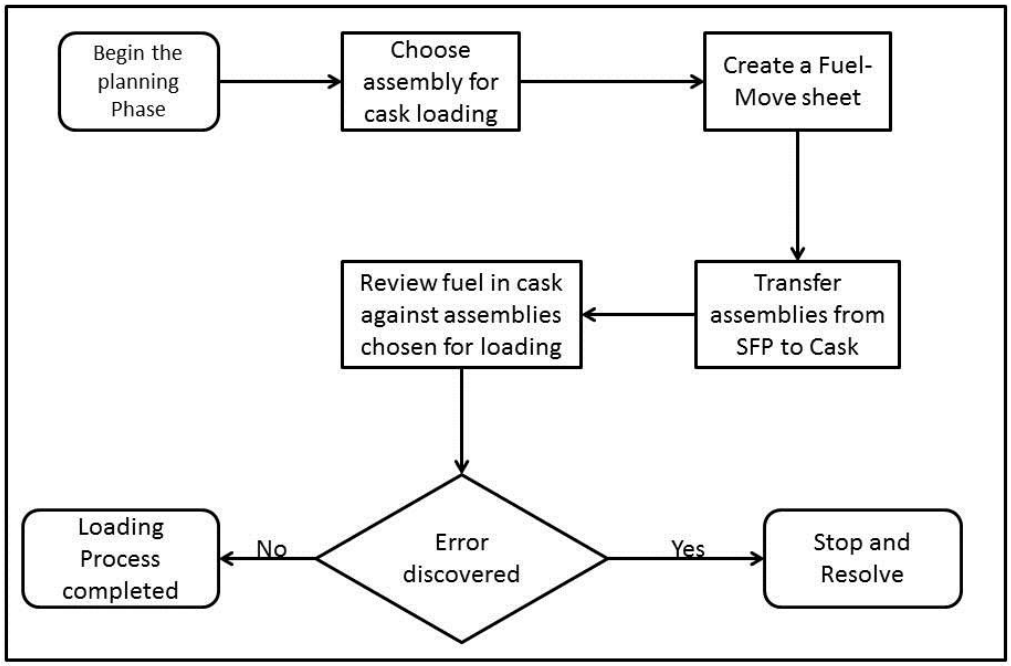

Figure 5.15 Generic dry cask loading activities [Knudsen, 2003**]**

Table 5.7 Summary of Human Error Probabilities used in this calculation [Knudsen, 2003].

Basic Event Name	**Mean Probability**
Choose Assembly to be loaded	4.84×10^{-3}
Move-sheet	4.84×10^{-3}
Fuel Transfer	8.70×10^{-3}
Final Review	1.61×10^{-2}
Independent Review	1.61×10^{-2}

The Human Error Probabilities (HEP) used in this study were taken from generic data published by the Electric Power Research Institute (EPRI) and other references [EPRI, 2008; EPRI, 2002; Knudsen, 2003] and are summarised in Table 5.7. It is important to note that the mean probabilities listed in this Table refer to the likelihood of failure of each individual activity with the loading process. Combining the failures to perform each of these steps yields the likelihood of misloading one or multiple assemblies within the cask. The event tree used in the analysis of misload events in this project is indicated in Figure 5.16. It is observed from

the event tree that multiple misloads have a higher probability of occurrence (4.84×10^{-3}) than a single misload.

This is due to common cause failure which increases with the number fuel assemblies. It has been observed that of the single misload that occurred, the probability due to error in the move-sheet which resulted in the incorrect fuel assembly being loaded in the cask and the error not being detected was higher ($2.22x10^{-6}$) than if the error was detected ($1.24x10^{-6}$).

Only sequences ending with single misload or multiple misload have been studied in this research. Each of the sequence of the event tree may be described as follows [Knudsen, 2003; EPRI, 2008];

- Sequence 1: Assemblies were correctly chosen, the move-sheet properly generated and all assemblies were correctly loaded.
- Sequence 2: Assemblies were correctly chosen and the move-sheet properly generated, but the fuel transfer error led to an incorrect fuel assembly being loaded into the cask. However, the error was identified in the final review.
- Sequence 3: Assemblies were correctly chosen and the move-sheet was properly generated, but a fuel transfer error led to an incorrect fuel assembly being loaded into the cask. The error was identified in the independent review.

Figure 5.16: Event tree for determining the likelihood of misloading the cask (Present study)

- Sequence 4: Assemblies were correctly chosen and the move-sheet was properly generated, but a fuel transfer error led to an incorrect fuel assembly being loaded into the cask. The error was not identified in the final review or independent review. A single assembly was misloaded.
- Sequence 5: Assemblies were correctly chosen, but error in the move-sheet led to an incorrect assembly being loaded. The error was identified in the final review.
- Sequence 6: Assemblies were correctly chosen, but an error in the move-sheet led to an incorrect assembly being loaded. The error was identified in the independent review.
- Sequence 7: Assemblies were correctly chosen, but an error in the move-sheet led to an incorrect assembly being loaded. The error was not identified in the final review or independent review. A single assembly was misloaded.
- Sequence 8: Assemblies were incorrectly chosen. Multiple assemblies were misloaded.

5.4.1.4 Comparison of Single versus Multiple Misload

According to EPRI in 2009 there were approximately 52000 fuel assemblies loaded into 1200 casks. As a result of this huge number of fuel assemblies being moved around, there was potential for misload [EPRI, 2002; EPRI, 2008]. Hence a study was launched determine the probability of misload of multiple fuel assemblies compared to a single misload.

If it is assumed that misloads are independent events and that multiple misloads occur as a result of multiple fuel transfer errors, rather than due to choosing fuel assemblies, then the probability of multiple misloads can be obtained by calculating the probability of x misloads in n trials given a misload probability of p. The single fuel movement transfer probability of $2.73X10^{-4}$ gives an error of probability of $8.70x10^{-3}$ per cask [EPRI, 2008; EPRI, 2002; Knudsen, 2003]. Thus, the probabilities for one to five independent misloads calculated using the same methods are summarised in Table 5.8. These must however be read in context taking into consideration that only the effect of the presence or absence of the reviews are taken into consideration and no other factors, and is the basis on which the event tree above Figure 5.16 was developed.

Therefore, because from Figure 5.16 multiple misloads have a higher probability of occurrence than single misloads, and the fact that they have higher k_{eff} than single misloads; the bounding accident scenario will, therefore, be where multiple fresh fuel assemblies are misloaded near the centre of the cask.

Table 5.8: Probability of Independent Multiple Misload [Knudsen, 2003].

	Number of misloads from fuel Transfer Errors				
	1	2	3	4	5
Without Final Review	8.66×10^{-3}	3.67×10^{-5}	1.00×10^{-7}	1.98×10^{-10}	3.03×10^{-13}
With Final Review	1.39×10^{-4}	5.91×10^{-7}	1.61×10^{-9}	3.19×10^{-11}	4.88×10^{-15}
With both Reviews	2.25×10^{-6}	9.50×10^{-9}	$2.60\text{Ex}10^{-11}$	5.14×10^{-14}	7.86×10^{-17}

CHAPTER 6

6 BURNUP CREDIT ANALYSES Effect of burnup on the neutron multiplication factor

As part of this research an analysis was performed to determine the effect of burnup on the k_{eff} using various burnup credit nuclide sets. The results obtained in this study shown in Figure 6.1 indicate that between 20 and 25 GWD/MTU there is an increase in k_{eff} **[**Leotlela, *et al.,* 2015**]**. This because it is too early in the cycle of the fuel, no fission products have been generated yet. Therefore because the material density of the fuel is higher than that of fission product there is an increase in k_{eff} **[**Leotlela, *et al.,* 2015**]**. From 25.8 GWD/MTU there is a sturdy decrease in k_{eff} as burnup increases **[**Leotlela, *et al.,* 2015**]**. This is consistent with the results in Figure 6.2 of a similar study conducted at Oak Ridge National Laboratory [Radulescu, *et al.,* 2008].

In addition to that, the results confirm findings that major actinides will have the lowest decrease in k_{eff} while major actinides + principal fission products will have the largest decrease. This further confirms that when burnup increases, it will result in an increase in the yield of some fissile nuclides such as ^{239}Pu and ^{241}Pu which will increase the k_{eff} while others like ^{155}Gd will tend to decrease it.

The decrease in the k_{eff} beyond 25.8 GWD/MTU which is the inflexion point is due to the presence of principal fission products: ^{243}Am, ^{237}Np, ^{99}Tc,^{133}Cs, ^{143}Nd ^{145}Nd, ^{147}Sm, ^{150}Sm, ^{151}Sm, ^{152}Sm, ^{151}Eu, ^{153}Eu, ^{155}Gd which were not present in the beginning of the cycle **[**Leotlela, *et al.,* 2015**]**. If the fuel burnup is increased beyond the design limit of the fuel assembly such as in thermal power uprates, there is a risk that the fuel cladding will begin to show signs of failure (due to radiation induced brittle fracture etc.) around the top limit of its burnup which for most of the present fuel types is in the region of 40-50 GWD/MTU.

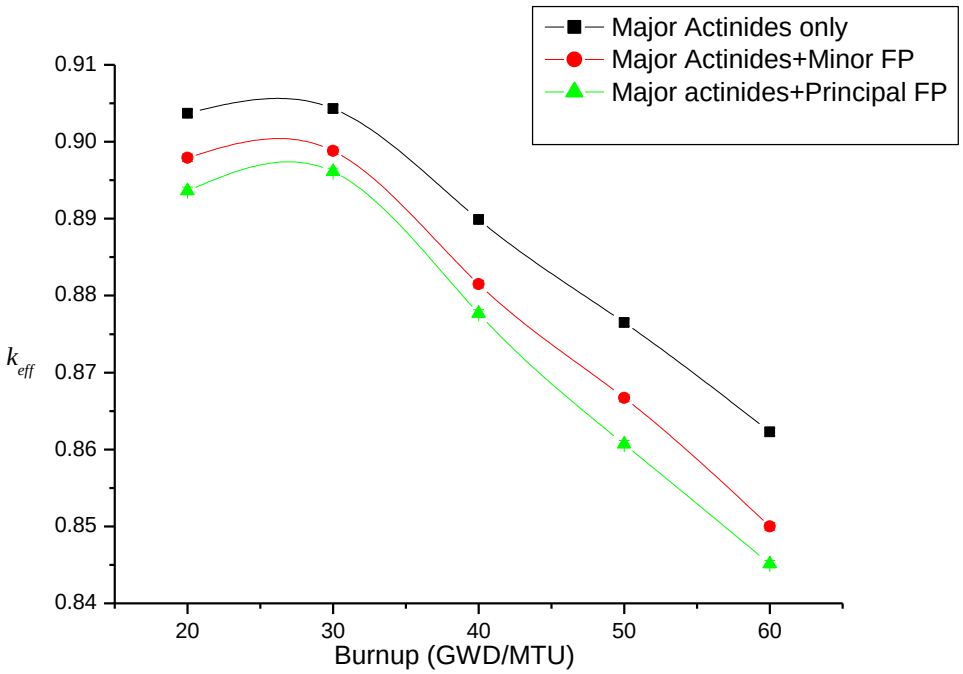

Figure 6.1: Comparison of k_{eff} of three burnup credit nuclide sets on the basis of Burnup [Leotlela, *et al.*, 2015]

Above this range, the periphery of the fuel pellet will have increased so much due to the *Rim Effect* that it will exert so much pressure against the cladding material that it will eventually lead to the fuel-cladding mechanical interaction (FCMI) between the pellet and the cladding. Given that the FCMI occurs round about 50 GWD/MTU [Lamarsh, 2002; Matzke, 1996; Matzke, *et al.*, 1997], this will eventually result in cladding failure that will lead to water ingress. As a result of that, the k_{eff} will then start to increase.

It has also been observed that nuclear criticality and premature cladding failure are not the only concerns on the increase in burnup, which will have a negative impact in thermal power uprates. Others include an increase in radiation levels and increased decay heat generation [Gauld, *et al.*, 2000; Broadhead, *et al.*, 2000; Broadhead, *et al.*, 1995] which are likely to be of great concern if thermal power uprates proceed without proper plant modification [Gauld, *et al.*, 2000]. Therefore a thorough study will need to be performed to determine the viability of thermal power uprates in the current design. Information gathered through this study indicates that shielding, nuclear criticality as well as premature component failure will need to be investigated thoroughly if future problems are to be avoided.

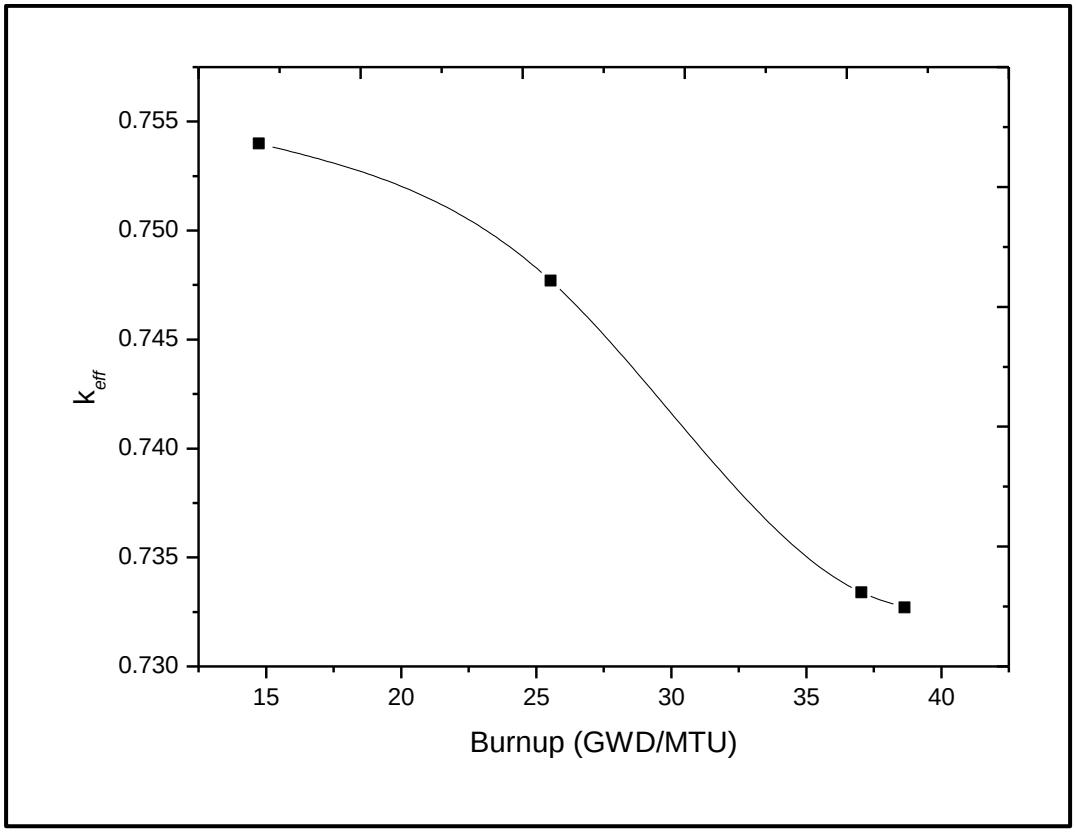

Figure 6.2 : Effect of Burnup in Criticality [Radulescu, *et al.*, 2008]

Burnup credit[17] plays a very important role in Criticality Safety Analysis in a sense that if the fuel is analysed as fresh fuel without taking credit for burn-up, there is usually a certain degree of conservatism built into the calculations which often results in over-estimation of k_{eff} and the corresponding margin, for example the distance between neighbouring spent fuel assemblies or absorber thickness needed to prevent criticality. If however, burn-up credit was taken into consideration, there could have been less distance/thickness needed to achieve the same criticality. Thus the application of burn-up credit often results in the saving of storage space allowing for more spent fuel to be stored in same size of the storage by removing over-conservatism associated with analysing spent fuel as fresh fuel, and at the same time meeting the sub-criticality requirement of safe storage of the fuel [P.Cousinou, 2001; Withee DE, 2000; Parks, *et al.*, 2006; Pesic, *et al.*, 1997].

[17] The phenomenon whereby credit is taken for the reduction in reactivity/criticality as a result of fuel burnup.

While burnup credit plays such an important role in criticality, not every burnup credit nuclides contributes the same towards burnup credit. As a results burrnup credit nuclides are grouped into three nuclide sets whose nuclides are described in Section 3.3.2.2.

4. Actinides-only burn-up Credits
5. Actinides + Minor Fission Products burn-up Credits
6. Major Actinides + Principal Fission Products burn-up credits

As shown in Figure 6.3, relative to fresh fuel, the major actinides only burnup credits reduce criticality quite substantially compared to fresh fuel. It is however still very conservative compared to the other two sets: Major Actinides + Fission Products and Major Actinides + Principal Fission Products.

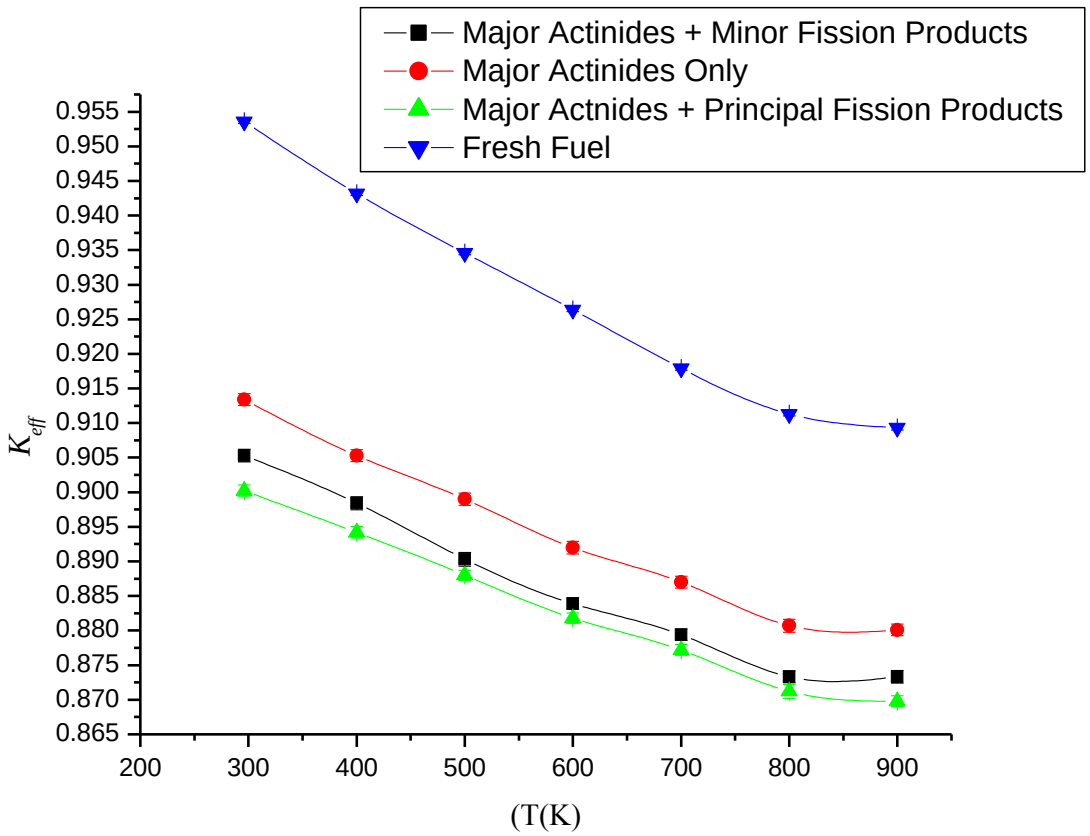

Figure 6.3: Comparison of burnup credits obtained from different sets of nuclides [modelled at BU=40 GWD/MTU and ^{235}U= 4.4 wt%]

According to Parks [Parks, *et al.*, 2001], in the USA authorisation to conduct research on burnup credits was given as far back as 2001 by the US Nuclear Regulatory Commission [NRC)] through the issue of the Interim Staff Guidance 8 (ISG8).

Since then the application of burnup credits for Major Actinides has been accepted for use in Transportation and Storage Cask. In South Africa it is uncertain whether credits for burnup of any nuclide are acceptable or not, however, in countries against which South Africa benchmarks its nuclear licensing strategies, such as the US and UK the application of Major Actinides is often preferred over other nuclide sets because of the amount of safety margin it allows the licensee before the regulatory limit of 0.95 is reached [IAEA, 2014]. Therefore, conservatism is the main reason why many nuclear regulators around the world have only accepted Major Actinides only burnup credits to be used in criticality safety analysis.

Because of the lack/absence of NNR position on burnup credit analyses, the licensees (Koeberg and NECSA) are often uncertain whether to take credit for burnup or not, and if so what nuclides sets to consider. Burnup credit analysis using Major Actinides + Principal Fission products on the other hand will need no additional countermeasures to prevent nuclear excursion because they decrease the k_{eff} of a system to such low levels that there is no additional nuclear criticality countermeasure needed other than burnup credits to prevent the system from being supercritical. This is one burnup credit scenario that the nuclear regulators are not interested in since it puts far too much risk on the system. However, for the licensee, this would be a much better option since they can put as many casks or fuel assemblies in as small a building as the system allows, thus saving the cost of transportation or of storage. As a result there will be more room for additional fuel assemblies if needed compared to Major Actinides. Calculation using data from Figure 6.3 at T = 296 K shows that relative to fresh fuel, the Δk_{eff} due to major actinides, major actinides + minor fission products and that of major actinides + principal fission products are; 0.0507, 0.0606 and 0.1193 respectively. According to Wagner, these translate to a storage space saving of 5.167%, 6.176% and 12.159% respectively [Wagner, 200; Wagner, 2006].

6.2.1 Relationship of the burnup and the position of the fuel assembly in the reactor core.

A PWR under consideration is a cylindrical reactor core whose volume is defined by the radius of a cylinder and its height. The volume V of the core is given by the equation of the volume of a cylinder:

$$V = \int_{a}^{b} 2\pi x f(x) dx \tag{6.0}$$

where x is the radius and $f(x)$ is the height of the cylinder. This in turn defines the power density (in units of MW/m^3 or MW/MTU) of the core. The power density and therefore, distribution of neutron flux in the core is not even. Depending on the loading pattern of the core, the type of control rods used, whether they are in or withdrawn, generally the central region will have a higher neutron flux than at the periphery partly because of neutron leakage (Duderstadt, *et al.*, 1976). Thus the fuel assemblies located in the centre of the core or the cask experience a much higher reaction rate because of the high neutron density in that area than the fuel assemblies in the edges are exposed to. Hence when the cask is designed, it is designed for a specific reactor design and for a specific burnup range. Therefore, this implies that no two dissimilar reactors can have exactly the same cask or no two similar reactors with different burnup can have the same cask. In that respect, then every cask is designed for a specific range of burnup, enrichment level and for a specific type of fuel [Taviv, 2013].

Thus a number of fuel assemblies located in the same region of the core are assumed to be exposed to the same neutron flux and the same burnup, and are thus grouped together as a batch. Therefore, when reload calculations are performed to determine the heat load of the fuel assembly, a group of fuel assemblies that see the same neutron flux are grouped together into a batch. Therefore, instead of calculating decay heat emission of each fuel assembly individually, only a few batches of the same region are analysed and the results obtained are found to be representative of every batch in that region [Taviv, 2013].

When one is preparing to load fuel assemblies into the casks or spent fuel pool, it is imperative that one takes into consideration its initial enrichment level, the burnup it experienced and the amount of decay heat. All of which are a function of the location in the core, the duration of the cycle and the power history of the reactor and out-of-reactor cooling

period. These are crucial points to be taken into account whenever one decides to purchase spent fuel casks. They will give an indication of how the design of the casks should be i.e. how much shielding material to provide, how far apart the fuel assemblies should be to prevent criticality and what the nuclide inventory is and therefore, what radiation protection and confinement provision to make [Taviv, 2013].

6.3 Burnup Credit Computation Methodology

Normally, burnup-credit calculations entail calculation of depletion of the nuclear material usually the fuel with the view of determining the spent nuclear fuel (SNF) isotopic composition. This will then be extracted from the depletion output file and be used in a criticality calculation model. Doing this manually can be a very lengthy and tedious process, as a result STARBUCS sequence was used in this thesis since it automates burnup-credit calculation thereby eliminating manual extraction of isotopic composition. STARBUCS couples the following SCALE code modules to achieve the automation; ORIGEN-ARP, ORIGEN-S, CSASI, WAX and KENO Va or KENO-VI depending on whether one uses SCALE5a or higher i.e. SCALE6 or SCALE6.1 [Gauld, *et al.*, 2000; Radulescu, *et al.*, 2006].

To ensure proper convergence and to reduce statistical uncertainty, KENO-VI was used in this study and all calculations were simulated using 10000 neutron generations, 10000 neutron histories per generation, and skipped 100 before averaging; thus each calculated k_{eff} is based on a minimum of 10 million neutron histories.

The burnup credit information will subsequently be used to determine a burnup-credit loading curve which will in turn be used to determine the burnup-enrichment combination. These are in turn used to determine whether the fuel assembly is suitable for loading into the cask or not [Radulescu, *et al.*, 2006; Wagner, 2001; Wagner, 2006].

It is also used to determine the effectiveness of a nuclide set in reducing the neutron multiplication factor of the system as indicated in Table 6.1, thereby benefitting the organisation in saving the spent fuel storage space which will subsequently translate in cost-savings [Parks, *et al.*, 2006; Radulescu, *et al.*, 2009].

6.4 Burnup-Credit Analyses for Castor X/28F

In this part of the study, the focus will entirely be on the burnup credit of a high capacity CASTOR X/28 cask.

There seem to be a consensus among nuclear regulators around the world to only accept calculations which only take burnup credit of actinides only in SNF with an assembly burnup of up to 50 GWD/MTU and the out-of-reactor cooling period of 1-40 years [Wagner, 2006; Mueller, *et al.*, 2005a; Parks, *et al.*, 2006].

In spite of this being the case it is important to note that computational techniques used in predicting the actinide compositions and for determining the k_{eff} value have to be verified and validated against a reputable reference standard. Normally, calculations of isotopic compositions are validated against destructive chemical assay measurements from SNF samples, while criticality analysis methods are validated against applicable critical experiments. Although only actinide burnup credits are acceptable to some nuclear regulators, in this thesis an analysis of the loading curve based on all three sets of nuclides listed in Table 6.1 were used so as to compare their effectiveness in as far as reducing the k_{eff} of a system and saving storage space is concerned. Unless stated otherwise, the following calculation assumptions and nuclide sets were used:

- Major Actinides Only: ^{234}U, ^{235}U, ^{238}U, ^{238}Pu, ^{239}Pu, ^{240}Pu, ^{241}Pu, ^{242}Pu and ^{241}Am.

Table 6.2: Required Burnup/Enrichment combination for a given enrichment to be acceptable for cask loading (Present study).

Nuclide Set	**Enrichment (^{235}U wt%)**	**Burnup (GWD/MTU)**
Major Actinides Only	2.65551948	28.6395553
Major Actinides + Minor FP	2.65551948	24.7483909
Major Actinides + Principal FP	2.65551948	22.1591574

- Major Actinides + Minor Fission Products: ^{234}U, ^{235}U, ^{238}U, ^{238}Pu, ^{239}Pu, ^{240}Pu, ^{241}Pu, ^{242}Pu, ^{241}Am, ^{243}Am, ^{237}Np, ^{133}Cs,^{143}Nd, ^{151}Sm and ^{155}Gd
- Major Actinides + Principal Fission Products: ^{234}U, ^{235}U, ^{238}U, ^{238}Pu, ^{239}Pu, ^{240}Pu, ^{241}Pu, ^{242}Pu, ^{241}Am, ^{243}Am, ^{237}Np, ^{99}Tc,^{133}Cs, ^{143}Nd ^{145}Nd, ^{147}Sm, ^{150}Sm, ^{151}Sm, ^{152}Sm, ^{151}Eu, ^{153}Eu, ^{155}Gd.
- Burnup dependent *axial profile* (No Radial Profile was taken into account)
- Isotopic Correction Factors (ICFs) of actinides listed above were obtained from various articles, notably from [Parks, *et al.*, 2006; Gauld, *et al.*, 2000 and Mueller, *et al.*, 2005b].
- Out-Of-Reactor cooling periods of 1 year, 5 years and 10 years.
- Operating parameters; Fuel Enrichment (^{235}U 1.8 wt% up to 5 wt%), Specific power (continuous operation at 40 GWD/MTU)

Results were compiled as three sets;

- Major Actinides Only, in three different cooling times (1 yr, 5 yrs and 10 year-cooling period)
- All three sets compared after a 10 year cooling period
- All three nuclide sets compared at three respective cooling times.

Studies show that the reduction in reactivity associated with fuel burnup is as a result of two competing processes [Radulescu, *et al.*, 2006; Wagner, 2006]:

Increase in fission product and other actinides with high parasitic absorption as result transmutation, decay or nuclear reactions. A literature survey shows that fission product found in irradiated UO_2 fuel can be grouped into the following categories [Patterson, *et al.*, 2010; Lamarsh, 2002];

1. **Volatile elements**: Rb, Cs, I, Sb, Cd and inert gasses which include Xe and Kr.
2. **Zr and the rare-earths**
3. **SrO and BaO** which are present as occlusion dispersed throughout the fuel.

4. **Noble Metals:** Mo, Ru, Tc, Pd, Rd and Ag. These metals are found in the un-alloyed state and occur as occlusion in the Equi-axed and columnar grains in the fuel. Mo may occur in the form of MoO_2 or MoO_3 in a region of high oxygen potential.

5. **Noble Metal Alloys**: The nominal composition of noble metal alloys generally located in the central voids of the fuel is 20% Mo, 17% Tc, 48% Ru, 13% Rh, and 2% Pd [Lamarsh, 2002; Patterson, *et al.*, 2010].

Decrease in concentration of fissile nuclides ^{235}U and ^{238}U. When treating decrease in fissile nuclides, it must always be borne in mind that ^{239}Pu and ^{241}Pu will be increasing and not decreasing thus adding positive reactivity to the system.

Therefore, if criticality calculations are performed based on the fresh fuel, they will only be accounting for a small fraction of fissile nuclides and a limited subset of absorbers, the calculated k_{eff} value will thus be conservative (i.e., k_{eff} is overestimated). To-date, according to the studies conducted at the Oak Ridge National Laboratory (ORNL), the proposed approach for burnup credit in storage and transportation casks is to qualify calculated isotopic predictions of nuclides that will be generated as result of the operation of the reactor (Gauld, 2003). This is done via validation against destructive assay measurements from SNF samples and also qualifies criticality analysis methods via validation against applicable critical experiments. Thus, the nuclides in a safety analysis process have primarily been limited by two important factors [Parks, *et al.*, 2006; Wagner, 2001]:

- The availability of chemical assay data and
- The applicable critical experiments.

The use of burnup credit necessitates that the reactor operating history experienced by the fuel assembly be taken into account when fuel assemblies are loaded into casks. Therefore, in comparison to analyses based on the fresh-fuel assumption, additional information and assumptions are needed for input to a burnup-credit evaluation. A related complication lies in the design of storage and transportation casks for a given reactor type. Therefore, because of previous operating history the fuel assembly has been exposed to, which leads to the build-up of the fission product and thereby a decrease in reactivity, this has to be taken into account when finally storing them. This leads to definition of the concept of Loading Curve which defines the criteria by which:

a) Fuel assemblies that are in the reactor core may either be declared as acceptable or not acceptable for loading in the spent fuel pool (decay heat loading requirement having been met) and

b) Fuel assemblies which are in the spent fuel pool will either be acceptable or not acceptable for cask loading.

The loading curve depicts the initial enrichment and minimum burnup combinations that define the boundary conditions for cask loading acceptability. All points on the curve represent burnup and enrichment combinations that yield the same value of k_{eff}. However, no credit is taken for burnup in the vertical part of the loading curve since this part corresponds to a region in which the reduction in reactivity due to burnup is dominated by the increase in reactivity associated with the conservatism in the burnup-credit evaluation [Parks, *et al.*, 2006; Wagner, 2001].

The shape and location of the loading curve depends on many factors some of which are:

- Decay or cooling period of the fuel assembly before it is loaded into the casks
- Type of burnup credit i.e. whether it is Major Actinides only, Major Actinides + Minor Fission Products or Major Actinides + Principal Fission Products or Full Burnup Credits.
- A combination of both, decay period and isotopic composition

These will determine whether the curve moves to the left or right of the x-axis of the loading curve of up or down the y-axis of the loading curve axis.

6.4.1 The effect of duration of decay period in Burnup credit application

The duration of the decay period plays a very significant role in the position of the loading curve with respect to one another and in the number of fuel assemblies acceptable for loading in the cask. This is because of the decrease in k_{eff} associated with the length of the cooling period of the fuel assembly. To illustrate, consider a fuel assembly with an enrichment of 4.4 wt% that has been irradiated in the reactor at a burnup of 40 GWD/MTU and a temperature of 400K. If only burnup credit of Major Actinides + Minor Fission Products are taken into consideration and the k_{eff} is plotted against the duration of cooling, a graph indicated in Figure 6.4 will be produced.

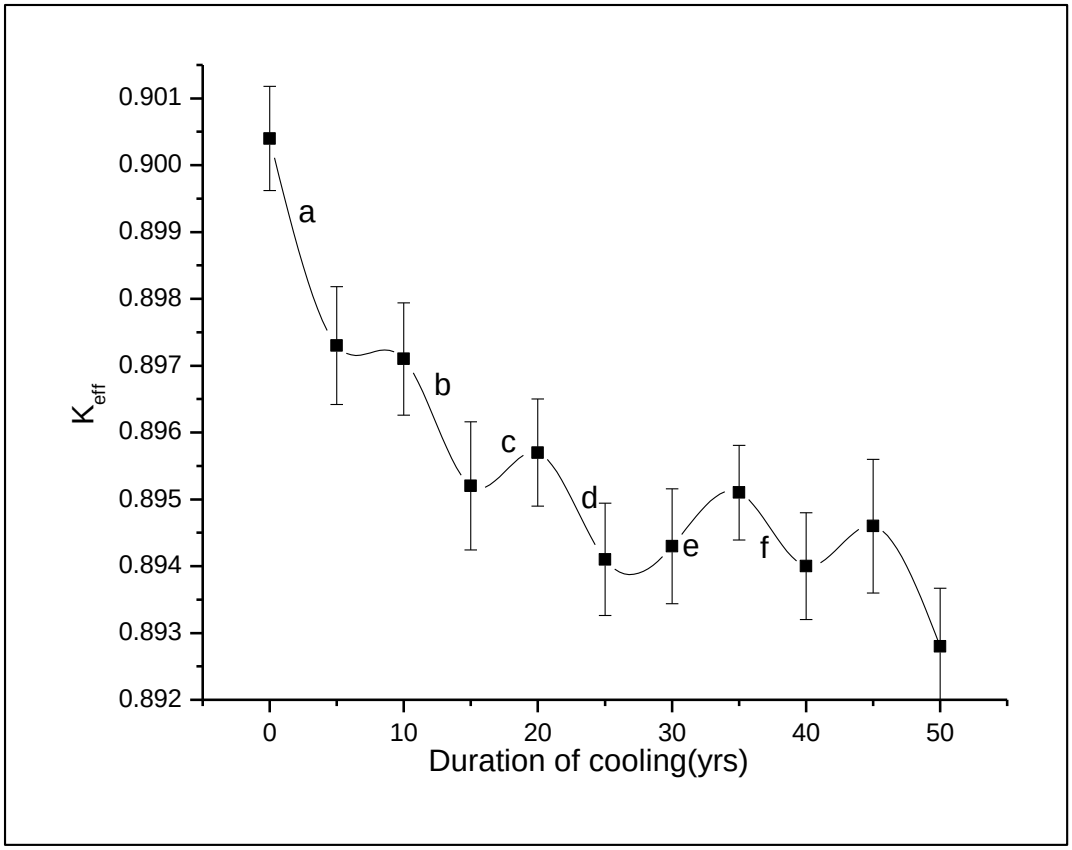

Figure 6.4: Effect of cooling period in criticality: 0-50 years [Actinides+Minor Fission Products at BU=40 GWD/MTU, 235=4.4 wt%] (Present study)

It is noted that the k_{eff} varies with duration of cooling as follows:

From 0 to 30 years: In the first thirty years there will be a significant decrease in k_{eff} ascribed to:

- the decay of short-lived nuclides such as ^{252}Cf ($t_{1/2}$ = 2.65 yrs) which undergoes spontaneous fission as well the decay of ^{241}Pu ($t_{1/2}$=14.290 yrs) and;
- the build-up of
  - ^{155}Gd from ^{155}Eu ($t_{1/2}$= 4.7 yrs)
  - ^{147}Sm from ^{147}Pm ($t_{1/2}$ = 2.62 yrs)
  - ^{152}Sm from ^{152}Eu (t ½ = 13.54 yrs)
  - ^{241}Am from ^{241}Pu (t ½ = 14.29 yrs)
  - ^{133}Cs from ^{133}Ba ($t_{1/2}$ = 10.51 yrs)

As a result of the opposing effect of nuclear fission and absorption, with absorption dominating, the net effect will be a decrease in k_{eff} and this is confirmed by the decrease in k_{eff} in Figure 6.4

From 30 to 50 years: The decrease is gradually slowing down because all short-lived fissile nuclides have decayed and as a result the k_{eff} has reached saturation. The causes of various peaks and dips in the graph labelled (a) through to (f) and are;

Region a is a decrease k_{eff} due to;

- Decay of ^{252}Cf ($t_{1/2}$ = 2.65yrs), and
- Build-up of ^{155}Gd from beta decay of ^{155}Eu ($t_{1/2}$ = 4.7yrs)
- Build-up of ^{147}Sm from beta decay of ^{147}Pm($t_{½}$ = 2.62 yrs)

Region b is a decrease in k_{eff} due to;

- decay of ^{241}Pu ($t_{1/2}$=14.290 yrs)
- Build-up of ^{152}Sm (from ^{152}Eu ($t_{1/2}$) =13.537yrs)
- Build-up of ^{241}Am (from ^{241}Pu ($t_{1/2}$ =14.290)
- Build-up of ^{133}Cs (from EC of ^{133}Ba ($t_{1/2}$ =10.51 yrs)

Region c is an increase in k_{eff} due to;

- SF[18] of ^{244}Cm ($t_{1/2}$ = 18.11 yrs)

Region d is a decrease k_{eff} due to;

- Build-up of ^{145}Nd (from EC[19] of ^{145}Pm ($t_{1/2}$ = 17.7 yrs)

Region e is an increase k_{eff} due to;

- SF of ^{243}Cm ($t_{1/2}$ = 29.1 yrs)

Region f is a decrease in k_{eff} due to:

[18] Spontaneous Fission
[19] Electron Capture

- The build-up of ^{151}Eu and ^{150}Sm from neutron capture of ^{150}Eu and EC of ^{150}Eu ($t_{1/2}$=36.9yr) respectively.

From 50 to 10^6 years: This period is better understood if divided into two time frames. This is because there are periods where there is an increase in k_{eff} and periods where there is decrease. If Figure 6.5 is divided into the following time frames: from 50 to 10^4 years and from 10^4 to 10^6 years, it is noted that the k_{eff} also changes due to the following reasons:

From 50 to 10^4 years: In this time period there will be an increase in the k_{eff} due to:

- Decay of ^{240}Pu ($t_{1/2}$ = 6560 y)
- Decay of ^{241}Am ($t_{1/2}$ = 433y)
- The build-up of ^{238}Pu from ^{238}Np ($t_{1/2}$ =2.12). ^{238}Pu undergoes spontaneous decay and adds to the increase in k_{eff}.
- The build-up of ^{239}Pu from ^{239}Am($t_{1/2}$ = 11.9 h), ^{239}Np ($t_{1/2}$ = 2.39 d) and ^{244}Cm ($t_{1/2}$ = 29yrs

From 10^4 to 10^6: In this time frame, there is a decrease in k_{eff} as a result of

- Decay of ^{239}Pu ($t_{1/2}$=2.411x10^4 yrs) which dominates. The build-up of other nuclide with short half-lives is insignificant, these include;
- ^{238}Pu from ^{238}Np ($t_{1/2}$ = 2.12 d)
- ^{241}Am from ^{241}Pu ($t_{1/2}$ = 14.29 yrs)
- ^{240}Pu from ^{240}Np ($t_{1/2}$) = 61.9 m)
- ^{234}U from ^{234}Pa ($t_{1/2}$=6.70 h) and also from SF of ^{234}Pa

Therefore, the choice of the duration of a cooling period is very important because if it is too long, i.e. more than 30 years the k_{eff} may be in the upward trend of a cycle (refer to Figure 6.4 and Figure 6.5). The cooling period must therefore be taken into account whenever the loading curve of the casks is evaluated. The importance of this can be seen in Figure 6.6 which clearly shows that if the cooling period is long relative to others, one will need much lower burnup to achieve the same k_{eff} compared to a shorter cooling period. This is consistent with the results obtained by Paul McConnell [McConnell, 2012].

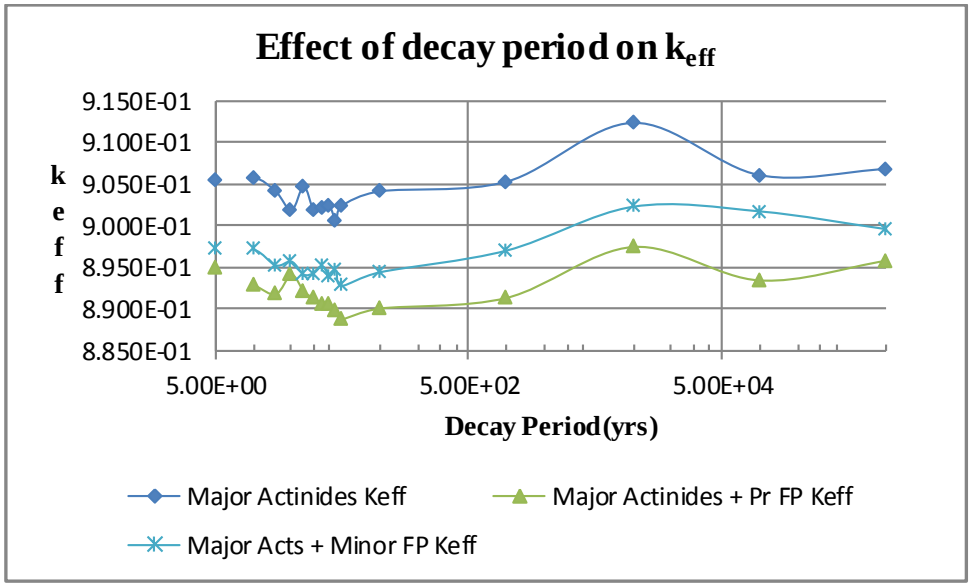

Figure 6.5: Effect of cooling period in criticality: 5.0 to10^6 years (Present study)

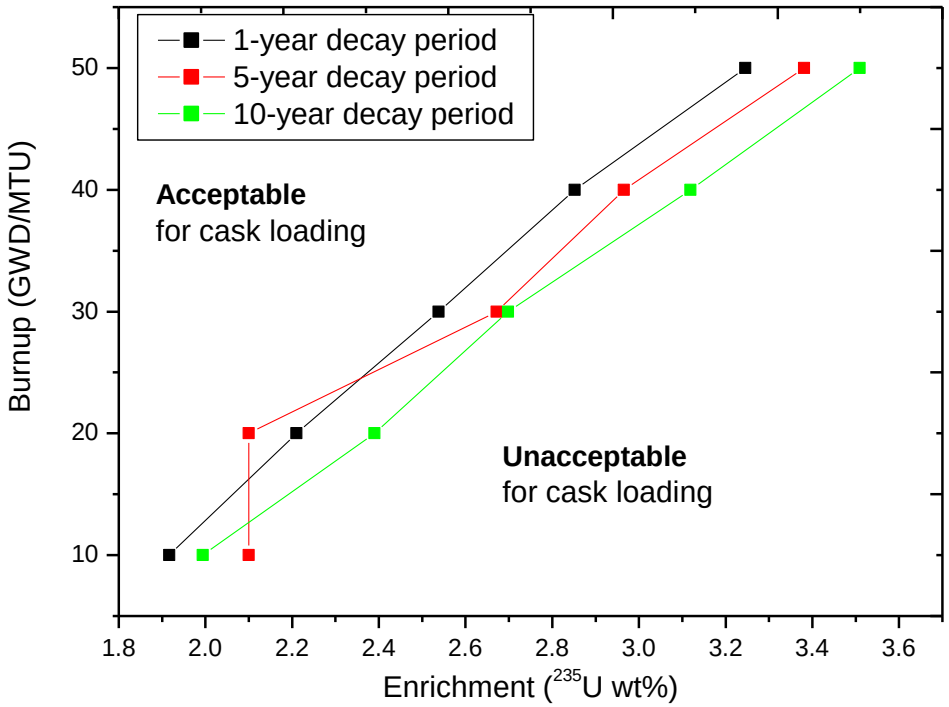

Figure 6.6: Effect of Decay Period on the Loading Curve (Major Actinides only) (Present study).

6.4.2 Effect of isotopic composition on the Loading Curve

In the previous section it was assumed that only one set of nuclides was active, the others were kept constant. This was done purposely because the objective was to study the effect of decay period on the k_{eff} and subsequently on the loading curve, and not the effect of isotopic composition, which is the subject of this section. In this section all three sets of nuclides described earlier are considered to be active and will be compared to one another on the bases of the effect they have on the loading curve.

Considering Figure 6.7, if one takes major actinides as a reference, one will note that it lies above those of Major Actinides + Minor Fission Products while that of Major Actinides + Principal Fission Products is below the other two. This implies that if we increase the number of nuclides with higher absorption cross-section e.g. fission products, there will be more nuclides taking part in the absorption process and not enough fission taking place to sustain the reaction, as a result fission product will result in lower k_{eff} than their actinides counterparts and the graph will move down.

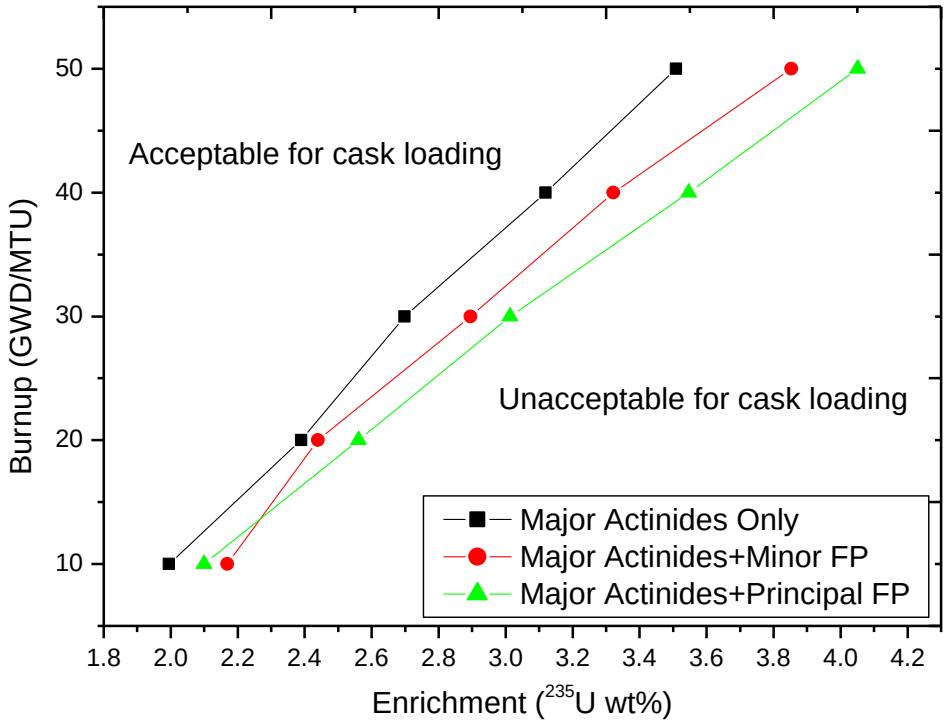

Figure 6.7: Effect of change in isotopic composition on the Loading Curve: 10 year decay period (Present study).

If, on the other hand, we take Major Actinides + Minor Fission Product as a reference and we increase the amount of Major Actinides, there will be more fissile material such ^{239}Pu, ^{240}Pu, ^{241}Pu and ^{242}Pu available for fission as a result the k_{eff} will increase relative to those of other nuclide, resulting in the graph moving up the burnup axis. Of the three sets, Major Actinides + Principal Fission Products (FP) has the greatest burnup credit effect, i.e. they will decrease the k_{eff} of the system to a much lower level than the other two could achieve. Therefore a small shift (up or down) in a cask loading curve can have a significant impact on the number of spent fuel nuclear fuel assemblies that are acceptable for loading.

Such broad qualification on cask contents requires an understanding of the effects of variations in reactor operating conditions and fuel assembly design characteristics on the reactivity of SNF to establish justifiable assumptions for a burnup-credit evaluation. A horizontal movement towards the right along the Enrichment axis at a constant burnup implies that the increase in k_{eff} can only be achieved by an increase in enrichment of fuel. If one makes a combination of the isotopic concentration, cooling time and burnup, one will obtain the Loading Curves indicated in Figure 6.8.

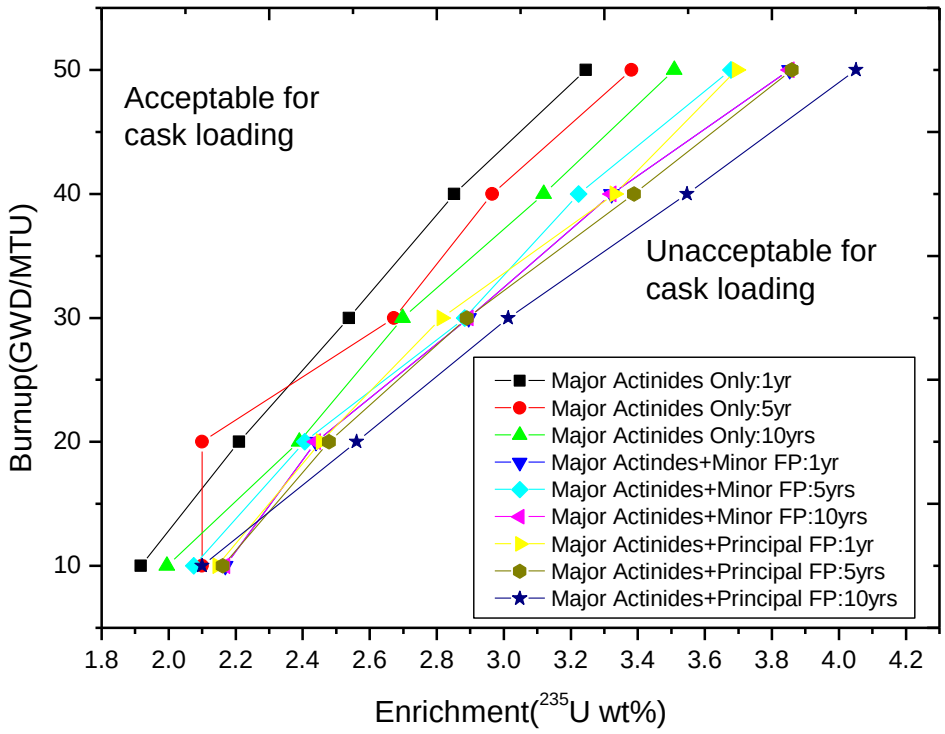

Figure 6.8: Comparison of loading curves of three nuclide sets at three different cooling times (Present study)

The three graphs show that an increase in allowable burnup credit can lower the burnup-enrichment loading curve and save the storage space and number of shipments. Therefore, given that to-date there is still a lot of uncertainty on the (NNR) National Nuclear Regulator's position regarding acceptability of burnup credit, it would be advisable that Eskom (Koeberg) and the Nuclear Energy Corporation of South Africa (NECSA) initiate discussions with the NNR to discuss the economic benefit of taking credit for burnup, if not all three sets, at least start with two; Major Actinides Only *and* Major Actinides + Minor Fission Products. This can make a significant difference in the storage space in the spent fuel pool, the number of casks Eskom must acquire, and on the number of shipments to be made to Vaalputs. If not, the application of neutron absorber inserts needs to be expanded to determine actual amount of space that can be saved if neutron absorbers inserts are used. This study, has been discussed in detail in section 4.4.1, and indicated that neutron absorber inserts can offer an alternative solution to the spent fuel storage capacity. It has been shown in this study that depending on the design or location the neutron absorber inserts on the fuel assembly; they can increase the storage capacity by up to 12% which is a significant saving in spent fuel pool storage space if implemented.

CHAPTER 7

7 SENSITIVITY AND UNCERTAINTY ANALYSES

7.1 PERTURBATION AND VARIATIONAL ANALYSIS OF A CRITICAL SYSTEM

There are a number of factors which can bring about a change in a nuclear system, and there are equally a number of parameters which can be perturbed to various degrees of perturbation to determine the response of that system to the parameters that are perturbed. The degree of response to perturbation depends on the parameter or material being perturbed, the magnitude of perturbation and the sensitivity of the response to the perturbed parameter. This chapter will first and foremost provide a brief background to the perturbation techniques available to nuclear analysis and finally present practical sensitivity and uncertainty analysis performed on several materials of spent fuel casks.

7.2 Variational methods and perturbation theory

Perturbation theory is a set of approximation schemes which have Applied Mathematics as their origin and have been applied in many branches of physical sciences and engineering [McCartin, 2009; Merzbacher, 1998]. One of these applications is in the Rayleigh-Schrödinger theory for symmetric matrix eigenvalue problems which has been applied quite extensively in variational analysis. Other variational theories where Rayleigh-Schrödinger theory has been applied include the WKB (Wentzel, Kramers & Brillouin) approximation which is directly related to mathematical perturbation for describing a complicated quantum mechanical system in terms of simpler ones [Merzbacher, 1998]. Perturbation theory is further divided into Linear and Non-Linear Perturbation Theory and is discussed in detail in the next section [Moro, *et al.*; McCartin, 2009; Merzbacher, 1998].

7.2.1 Linear perturbation theory

There are many research articles published in the field of linear perturbation theory, and all concur that when the matrix A_0 is subjected to a small symmetric linear perturbation due to some inhomogeneity, the result will be in the form of a linear equation; $A = A_0 + \epsilon A_1$. These

techniques have a wide range of application in many areas of physics, particularly in the field of mathematical and theoretical physics through which physics problems which were believed to have no solution such as the Schrödinger Wave equation in quantum physics were solved [McCartin., 2009; Merzbacher, 1998]

In nuclear physics, particularly in reactor physics it finds wide application in predicting what the outcome of the neutron multiplication factor would be if a small perturbation in some reactor parameters such as the nuclide cross-section were to occur as a result of, for example, an increase in fuel or moderator temperature. If such a strain (i.e. increase in temperature) were to be brought to bear upon the system, then discrete mathematical analysis would be used to analyse the Boltzmann Transport Equation to determine how this would affect neutron transport in general [McCartin., 2009; Merzbacher, 1998].

7.2.2 Non-linear perturbation

In Non-linear Perturbation on the other hand, the differential operator of a real symmetric matrix A_0 is evaluated by discrete mathematics. According to Merzbacher and McCartin, if the matrix is subjected to a small symmetric perturbation which may be due to some physical inhomogeneity in the system which is in turn analytic in small parameter,ϵ; the results will be in the power form of ϵ; $A(\epsilon) = A_0 + \epsilon A_1 + \epsilon^2 A_2 + \in^3$ ....

In either case, regardless of whether one uses linear or analytic perturbation, the results will be statistically the same [McCartin., 2009; Merzbacher, 1998; Johnson, 2005]. According to Johnson [Johnson, 2005], the solutions to the eigenvalues and eigenvectors are approximations of matrix A_0, which is produced by a sequence of successive higher order corrections to the initial eigenvalues and eigenvectors. This has been confirmed by studies conducted by Down in which it was observed that although the results were statistically similar, when applied to density contrast, linear perturbation is more accurate than non-linear [Down, 2006].

The linear and non-linear techniques both have boundary conditions as a common denominator (Sanchez, *et al.*, 2001); therefore, in either case one will have to perform an analyses where the boundary conditions are brought to bear upon the system. In the case of nuclear criticality analyses the boundary conditions often encountered are geometrical and albedo conditions [Sanchez, *et al.*, 2001]. Other forms of boundaries may either be time, material density, neutron energy, etc., all of which may act for a certain period of time, hence

they are time-dependent. According to Rearden [Rearden, 2004], it is immaterial whether one applies linear or non-linear perturbation; they all start with a simple system of Hamiltonian $H^{(0)}$ for which the exact solution $\psi^{(0)}$ is known, such that

$$H^{(0)}\psi_n^{(0)} = E_n^{(0)}\psi_n^{(0)} \tag{7.1}$$

and a small "*perturbing*" $\lambda H^{(1)}$ Hamiltonian representing a small change in the system is added. If the change is not too large, the various physical quantities associated with the perturbed system (e.g. its energy or eigenvalue) can, from considerations of continuity, be expressed as 'corrections' to those of the simple system, as shown in Eqn (7.2) and Eqn (7.3)

$$\begin{aligned} H &= H^{(0)} + \lambda H^{(1)} + \lambda^2 H^2 + \ldots \\ \psi_n &= \psi_n^{(0)} + \lambda\psi_n^{(1)} + \lambda^2\psi_n^{(2)} + \ldots \\ E_n &= E_n^{(0)} + \lambda E_n^{(1)} + \lambda^2 E_n^{(2)} + \ldots \end{aligned} \tag{7.2}$$

and

$$H\psi_n = E_n\psi_n \tag{7.3}$$

where λ is the perturbation parameter; the terms $\phi_n^{(1)}$ and $E_n^{(1)}$ are the first order corrections to the wave function and energy respectively, and $\phi_n^{(2)}$ and $E_n^{(2)}$ are the second order corrections. These corrections, being 'small' compared to the size of the quantities themselves, can be calculated using approximate methods such as asymptotic series [Moro, *et al.*, 2000, Johnson, 2005.]. According to Mueller the variation must be within the range of ±10% around the nominal value of the parameter that is being perturbed. Using the nuclear criticality background, Mueller argued that "*if the variation used is too narrow, the Direct Perturbation (DP) sensitivity coefficient is likely to be driven mainly by the statistical variation in k_{eff} between high- and low- density calculation than by the actual sensitivity. If on the other hand the delta used is too large, the DP sensitivity coefficient may miss some local non-linear behaviour of k_{eff} as a function of density*" [Mueller, *et al.*, 2005].

Therefore, as stated earlier the complicated system can therefore, be studied based on knowledge of the simpler one and what seemed difficult and impossible to solve can now be solved because of the simplified version of the complicated system.

7.3 SENSITIVITY AND UNCERTAINTY ANALYSIS

7.3.1 Sensitivity Generation

Using the basic principle of variational analysis and the background given in the previous section it is noted that for every fractional change in an input parameter, there will be a corresponding fractional change on the system's response. The relationship between these two is a factor known as the *sensitivity coefficient* [Rearden, *et al.*, 2008].

One specific example that will be seen later is the effect of change in the moderator density which has led to a statistically equivalent change in the eigenvalue. It has also been noted that not all material responds the same way to the same change in input; these will be studied in detail in following sections.

There are as many techniques that one can use to perform sensitivity analysis as there are variational and approximation methods, but not every method is applicable in every situation. In this study, sensitivity and uncertainty analysis will be based on the adjoint-based perturbation theory because of its credibility and reliability in nuclear criticality safety analysis and also because it is the approximation model used in TSUNAMI-3D code which will be used in this study [Mueller, *et al.*, 2005]. The adjoint-based perturbation theory specific for the generation of sensitivity of k_{eff} is presented as the Boltzmann transport equation as [Mueller, *et al.*, 2005b]

$$[\mathrm{A} - \lambda \mathrm{B}]\phi = 0 \tag{7.4}$$

where A and B are the loss and production operators , ϕ is the angular neutron flux and λ represents the eigenvalues where the largest eigenvalue is $1/k_{\text{eff}}$. The perturbed transport operators and eigenvalue are then defined as

$$\begin{aligned} \mathrm{A}' &= \mathrm{A} + \delta\mathrm{A} \\ \mathrm{B}' &= \mathrm{B} + \delta\mathrm{B} \\ \lambda' &= \lambda + \delta\lambda \end{aligned} \tag{7.5}$$

where δA and δB are fractional linear perturbations in their respective transport operators and $\delta\lambda$ represents the corresponding fractional change in the eigenvalues. Therefore, the perturbed transport equation can then be given as [Mueller, *et al.*, 2005a; Mueller, *et al.*, 2005]

$$[\mathrm{A}' - \lambda' B']\phi' = 0 \tag{7.6}$$

and the adjoint equation is given by,

$$[\mathrm{A}^* - \lambda \mathrm{B}^*]\phi = 0, \tag{7.7}$$

where ϕ^* is the adjoint flux, also known as the *importance function*, and A^* and B^* are adjoint operators corresponding to *A* and *B*.

If Eqn (7.6) is multiplied by ϕ^*, and integrated over all phase-spaces, it will result in

$$\left\langle \phi^* \left(\mathrm{A}' - \lambda' B'\right)\phi \right\rangle = 0, \tag{7.8}$$

where $\langle\ \rangle$ represents integration over all phase and space, i.e. volume, energy and direction.

Expanding Eqn (7.8) in terms of Eqn (7.5) will result in

$$\left\langle \phi^* \left(\mathrm{A} - \lambda \mathrm{B} + \delta \mathrm{A} - \lambda \delta \mathrm{B} - \mathrm{B}\delta\lambda - \delta\lambda\delta \mathrm{B}\right)\phi' \right\rangle = 0 \quad . \tag{7.9}$$

Since the requirement for adjointedness is that;

$$\left\langle \phi^* \left(\mathrm{A} - \lambda \mathrm{B}\right)\phi' \right\rangle = \left\langle \phi' \left(\mathrm{A}^* - \lambda \mathrm{B}^*\right)\phi^* \right\rangle, \tag{7.10}$$

and using the property of adjointedness and Eqn (7.7) to reduce the number of terms of Eqn (47.9) will yield,

$$\left\langle \phi^* \left(\delta \mathrm{A} - \lambda \delta \mathrm{B} - \mathrm{B}\delta\lambda - \delta\lambda\delta \mathrm{B}\right)\phi' \right\rangle = 0 . \tag{7.11}$$

If $\delta\lambda\delta B$ is ignored and ϕ' is substituted with ϕ, it will be noted that the perturbations in the transport operators do not cause significant perturbations in the flux solutions [Mueller, *et al.*, 2005a; Mueller, *et al.*, 2005b; Rearden, *et al.*, 2008; Rearden, 2004]. Therefore, the eigenvalue perturbation becomes

$$\frac{\delta\lambda}{\lambda} = \frac{\left\langle \phi^* \left(\delta \mathrm{A} - \lambda \delta \mathrm{B}\right)\phi \right\rangle}{\left\langle \phi^* \left(\lambda \mathrm{B}\right)\phi \right\rangle} \tag{7.12}$$

if we replace the perturbation terms with partial derivatives with respect to a particular nuclide-reaction pair macroscopic cross-section $\sum_x$ the relative sensitivity of λ will be [Mueller, *et al.*, 2005a; Mueller, *et al.*, 2005b; Rearden, 2004].

$$\frac{\Sigma_x}{\lambda}\frac{\partial\lambda}{\partial\Sigma_x} = \frac{\Sigma_x}{\lambda}\frac{\left\langle \phi^*\left(\frac{\partial A}{\partial\Sigma_x} - \lambda\frac{\partial B}{\partial\Sigma_x}\right)\right\rangle}{\left\langle \phi^* B\phi\right\rangle}. \tag{7.13}$$

Since

$$\lambda = 1/k_{eff} \tag{7.14}$$

then

$$\partial\lambda/\lambda = -\partial k_{eff}/k_{eff} \tag{7.15}$$

such that sensitivity of k_{eff} to some macroscopic cross-section is defined as

$$\begin{aligned} S_{k,\Sigma x} &= \frac{\Sigma_x}{k_{eff}}\frac{\partial k_{eff}}{\partial\Sigma_x} = -\frac{\Sigma_x}{\lambda}\frac{\partial\lambda}{\partial\Sigma_x} \\ &= -\frac{\Sigma_x}{k_{eff}}\frac{\left\langle \phi^*\left(\frac{\partial A}{\partial\Sigma_x} - \frac{1}{k_{eff}}\frac{\partial B}{\partial\Sigma_x}\right)\phi\right\rangle}{\left\langle \phi^*\frac{B}{k_{eff}^2}\phi\right\rangle}, \end{aligned} \tag{7.16}$$

where $\partial A/\partial\sum_x$ and $\partial B/\partial\sum_x$ are the functions of scattering, capture and fission cross-section data. The evaluation of Eqn (7.16) results in the integration of the forward and adjoint fluxes *and* the cross-section over the entire phase-space.

According to Mueller and Rearden [Rearden, *et al.*, 2008; Mueller, *et al.*, 2005b], the energy-dependence of the cross-section data is generally obtained by averaging the $\sum_x$ quantities over energy groups g and is represented as $\sum_{x,g}$. If these groups are inserted in Eqn (7.16), it will result in the sensitivity of k_{eff} to perturbation in a single energy group of a particular nuclide-reaction pair given by [Broadhead, *et al.*, 2004]:

$$S_{k,\sum_{x,g}} = \frac{\sum_{x,g}}{k_{eff}} \frac{\partial k_{eff}}{\partial \sum_{x,g}}. \tag{7.17}$$

If the value of g is changed to obtain the sensitivity of all energy groups across the energy range, then an energy-dependent sensitivity profile is generated. In 2004 Broadhead and Rearden [Broadhead, *et al.*, 2004] noted that the sensitivity coefficient as computed in Eqn (7.17) only accounts for *explicit sensitivity*. In order to be complete, it needs another term that will account for first-order *implicit sensitivity*. Therefore, the implicit portion of the sensitivity coefficient is thus defined by [Broadhead, *et al.*, 2004; Rearden, *et al.*, 2008]:

$$S_{\sum_{x,g,\omega_i}} = \frac{\omega_i}{\sum_{g,x}} \frac{\partial \sum_{x,g}}{\partial \omega_i}, \tag{7.18}$$

where ω_i is the number density of a particular material or a certain nuclear data component. The total sensitivity accounting for both implicit and explicit sensitivity where the implicit sensitivity is added to the explicit sensitivity is then defined by

$$\left(S_{k,\sum x,g} \right)_{total} = S_{k,\sum x,g} + \sum_i \sum_y \sum_h S_{k,\sum y,h} S_{\sum y,h,\omega_i} S_{\omega_i,\sum x,g} \tag{7.19}$$

where *i* is summed over all parameters that are dependent on the group-wise cross-section $\sum x,g$, and y and h are summed over all nuclide-reaction pairs and energy groups that are dependent on ω_i. The two components of sensitivity, i.e. explicit and implicit sensitivity will be described in detail in the following two sections.

7.3.1.1 Explicit Sensitivity Generation

As stated in the previous section Sensitivity is made up of two parts; explicit and implicit sensitivity. The explicit sensitivity as described by Rearden and Mueller expresses the sensitivity of k_{eff} to a particular group-wise cross-section data. It is derived from the eigenvalue neutron-transport equation expressed in operator notation as [Broadhead, *et al.*, 2004; Mueller, *et al.*, 2005a; Mueller, *et al.*, 2005b; Rearden, 2004]:

$$A\phi = \frac{1}{k} B\phi, \tag{7.20}$$

where

ϕ = neutron flux

$k = k_{\text{eff}}$

A = operator that represents all transport equations except for the fission term

B = operator which represents the fission term of the transport equation.

The adjoint form of the transport equation is written as

$$\mathrm{A}^{*}\phi^{*} = \frac{1}{k}\mathrm{B}^{*}\phi^{*}, \tag{7.21}$$

where, as stated, ϕ^{*} is the adjoint flux which has a special physical significance as the 'neutron importance' of the system. By applying linear perturbation theory, it can be shown that a relative change in k due to a small perturbation in macroscopic cross-section Σ of the transport operator at some point r, can be expressed as [Broadhead, *et al.*, 2004; Mueller, *et al.*, 2005a; (Mueller, *et al.*, 2005b; Rearden, 2004]:

$$S_{\mathrm{k},\Sigma(\vec{\mathrm{r}})} \equiv \frac{\Sigma(\vec{\mathrm{r}})}{k}\frac{\partial k}{\partial \Sigma(\vec{\mathrm{r}})} = -\frac{\Sigma(\vec{\mathrm{r}})}{k}\frac{\left\langle \phi^{*}(\vec{\xi})\left(\frac{\partial \mathrm{A}\left[\Sigma(\vec{\xi})\right]}{\partial \Sigma(\vec{\mathrm{r}})} - \frac{1}{k}\frac{\partial \mathrm{B}\left[\Sigma(\vec{\xi})\right]}{\partial \Sigma(\vec{\mathrm{r}})}\right)\phi(\vec{\xi})\right\rangle}{\left\langle \phi^{*}\left(\vec{\xi}\right)\frac{1}{k^{2}}\mathrm{B}\left[\Sigma(\vec{\xi})\right]\phi(\vec{\xi})\right\rangle}, \tag{7.22}$$

where $\vec{\xi}$ is the phase-space vector.

Thus the sensitivity of k to a particular cross-section can be calculated from Eqn (7.22), using discrete ordinates from the Boltzmann neutron transport equation.

Regarding the sensitivity of nuclear reaction x, due to isotope i of energy group g in a computational region z of the system, Mueller and Rearden have demonstrated that it can be represented as [Broadhead, *et al.*, 2004; Mueller, *et al.*, 2005a; Mueller, *et al.*, 2005b]

$$S_{\mathrm{k},\Sigma^{\mathrm{i}}_{\mathrm{x,g,z}}} = \frac{T^{\mathrm{i}}_{1,\mathrm{x,g,z}} + T^{\mathrm{i}}_{2,\mathrm{x,g,z}} + T^{\mathrm{i}}_{3,\mathrm{x,g,z}}}{D}, \tag{7.23}$$

where

$$D = \frac{1}{k}\sum_{\mathrm{i}=1}^{\mathrm{I}}\sum_{z=1}^{\mathrm{R}} V_{\mathrm{z}}\sum_{g=1}^{\mathrm{G}}\left(\bar{\nu}^{\mathrm{i}}_{\mathrm{g,z}}\Sigma^{\mathrm{i}}_{\mathrm{f,g,z}}\ \phi_{\mathrm{g,z}}\right)\sum_{\mathrm{g}'=1}^{G}\left(\chi^{\mathrm{i}}_{\mathrm{g}',\mathrm{z}}\phi^{*}_{\mathrm{g}',\mathrm{z}}\right) \tag{7.24}$$

and

$\chi^{i}_{g',z}$ = average fraction of fission neutrons emitted into energy group g′ from isotope *i* in region *z*.

$\bar{\nu}^{i}_{g,z}$ = average number of fission neutrons emitted from fission of isotope *i* in region z and in energy group g.

$\sum^{i}_{f,g,z}$ = macroscopic cross-section for fission of isotope *i* in region z and energy group g.

I = number of isotopes in the system model

R = number of computational regions in the system model.

G = number of neutron energy groups in the system model

The energy integrated coefficients are obtained by summing the group-wise coefficients over all the energy groups. Mueller and Rearden [Mueller, *et al.*, 2005] further added that the *T* terms in Eqn (7.23) represent the transport process for neutron loss, fission production, and scattering to the group of interest in T_1, T_2 and T_3 respectively [Mueller, *et al.*, 2005]. These terms are in turn defined as;

$$T^{\mathrm{i}}_{1,\mathrm{x,g,z}} = -\Sigma^{\mathrm{i}}_{\mathrm{x,g,z}}\ \mathrm{V_z} \sum_{\mathrm{j=0}}^{\mathrm{NMOM}} (2\ell+1)\tilde{\phi}^{*\mathrm{j}}_{\mathrm{g,z}}\tilde{\phi}^{\mathrm{j}}_{\mathrm{g,z}}\ , \tag{7.25}$$

$$T^{\mathrm{i}}_{2,\mathrm{g,z}} = \frac{1}{k}\mathrm{V_z}\bar{\nu}^{\mathrm{i}}_{\mathrm{g,z}}\sum\nolimits^{\mathrm{i}}_{\mathrm{f,g,z}}\ \phi_{\mathrm{g,z}}\sum_{\mathrm{g'=1}}^{\mathrm{G}}\ \phi^{*}_{\mathrm{g',z}}\chi_{\mathrm{g',z}} \tag{7.26}$$

and

$$T^{i}_{3,g,z} = \sum_{j=0}^{\mathrm{NMOM}}\ V_z\sum_{g'=1}^{G}\ \tilde{\phi}^{*j}_{g,z}\tilde{\phi}^{j}_{g,z}\sum\nolimits^{\ell,i}_{x,g'\to g,z} \tag{7.27}$$

where

$\sum^{i}_{x,g,z}$ = macroscopic cross-section for some reaction x, of isotope I, energy group g in region z.

ℓ = Legendre order that corresponds to the jth real-valued flux moments.

$\tilde{\phi}^{*j}_{g,z}$ = jth component real valued adjoint flux moment for energy group g, and region z.

NMOM = total number of real valued flux moments corresponding to the desired Legendre order of expansion

$\sum_{x,g'\to g,z}^{\ell,i}$ = ℓ^{th} moment of the transfer cross-section for reaction *x* of isotope *i* from energy group g' to energy g in region z.

According to Rearden and Mueller, not all T terms defined above are used to calculate every sensitivity coefficient [Broadhead, *et al.*, 2004; Mueller, *et al.*, 2005a; Mueller, *et al.*, 2005b]. For example in;

- Capture reaction sensitivity: only $T_1$is used ,
- Fission reaction sensitivity*:* T_1 and T_2 are used.
- $\bar{\nu}$ (nu bar) sensitivity : only T_2 is used.
- χ sensitivity: only T_2 is required
- All Scattering reactions: T_1 and T_3 are required.
- Total reaction sensitivity: all three T_1, T_2 and T_3 terms are required.

7.3.1.2 Implicit Sensitivity Generation

In the previous section the first part of total sensitivity, explicit sensitivity was described. In this section the study will focus on the implicit sensitivity of k_{eff}, which may be due to sensitivity of some subcomponents (e.g. fuel or moderator) of the system to the parameter (e.g. material density or temperature) that is being perturbed. For example there is a linear relationship between the water density and k_{eff} of the system. Since hydrogen and oxygen are both components of water, and the density of water has a certain fraction of sensitivity to oxygen and hydrogen densities, what is then 'implied' is that the k_{eff} is 'indirectly' sensitive to the sensitivity of water density which in itself is sensitive to the density of oxygen and hydrogen. Therefore, k_{eff} is indirectly sensitive to the material density of hydrogen and oxygen [Mueller, *et al.*, 2005a; Mueller, *et al.*, 2005b]

If one considers sensitivity of k_{eff} to resonance self-shielding then Eqn (7.23) needs to be modified with an additional term that will specifically account for the firs-order implicit effects of perturbations on k_{eff}. Thus, the implicit part of the sensitivity coefficient, is given by;

$$S_{\sum x,g,\omega_i} = \frac{\omega_i}{\sum_{x,g}} \frac{\partial \sum_{x,g}}{\partial \omega_i}, \tag{7.28}$$

where the ω_i represents an input data, which could be the material number density of a particular nuclide, or the physical dimensions of the system. If, on the other hand, ω_i is a certain cross-section data component for process (y) of nuclide (j) in energy group (h) expressed as $\sum_{y,h}^{j}$, which is sensitive to perturbations in process (x) in energy group (g) for nuclide (i) expressed as $\sum_{x,g}^{i}$, then the complete sensitivity of k_{eff} due to perturbation $\sum_{x,g}^{i}$ can be defined as (derived from the chain rule of derivatives)

$$\left(S_{k,\sum_{x,g}^{i}} \right)_{\text{total}} = \frac{\sum_{x,g}^{i}}{k} \frac{dk}{d\sum_{x,g}^{i}} = \frac{\sum_{x,g}^{i}}{k} \frac{\partial k}{\partial \sum_{x,g}^{i}} + \sum_{j}\sum_{h} \frac{\sum_{y,h}^{j}}{k} \frac{\partial k}{\partial \sum_{y,h}^{j}} \times \frac{\sum_{x,g}^{i}}{\sum_{y,h}^{j}} \frac{\partial \sum_{y,h}^{j}}{\partial \sum_{x,g}^{i}} \tag{7.29}$$

$$= S_{k,\sum_{x,g}^{i}} + \sum_{j}\sum_{h} S_{k,\sum_{y,h}^{j}} S_{\sum_{y,h}^{j} \sum_{x,g}^{j}}$$

where the sensitivity coefficients with respect to k_{eff} are the explicit components as computed in Eqn (47.23) with the regions subscript z omitted, and j and h are varied to include all processes that are influenced by the value of $\sum_{x,g}^{i}$.

7.4 Overview of uncertainty

Modelling of physical systems is often complicated by the presence of a number of uncertainties in the system, which may either be statistical or due to measurement errors in nature which are typically categorised as Type A and Type B errors respectively [Labuschagne, *et al.*, 2007; Young, 1962]. The implications of these uncertainties are particularly important in the assessment of several criticality safety analysis options. This is primarily due to uncertainties which may arise in the neutron multiplication factor of the system as a result of a small perturbation of a material composition of a system or any physical parameter such as the fuel or moderator's temperature, or even a fractional change in the geometry of the system. Perturbation of geometry can be achieved by, for example, changing the separation gap among adjacent fuel assemblies or spent fuel casks or even re-arranging storage array which can subsequently change the neutron density, fission density or neutron importance and subsequently the k_{eff} of the system.

According to Labuschagne and Young [Labuschagne, *et al.*, 2007; Young, 1962] a systematic uncertainty analysis provides insight into the level of confidence in model estimates, and can aid in assessing how various possible model estimates should be weighed so that the errors arising from uncertainty are accounted for in the final results [Labuschagne, *et al.*, 2007; Young, 1962]. It can also lead to the identification of key sources of uncertainty, such as data gaps or measurement discrepancies which may require more data to be taken to determine if there is a significant[20] difference in the results as well as the sources of uncertainty that are not important to the given response.

Quantitative uncertainty analysis on the other hand aims at quantifying the degree of confidence in the data at hand and the model being used. Even though the applicability of a model is limited by the model assumptions and the uncertainties in the evaluation data, understanding the judgments associated with the modelling process is more valuable than side-stepping the uncertainty analysis. In fact, it is precisely for problems where data are limited and where simplifying assumptions have been used that a quantitative uncertainty analysis can provide a significant insight into the problem being investigated [Labuschagne, *et al.*, 2007; Young, 1962].

Young argued that the information obtained from measurement of a certain physical quantity, x, which could be the radius of the fuel pellet does not only consist of a single value, but of a

[20] significant in this context means greater or equal to 3sigma ($\geq 3\sigma$)

whole probability distribution i.e. a distribution of discrete probabilities p_j of possible x_j values from a discrete set or infinitesimal probabilities $p(x)dx$ of the true value which lies between x and $x+dx$ if they form a continuum with probability density function $p(x)$. According to decision theory [Labuschagne, et al., 2007], if the distribution is to be based on just two numbers, it is best to use its mean $\bar{x}$ rather than its variance (var x) and the mean is given by

$$\bar{x} = \frac{1}{N}\sum_{i=1}^{N} x_i \tag{7.30}$$

where N is the number of observations, which in this case is 2, and the variance is given by

$$\sigma^2 = \frac{1}{N}\sum\left(x-\bar{x}\right)^2 \tag{7.31}$$

Therefore, the measured or calculated results must be reported as

$$\bar{x} \pm \sigma \tag{7.32}$$

where σ is standard deviation given by [Labuschagne, *et al.*, 2007]

$$\sigma = \sqrt{\frac{1}{N}\sum_{i=1}^{N}\left(x_i-\bar{x}\right)^2} \tag{7.33}$$

7.4.1 Variance reduction techniques

Variance Reduction may be described using a detector which is set up to detect particles e.g. neutrons from a certain source. It is expected that there will be a region around the detector where there will be neutrons at higher energies and other regions with neutrons at lower energies/velocities [Peplow, *et al.*, 2006; Blakeman, *et al.*, 2007]. If low energy neutrons do not activate the detector, the analyst may decide to ignore or reduce the counting time/efficiency of low energy neutron and compensate this reduction by adding it in the high energy neutrons. Thus Variance Reduction in this context means reduction of the counting time or detection efficiency in the low energy neutron and increasing the counting time/detection time in the high energy neutrons by the same amount [Blakeman, *et al.*, 2007;

Peplow, *et al.*, 2006]. There are a number of techniques used by SCALE 6.1.3 to achieve the desired variance reduction but these will be discussed in detail in their respective sections [Wagner, *et al.*, 2013; Broadhead, *et al.*, 2004].

7.4.2 The uncertainty of the neutron multiplication factor

The objective of this calculation is to find the effect of making a small variation of either of the parameters (atom densities, density of fuel, moderator or fuel temperature) on the k_{eff} of the system. In some literature it is called k, in this thesis, k_{eff} and k will be used interchangeably. Assume that the uncertainty u_i of parameter i is small enough to have a first order effect on k. This implies that for $\Delta x_i \leq u_i$, the change in k produced by Δx_i is proportional to the magnitude of Δx_i [Rearden, *et al.*, 2008].

If the perturbation parameter is δx_i, it must be sufficiently large to minimise errors associated with rounding off, but at the same time small enough not to violate the linearity (first-order effect) assumptions so that both u_i and δx_i are proportional to the corresponding changes in k by the same factor [Mueller, *et al.*, 2005a; Rearden, 2004]. Then the desired reactivity effect is given by

$$\Delta k_i = u_i \delta k_i / \delta x_i , \tag{7.34}$$

and the proportionality factor $\delta k_i / \delta x_i$ is the sensitivity of k_{eff} to x_i. If u_i is not linear perturbation, then it is necessary to determine whether the sensitivity of k is not too large. However if Δk_i due to u_i is not too large, then it is imperative to calculate the effects of both ($+u_i$) and ($-u_i$) perturbation. If the two resulting values of Δk_i are comparable or are small, then it is acceptable to average the magnitudes and move on to the uncertainty-combining steps. However, if the two values of Δk_i are large and significantly different, they should be treated as asymmetric uncertainty.

The easiest way of finding the effect of each parameter on k which will be used in direct perturbation of fuel and moderator temperature in this thesis, is to perform a systematic analysis; changing one parameter at a time and observe its effect on the k_{eff}. First the reference k (k_{ref}) is calculated using unperturbed parameters, then the parameter x_i is perturbed while all other parameters are kept constant, then k_i corresponding to the perturbation u_i is calculated [Mueller, *et al.*, 2005a; Mueller, *et al.*, 2005b; Rearden, *et al.*, 2008]. The change in k given by Eqn (7.35),

$$\Delta k_{\mathrm{i}} = k_{\mathrm{i}} - k_{\mathrm{ref}} \tag{7.35}$$

is the reactivity effect of u_i on k.

There are several techniques to calculate the effect of perturbation of u_i on k, but the most common ones are analytical techniques, deterministic and Monte Carlo techniques. For simple configurations the analytical techniques could be used and have indeed been used quite extensively in the past before the advent of high performance computers. The concern is that it relies too much on manual labour, calculating each value manually which opens it to the risk of human error and it is also a very slow and tedious process [Labuschagne, *et al.*, 2007; Young, 1962].

7.4.2.1 Uncertainties of calculated uncertainties

When using Monte Carlo codes such KENO and MCNP to calculate the k_{eff} of the reference configuration and the k_{eff} of the parameter, statistical uncertainty of the calculation by the Monte Carlo (S_{MC}) must be taken into account [Dupree, *et al.*, 2002; Landau, *et al.*, 2005]. For large data such as in nuclear analysis the variance is often preferred over the mean, and when it is found that there is no correlation among parameter uncertainties, then the variance of the k_{eff} uncertainty caused by the parameter is given by [Rearden, 2004; Mueller, et al., 2005b]

$$\left(\Delta k_{\mathrm{i}}\right)^2 = \frac{u_{\mathrm{i}}^2}{\delta x_{\mathrm{i}}^2}\left[\left(k_{\delta \mathrm{x}_{\mathrm{i}}} - k_{\mathrm{ref}}\right)^2 \pm \left(S_{\mathrm{MC},\delta \mathrm{x}_{\mathrm{i}}}^2 + S_{\mathrm{MC,ref}}^2\right)\right] \tag{7.36}$$

where $\left(k_{\delta x_i} - k_{ref}\right)$ indicates the change in k_{eff} as a result of change δx_i in parameter x_i u_i is the standard uncertainty of parameter x_i, $S_{MC,\delta xi}$ and $S_{MC,ref}$ are the statistical standard deviations of the two calculations of k_{eff}. Generally the $S_{MC,\delta x}$ is typically the same as $S_{MC,ref}$ and in that case Eqn (7.36) is simplified to

$$\left(\Delta k_{\mathrm{i}}\right)^2 = \frac{u_{\mathrm{i}}^2}{\delta x_{\mathrm{i}}^2}\left[\left(k_{\delta \mathrm{x}_{\mathrm{i}}} - k_{\mathrm{ref}}\right)^2 \pm 2\left(S_{\mathrm{MC}}^2\right)\right] \tag{7.37}$$

Therefore, the contribution to the standard uncertainty of k_{eff} from the standard parameter is thus given by [Mueller, *et al.*, 2005b; Rearden, 2004]:

$$\Delta k_{\mathrm{i}} = \frac{u_{\mathrm{i}}}{\delta x_{\mathrm{i}}}\left(k_{\delta x_{\mathrm{i}}} - k_{\mathrm{ref}} \right), \tag{7.38}$$

and the uncertainty of uncertainty is equal to $\frac{u_{\mathrm{i}}}{\delta x_{\mathrm{i}}}\sqrt{2S_{\mathrm{MC}}}$

Ideally the uncertainty of uncertainty should be very small compared to the uncertainty itself. This may be achieved by making δx_i very large. Alternatively, this may be achieved by calculating a relatively large number of histories which may be obtained by running the simulation at 10^4 neutron generations and 10^4 neutrons per generations (Rearden, 2004; Rearden, et al., 2008) [Rearden, 2004; Rearden, *et al.*, 2008]. In that way it is possible that $S_{MC} < 0.0002$ and the uncertainty of uncertainty will be < 0.0003.

Other factors which contribute to the uncertainty in uncertainty other than Monte Carlo statistics are often due to Multigroup Monte Carlo calculations which result from uncertainty in cross-section processing approximations just as it happens with deterministic calculations.

7.4.3 The General Equation of the total Standard Uncertainty

In the previous section the equation for determining Δk_i , the effect of u_i on k_{eff} were derived. However, in all those cases it was only for a single parameter *i*. If on the other hand there are *N* important parameters brought to bear in a critical system, then total uncertainty Δk_{tot} needs to be calculated and its effect on the final k_{eff} evaluated. In that case then the general formula for the combined variance due to *N* parameters is given by [Dean, *et al.*, 2007]

$$\begin{aligned}\left(\Delta k_{\mathrm{tot}}\right)^2 &= \sum_{\mathrm{i}=1}^{\mathrm{N}}\left[\frac{\partial k_{\mathrm{eff}}}{\partial x_{\mathrm{i}}}\right]^2 u_{\mathrm{i}}^2 + 2\sum_{\mathrm{i}=1}^{\mathrm{N-1}}\sum_{\mathrm{j}=\mathrm{i}+1}^{\mathrm{N}}\frac{\partial k_{\mathrm{eff}}}{\partial x_{\mathrm{i}}}\frac{\partial k_{\mathrm{eff}}}{\partial x_{\mathrm{j}}}\mathrm{r}_{\mathrm{i,j}}u_{\mathrm{i}}u_{\mathrm{j}} \\ &= \sum_{\mathrm{i}=1}^{\mathrm{N}}\left(\Delta k_{\mathrm{i}}\right)^2 + 2\sum_{\mathrm{i}=1}^{\mathrm{N}-1}\sum_{\mathrm{j}=\mathrm{i}+1}^{\mathrm{N}}\left(\Delta k_{\mathrm{i}}\right)\left(\Delta k_{\mathrm{j}}\right)\mathrm{r}_{\mathrm{i,j}}.\end{aligned} \tag{7.39}$$

Each individual Δk_i indicates the change in k_{eff} when a particular physical parameter x_i is perturbed by an amount equal to u_i, the standard uncertainty of that parameter. Since to find Δk_i, the value of k_{ref} was calculated first, which is the k for all parameters equal to or very close to their nominal values. Then k is calculated for a variation in parameter x_i, with all other parameters held constant. The difference in the two k values, δk_i, divided by the parameter variation in the calculation, δx_i i.e. $(\delta k_i / \delta x_i)$ represents the sensitivity $(\partial k_{\mathrm{eff}}/\partial x_i)$, of k to the parameter x_i. When the sensitivity is multiplied by the standard

uncertainty, u_i , of parameter x_i, we get the k_{eff} uncertainty due to the standard uncertainty in that particular parameter, i.e. $\Delta k_i = \frac{\delta k_i}{\delta x_i} u_i = \frac{\partial k_{eff}}{\partial x_i} u_i$ [Dean, *et al.*, 2007].

7.4.4 Estimation of the neutron multiplication factor of an array.

Being able to calculate k_{eff} of an array (i.e. k_{array}) of a number of fissile materials is of great importance to the storage of spent fuel assemblies and fuel assembly casks stored in the interim or final storage facility. Variation of the pitch among adjacent fuel rods or casks is one of the most important variables in criticality safety but certainly not the only one. Not being able to determine the k_{eff} of an array also called k_{array}, may lead to the array going supercritical depending on the initial enrichment levels and the power history they were subjected to [Dean, *et al.*, 2007].

According to Dean to find the effect the random variation of a parameter like distance among adjacent casks or fuel rods in an array has on the k_{eff}, the Δk_{eff} may be estimated by dividing, the number of units e.g. casks, fuel rods or fuel assemblies in the array by $\sqrt{N}$. The Δk of an array (Δk_{array}) can then be derived from $\Delta k_{array} = \Delta k_{eff}/\sqrt{N}$. This approximation has received criticism from several scientists on the basis that it is not realistic since it fails to take into account the fact that in a fuel assembly the fuel rods near the centre of the array have a much higher neutron importance than the rods in the periphery of the array. Furthermore, because the effects from each of the fuel rods or casks are added in quadrature (i.e. square root of sum of squares), this uneven weighting must be taken into account if the effect of random variation in the k_{eff} is to be determined, which is a subject of discussion in the next section.

7.4.4.1 Uncertainty arising from spacing of fissile materials

If we take a case of an array of *N* equally spaced fuel rods, spent fuel assemblies or casks, the uncertainty of the pitch due to either variation in rod position or uncertainty of measurements in the fuel rod or fuel assembly, depends on the grid for the rods or units and their placement (which includes pattern and gaps among different units) in the grid. In the case of fuel rods, random variation is due to the gaps among the rods and the grid hole and also due to the location of the hole itself in the grid. In rare cases it may be affected by slightly bowing of the rods [Dean, *et al.*, 2007].

If the standard deviation of the distance among fissile units has been determined, and Δk is calculated for an increase in the distance among all units by that amount, the effect from each unit may be estimated roughly as Δk/N. However, this is only a rough estimation of the Δk partly because the value of a pitch at the centre of the assembly has a larger effect than the value of pitch near the edges due to higher neutron importance at the centre of the fuel assembly. The total effect on the k_{eff} of the random variation among unit positions is therefore, the total of the effects from each, combined as the square root of the sum of their square values as indicated in Eqn (4.40) [Dean, *et al.*, 2007];

$$\sqrt{\sum_{i}^{N}\left(\frac{\Delta k}{N}\right)^2} = \sqrt{N\frac{(\Delta k)^2}{N^2}} = \frac{\Delta k}{\sqrt{N}} \tag{7.40}$$

7.5 Boundary conditions

For the purpose of describing the concept of boundary conditions it is assumed that the region of interest where the reaction takes place is surrounded by a convex surface, therefore, a neutron leaving the region through the surface cannot interact with the surface again. If however neutrons enter such a region from the external source the incoming flux must be specified; if on the other hand no neutrons from the external source enter the region and if a neutron that leaves the surface cannot return into the region, then that surface is known as a free surface and there exists a condition described by; [Becker, 2010; Hollenbach, *et al.*, 2004; Hollenbach, *et al.*, 2005]

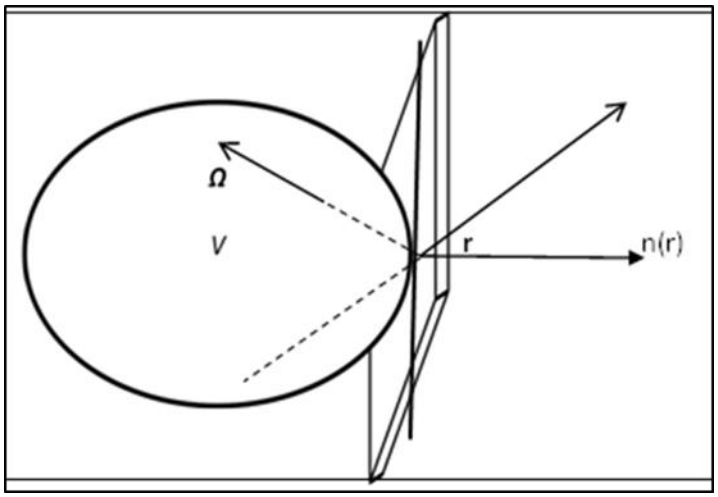

Figure 7.1: Illustrations of directions of Ω and $\mathbf{\Omega}'$ used in boundary conditions.

$$N(r,\Omega,E,t)=0 \qquad \text{if } n\cdot\Omega<0, \tag{7.41}$$

where n is a unit vector in a direction of the outward normal at position r on the surface (see Figure 7.1). Such a condition will exist if the region is surrounded by a vacuum or a perfect absorber. In practice one finds a number of situations where a vacuum boundary is applicable but hardly ever finds a perfect absorber.

As such boundary conditions are classified according to how neutrons are reflected back into the vessel. To give a qualitative context to this description, the main function of the boundary conditions is to specify or describe mathematically the amount of angular flux that comes from the outside of the vessel into the vessel, in a direction $\mathbf{\Omega_{in}}$ such that $\mathbf{\Omega_{in}\cdot n<0}$, where **n** as already stated denotes the unit outward normal to the boundary as indicated in Figure 7.1. The meaning of each boundary condition in a reactor physics context is described in the next section [Hollenbach, *et al.*, 2004; Hollenbach, *et al.*, 2005, Sanchez, *et al.*, 2001]

7.5.1 The Vacuum Boundary Condition

The vacuum boundary conditions are often referred to as zero (incoming) flux boundary conditions since they demand that the angular flux (ψ) on the boundary of the region of interest is zero for all incoming directions, i.e. $\phi(\mathrm{r},\mathrm{E},\Omega)=0$ when $\mathbf{\Omega\cdot n(r)} < \mathbf{0}$, $\mathrm{r}\in\partial\mathrm{V}$, where **n(r)** is an outward normal at $\mathrm{r}\in\partial\mathrm{V}$ and V is the boundary (see Figure 7.1). Since as per the requirements of boundary conditions no neutron will re-enter the system, a neutron exiting the system through a vacuum boundary is permanently lost to the system.

7.5.2 White boundary condition

The white boundary on the other hand is a boundary condition where the outgoing flux is reflected isotropically (with an equal distribution in angle) back into the system. If expressed in terms of the normal plane a particle scattered from a white boundary will be reflected with a cosine distribution $\mathrm{p}(\mu)=\mu$ relative to the normal plane. White boundaries are very important in comparing results of two codes such as in a verification and validation (V&V) of codes that have white boundary conditions such as e.g. MCNP and SCALE. It makes no sense in using them in problems with next-event estimators such as detectors [Hollenbach, *et al.*, 2005; Hollenbach, *et al.*, 2004]

7.5.3 Periodic Boundaries

The Periodic boundary conditions can be depicted as a number of pairs of parallel planes used to simulate an infinite lattice. Thus the incoming angular flux on a boundary is set equal to the outgoing angular flux on the opposite side, which results in a neutron leaving one boundary being returned at the same quantity and angle on the opposite boundary. In reactor lattice calculations, for example, the geometry may consist of a single fuel assembly, often infinite in the axial direction, which is surrounded by reflective or periodic boundary conditions. This means that the solution corresponds to a repeated lattice of identical fuel assemblies, infinite in all spatial directions. Therefore, instead of, for example performing criticality analysis of a 4×4 array of casks, one could use 2×2 array and change the boundary conditions to periodic and obtain the results of a 4×4 array. Although the scattering and other aspects of Monte Carlo random walk dominates the running time, the computer time gained by using periodic boundaries is lost to the scattering [Hollenbach, *et al.*, 2005; MCNP_X5_Team, 2003].

7.5.4 Reflective boundary conditions

This requires that the flux at the boundary in the *incoming* direction Ω is the same as the flux in the *outgoing* direction Ω' at that point, where $\Omega' = \Omega - 2[\Omega \cdot \mathrm{n}(\mathrm{r})]\mathrm{n}(\mathrm{r})$ is the reflected direction as shown in Figure 7.1 and satisfies $(\Omega \times \Omega') \cdot \mathrm{n}(\mathrm{r}) = 0$. In simple terms this means angle of incidence equals the angle of reflection. In the context of criticality calculations it means the escaped neutrons are reflected back into the core or any vessel of the system in the same plane in which they left. This implies that there is no loss of neutrons and therefore, no change in fission density. The reflective boundary condition can thus summarised mathematically as follows,

$$\boldsymbol{\psi}(\mathbf{r}, \mathbf{E}, \boldsymbol{\Omega}) = \boldsymbol{\psi}(\mathbf{r}, \mathbf{E}, \boldsymbol{\Omega}') \text{ when } \boldsymbol{\Omega} \cdot \mathbf{n}(\mathbf{r}) < \mathbf{0}, \ \boldsymbol{r} \in \boldsymbol{\partial V} \tag{7.42}$$

7.5.5 The Albedo boundary condition

The albedo forms a link between the vacuum and specular reflection condition in the following way; if in specular reflection a fraction α of escaped neutrons is reflected back into the system and (1-α) passes through the boundary, α can be adjusted so that either all escaped

neutrons are reflected back into the vessel or all are transmitted through the boundary [McCartin., 2009]. When α is set at zero (0) all neutrons will pass through the boundary and that boundary condition is known as vacuum. However, when α is set at one (1), all neutrons are reflected at the boundary and that boundary condition is referred to as reflective boundary conditions. Generally the albedo coefficient α varies with the reflector properties and the selection of the albedo coefficient should be such that it can capture angular and energetic redistribution of reflected neutrons as they diffuse through the reflector [Hollenbach, *et al.*, 2005; MCNP_X5_Team, 2003, Sanchez, *et al.*, 2001].

7.6 Neutron importance

Neutron Importance refers to the fact that every neutron in a system has an equal chance of causing an event [Lewins, 1965], which can either be a fission process or reaching a neutron detector thereby registering a signal. Research conducted by Soodak and Lewins has shown that the neutron importance is a function of the distance *x* from the detector, or in this case the distance from the fuel and the number of its progeny sometimes *t* later. A neutron progeny in this context refers to "*the neutron generations which trace their existence to a parent neutron through either scattering or fission"* [Lewins, 1965]. Therefore, because every neutron generation has as much chance of registering a signal in a detector, Lewins derived the following postulate to indicate the importance of neutron progeny in an event;

Postulate: "*A particle is as important as its progeny. This axiom expresses the requirement that a particle only contributes to the future meter reading through its progeny and the total importance of these progeny must be conserved up to the moment the meter is read*" [Lewins, 1960; Lewins, 1965]

The progeny only captures the time factor of neutron importance. The other equally important factor in neutron importance is distance *x* of a neutron from the detector which, according to Lewins plays an equally important role in defining neutron importance. He subsequently derived the following definition.

Definition: "*The importance N+(x,t), is defined as the expected or probable contribution of one particle at x at time t to the meter reading at time* t_f. *Thus a particle is 'important' to the (future) observable reading*" [Lewins, 1960; Lewins, 1965].

In the context of storage array, this implies that the neutron in the middle of the casks or array has much higher importance than those at the periphery which is in agreement with the Lewins findings which state that "*neutrons near the outer surface have a higher probability of leaking out of the system without leaving any progeny behind and therefore, without affecting the meter reading. Hence the neutron importance will be lower near the outer surface than near the centre of the array*" [Lewins, 1960; Lewins, 1965]. This seems to confirm why the 2×2 array has a much higher k_{eff} than the 1×4 array.

7.6.1 Neutron Generation Importance

Neutron importance is interpreted in different ways depending on the intention of the author and on the criticality of the reactor [Lewis, 2008] and has been found to be applicable to both critical and steady state subcritical system. In attempting to describe the concept of generation importance, one has to assume that there are a number of cycles of neutron generations radiating out of the neutron source and each cycle must be seen as separate from the others [Lewins, 1965; Lewins, 1984]. Also, each of the particles radiating out of the source exists in its own (first) generation until it is removed by the process represented by R. Whilst in its cycle, each neutron is producing progeny[21] for the next generation according to the probability represented by P [Lewins, 1960; Lewins, 1965]. Therefore, if $N^{+(1)}(x)$ is the importance of a particle in its own generation (i.e. its own effect on the detector or criticality without regard to that of its progeny) and if R^* describes the distribution with which it is being removed from its generation, then $R^*N^{+(1)}$ is the rate at which the particle is giving up its importance in the system, and this is equal to its immediate effect to criticality or to the detector given by , $H^+(x)$:

$$\text{where,} \qquad R^*N^{+(1)} = H^+ \tag{7.43}$$

It must be noted that the neutron multiplication factor of the system is also being affected by the progeny of the particles emitted from the source in the previous generation. If the preceding generation $i = 2$ and the present generation $i = 1$, then the particle in generation 2 has importance $N^{+(2)}$ and is being lost to its generation with probability distribution R^* . However, its progeny in the next generation are being produced with the probability distribution P* and each will have an importance of $N^{+(1)}$. Since the conservation of importance in the steady state requires that [Lewins, 1960; Lewins, 1965]:

[21] Daughter products

$$\mathbf{R}^{*}\mathbf{N}^{+(1)} = \mathbf{P}^{*}\mathbf{N}^{+(1)} \tag{7.44}$$

then the general equation that describes the importance of previous generation is written as

$$\mathrm{R}^{*}\mathrm{N}^{+(\mathrm{i}+1)} = \mathrm{P}^{*}\mathrm{N}^{+(\mathrm{i})}, \tag{7.45}$$

where $\mathrm{N}^{+(\mathrm{i}+1)}$ is the importance of a particle through its progeny *i* later.

Apart from the neutron importance, the system must also take into account the neutron source importance, which is *defined as the sum of the particle generation importance* given by:

$$\mathbf{S}^{+}(\mathbf{x}) = \sum_{1}^{\infty} \mathbf{N}^{+(\mathbf{i})}(\mathbf{x}) \tag{7.46}$$

In a subcritical system where there are no progeny left after a number of generations, this can be represented mathematically as [Lewins, 1960; Lewins, 1965; Lewins, 1984];

$$\mathbf{N}^{+(\mathbf{i})} \rightarrow \mathbf{0} \ \mathbf{as} \ \boldsymbol{i} \rightarrow \infty. \tag{7.47}$$

However, this is not the case in a critical system since there will always be a number of progeny left after a several generations in which case $\mathrm{N}^{+(\mathrm{i})}$ remains finite. Therefore, the sum corresponding to that is not finite but instead $\mathrm{N}^{(+\mathrm{i})}$ converges to N^{+} for a large i. [Lewins, 1960; Lewins, 1965].

In subcritical and critical systems the neutron importance is associated with the asymptotic neutron population [Lewis, 2008]. Therefore, if the system is slightly perturbed by inserting neutrons in a critical system the neutron population will increase depending on the location of insertion, their energy and the directions of initial neutrons whether they are moving away or towards the fuel. For a critical nuclear system having an initial N_0 neutron population, the neutron population will change by ΔN after an insertion of neutrons and will stabilize at a new neutron density level of $N_o+\Delta N$. In a critical system, the variation of neutrons population per inserted neutron is known as "*neutron importance*" and depends on the direction, energy and location of insertion. Therefore, in this regard the concept of neutron importance is related to any quantity proportional to the asymptotic power of a reactor core [[Lewins, 1960, Lewins, 1965].

7.6.2 Time-Dependent Neutron Importance

The other school of thought is of the opinion that *"the importance concept implies that the contribution of any one neutron to some final operationally determinable characteristics of a nuclear reactor such as perturbation of criticality is as important as any other neutron generation, irrespective of whether it is the first or n^{th} generation"* [Lewins, 1960]. This is the basis of the derivation of adjoint equation and the boundary condition of the Boltzmann Transport Equation for simple and multigroup diffusion theory and also for the continuous slowing down model. Adjoint functions which are solutions to the adjoint Boltzman equation were first introduced in reactor physics in 1945, but their application in the first-order perturbation theory was not until later [Lewins, 1960; Lewins, 1965]

Regardless of which school of thought one subscribes to, it is agreed that for many problems in reactor physics it is necessary to describe the state of the reactor by using a single overall characteristic, e.g. reactivity, instead of describing the neutron behaviour in detail throughout the reactor core [Lewins, 1960; Lewins, 1984]. However, contrary to the general belief, the neutron density cannot be separated into a function of time and the remaining variables, because then the notion of criticality loses its meaning. This led to the derivation of the time-dependent adjoint equation of neutron importance where the importance of a neutron is believed to be in three different time-zones relative to the position of the projectile to that of a target nuclide [Lewins, 1960; Lewins, 1965]:.

- before time *t*, in which case the neutron has not yet interacted with target nuclide (neutron still approaching).
- at time *t* where interaction of a neutron is actually in progress, in which there is transfer of energy, charge or other particles between the projectile and the target nuclide, and
- after time *t* where new nuclides/isotopes are created as a result of the interaction.

These are different time zones or stages through which nuclear reactions take place, and must be interpreted in the context of nuclear reaction analysis with reference to Figure 2.5.

7.7 PERTURBATION OF PARAMETERS IMPORTANT TO NUCLEAR CRITICALITY SAFETY OF CASTOR X/28F SPENT FUEL CASKS

In this thesis, sensitivity and uncertainty analysis was performed in two separate phases; in the first instance the focus was on fresh fuel, perturbing some of the important parameters to criticality with the view of determining what the effect of small perturbation will be on the k_{eff}.

7.7.1 Direct perturbation of fresh fuel parameters

The sensitivity and uncertainty analysis of fresh fuel was based on Direct Perturbation (DP) technique where KENO-IV was used to calculate k_{eff}. The resulting k_{eff} value is then used to manually calculate a total sensitivity coefficient that will then be compared to the total sensitivity coefficient calculated using TSUNAMI-1D or TSUNAMI-3D [Mueller, *et al.*, 2005a]. In this case, the study was divided into the following categories

- Perturbation of ^{10}B in the boral plate of the cask basket.
- Perturbation of moderator density,
- Perturbation of Moderator Temperature.
- Perturbation of Polyethylene Temperature.

The initial input parameters were as follows;

- Enrichment: 3.9 wt%,
- Cross-section library: v7-238
- Number of neutron generations (gen) = 10000
- Number of neutrons per generation (npg) = 10000
- Number of generations skipped (nsk) = 100
- Standard deviation (sig) = 0.0001

A sensitivity coefficient is thus defined *as the relative impact of a change in some nuclear data e.g. the macroscopic absorption cross-section* ($\sum_a$) *on the systems* k_{eff} and is defined as

$$S_a = {dk/k}\big/{d\alpha/\alpha}, \tag{7.48}$$

where α is nuclear data of interest [Rearden, *et al.*, 2008; Rearden, 2004]

The coefficients therefore, directly reflect the relative importance of data parameters to the results of a computer simulation. Studies conducted by Mueller have shown that TSUNAMI-3 and Direct Perturbation results should be within 1 or 2 standard deviations of each other [Rearden, 2004; Rearden, *et al.*, 2008]

As stated, Sensitivity coefficients may be further divided into explicit and implicit components. The explicit component results from the sensitivity of k_{eff} to variation of the resonance self-shielded macroscopic cross-section. The implicit component on the other hand results from cross-section adjustments in the resonance self-shielding calculation. For example, the explicit sensitivity of hydrogen in the moderator around a fuel pin results directly from the sensitivity of k_{eff} to changes in the hydrogen cross-section. Implicit sensitivity on the other hand includes the effects of the sensitivity of the fuel macroscopic cross-section to change in the moderator cross-section. The implicit component is calculated using derivatives produced during problem-dependent cross-section processing [Mueller, *et al.*, 2005a; Rearden, *et al.*, 2008].

7.7.1.1 Perturbation of ^{10}B Concentration

In this study, the fraction of ^{10}B was taken as the nominal amount of ^{10}B in the borated steel. It was then perturbed by ±5% and ±10% and in each case the effect of perturbation on the k_{eff} recorded for further analysis using Direct Perturbation techniques discussed earlier [Mueller, 2013a, Leotlela, *et al.*, 2015].

The results shown in Figure 7.2 indicate that as the fraction of ^{10}B in boral plates (or poison panels as some authors call it) is increased, there is a corresponding decrease in k_{eff} until one approaches a saturation level where no further decrease in k_{eff} can be achieved by any increase in ^{10}B. This may be ascribed to the fact that the neutron population available for absorption by ^{10}B has decreased so much that any excess of ^{10}B will have no neutrons left to absorb. If one keeps on increasing the ^{10}B concentration it will reach the point where the slope of the curve (i.e. the sensitivity) approaches zero but never actually gets to zero. This is a classic case of the non-linear behaviour that is exhibited by some materials [Mueller, 2013c, Leotlela, *et al.*, 2015]

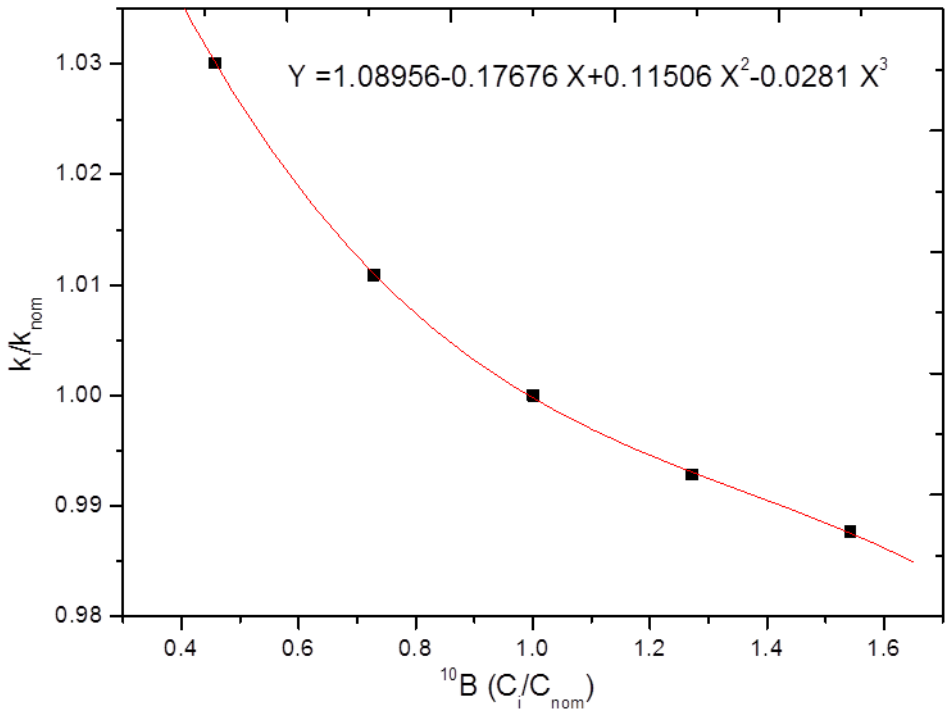

Figure 7.2: Perturbation of ^{10}B concentration of Boral plate [Leotlela, *et al.*, 2015]

What has been observed by changing the order of polynomial function is that when either of the polynomial fit is performed, the trend line tends to fit the graph better. As a result three equations were obtained [Leotlela, *et al.*, 2015];

1. Exponential decay equation

$$Y_0 = A_1 e^{-x/t_1}$$

$Y_0 = 0.98145 \quad \sigma = 3.25425\text{E-}4$

$A_1 = 0.11166 \quad \sigma = 5.47223\text{E-}4$

$t_1 = 0.55025 \quad \sigma = 0.00684$

$R^2 = 0.99975$

$\chi^2/\text{DoF}=19.6245$

2. 2nd Order Polynomial Equation

$$Y = A + B_1 x + B_2 x^2$$

$A = 1.07199, \sigma = 2.5984\times10^{-4}$

$B_1 = 0.10802, \sigma = 6.79124\times10^{-4}$

$B_2 = 0.03514, \sigma = 3.37549\times10^{-4}$

R^2 = 0.99748

SD =14.1196

3. 3rd Order Polynomial Equation

$Y=A+B_1x+B_2x^2+B_3x^3$

$A = 1.08956, \sigma = 9.27283E-4$

$B_1 = -0.17676, \sigma = 0.000355$

$B_2 = 0.11506, \sigma = 0.00403$

$B_3 = -0.0281, \sigma = 0.00403$

R^2 = 0.99994

SD =3.01384

Looking at the linear fit of all three equations, it is noted that the 3rd order polynomial has the best fit (R^2 = 0.99994) as the trend line fit seems to capture all data much better than any other equation above. To add to that, it also has the lowest standard deviation of them all. It is therefore, expected that the decrease in k_{eff} as the fraction of ^{10}B is increased will follow the 3rd order polynomial described by [Leotlela, *et al.*, 2015];

$$Y=1.08956 - 0.17676x+0.11506x^2 - 0.0281x^3. \quad (7.49)$$

The sensitivity coefficient can be obtained by finding the derivative (slope) of this equation at a particular point. Applying the basic differentiation rule in calculus wherein if n is a positive integer and y is a function defined by $y = x^n$ then the derivative is given by $dy/dx = nx^{n-1}$ [Finney, *et al.*, 1990]. Therefore the general equation for the sensitivity of k_{eff} to ^{10}B concentration is given by [Leotlela, *et al.*, 2015]:

$$dy/dx = -0.17676 + 0.23012x - 0.0843x^2 \quad (7.50)$$

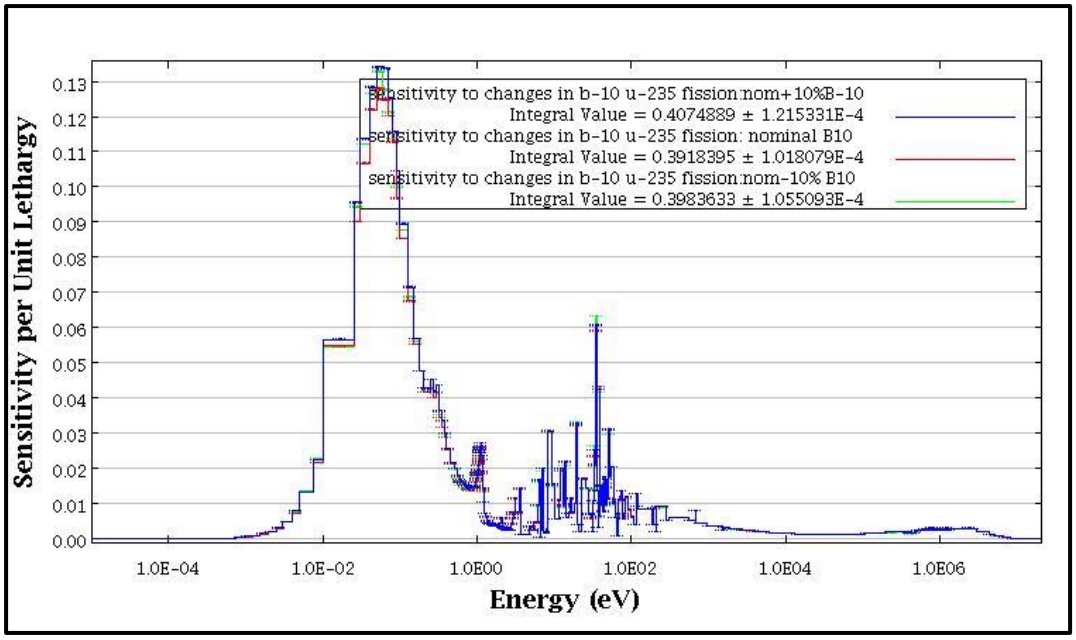

Figure 7.3 : Sensitivity of ^{235}U fission to changes in ^{10}B concentration **[**present study**]**

Therefore at $^{10}B(C_i/C_{nom}) = 1$ (i.e. x = 1), then k_i/k_{nom} will be [Leotlela, *et al.*, 2015];

$$\left| dy/dx \right|_{x=1} = -0.03094 \pm 1.10 \times 10^{-04}. \qquad 7.51$$

which is the sensitivity coefficient at that concentration and is consistent with the coefficient obtained by Mueller *et al* [Mueller, *et al.*, 2005].

The relationship between sensitivity of ^{235}U to changes in ^{10}B concentration is shown in Figure 7.3

7.7.1.2 Perturbation of Moderator Density.

When the density of water is increased, there is a linear increase in the k_{eff} of the system. This is because the increase in water density results in the increase in the density of hydrogen atoms in the system. And because light elements such as hydrogen have a much higher moderation power than their heavier counterparts e.g. oxygen in this case, they have a much higher propensity of slowing neutrons down to their thermal energy range, thus increasing the rate of fission thereby increasing the k_{eff}. The graphical relationship between these two parameters is shown in Figure 7.4 which is summarised mathematically by Eqn (7.52 [Leotlela, *et al.*, 2015])**.**

$Y = 0.61451 + 0.3841x$
A = 0.61451 σ = 6.94405E-4
B = 0.3841 σ = 6.97119E-4
$R^2 = 0.99933$

(7.52)

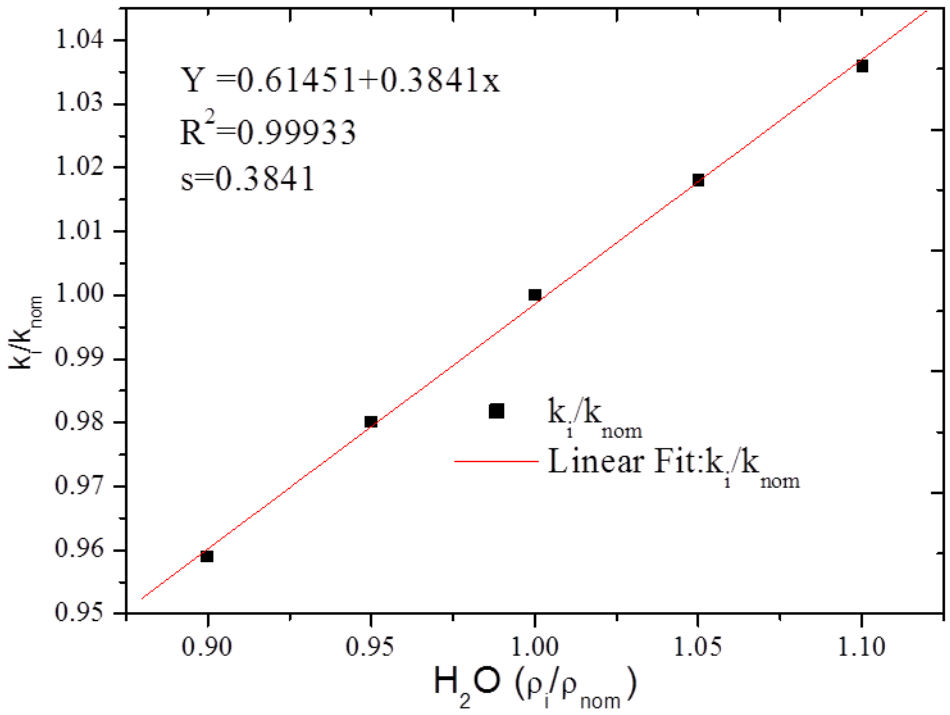

Figure 7.4: Effect of Perturbation of Moderator Density in the k_{eff} **[**Leotlela, *et al.*, 2015**]**

7.7.1.3 Perturbation of moderator and fuel temperatures

Perturbation of fuel and moderator temperatures reveals that there is a linear relationship between an increase temperature in both materials and a decrease in the k_{eff} of the system [Leotlela, *et al.*, 2015]. This is largely due to Doppler broadening effect of the temperature on the cross-sections of the two materials. Since the two materials i.e. fuel and moderator have different absorption and capture cross-sections, the mode of reaction with neutrons will also be different..

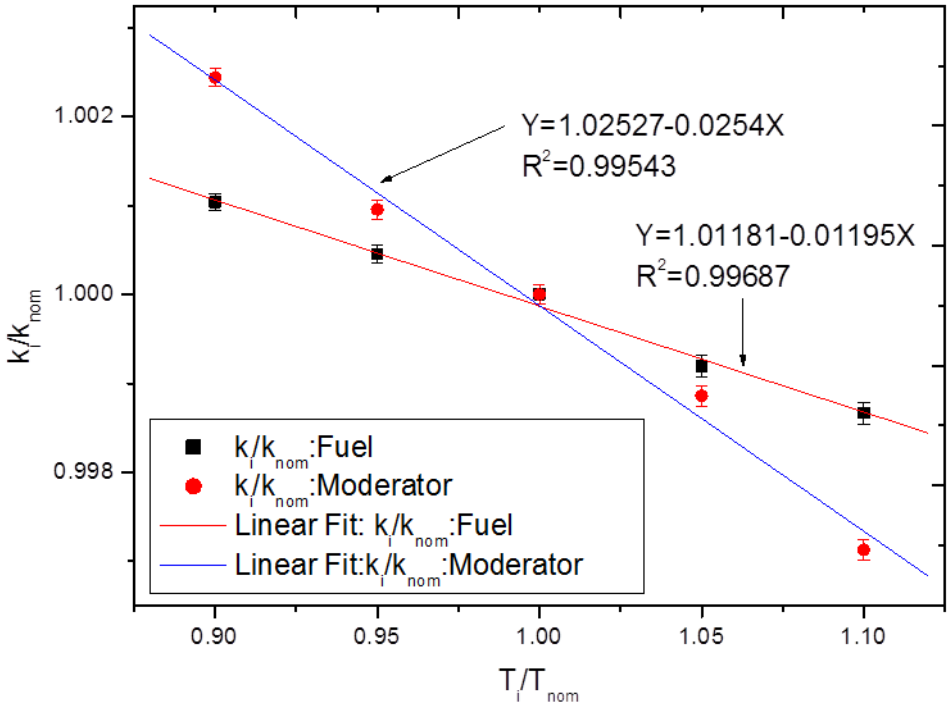

Figure 7.5: Comparison of Effects of Perturbation of Fuel and Moderator Temperature in k_{eff} **[**Leotlela, *et al.*, 2015**]**

In the fuel ^{238}U accounts for the largest fraction of Doppler broadening because of the resonance escape probability and the negative temperature coefficient being more affected than in other materials. However, because of its fission cross-section, it will tend to decrease the k_{eff} much slower than the moderator will do as shown in Figure 7.5, hence a lower sensitivity coefficient (B = - 0.01195) compared to that of the moderator (B = -0.02527) [Leotlela, *et al.*, 2015]. The relationship between these two parameters as summarised by the mathematical equation are shown in Table 7.1.

Table 7.1:Mathematical relationship between temperature and criticality (fuel and moderator) **[**Leotlela, *et al.*, 2015**]**

	Fuel	Moderator
Equation	$Y = 1.01181 - 0.01195x$ A=1.01181 $\sigma = 6.75509\times10^{-4}$ B=-0.01195 $\sigma = 6.82307\times10^{-4}$	$y = 1.02527 - 0.0254x$ A=1.02527 $\sigma = 6.835\times10^{-4}$ B=-0.0254 $\sigma = 6.88072\times10^{-4}$
R	0.99687	0.99543
SD	0.80144	2.04404

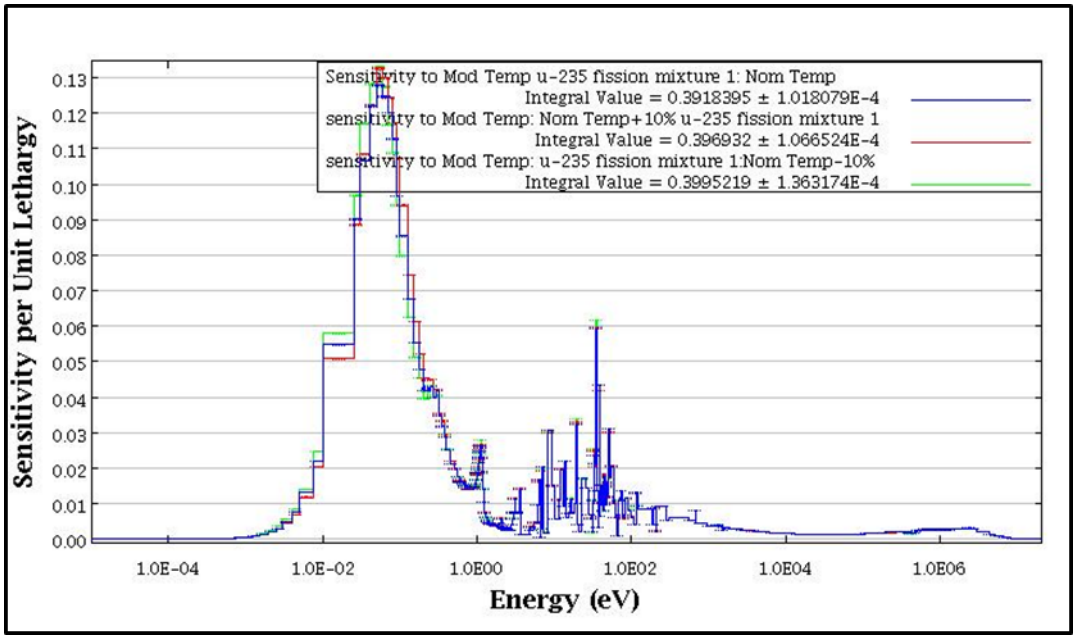

Figure 7.6: Sensitivity of ^{235}U fission to Moderator Temperature (Present study)

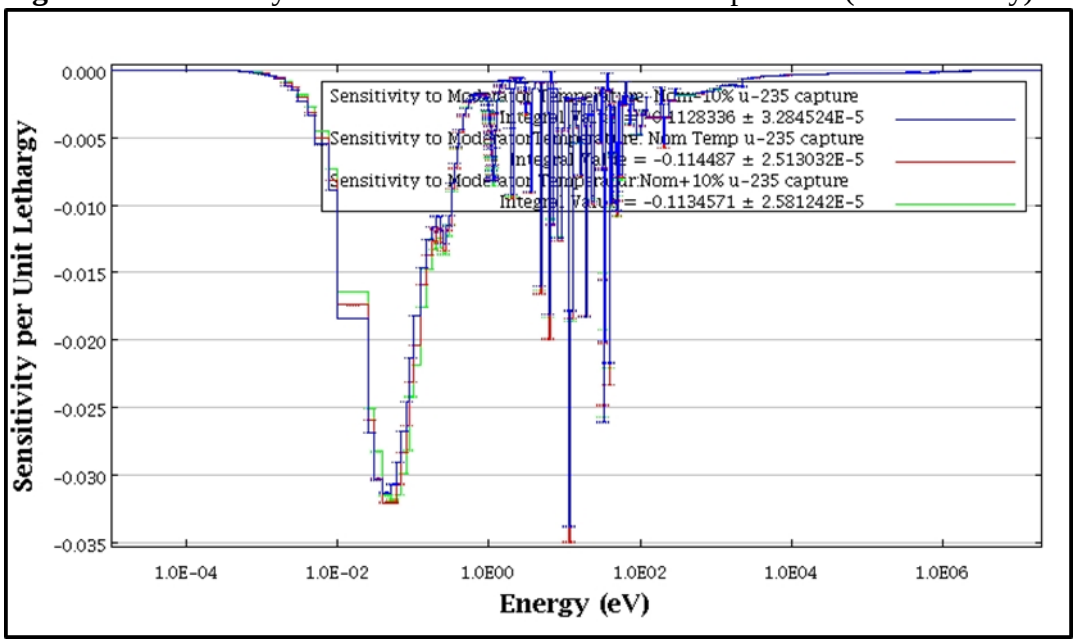

Figure 7.7: Sensitivity of ^{235}U capture to moderator temperature (Present study)

The sensitivity per unit lethargy for fission and capture of ^{235}U to moderator temperature is indicated in Figure 7.6 and Figure 7.7 respectively, which confirms the trend obtained in Figure 7.5.

7.7.1.4 Perturbation of polyethylene temperature

Before one can go to study the effect of perturbation of polyethylene to temperature, one has to understand what polyethylene is and what its chemical structure is and what happens when it is subjected to slight changes in temperature or when it is irradiated.

There have been a number of studies conducted to determine whether polyethylene will lose its shielding effectiveness when stored for a long time, subjected to high temperature changes or exposure to radiation. The studies were initiated as a result of concern that when polyethylene is stored for a long time or exposed to high temperatures or radiation exposure, it will result in deformation of the molecules or result in change in density due to changes in temperature (from decay heat, day light etc.) thereby resulting in premature failure in its effectiveness to provide neutron shielding.

One such study was conducted by Rodel, *et al.* [1998] of the German Nuclear Regulatory Authority in which all components of Castor X/28F were analysed for their mechanical and thermal stability. Their results indicated that there was no substantial change in polyethylene shielding effectiveness after it had been subjected to changes in temperature and pressure.

Polyethylene is one type of what in organic chemistry is referred to *n*-paraffin made-up of carbon and hydrogen of various carbon chain lengths such as,

- *n*-$C_{28}H_{58}$, *n*-$C_{35}H_{72}$,
- *n*-$C_{44}H_{90}$ and
- *n*-$C_{94}H_{190}$.

In the nuclear industry, polyethylene is used as neutron absorber in the spent fuel casks where it is continuously exposed to radiation from the spontaneous fission process. Studies conducted by Kawaguchi indicate that when polyethylene is irradiated with charged particles, it undergoes crystal structural deformation in the following order [Kawaguchi, *et al.*, 1982; Rodel, *et al.*, 1998]

- n-$C_{22}H_{44}$ and $C_{24}H_{50}$: undergo transition from triclinic to orthorhombic form.
- $C_{28}H_{58}$, $C_{36}H_{74}$ and $C_{44}H_{90}$: Undergo transition from monoclinic to orthorhombic phase [Kawaguchi, *et al.*, 1982]

The transition to a phase with high energy (orthorhombic phase) results in radiation-induced stresses. The excess strain energy produced by cross-links in structure is believed to be equal

to the enthalpy change of the phase transition, and the number of cross-links required to induce the phase transition is estimated as one per volume of about ten molecular chains [Kawaguchi, *et al.*, 1981].

In the study conducted by Rodel, it was concluded that because of change in structures, the performance of polyethylene as neutron absorber will be negatively affected. Kawaguchi [Kawaguchi, *et al.*, 1982] argued that, this depends on the molecular weight of the paraffin and the radiation dose it received. Kawaguchi was able to show that irradiation of any of the polyethylene monomers results in the widening of the lattice spacings, and that the degree of widening of the lattice spacings increases with irradiation dose and the molecular weight of the paraffin. In addition to an increase in the lattice spacings as a lattice defect, Kawaguchi *et al.* noted that irradiation of shorter paraffins resulted in amorphous patches being segregated out of the crystal lattice, thus improving the crystalinity of the paraffin [Kawaguchi, *et al.*, 1982].

Other factors which Kawaguchi identified to be the causes of phase transitions in polyethylene were the presence of impurity and temperature. As was the case in radiation study where the signs of structural defect were lattice spacings, in the case of temperature effects it is change in structure. Kawaguchi [Kawaguchi, *et al.*, 1981] noted that different paraffins of different structure are affected by temperature differently; the results show that an increase in temperature hardly ever induces phase transition of the triclinic form to the monoclinic form, while changing to orthorhombic takes place quite easily [Kawaguchi, *et al.*, 1981].

With regard to the effect of impurities on the stability of the paraffins, Kawaguchi observed that addition of a small fraction of impurities such as other homologs (i.e. other paraffins of a different carbon chain length from that of a base material) in the base material causes crystal transformation to take place in the base material paraffin of various modifications [Kawaguchi, *et al.*, 1982].

Therefore, based on this, it would be expected that the longer the carbon chain of a homolog, the better the shielding effectiveness will be because of the sheer number of light elements available for scattering.

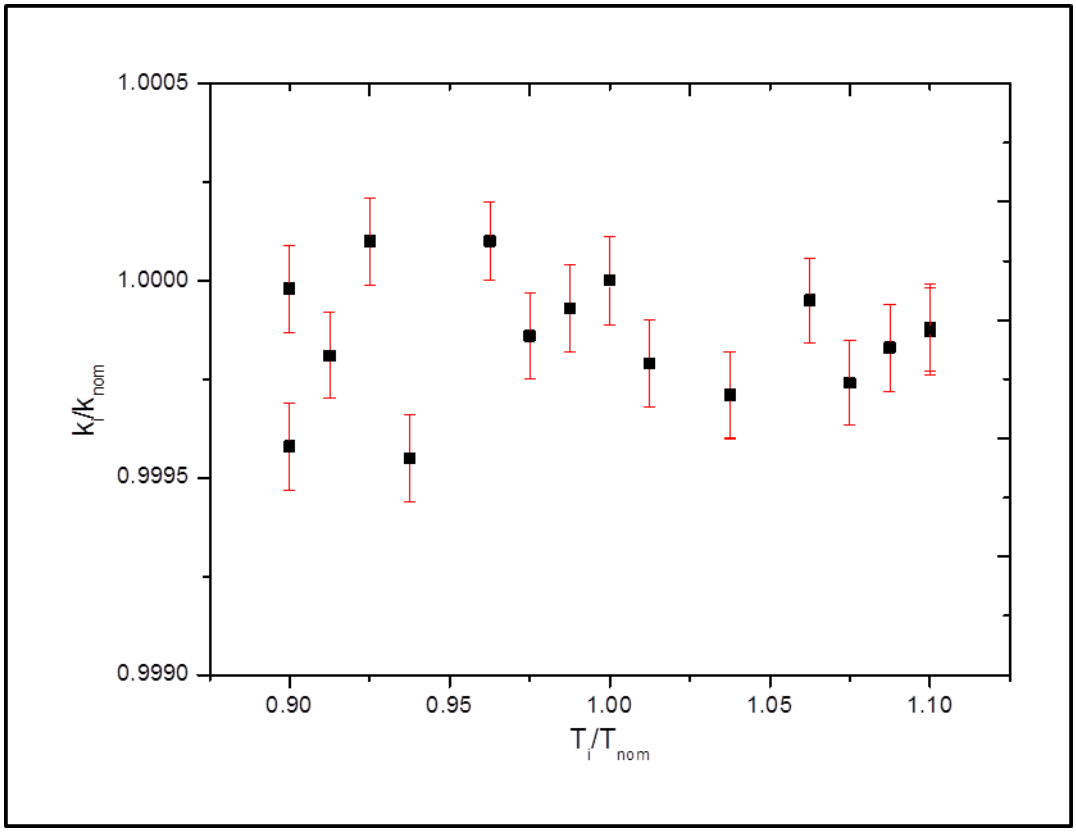

Figure 7.8: Perturbation of polyethylene (Present study)

In spent fuel storage technology, these paraffins are used quite extensively in neutron moderation because of light nuclide in their composition. For example the Castor X/28 F cask has 70 polyethylene rods which are of 7 cm in diameter and 370 cm in length distributed evenly around a radius of 104.5 cm to provide neutron shielding.

As shown in Figure 7.8, the results indicate that the k_{eff} has little or no sensitivity to temperature of polyethylene, which correlates very well with the findings of Kawaguchi and Rodel [Kawaguchi, *et al.*, 1981; Rodel, *et al.*, 1998]. In this study the density was held constant and only the temperature was varied, because of this the most significant contributor which seem to increase the attenuation coefficient of polyethylene to an exceptional neutron shielding material that it is, is how the H and C are arranged in the chemical structure of polyethylene.

Although polyethylene does not lose its shielding qualities, being exposed to radiation for an extended period of time accelerates its aging.

A classical example of this are the problems the US nuclear plants have with Boraflex, (which is a polymer loaded with B_4C crystals). After being irradiated for quite some time, boraflex panels shrink, forming gaps of unshielded areas in fuel racks, and also exhibit enhanced dissolution in spent fuel pools [US NRC, 2010; Northeast Technology Corp, 2008 (O'Leary, *et al.*, 1996)].

7.7.2 Perturbation of spent fuel parameters

7.7.2.1 Sensitivity to burnup changes

In 2002 Seong Hee Lee *et al.* conducted a study with a view of determining the effect of axial profile on the k_{eff} [Lee, *et al.*, 2002]. In that study Seong Hee Lee used various combinations of a flat burnup (where axial burnup profile was not taken into account) and an actual axial burnup profile and coupled these with different enrichment levels to determine what the effect of each combination would be in the k_{eff}. The results showed different trends depending on the enrichment level and whether a flat or actual axial burnup profile was used [Lee, *et al.*, 2002];

Table 7.2: The neutron multiplication factor as function of spent fuel burnup for GBC cask [Radulescu, *et al.*, 2008]

Average burnup (GWD/MTU)	Initial Enrichment (wt% ^{235}U)	Fuel Temperature (K)	EALF[22] (eV)	k_{eff}	σ
10	1.9972	293	2.09E-1	0.8975	0.0005
20	2.5563	293	2.42E-1	0.8854	0.0006
30	3.2025	293	2.67E-01	0.8807	0.0005
40	3.777	293	2.84E-01	0.8776	0.0004
50	4.3427	293	2.99E-01	0.8755	0.0006
60	4.8819	293	3.14E-01	0.8703	0.0005

[22] Energy of Average Lethargy for causing Fission

A. For a High Enrichment (4.6 wt%) and High Burnup (54 GWD/MTU) : A flat burnup distribution resulted in lower k_{eff} than the actual burnup distribution which became more severe (even lower k_{eff}) in longer cooling times.

B. At relatively low initial enrichment (3.0 wt %) and high burnup (54 GWD/MTU), the flat burnup distribution yields lower k_{eff} than those obtained from axial profile distribution. The k_{eff} was further decreased by a long cooling time. However, the degree of difference was less than was seen in the case of high enrichment and high burnup case.

C. For a high enrichment (4.6 wt%) and relatively low burunp (18 GWD/MTU): The flat burnup distribution yields higher k_{eff} than what is obtained with the actual axial profile at no cooling time and 1 year cooling time. However, the flat burnup results in lower k_{eff} than that obtained in axial profile burnup with a 5 year cooling.

D. In a 5 year cooling time case, the flat burnup distribution resulted in lower k_{eff} than is seen with axial profile.

7.7.2.1.1 Sensitivity and Uncertainty analysis of neutron multiplication factor to burnup by Direct Perturbation Technique

A similar study was performed at Oak Ridge National Laboratory and the results confirmed Lee's findings and the results are tabulated in Table 7.2 [Radulescu, *et al.*, 2008]. To determine sensitivity of k_{eff} to burnup, two techniques were used, in the first instance Direct Perturbation technique summarised by Eqn 7.53 was applied. The second technique entails using TSUNAMI-3D computer code and will be described in detail the following section. Also instead of using a three point DP technique, a multipoint DP technique was used which is described by [Mueller, *et al.*, 2005; Mueller, *et al.*, 2005a].

$$s = \frac{(k_1 - k_2)/k_{\text{nominal}}}{(\rho_1 - \rho_2)/\rho_{\text{nominal}}} \tag{7.53}$$

where k_1, k_2, k_{nominal} are the k_{eff} of the perturbed system, using the new values ρ_1 and ρ_2 from the perturbed system and the uncertainty coefficient is calculated using the following equation [Mueller, *et al.*, 2005a; Mueller, *et al.*, 2005]:

$$\sigma_s = \frac{1}{k_{\text{nominal}}}\left[\sigma_{k_1}^2 + \sigma_{k_2}^2 + \left(\frac{k_1 - k_2}{k_{\text{nominal}}}\right)^2 \sigma_{k_{\text{nominal}}}^2\right]^{0.5} \frac{\rho_{\text{nominal}}}{|\rho_1 - \rho_2|} \tag{7.54}$$

where σ_{k1} , σ_{k2} and $\sigma_{knominal}$ are calculated standard deviation associated with k_1, k_2, and $k_{nominal}$. It was found that sensitivity of k_{eff} of various nuclide sets to burnup obey the following respective equations [Leotlela, *et al.*, 2015]

$$\begin{aligned} y_{actinides} &= -852.07x^5 + 4466.4x^4 - 9325x^3 + 9694.6x^2 - 5019.6x + 1036.7 \\ R^2_{Major\ actinides} &= 0.9908 \end{aligned} \quad (7.55)$$

$$\begin{aligned} y_{Major\ actinides+Minor\ FP} &= -1492.1x^5 + 7678.6x^4 - 15765x^3 + 16139x^2 - 8239.7x + 1679.2 \\ R^2_{Major\ actinides+Minor\ FP} &= 0.9864 \end{aligned} \quad (7.56)$$

$$\begin{aligned} y_{Major\ actinides+Principal\ FP} &= 335.36x^5 - 1364.4x^4 + 2110.9x^3 - 1504x^2 + 455.92x - 32.745 \\ R^2_{Major\ actinides+Principal\ FP} &= 0.9978 \end{aligned} \quad (7.57)$$

where, $y = k_i/k_{nom}$ and $x = BU_i/BU_{nom}$

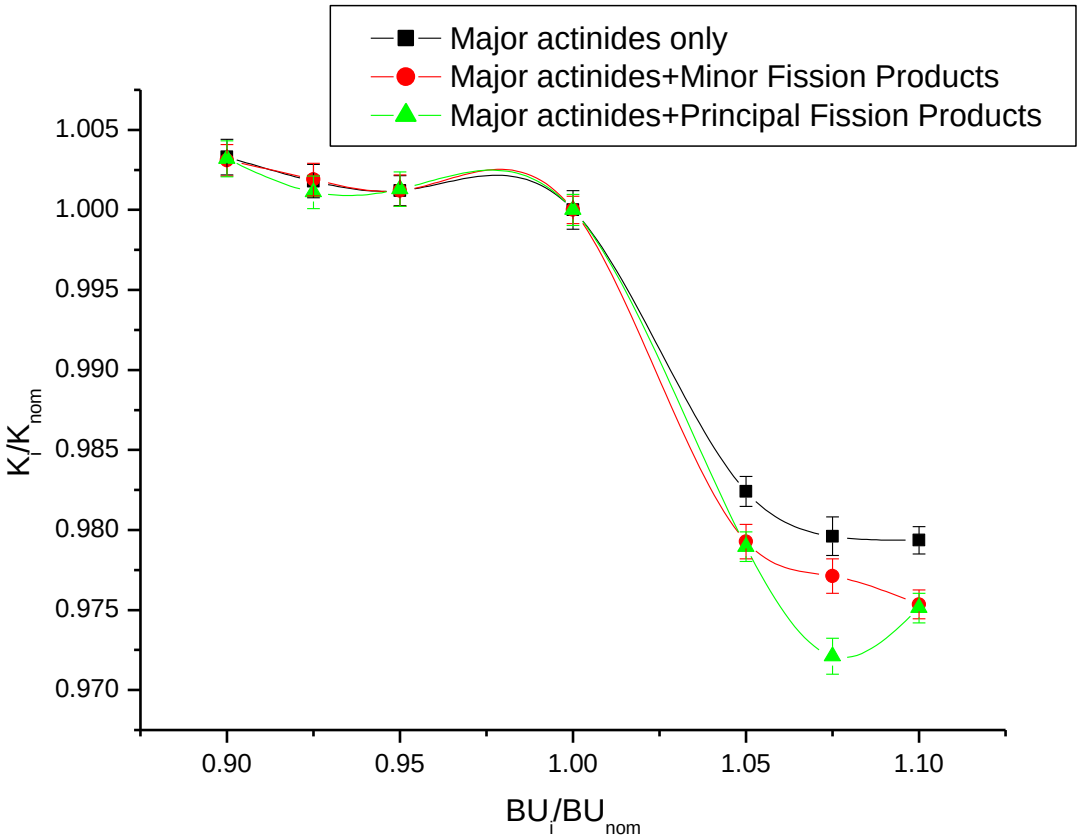

Figure 7.9: Sensitivity of the three nuclide sets to burnup used in the analysis of CASTOR X/28. [Leotlela, *et al.*, 2015]

The study started with an initial enrichment of 3.9 wt% and nominal burnup of 40 GWD/MTU. The burnup was increased by values ranging from +/-2.5%, to +/-10% and in each case all three burnup credit nuclide sets were taken into account [Leotlela, *et al.*, 2015]. After each simulation the k_i/k_{nom} and the Bu_i/Bu_{nom} were calculated using Eqn 7.53 and instead of using Eqn 7.54 to calculate σ_s direct difference method was used and the results are indicated in Figure 7.9. It is observed that there is a decrease in k_{eff} as burnup increases. It is, however, observed that the decrease is not uniform; at lower burnups between 36 GWD/MTU and 38 GWD/MTU it is much slower and between 40 GWD/MTU and 43 GWD/MTU it is much more rapid. Looking at the graph, it is observed that there is a *cliff-edge* at (BU_i/BU_{nom} = 0.981655844, k_i/k_{nom}= 1.00257314) and that the co-ordinates of the *cliff-edge* for the three nuclides sets coincides. The relationship between k_i/k_{nom} and Bu_i/Bu_{nom} and their respective correlation coefficients for all three nuclide sets is summarised mathematically by equations (7.55), (7.56) and (7.57). The total sensitivity coefficients of any of these nuclide sets indicated in the graph may be obtained by determining the differential of the respective equation at the point of interest [Leotlela, *et al.*, 2015].

7.7.2.2 Tsunami-3D sensitivity and uncertainty analysis of major actinides

The study of sensitivity of major actinides was largely driven by similar research that was done in 2005 by Oak Ridge National Laboratory (ORNL) aimed at investigating the accuracy of each Burnup Fission Product cross-section [Radulescu, *et al.*, 2008; Mueller, 2013c].

The main aim of Major Actinides Sensitivity analysis as carried out in this thesis is to use TSUNAMI-3 to determine by how much the k_{eff} of the system is affected by the variation in cross-section of a given fuel composition, which is what TSUNAMI-3 tells an analyst. On the other hand, the sensitivity of k_{eff} to a particular nuclide-reaction pair macroscopic cross-section $\left(\sum_x^n\right)$ referred to as sensitivity coefficient, provides a measure of a first-order effect of perturbation in nuclear reaction x for nuclide n upon k_{eff}. A sensitivity coefficient is computed as a sum over all energy groups of the sensitivities of k_{eff} to group-wise cross-section. [Radulescu, *et al.*, 2008; Mueller, 2013c]

Based on the definition of sensitivity above, one can deduce that it is important that the accuracy of a cross-section of a particular nuclide for a specific reaction is known. Therefore, in that regard the accuracy of actinide cross-section is very important to criticality analyses for the following reasons;

- the microscopic cross-section of the nuclide determines the reactivity worth of actinide in spent fuel when determining the importance or fractional contribution of that nuclide to burnup credit (BUC) of the entire set of Major Actinide [Mueller, *et al.*, 2005a],
- the cross-section of the nuclide determines the reaction rate during the depletion/irradiation of the fuel and determines the degree of accuracy to which the final concentrations of various nuclides in the spent fuel can be predicted [Mueller, *et al.*, 2005a];
- the radiation damage of the material and consequently crystal structure transformation that results from irradiation [Matzke, 1992].

This research will only evaluate the effect cross-section of Major Actinides in the k_{eff} of the system and not fission products or any of the precursor nuclides since they have already been studied. The methodology for this part was divided into two stages;

- **Phase 1**

The Burnup Credit is the first phase of the TSUNAMI-3D sensitivity and uncertainty calculation. It involves application of STARBUCS (Standardized Analysis of Reactivity for Burnup Credit using Scale) sequence to create *sysin2file* criticality input file by making use of the *shell* command, which is written at the end of the depletion input file (i.e. at the End of STARBUCS) as follows [Mueller, *et al.*, 2005a; Mueller, *et al.*, 2005b; Radulescu, *et al.*, 2008];

```
#shell

copy sysin2 "%RTNDIR%\%why%.buc.input"

end.
```

This will copy the **sysin2file** with the file name ***why*** to the same directory where STARBUCS was executed and append it with .buc file extension e.g. *%why%.buc.input* (Refer to APPENDIX 3) [Leotlela, *et al.*, 2015]. The initial enrichment of the fuel was 3.9

wt% ^{235}U and it was subjected to three different burnups; 20 GWD/MTU, 40 GWD/MTU and 60 GWD/MTU and the cooling time of each burnup level was divided into three different categories; 1 year, 5 years and 10 years [Mueller, 2013d].

There are other similar studies which have been done before, however the approach was different in the sense that the cooling time was kept constant (5 years) but enrichment increased as burnup is increased. These include those published by Radulescu and Mueller [Radulescu, *et al.*, 2008].

For the purpose of this analysis the cask was modelled as fully loaded (28 fuel assemblies) with a 17×17 PWR fuel assemblies and all the air-gaps in the interior of the cask replaced with water. The nuclide whose cross-sections were investigated were Major Actinide nuclides.

- **Phase II**

In the second phase the **sysin2file** that was created in the STARBUCS depletion phase was imported into the TSUNAMI-3D input file and the cell data divided into 18 axial sections with their corresponding media alongside each component of the cell data. The geometry in unit 1 was also divided into 18 axial fuel zones and used the 18 fuel mixtures in the media cards for unit 1, and finally added the *read* SAMS block. The parameter input deck was as follows [Mueller, 2013a; Mueller, 2013d, Leotlela, *et al.*, 2015,];

read parameter

gen = 10000, npg = 10000, nsk = 100, htm = yes, nub = no, apg = 20000, agn = 20000, ask = 200, sig = 0.0001, as g= 0.001, tfm = no , pnm = 1, mfx = yes msh = 10

end parameter.

The programme was then executed and sensitivity coefficient of each nuclide read from the output file.

It is important to note that under normal conditions the fuel burned in the PWR core exhibits an axial burnup profile as a result of uneven distribution of neutron flux caused by neutron leakage and temperature gradient along the length of fuel assembly. This leads to a high concentration of fission products around the middle of the fuel assembly and low concentrations at the top and bottom ends of the fuel assembly, creating the *end-effect* as has already been discussed in the previous section. In a storage situation there is no such

temperature gradient, hence the axial fission distribution is much higher near the top compared to the same fuel assembly in the core [Mueller, *et al.*, 2005b]. As a result of changes in isotopic composition along the length of the fuel assembly, the results were taken from the total integrated sensitivities from the 18 mixtures. The results are summarised in APPENDIX 4[Leotlela, *et al.*, 2015].

Oak Ridge National Laboratory conducted a study to determine the relative sensitivity coefficients of a number of nuclides with a view to ranking the nuclide cross-sections that need to be revised. The results were documented in ORNL/TM-2005/48 [Mueller, *et al.*, 2005a; Mueller, 2013]. The Fission Product nuclides which were investigated in the study by Gauld, *et al.* were;

^{99}Mo, ^{99}Tc, ^{101}Ru, ^{103}Rh, ^{109}Ag, ^{133}Cs, ^{143}Nd, ^{147}Sm, $^{149\text{-}152}$Sm, ^{155}Gd and ^{153}Eu.

Because the concentration of nuclear reaction products changes dramatically during irradiation the sensitivity coefficients are thus burnup-,time- and region-dependent, the burnup in that case was held constant at 43 GWD/MTU [Mueller, *et al.*, 2005a].

Also, because burnup credit fission products are in many cases stable; their coefficients also do not change appreciably from discharge from the reactor.

However for those fission products that changed appreciably after fuel discharge e.g. ^{147}Sm and ^{155}Gd the coefficients were calculated after the cooling period of 5 and 20 years while in other cases 1 year cooling was sufficient. It is important to note that the coefficients represent the relative importance of the fission product cross-section to the predicted concentration of each burnup credit fission product.

The coefficients were evaluated with respect to the radiative capture cross-sections $\sigma(n,\gamma)$ [Gauld, *et al.*, 2005]. The results showed that the relative sensitivity coefficients for each burnup credit fission product are as illustrated in ORNL/TM-2005/48 [Gauld, *et al.*, 2005]. The Figure shows that the concentration of many fission products is sensitive to their own cross-section. However, ^{133}Cs, ^{145}Nd, ^{99}Tc, ^{95}Mo and ^{101}Ru exhibit relatively low cross-section sensitivities, with sensitivities coefficients of less than 0.2 [Gauld, *et al.*, 2005].

The other fission products (^{103}Rh, ^{109}Ag, ^{143}Nd, $^{147,149\text{-}152}$Sm, ^{155}Gd and ^{153}Eu) display larger cross-section sensitivity. Most fission products show relative sensitivity to their own cross-section with the exception of ^{151}Sm, ^{155}Gd, ^{153}Eu and ^{147}Sm which exhibit sensitivity to the

cross-section of their precursors. Gauld further lists sensitivity coefficients as follows; ^{150}Sm(S=0.4), ^{155}Eu(S= -0.95), ^{152}Sm(S = 0.32) and ^{147}Pm(S = -0.48) respectively. Gauld and Mueller commented further that the reason for the high sensitivity to the precursor fission product is that production by neutron capture and not directly by fission is a dominant mode of production [Gauld, *et al.*, 2005].

TSUNAMI-3 calculations were only run on nominal concentration and the sensitivity coefficient is read directly from the TSUNAMI-3 output [Leotlela, *et al.*, 2015].

CHAPTER 8

8.0 CONCLUSION AND RECOMMENDATIONS

8.1 Acceptability of the present design for use in higher fuel enrichment

As stated in Section 1.2 the two primary objectives of this project were to: i) ascertain whether the present cask design can be used to store fuel assemblies with higher enrichment given that they are only licensed for 3.5 wt%; ii) and to determine if there was a significant difference in criticality between fuel assemblies from AREVA (AFA-3G) and the one from Westinghouse (374-RFA).

Considering Table 5.3, when the three enrichment levels are compared at 600 K, it is observed that at the 3.9 wt% and 4.4 wt% enrichment the results are well below the regulatory safety limit of k_{eff} = 0.95, while at 5.0 wt% both fuel assemblies are above the regulatory limit. Also, at 4.4 wt%, their k_{eff} are so close to the safety limit that the safety margin is only 2.5%, which is below the recommended 10%. Therefore, neither of the two fuel assemblies can be stored in the present consignment of casks.

On the question of which one of the two fuel assemblies is more reactive, it is observed that at 600 K, AFA-3G is more reactive at lower enrichment (3.9 wt%) than 374-RFA by 0.056% and at higher enrichments (5 wt%) 374-RFA is more reactive by the same percentage margin.

8.2 Sensitivity of k_{eff} to parameters important to criticality nuclear safety of Castor X/28 spent fuel Cask

Sensitivity and uncertainty analysis was performed on both fresh fuel and on spent fuel. On the fresh fuel, analysis was largely performed by Direct Perturbation (DP) while for spent fuel, TSUNAMI-3D was used [Leotlela, *et al.*, 2015]. The parameters investigated for *fresh fuel* are discussed in detail in section 7.7.1 while those of spent fuel are discussed in 7.7.2 .

8.2.1 Sensitivity to ^{10}B concentration

The results indicate that the sensitivity of k_{eff} to ^{10}B concentration follows a non-linear relationship defined by the differential equation given in section 7.7.1.1 derived from Figure 7.2 [Leotlela, *et al.*, 2015]. This is implies that the concentration of ^{10}B can only be increased up to a certain point where the k_{eff} will still decrease; beyond that point it reaches a saturation point where no further increase in ^{10}B concentration will result in further decrease of k_{eff}.

8.2.2 Sensitivity to temperature

With regard to sensitivity of k_{eff} to fuel and moderator temperature, it is noted that the moderator with a sensitivity coefficient of - 0.0254 is much more sensitive to temperature perturbation than the fuel which has the sensitivity coefficient of - 0.01195. This implies that when the temperature of the system increases and there is a corresponding decrease in k_{eff}; the decrease will largely be due to the effect of the moderator rather than due to the effect of temperature on the fuel (Figure 7.5).

8.2.3 Sensitivity to moderator density

On the moderator density, the results show that as the moderator density increases so will the k_{eff}, and the sensitivity coefficient has been found to be 0.3841 (Figure 7.4). This may be understood if one considers neutron moderation in the presence of hydrogen where absorption is ignored. If one takes into account the logarithmic energy decrement of all light elements, one will notice that hydrogen has the highest logarithmic energy decrement of all isotopes in the geometry and ^{238}U has the lowest which are 1.00 and 0.00838 respectively. As the density of water is increased, it implies that there will be more hydrogen molecules in the system available to cause scattering which subsequently results in thermalisation of neutrons. As a result of the gradual increase in the number of neutrons in the thermal energy range caused by an increase in moderator density, there will be a corresponding increase in k_{eff} as moderator density increases [Leotlela, *et al.*, 2015].

8.2.4 Sensitivity to polyethylene temperature

Research indicates that when polyethylene is irradiated, it undergoes crystal structure deformation in the following order [Kawaguchi, *et al.*, 1982; Rodel, *et al.*, 1998]

- n-$C_{22}H_{44}$ and $C_{24}H_{50}$: undergo transition from triclinic to orthorhombic form.
- $C_{28}H_{58}$, $C_{36}H_{74}$ and $C_{44}H_{90}$: undergo transition from monoclinic to orthorhombic phase [Kawaguchi, *et al.*, 1982]

The transition to a phase with high energy (orthorhombic phase) results in radiation-induced stresses. The excess strain energy produced by cross-links in structure is believed to be equal to the enthalpy change of the phase transition. The number of cross-links required to induce the phase transition is estimated to be one per volume of about ten molecular chains [Kawaguchi, *et al.*, 1981].

With regard to the effect of increase in temperature structural changes, it has been observed that different paraffins of different structure are affected by temperature differently. For example, an increase in temperature hardly ever induces phase transition of the triclinic form to the monoclinic form, whereas changing to orthorhombic takes place quite easily [Kawaguchi, *et al.*, 1981].

It has also been noted that the longer the carbon chain of a homolog, the better will be the shielding effectiveness of that paraffin compared to the shorter carbon chain homologs.

8.3 Selection of the optimum storage array

In this section the objective of the study was to ascertain what the effect of: 1) different storage arrays and 2) changing the distances among adjacent casks would be on the k_{eff}. Two cases were investigated which involved four casks and thirty casks in two different arrays. In the case of four casks, one scenario focussed on the linear (1X4) array while the other focussed on the 2X2 square array. Similarly, the thirty casks were arranged in 2X15 and in 3X10 arrays and the change in k_{eff} plotted as a function of the separation gap among adjacent casks. The cases were further divided into misaligned casks and compared to traditional storage arrays where all casks were at the same level. The results in Figure 4.11 indicate that the k_{eff} from the misaligned array is lower than in the traditional 2X15 array by an average Δk of 0.0050. Since the distance between the two rows were the same in both arrays, the difference in the k_{eff} may be ascribed to the change in the Dancoff factor when one changes the array and the end-effect which becomes less effective as the distance between the adjacent casks increases.

It has further been proven that the casks in misaligned 3X10 storage arrays, irrespective of whether they are horizontal or vertical, result in much lower k_{eff} than those in a traditional 3X10 vertical orientation. Since the gaps between the rows of the two arrays were kept constant, the difference in k_{eff} will be as a result of misalignment of the two reactive ends of adjacent casks which resulted in the decrease in the k_{eff}.

When on compares vertical and horizontal casks, it is observed that there is no significant difference in the neutron multiplication factor of the two arrays, the wave-like variation in k_{eff} from one position to the next is due to stochastic variation the number of neutrons in the thermal energy range.

In the case of four casks, it was observed that the linear arrays (1X4) will yield much lower k_{eff} compared to the square arrays (2X2) for every unit separation made among the adjacent rows. Comparing different configurations of 1X4, it was observed that the *staggered/misaligned* storage array resulted in lower k_{eff} compared to the *traditional* 1X4 linear matrix. This is due to the fact that the reactive top and bottom ends of adjacent casks are misaligned and when the casks stand next to each other the reactive end of one cask fits in the non-reactive middle part of its adjacent partner. As a result of this, misaligned casks result in lower fission rate than in traditional 1X4 array where the reactive ends are aligned. Similarly the 3X10 array will yield much lower k_{eff} than their 2X15 counterparts. The common denominator between the 1X4 array and the 3X10 is that they both have a middle array which acts as a neutron absorber for neutron origination from the outer rows. Resonance- and spatial self-shielding are the two most important elements of shielding which will add to neutron absorption in the two arrays and consequently lead to a decrease in k_{eff}. The absence of spatial shielding in the 2X15 and 2X2 arrays combined with the fact that as the distance between two rows increases it will result in neighbouring casks moving away from the influence of End-Effect of one another, thereby resulting in a decrease in k_{eff}. This, combined with the fact that as adjacent casks move away from one another, the total volume occupied by the array of casks will also increase and thus decrease the flux density. Since neutrons have very short mean free path, their neutron importance will decrease which will subsequently lead to a decrease in k_{eff}. However, because these do not have the middle row, their decrease in k_{eff} per distance of separation is much slower than those containing the middle row. This slow decrease in k_{eff} is further exacerbated by the fact that as the distance among adjacent casks is increased, the cask actually moves closer to the walls of the building,

resulting in an increase in back scattering of neutrons back to the cask. The net effect is that 2X15 and 2X2 have a much slower decrease in k_{eff} compared to the 3X10 or 1X4 array. Therefore, if there are only a few casks to store, it would be recommended that they be stored in such a manner that they shield one another rather than not. Therefore, in a case where there are four fully loaded casks to be stored, it would be recommended that they are stored in a staggered 1X4 array rather than in a 2X2 array.

If one is to choose between changing storage array or to use burnup credit to increase the capacity of the spent fuel. It has been proved that the degree of burnup has a much greater effect in the reduction of the k_{eff} than the type of an array has. This implies that although the choice of the storage array can make a significant contribution in increasing the capacity of the storage facility, this is more relevant to fresh fuel than in used fuel. In spent fuel, burnup credit is by far the most effect means to achieve this goal.

8.4 Risks that can lead to an increase in the k_{eff} of the system

Two accident scenarios were investigated, Water Ingress and Misload accident scenarios. The water ingress has always been one of the top priority accident scenarios because of the potential accident that can happen while being transported to the Radioactive Waste Storage facility. Its importance and popularity was further heightened by the Fukushima Daiichi Nuclear Plant accident.

The second scenario which proved to be of importance because of its high probability is the misload accident scenario.

8.4.1 Water-ingress

8.4.1.1 The neutron multiplication factor as a function of rising water levels

On the relationship between rising levels of water and the k_{eff}, it has been shown in both horizontal and vertical cases that the most critical amount of water from nuclear criticality safety point of view is the first few litres (up to 10% of empty space) since it has the greatest effect in the k_{eff} of the system. It will increase the k_{eff} of the system from the lowest k_{eff} (of 0.21 and 0.34 in vertical and horizontal casks respectively) when filled with air to its highest

(0.92 and 0.938 respectively) irrespective of whether the cask is horizontal or vertical. From there onward, the k_{eff} will stay constant regardless of the amount of water added.

It has also been shown that water ingress in a horizontal cask resulted in higher k_{eff} than in vertical casks by an average $\Delta k \approx 0.02$ at any level of water in the cask. However when two scenarios are compared at 100% full, the horizontal cask has a lower k_{eff} than in the vertical cask.

8.4.1.2 Freshwater versus Seawater

When the fresh water is compared to the seawater, the results show that the cask flooded with freshwater results in higher k_{eff} compared to that containing seawater. This may be ascribed to the fact that seawater contains significantly more chemical elements than pure freshwater, some of which have a very high neutron absorption cross-section e.g. chlorine and bromine. The neutron absorption cross-section will reduce the number of neutrons participating in fission and subsequently lead to a reduction in k_{eff}. Therefore, because of this, seawater will tend to make cask less reactive and safer compared to the freshwater. Therefore, in an accident situation where the spent fuel pools are running dry and fuel temperature is increasing as has been the case at the Fukushima Daiichi Nuclear Reactor, it is recommended that they are cooled with seawater instead of freshwater.

8.4.2 Fuel assembly misload

The study has found that there is a direct correlation between the number of fuel assembly surrounding the misloaded fuel assembly and magnitude of the neutron multiplication factor; and also between the distance between the misloaded fuel assembly and its neighbouring fuel assemblies. The research findings indicate that the higher the number of fuel assemblies surrounding the misloaded cask the higher the k_{eff}, and the wider the gap between the misloaded fuel assembly and its neighbouring units the lower the k_{eff}. This is to be expected since; if the misloaded fuel assembly is surrounded by four neighbouring fuel assemblies as is the case with (16.25; 16.25), which is the maximum number of nearest fuel assemblies it can be surrounded with, it will be exposed to neutrons escaping from 4 fuel assemblies compared to those at (46.95;16.25) and (94.9;0) which only have two fuel assemblies around them. Therefore, the misloaded fuel assembly with higher neighbouring fuel assembly will yield higher k_{eff} .

Secondly if the neighbouring fuel assemblies are farther away from the misloaded fuel assembly, the k_{eff} will decrease because the mean free path of neutrons is very short, hence as the gap between the neighbour and the misloaded fuel assembly increases, the k_{eff} decreases.

Where multiple misloads are considered, it has been found that the neutron multiplication factor is a function of a number of misloaded fuel assemblies and the location of misloaded fuel assemblies; for a constant number of fuel assemblies, it has been found that;

- the k_{eff} will be higher in a case where all misloaded fuel assemblies are near the centre of the cask e.g. (16.25; 16.25), compared to those that are farther away (46.95;16.25) and (94.9;0) and fuel assemblies misloaded in the periphery (94.9;0) will have the lowest k_{eff}.
- In a case of two misloaded fuel assemblies, the study shows that if one of the misloaded fuel assemblies is near the centre of the cask (16.25;16.25), and the other at (46.95;16.25) the k_{eff} will be higher compared to the case when one of the casks is at (46.95;16.25) and the other at the periphery (94.9;0).

8.5 Taking credit for burnup of major actinides + minor fission products

In light of the shortage of storage space in the spent fuel pool and the fact that this already has taken credit of Major Actinides, it is recommended that consideration be given to taking credit of *Major Actinides + Minor Fission Products* nuclide sets. The results of the study show that this nuclide set can decrease the k_{eff} quite considerably compared to the *Major Actinides Only* nuclide sets and still leave a reasonable safety margin compared to the *Major Actinides+Principal Fission Products* nuclide sets. As Wagner (Wagner, 2006) indicated, inclusion of fission products in burnup credit calculations will increase the number of acceptable fuel assemblies from 11% to 58%. This is a significant amount of increase in the number of acceptable fuel assemblies to be loaded in the casks and can buy Eskom (Koeberg) a fair amount of time and storage space while maintaining the safety margin within the regulatory limit.

Not only does it save Eskom storage space, there will also be a reduction in the number of consignments to the Interim Spent Fuel Storage Installation, thus reducing the risk of nuclear related accidents associated with transportation of spent fuel to the storage facility.

Also, given that Rimpler and Buchiller proved that neutrons can travel as far as 10 m from the cask, it is recommended that a 10 m dose rate measurement from the cask be performed regularly in addition to current contact and 1 m dose rate measurements.

In a case where the casks are stored out in the open field (not inside the building) it is recommended that a fence is erected around them to prevent members of the public coming too close. The casks must be at least 10 m away from the fence.

Based on the fact that both Eskom and NECSA could save a significant amount of storage space if burnup credit were taken into account, it would be tremendously helpful if NNR's position on this matter were known to its licensees. This could be done by being forthright, that is, by developing its own requirements document (RD) that specifically addresses the requirements for nuclear criticality safety, as it did with other aspects of nuclear safety (please refer to http://www.nnr.co.za/acts-regulations/regulatory-documents/ for a list of NNR regulatory documents). If this were done, both Koeberg and NECSA would know what nuclide sets are acceptable for burnup credit analysis relating to the spent fuel pool and for casks, and what nuclides constitute these nuclide sets. Being forthright about this matter, and informing the public and the licensees about what nuclide sets can be taken into account for burnup credit in nuclear criticality safety analysis, would not make the public and the environment any less safe than it would be if the licensees were to propose the nuclide sets and the NNR to accept the proposal.

8.6 CONCLUSION

In conclusion, under the current state of affairs of the spent fuel pool, taking into consideration that the present casks cannot be used for higher enrichment and the lengthy period of procurement for new casks, it is recommended that burnup credit and neutron absorber inserts be given consideration to relieve the demand in the spent fuel pool storage space. There role of crystal structure transformation on the neutron multiplication factor of the system has been greatly undervalued/underestimated. It is therefore prudent that when surveillance of a Reactor Pressure Vessel (RPV) is performed, one does not only look at signs of material degradation like corrosion only which are easily observable to unaided eye, but also perform microscopic analysis of the SSC to determine if there is any crystal structure transformation which may not only result in material degradation but also have an effect on the k_{eff} of the system.

ACRONYMS 1

BCC	Body Centred Cubic
BOC	Beginning of cycle
BUC	Burnup Credit
CAFTA	Computer Aided Fault Tree Analysis
EOC	End of cycle
EPRI	Electric Power Research Institute
FA	Fuel Assembly
FCC	Face-Centred-Cubic
GNB	Gesselschaft für Nuklear-Behalter mBH
GWD/MTU	Giga Watt Day per Mega tonne of Uranium
HAW	High Active Waste
HEP	Human Error Probabilities
IAEA	International Atomic Energy Agency
ISFSF	Interim Spent Fuel Storage Facility
ISG8	Interim Staff Guidance 8
KW	Kilowatt
MCNP	Monte Carlo N-Particle
MWD/MTU	Mega Watt Day per Mega tonne of Uranium
NNR	National Nuclear Regulator
NRC	Nuclear Regulatory Commission
O/M	Oxygen-to-Metal ratio
ORNL	Oak Ridge National Laboratory

PWR	Pressurized Water Reactor.
RWMP	Radioactive Waste Management Policy
SCALE	Standardized Computer Analysis for Licensing Evaluation
SNF	Spent Nuclear Fuel
STARBUCS	Standardized Analysis of Reactivity for Burnup Credit using Scale
TRS	Technical Requirement Specification
TSUNAMI	Tools for Sensitivity and Uncertainty Analysis Methodology Implementation
UO_2	Uranium dioxide
URS	User-requirement Specification
WKB	Wentzel, Kramers & Brillouin approximation

APPENDIX 1: Design data of Castor X/28 Cask

Borated stainless steel								
Thickness (cm)	1		Cross-sections (barns)					
Density (g/cm^3)	7.8	ξ	σ_a	σ_s	σ_t	Σ_a	Σ_s	Σ_t
Borated Steel composition (%)								
Boron(nat)	0.9	0.171	755	4	759	103	0.346	104
Silicon (Si)	1	0.0698	0.16	1.7	1.8	0.008	0.089	0.097
Manganese (Mn)	2	0.0359	13.2	2.3	15.5	1.04	0.181	1.22
Chromium (Cr)	19	0.0385	3.1	3	6.1	0.255	0.247	0.501
Iron(Fe)	67.1	0.0353	2.62	11	13.6	0.222	0.933	1.15
Nickel (Ni)	10.0	0.0335	4.6	17.5	22.1	0.420	1.60	2.02
Stainless Steel								
Thickness(cm)	1							
Density(g/cm^3)	7.8							
Stainless Steel composition (%)								
Chromium(Cr)	18	0.0385	3.1	3	6.1	0.255	0.247	0.501
Manganese(Mn)	2	0.0359	13.2	2.3	15.5	1.04	0.181	1.22
Iron (Fe)	69.5	0.0353	2.62	11	13.6	0.222	0.933	1.15
Nickel (Ni)	10.5	0.0335	4.6	17.5	22.1	0.420	1.60	2.02
Cask Body Specification								
Density g.cm^{-3}	7.8							
Composition (%)								
Iron (Fe)	92.63	0.0353	2.62	11	13.6	0.222	0.933	1.15
Graphite (C)	3.5	0.158	0.004	4.8	4.8	32[23]	0.385	0.385
Silicon(Si)	1.96	0.0698	0.16	1.7	1.8	0.008	0.089	0.097
Nickel (Ni)	1.31	0.0335	4.6	17.5	22.1	0.420	1.60	2.02
Manganese (Mn)	0.60	0.0359	13.2	2.3	15.5	1.04	0.181	1.22

[23] Value has been multiplied by 10^5

APPENDIX 2 : X-Y-co-ordinates of fuel assemblies on the outer source of the cask (z= 0, a2= 0, a3= 0)

Fuel Assembly #	XY-Co-ordinates		β (a1)
	X	Y	
1	94.9	0	0
2	0	94.9	0
3	87.676	36.316	20
4	36.316	87.676	-20
5	67.105	67.105	-45
6	-94.9	0	0
7	-87.676	36.316	-20
8	-67.105	67.105	45
9	-36.316	87.676	20
10	-87.676	-36.316	20
11	-67.105	-67.105	45
12	-36.316	-87.676	-20
13	88.6	-36.699	-20
14	67.105	-67.105	45
15	36.316	-87.676	20
16	0	-94.9	0

APPENDIX 3: Sysin2 file for 40 GWD/MTU

```
u-234      101   0  5.4693E-06   400.0 end
 u-235      101   0  7.4657E-04   400.0 end
 u-238      101   0  2.3128E-02   400.0 end
np-237      101   0  1.6330E-06   400.0 end
pu-238      101   0  1.8883E-07   400.0 end
pu-239      101   0  9.5485E-05   400.0 end
pu-240      101   0  1.2623E-05   400.0 end
pu-241      101   0  3.5000E-06   400.0 end
pu-242      101   0  3.6597E-07   400.0 end
am-241      101   0  1.3476E-06   400.0 end
am-243      101   0  1.9505E-08   400.0 end
tc-99       101   0  9.8850E-06   400.0 end
cs-133      101   0  1.6531E-05   400.0 end
nd-143      101   0  1.4172E-05   400.0 end
nd-145      101   0  1.0065E-05   400.0 end
sm-147      101   0  3.4750E-06   400.0 end
sm-150      101   0  1.9656E-06   400.0 end
sm-151      101   0  2.0038E-07   400.0 end
eu-151      101   0  1.7248E-08   400.0 end
sm-152      101   0  1.2175E-06   400.0 end
eu-153      101   0  5.2355E-07   400.0 end
gd-155      101   0  1.5033E-08   400.0 end
 o-16       101   0  4.8904E-02   400.0 end
zr-90         2   0  2.1891E-02   400.0 end
zr-91         2   0  4.7740E-03   400.0 end
zr-92         2   0  7.2971E-03   400.0 end
zr-94         2   0  7.3950E-03   400.0 end
zr-96         2   0  1.1914E-03   400.0 end
sn-112        2   0  4.6807E-06   400.0 end
sn-114        2   0  3.1365E-06   400.0 end
sn-115        2   0  1.7372E-06   400.0 end
sn-116        2   0  7.0113E-05   400.0 end
sn-117        2   0  3.7059E-05   400.0 end
sn-118        2   0  1.1687E-04   400.0 end
sn-119        2   0  4.1402E-05   400.0 end
sn-120        2   0  1.5726E-04   400.0 end
sn-122        2   0  2.2342E-05   400.0 end
sn-124        2   0  2.7939E-05   400.0 end
fe-54         2   0  5.6347E-06   400.0 end
fe-56         2   0  8.7595E-05   400.0 end
fe-57         2   0  2.0056E-06   400.0 end
fe-58         2   0  2.6741E-07   400.0 end
cr-50         2   0  3.3012E-06   400.0 end
cr-52         2   0  6.3662E-05   400.0 end
cr-53         2   0  7.2179E-06   400.0 end
```

```
cr-54        2   0  1.7969E-06    400.0 end
ni-58        2   0  2.5275E-05    400.0 end
ni-60        2   0  9.6629E-06    400.0 end
ni-61        2   0  4.1836E-07    400.0 end
ni-62        2   0  1.3291E-06    400.0 end
ni-64        2   0  3.3691E-07    400.0 end
hf-174       2   0  3.5856E-09    400.0 end
hf-176       2   0  1.1523E-07    400.0 end
hf-177       2   0  4.1182E-07    400.0 end
hf-178       2   0  6.0418E-07    400.0 end
hf-179       2   0  3.0166E-07    400.0 end
hf-180       2   0  7.7688E-07    400.0 end
o-16         3   0  3.3376E-02    400.0 end
h-1          3   0  6.6751E-02    400.0 end
co-59        3   0  1.0000E-20    400.0 end
o-16         4   0  6.4741E-02    400.0 end
b-10         4   0  4.0445E-04    400.0 end
b-11         4   0  1.6280E-03    400.0 end
c            4   0  5.0810E-04    400.0 end
al-27        4   0  4.3161E-02    400.0 end
fe-54        5   0  3.4542E-03    400.0 end
fe-56        5   0  5.3698E-02    400.0 end
fe-57        5   0  1.2295E-03    400.0 end
fe-58        5   0  1.6393E-04    400.0 end
cr-50        5   0  7.5918E-04    400.0 end
cr-52        5   0  1.4640E-02    400.0 end
cr-53        5   0  1.6599E-03    400.0 end
cr-54        5   0  4.1323E-04    400.0 end
ni-58        5   0  5.2841E-03    400.0 end
ni-60        5   0  2.0202E-03    400.0 end
ni-61        5   0  8.7463E-05    400.0 end
ni-62        5   0  2.7787E-04    400.0 end
ni-64        5   0  7.0435E-05    400.0 end
c            5   0  3.1848E-04    400.0 end
si-28        5   0  1.5702E-03    400.0 end
si-29        5   0  7.9507E-05    400.0 end
si-30        5   0  5.2778E-05    400.0 end
p-31         5   0  6.9468E-05    400.0 end
mn-55        5   0  1.7407E-03    400.0 end
fe-54        6   0  3.3300E-03    400.0 end
fe-56        6   0  5.1768E-02    400.0 end
fe-57        6   0  1.1853E-03    400.0 end
fe-58        6   0  1.5804E-04    400.0 end
cr-50        6   0  7.4580E-04    400.0 end
cr-52        6   0  1.4382E-02    400.0 end
cr-53        6   0  1.6306E-03    400.0 end
cr-54        6   0  4.0594E-04    400.0 end
ni-58        6   0  5.4642E-03    400.0 end
ni-60        6   0  2.0890E-03    400.0 end
ni-61        6   0  9.0443E-05    400.0 end
```

```
ni-62          6   0  2.8734E-04    400.0 end
ni-64          6   0  7.2834E-05    400.0 end
b-10           6   0  7.7817E-04    400.0 end
b-11           6   0  3.1322E-03    400.0 end
si-28          6   0  1.5425E-03    400.0 end
si-29          6   0  7.8105E-05    400.0 end
si-30          6   0  5.1847E-05    400.0 end
mn-55          6   0  1.7100E-03    400.0 end
al-27          7   0  6.0200E-02    400.0 end
o-16           8   0  3.3376E-02    400.0 end
h-1            8   0  6.6751E-02    400.0 end
c              9   0  3.9499E-02    400.0 end
h-poly         9   0  7.8998E-02    400.0 end
fe-54         10   0  4.1609E-03    400.0 end
fe-56         10   0  6.4684E-02    400.0 end
fe-57         10   0  1.4810E-03    400.0 end
fe-58         10   0  1.9747E-04    400.0 end
ni-58         10   0  6.4790E-04    400.0 end
ni-60         10   0  2.4770E-04    400.0 end
ni-61         10   0  1.0724E-05    400.0 end
ni-62         10   0  3.4070E-05    400.0 end
ni-64         10   0  8.6361E-06    400.0 end
si-28         10   0  2.7365E-03    400.0 end
si-29         10   0  1.3856E-04    400.0 end
si-30         10   0  9.1980E-05    400.0 end
mn-55         10   0  4.6434E-04    400.0 end
c-graphite    10   0  1.2401E-02    400.0 end
fe-54         11   0  3.4491E-03    400.0 end
fe-56         11   0  5.3619E-02    400.0 end
fe-57         11   0  1.2277E-03    400.0 end
fe-58         11   0  1.6369E-04    400.0 end
cr-50         11   0  7.0654E-04    400.0 end
cr-52         11   0  1.3625E-02    400.0 end
cr-53         11   0  1.5448E-03    400.0 end
cr-54         11   0  3.8457E-04    400.0 end
ni-58         11   0  5.7374E-03    400.0 end
ni-60         11   0  2.1934E-03    400.0 end
ni-61         11   0  9.4965E-05    400.0 end
ni-62         11   0  3.0170E-04    400.0 end
ni-64         11   0  7.6476E-05    400.0 end
mn-55         11   0  1.7100E-03    400.0 end
'Node[02][01]    major actinides + principal fission products
 u-234       102   0  5.0099E-06    400.0 end
 u-235       102   0  6.0141E-04    400.0 end
 u-238       102   0  2.3022E-02    400.0 end
np-237       102   0  3.2413E-06    400.0 end
pu-238       102   0  6.0628E-07    400.0 end
pu-239       102   0  1.2350E-04    400.0 end
pu-240       102   0  2.3607E-05    400.0 end
pu-241       102   0  8.4440E-06    400.0 end
```

```
pu-242      102   0  1.5360E-06   400.0 end
am-241      102   0  3.2482E-06   400.0 end
am-243      102   0  1.4019E-07   400.0 end
tc-99       102   0  1.5545E-05   400.0 end
cs-133      102   0  2.5928E-05   400.0 end
nd-143      102   0  2.1260E-05   400.0 end
nd-145      102   0  1.5587E-05   400.0 end
sm-147      102   0  4.9711E-06   400.0 end
sm-150      102   0  3.3366E-06   400.0 end
sm-151      102   0  2.3612E-07   400.0 end
eu-151      102   0  1.9879E-08   400.0 end
sm-152      102   0  2.0130E-06   400.0 end
eu-153      102   0  1.0474E-06   400.0 end
gd-155      102   0  2.6880E-08   400.0 end
 o-16       102   0  4.8903E-02   400.0 end
zr-90       202   0  2.1891E-02   400.0 end
zr-91       202   0  4.7740E-03   400.0 end
zr-92       202   0  7.2971E-03   400.0 end
zr-94       202   0  7.3950E-03   400.0 end
zr-96       202   0  1.1914E-03   400.0 end
sn-112      202   0  4.6807E-06   400.0 end
sn-114      202   0  3.1365E-06   400.0 end
sn-115      202   0  1.7372E-06   400.0 end
sn-116      202   0  7.0113E-05   400.0 end
sn-117      202   0  3.7059E-05   400.0 end
sn-118      202   0  1.1687E-04   400.0 end
sn-119      202   0  4.1402E-05   400.0 end
sn-120      202   0  1.5726E-04   400.0 end
sn-122      202   0  2.2342E-05   400.0 end
sn-124      202   0  2.7939E-05   400.0 end
fe-54       202   0  5.6347E-06   400.0 end
fe-56       202   0  8.7595E-05   400.0 end
fe-57       202   0  2.0056E-06   400.0 end
fe-58       202   0  2.6741E-07   400.0 end
cr-50       202   0  3.3012E-06   400.0 end
cr-52       202   0  6.3662E-05   400.0 end
cr-53       202   0  7.2179E-06   400.0 end
cr-54       202   0  1.7969E-06   400.0 end
ni-58       202   0  2.5275E-05   400.0 end
ni-60       202   0  9.6629E-06   400.0 end
ni-61       202   0  4.1836E-07   400.0 end
ni-62       202   0  1.3291E-06   400.0 end
ni-64       202   0  3.3691E-07   400.0 end
hf-174      202   0  3.5856E-09   400.0 end
hf-176      202   0  1.1523E-07   400.0 end
hf-177      202   0  4.1182E-07   400.0 end
hf-178      202   0  6.0418E-07   400.0 end
hf-179      202   0  3.0166E-07   400.0 end
hf-180      202   0  7.7688E-07   400.0 end
o-16        302   0  3.3376E-02   400.0 end
```

```
 h-1          302   0  6.6751E-02    400.0 end
'Node[03][01]    major actinides + principal  fission  products
  u-234       103   0  4.8316E-06    400.0 end
  u-235       103   0  5.4778E-04    400.0 end
  u-238       103   0  2.2976E-02    400.0 end
 np-237       103   0  3.9876E-06    400.0 end
 pu-238       103   0  8.6466E-07    400.0 end
 pu-239       103   0  1.3146E-04    400.0 end
 pu-240       103   0  2.8142E-05    400.0 end
 pu-241       103   0  1.0650E-05    400.0 end
 pu-242       103   0  2.3094E-06    400.0 end
 am-241       103   0  4.0923E-06    400.0 end
 am-243       103   0  2.4836E-07    400.0 end
 tc-99        103   0  1.7815E-05    400.0 end
 cs-133       103   0  2.9677E-05    400.0 end
 nd-143       103   0  2.3891E-05    400.0 end
 nd-145       103   0  1.7760E-05    400.0 end
 sm-147       103   0  5.4787E-06    400.0 end
 sm-150       103   0  3.9399E-06    400.0 end
 sm-151       103   0  2.4881E-07    400.0 end
 eu-151       103   0  2.0820E-08    400.0 end
 sm-152       103   0  2.3246E-06    400.0 end
 eu-153       103   0  1.2992E-06    400.0 end
 gd-155       103   0  3.3314E-08    400.0 end
  o-16        103   0  4.8903E-02    400.0 end
 zr-90        203   0  2.1891E-02    400.0 end
 zr-91        203   0  4.7740E-03    400.0 end
 zr-92        203   0  7.2971E-03    400.0 end
 zr-94        203   0  7.3950E-03    400.0 end
 zr-96        203   0  1.1914E-03    400.0 end
 sn-112       203   0  4.6807E-06    400.0 end
 sn-114       203   0  3.1365E-06    400.0 end
 sn-115       203   0  1.7372E-06    400.0 end
 sn-116       203   0  7.0113E-05    400.0 end
 sn-117       203   0  3.7059E-05    400.0 end
 sn-118       203   0  1.1687E-04    400.0 end
 sn-119       203   0  4.1402E-05    400.0 end
 sn-120       203   0  1.5726E-04    400.0 end
 sn-122       203   0  2.2342E-05    400.0 end
 sn-124       203   0  2.7939E-05    400.0 end
 fe-54        203   0  5.6347E-06    400.0 end
 fe-56        203   0  8.7595E-05    400.0 end
 fe-57        203   0  2.0056E-06    400.0 end
 fe-58        203   0  2.6741E-07    400.0 end
 cr-50        203   0  3.3012E-06    400.0 end
 cr-52        203   0  6.3662E-05    400.0 end
 cr-53        203   0  7.2179E-06    400.0 end
 cr-54        203   0  1.7969E-06    400.0 end
 ni-58        203   0  2.5275E-05    400.0 end
 ni-60        203   0  9.6629E-06    400.0 end
```

```
 ni-61       203   0  4.1836E-07    400.0 end
 ni-62       203   0  1.3291E-06    400.0 end
 ni-64       203   0  3.3691E-07    400.0 end
 hf-174      203   0  3.5856E-09    400.0 end
 hf-176      203   0  1.1523E-07    400.0 end
 hf-177      203   0  4.1182E-07    400.0 end
 hf-178      203   0  6.0418E-07    400.0 end
 hf-179      203   0  3.0166E-07    400.0 end
 hf-180      203   0  7.7688E-07    400.0 end
 o-16        303   0  3.3376E-02    400.0 end
 h-1         303   0  6.6751E-02    400.0 end
'Node[04][01]    major actinides + principal fission products
  u-234      104   0  4.8241E-06    400.0 end
  u-235      104   0  5.4557E-04    400.0 end
  u-238      104   0  2.2974E-02    400.0 end
 np-237      104   0  4.0202E-06    400.0 end
 pu-238      104   0  8.7688E-07    400.0 end
 pu-239      104   0  1.3176E-04    400.0 end
 pu-240      104   0  2.8334E-05    400.0 end
 pu-241      104   0  1.0744E-05    400.0 end
 pu-242      104   0  2.3463E-06    400.0 end
 am-241      104   0  4.1283E-06    400.0 end
 am-243      104   0  2.5398E-07    400.0 end
 tc-99       104   0  1.7911E-05    400.0 end
 cs-133      104   0  2.9835E-05    400.0 end
 nd-143      104   0  2.3999E-05    400.0 end
 nd-145      104   0  1.7852E-05    400.0 end
 sm-147      104   0  5.4989E-06    400.0 end
 sm-150      104   0  3.9662E-06    400.0 end
 sm-151      104   0  2.4934E-07    400.0 end
 eu-151      104   0  2.0859E-08    400.0 end
 sm-152      104   0  2.3377E-06    400.0 end
 eu-153      104   0  1.3103E-06    400.0 end
 gd-155      104   0  3.3608E-08    400.0 end
  o-16       104   0  4.8903E-02    400.0 end
 zr-90       204   0  2.1891E-02    400.0 end
 zr-91       204   0  4.7740E-03    400.0 end
 zr-92       204   0  7.2971E-03    400.0 end
 zr-94       204   0  7.3950E-03    400.0 end
 zr-96       204   0  1.1914E-03    400.0 end
 sn-112      204   0  4.6807E-06    400.0 end
 sn-114      204   0  3.1365E-06    400.0 end
 sn-115      204   0  1.7372E-06    400.0 end
 sn-116      204   0  7.0113E-05    400.0 end
 sn-117      204   0  3.7059E-05    400.0 end
 sn-118      204   0  1.1687E-04    400.0 end
 sn-119      204   0  4.1402E-05    400.0 end
 sn-120      204   0  1.5726E-04    400.0 end
 sn-122      204   0  2.2342E-05    400.0 end
 sn-124      204   0  2.7939E-05    400.0 end
```

```
 fe-54       204   0  5.6347E-06   400.0 end
 fe-56       204   0  8.7595E-05   400.0 end
 fe-57       204   0  2.0056E-06   400.0 end
 fe-58       204   0  2.6741E-07   400.0 end
 cr-50       204   0  3.3012E-06   400.0 end
 cr-52       204   0  6.3662E-05   400.0 end
 cr-53       204   0  7.2179E-06   400.0 end
 cr-54       204   0  1.7969E-06   400.0 end
 ni-58       204   0  2.5275E-05   400.0 end
 ni-60       204   0  9.6629E-06   400.0 end
 ni-61       204   0  4.1836E-07   400.0 end
 ni-62       204   0  1.3291E-06   400.0 end
 ni-64       204   0  3.3691E-07   400.0 end
 hf-174      204   0  3.5856E-09   400.0 end
 hf-176      204   0  1.1523E-07   400.0 end
 hf-177      204   0  4.1182E-07   400.0 end
 hf-178      204   0  6.0418E-07   400.0 end
 hf-179      204   0  3.0166E-07   400.0 end
 hf-180      204   0  7.7688E-07   400.0 end
 o-16        304   0  3.3376E-02   400.0 end
 h-1         304   0  6.6751E-02   400.0 end
'Node[05][01]    major actinides + principal fission products
  u-234      105   0  4.8252E-06   400.0 end
  u-235      105   0  5.4589E-04   400.0 end
  u-238      105   0  2.2974E-02   400.0 end
 np-237      105   0  4.0156E-06   400.0 end
 pu-238      105   0  8.7513E-07   400.0 end
 pu-239      105   0  1.3171E-04   400.0 end
 pu-240      105   0  2.8306E-05   400.0 end
 pu-241      105   0  1.0731E-05   400.0 end
 pu-242      105   0  2.3410E-06   400.0 end
 am-241      105   0  4.1232E-06   400.0 end
 am-243      105   0  2.5317E-07   400.0 end
 tc-99       105   0  1.7897E-05   400.0 end
 cs-133      105   0  2.9813E-05   400.0 end
 nd-143      105   0  2.3984E-05   400.0 end
 nd-145      105   0  1.7839E-05   400.0 end
 sm-147      105   0  5.4961E-06   400.0 end
 sm-150      105   0  3.9624E-06   400.0 end
 sm-151      105   0  2.4927E-07   400.0 end
 eu-151      105   0  2.0853E-08   400.0 end
 sm-152      105   0  2.3358E-06   400.0 end
 eu-153      105   0  1.3087E-06   400.0 end
 gd-155      105   0  3.3566E-08   400.0 end
  o-16       105   0  4.8903E-02   400.0 end
 zr-90       205   0  2.1891E-02   400.0 end
 zr-91       205   0  4.7740E-03   400.0 end
 zr-92       205   0  7.2971E-03   400.0 end
 zr-94       205   0  7.3950E-03   400.0 end
 zr-96       205   0  1.1914E-03   400.0 end
```

```
sn-112      205   0  4.6807E-06   400.0 end
sn-114      205   0  3.1365E-06   400.0 end
sn-115      205   0  1.7372E-06   400.0 end
sn-116      205   0  7.0113E-05   400.0 end
sn-117      205   0  3.7059E-05   400.0 end
sn-118      205   0  1.1687E-04   400.0 end
sn-119      205   0  4.1402E-05   400.0 end
sn-120      205   0  1.5726E-04   400.0 end
sn-122      205   0  2.2342E-05   400.0 end
sn-124      205   0  2.7939E-05   400.0 end
fe-54       205   0  5.6347E-06   400.0 end
fe-56       205   0  8.7595E-05   400.0 end
fe-57       205   0  2.0056E-06   400.0 end
fe-58       205   0  2.6741E-07   400.0 end
cr-50       205   0  3.3012E-06   400.0 end
cr-52       205   0  6.3662E-05   400.0 end
cr-53       205   0  7.2179E-06   400.0 end
cr-54       205   0  1.7969E-06   400.0 end
ni-58       205   0  2.5275E-05   400.0 end
ni-60       205   0  9.6629E-06   400.0 end
ni-61       205   0  4.1836E-07   400.0 end
ni-62       205   0  1.3291E-06   400.0 end
ni-64       205   0  3.3691E-07   400.0 end
hf-174      205   0  3.5856E-09   400.0 end
hf-176      205   0  1.1523E-07   400.0 end
hf-177      205   0  4.1182E-07   400.0 end
hf-178      205   0  6.0418E-07   400.0 end
hf-179      205   0  3.0166E-07   400.0 end
hf-180      205   0  7.7688E-07   400.0 end
o-16        305   0  3.3376E-02   400.0 end
h-1         305   0  6.6751E-02   400.0 end
'Node[06][01]    major actinides + principal fission products
 u-234      106   0  4.8316E-06   400.0 end
 u-235      106   0  5.4778E-04   400.0 end
 u-238      106   0  2.2976E-02   400.0 end
np-237      106   0  3.9876E-06   400.0 end
pu-238      106   0  8.6466E-07   400.0 end
pu-239      106   0  1.3146E-04   400.0 end
pu-240      106   0  2.8142E-05   400.0 end
pu-241      106   0  1.0650E-05   400.0 end
pu-242      106   0  2.3094E-06   400.0 end
am-241      106   0  4.0923E-06   400.0 end
am-243      106   0  2.4836E-07   400.0 end
tc-99       106   0  1.7815E-05   400.0 end
cs-133      106   0  2.9677E-05   400.0 end
nd-143      106   0  2.3891E-05   400.0 end
nd-145      106   0  1.7760E-05   400.0 end
sm-147      106   0  5.4787E-06   400.0 end
sm-150      106   0  3.9399E-06   400.0 end
sm-151      106   0  2.4881E-07   400.0 end
```

```
 eu-151      106   0  2.0820E-08    400.0 end
 sm-152      106   0  2.3246E-06    400.0 end
 eu-153      106   0  1.2992E-06    400.0 end
 gd-155      106   0  3.3314E-08    400.0 end
  o-16       106   0  4.8903E-02    400.0 end
 zr-90       206   0  2.1891E-02    400.0 end
 zr-91       206   0  4.7740E-03    400.0 end
 zr-92       206   0  7.2971E-03    400.0 end
 zr-94       206   0  7.3950E-03    400.0 end
 zr-96       206   0  1.1914E-03    400.0 end
 sn-112      206   0  4.6807E-06    400.0 end
 sn-114      206   0  3.1365E-06    400.0 end
 sn-115      206   0  1.7372E-06    400.0 end
 sn-116      206   0  7.0113E-05    400.0 end
 sn-117      206   0  3.7059E-05    400.0 end
 sn-118      206   0  1.1687E-04    400.0 end
 sn-119      206   0  4.1402E-05    400.0 end
 sn-120      206   0  1.5726E-04    400.0 end
 sn-122      206   0  2.2342E-05    400.0 end
 sn-124      206   0  2.7939E-05    400.0 end
 fe-54       206   0  5.6347E-06    400.0 end
 fe-56       206   0  8.7595E-05    400.0 end
 fe-57       206   0  2.0056E-06    400.0 end
 fe-58       206   0  2.6741E-07    400.0 end
 cr-50       206   0  3.3012E-06    400.0 end
 cr-52       206   0  6.3662E-05    400.0 end
 cr-53       206   0  7.2179E-06    400.0 end
 cr-54       206   0  1.7969E-06    400.0 end
 ni-58       206   0  2.5275E-05    400.0 end
 ni-60       206   0  9.6629E-06    400.0 end
 ni-61       206   0  4.1836E-07    400.0 end
 ni-62       206   0  1.3291E-06    400.0 end
 ni-64       206   0  3.3691E-07    400.0 end
 hf-174      206   0  3.5856E-09    400.0 end
 hf-176      206   0  1.1523E-07    400.0 end
 hf-177      206   0  4.1182E-07    400.0 end
 hf-178      206   0  6.0418E-07    400.0 end
 hf-179      206   0  3.0166E-07    400.0 end
 hf-180      206   0  7.7688E-07    400.0 end
 o-16        306   0  3.3376E-02    400.0 end
 h-1         306   0  6.6751E-02    400.0 end
'Node[07][01]    major actinides + principal fission products
  u-234      107   0  4.8434E-06    400.0 end
  u-235      107   0  5.5126E-04    400.0 end
  u-238      107   0  2.2979E-02    400.0 end
 np-237      107   0  3.9364E-06    400.0 end
 pu-238      107   0  8.4566E-07    400.0 end
 pu-239      107   0  1.3097E-04    400.0 end
 pu-240      107   0  2.7839E-05    400.0 end
 pu-241      107   0  1.0502E-05    400.0 end
```

pu-242 107 0 2.2520E-06 400.0 end
am-241 107 0 4.0356E-06 400.0 end
am-243 107 0 2.3971E-07 400.0 end
tc-99 107 0 1.7664E-05 400.0 end
cs-133 107 0 2.9429E-05 400.0 end
nd-143 107 0 2.3720E-05 400.0 end
nd-145 107 0 1.7617E-05 400.0 end
sm-147 107 0 5.4466E-06 400.0 end
sm-150 107 0 3.8988E-06 400.0 end
sm-151 107 0 2.4798E-07 400.0 end
eu-151 107 0 2.0757E-08 400.0 end
sm-152 107 0 2.3040E-06 400.0 end
eu-153 107 0 1.2818E-06 400.0 end
gd-155 107 0 3.2854E-08 400.0 end
o-16 107 0 4.8903E-02 400.0 end
zr-90 207 0 2.1891E-02 400.0 end
zr-91 207 0 4.7740E-03 400.0 end
zr-92 207 0 7.2971E-03 400.0 end
zr-94 207 0 7.3950E-03 400.0 end
zr-96 207 0 1.1914E-03 400.0 end
sn-112 207 0 4.6807E-06 400.0 end
sn-114 207 0 3.1365E-06 400.0 end
sn-115 207 0 1.7372E-06 400.0 end
sn-116 207 0 7.0113E-05 400.0 end
sn-117 207 0 3.7059E-05 400.0 end
sn-118 207 0 1.1687E-04 400.0 end
sn-119 207 0 4.1402E-05 400.0 end
sn-120 207 0 1.5726E-04 400.0 end
sn-122 207 0 2.2342E-05 400.0 end
sn-124 207 0 2.7939E-05 400.0 end
fe-54 207 0 5.6347E-06 400.0 end
fe-56 207 0 8.7595E-05 400.0 end
fe-57 207 0 2.0056E-06 400.0 end
fe-58 207 0 2.6741E-07 400.0 end
cr-50 207 0 3.3012E-06 400.0 end
cr-52 207 0 6.3662E-05 400.0 end
cr-53 207 0 7.2179E-06 400.0 end
cr-54 207 0 1.7969E-06 400.0 end
ni-58 207 0 2.5275E-05 400.0 end
ni-60 207 0 9.6629E-06 400.0 end
ni-61 207 0 4.1836E-07 400.0 end
ni-62 207 0 1.3291E-06 400.0 end
ni-64 207 0 3.3691E-07 400.0 end
hf-174 207 0 3.5856E-09 400.0 end
hf-176 207 0 1.1523E-07 400.0 end
hf-177 207 0 4.1182E-07 400.0 end
hf-178 207 0 6.0418E-07 400.0 end
hf-179 207 0 3.0166E-07 400.0 end
hf-180 207 0 7.7688E-07 400.0 end
o-16 307 0 3.3376E-02 400.0 end

```
 h-1          307   0  6.6751E-02    400.0 end
'Node[08][01]    major actinides + principal fission products
  u-234       108   0  4.8519E-06    400.0 end
  u-235       108   0  5.5379E-04    400.0 end
  u-238       108   0  2.2981E-02    400.0 end
 np-237       108   0  3.8992E-06    400.0 end
 pu-238       108   0  8.3198E-07    400.0 end
 pu-239       108   0  1.3062E-04    400.0 end
 pu-240       108   0  2.7619E-05    400.0 end
 pu-241       108   0  1.0394E-05    400.0 end
 pu-242       108   0  2.2107E-06    400.0 end
 am-241       108   0  3.9943E-06    400.0 end
 am-243       108   0  2.3355E-07    400.0 end
 tc-99        108   0  1.7554E-05    400.0 end
 cs-133       108   0  2.9247E-05    400.0 end
 nd-143       108   0  2.3595E-05    400.0 end
 nd-145       108   0  1.7512E-05    400.0 end
 sm-147       108   0  5.4230E-06    400.0 end
 sm-150       108   0  3.8689E-06    400.0 end
 sm-151       108   0  2.4737E-07    400.0 end
 eu-151       108   0  2.0712E-08    400.0 end
 sm-152       108   0  2.2890E-06    400.0 end
 eu-153       108   0  1.2692E-06    400.0 end
 gd-155       108   0  3.2523E-08    400.0 end
  o-16        108   0  4.8903E-02    400.0 end
 zr-90        208   0  2.1891E-02    400.0 end
 zr-91        208   0  4.7740E-03    400.0 end
 zr-92        208   0  7.2971E-03    400.0 end
 zr-94        208   0  7.3950E-03    400.0 end
 zr-96        208   0  1.1914E-03    400.0 end
 sn-112       208   0  4.6807E-06    400.0 end
 sn-114       208   0  3.1365E-06    400.0 end
 sn-115       208   0  1.7372E-06    400.0 end
 sn-116       208   0  7.0113E-05    400.0 end
 sn-117       208   0  3.7059E-05    400.0 end
 sn-118       208   0  1.1687E-04    400.0 end
 sn-119       208   0  4.1402E-05    400.0 end
 sn-120       208   0  1.5726E-04    400.0 end
 sn-122       208   0  2.2342E-05    400.0 end
 sn-124       208   0  2.7939E-05    400.0 end
 fe-54        208   0  5.6347E-06    400.0 end
 fe-56        208   0  8.7595E-05    400.0 end
 fe-57        208   0  2.0056E-06    400.0 end
 fe-58        208   0  2.6741E-07    400.0 end
 cr-50        208   0  3.3012E-06    400.0 end
 cr-52        208   0  6.3662E-05    400.0 end
 cr-53        208   0  7.2179E-06    400.0 end
 cr-54        208   0  1.7969E-06    400.0 end
 ni-58        208   0  2.5275E-05    400.0 end
 ni-60        208   0  9.6629E-06    400.0 end
```

```
ni-61       208   0  4.1836E-07    400.0 end
ni-62       208   0  1.3291E-06    400.0 end
ni-64       208   0  3.3691E-07    400.0 end
hf-174      208   0  3.5856E-09    400.0 end
hf-176      208   0  1.1523E-07    400.0 end
hf-177      208   0  4.1182E-07    400.0 end
hf-178      208   0  6.0418E-07    400.0 end
hf-179      208   0  3.0166E-07    400.0 end
hf-180      208   0  7.7688E-07    400.0 end
o-16        308   0  3.3376E-02    400.0 end
h-1         308   0  6.6751E-02    400.0 end
'Node[09][01]    major actinides + principal fission products
 u-234      109   0  4.8530E-06    400.0 end
 u-235      109   0  5.5411E-04    400.0 end
 u-238      109   0  2.2981E-02    400.0 end
np-237      109   0  3.8946E-06    400.0 end
pu-238      109   0  8.3028E-07    400.0 end
pu-239      109   0  1.3057E-04    400.0 end
pu-240      109   0  2.7592E-05    400.0 end
pu-241      109   0  1.0380E-05    400.0 end
pu-242      109   0  2.2055E-06    400.0 end
am-241      109   0  3.9892E-06    400.0 end
am-243      109   0  2.3279E-07    400.0 end
tc-99       109   0  1.7541E-05    400.0 end
cs-133      109   0  2.9225E-05    400.0 end
nd-143      109   0  2.3580E-05    400.0 end
nd-145      109   0  1.7499E-05    400.0 end
sm-147      109   0  5.4201E-06    400.0 end
sm-150      109   0  3.8652E-06    400.0 end
sm-151      109   0  2.4729E-07    400.0 end
eu-151      109   0  2.0706E-08    400.0 end
sm-152      109   0  2.2872E-06    400.0 end
eu-153      109   0  1.2676E-06    400.0 end
gd-155      109   0  3.2481E-08    400.0 end
 o-16       109   0  4.8903E-02    400.0 end
zr-90       209   0  2.1891E-02    400.0 end
zr-91       209   0  4.7740E-03    400.0 end
zr-92       209   0  7.2971E-03    400.0 end
zr-94       209   0  7.3950E-03    400.0 end
zr-96       209   0  1.1914E-03    400.0 end
sn-112      209   0  4.6807E-06    400.0 end
sn-114      209   0  3.1365E-06    400.0 end
sn-115      209   0  1.7372E-06    400.0 end
sn-116      209   0  7.0113E-05    400.0 end
sn-117      209   0  3.7059E-05    400.0 end
sn-118      209   0  1.1687E-04    400.0 end
sn-119      209   0  4.1402E-05    400.0 end
sn-120      209   0  1.5726E-04    400.0 end
sn-122      209   0  2.2342E-05    400.0 end
sn-124      209   0  2.7939E-05    400.0 end
```

```
 fe-54       209   0  5.6347E-06   400.0 end
 fe-56       209   0  8.7595E-05   400.0 end
 fe-57       209   0  2.0056E-06   400.0 end
 fe-58       209   0  2.6741E-07   400.0 end
 cr-50       209   0  3.3012E-06   400.0 end
 cr-52       209   0  6.3662E-05   400.0 end
 cr-53       209   0  7.2179E-06   400.0 end
 cr-54       209   0  1.7969E-06   400.0 end
 ni-58       209   0  2.5275E-05   400.0 end
 ni-60       209   0  9.6629E-06   400.0 end
 ni-61       209   0  4.1836E-07   400.0 end
 ni-62       209   0  1.3291E-06   400.0 end
 ni-64       209   0  3.3691E-07   400.0 end
 hf-174      209   0  3.5856E-09   400.0 end
 hf-176      209   0  1.1523E-07   400.0 end
 hf-177      209   0  4.1182E-07   400.0 end
 hf-178      209   0  6.0418E-07   400.0 end
 hf-179      209   0  3.0166E-07   400.0 end
 hf-180      209   0  7.7688E-07   400.0 end
 o-16        309   0  3.3376E-02   400.0 end
 h-1         309   0  6.6751E-02   400.0 end
'Node[10][01]    major actinides + principal fission products
  u-234      110   0  4.8487E-06   400.0 end
  u-235      110   0  5.5284E-04   400.0 end
  u-238      110   0  2.2980E-02   400.0 end
 np-237      110   0  3.9131E-06   400.0 end
 pu-238      110   0  8.3710E-07   400.0 end
 pu-239      110   0  1.3075E-04   400.0 end
 pu-240      110   0  2.7702E-05   400.0 end
 pu-241      110   0  1.0434E-05   400.0 end
 pu-242      110   0  2.2261E-06   400.0 end
 am-241      110   0  4.0098E-06   400.0 end
 am-243      110   0  2.3585E-07   400.0 end
 tc-99       110   0  1.7596E-05   400.0 end
 cs-133      110   0  2.9315E-05   400.0 end
 nd-143      110   0  2.3642E-05   400.0 end
 nd-145      110   0  1.7552E-05   400.0 end
 sm-147      110   0  5.4319E-06   400.0 end
 sm-150      110   0  3.8801E-06   400.0 end
 sm-151      110   0  2.4760E-07   400.0 end
 eu-151      110   0  2.0729E-08   400.0 end
 sm-152      110   0  2.2947E-06   400.0 end
 eu-153      110   0  1.2739E-06   400.0 end
 gd-155      110   0  3.2647E-08   400.0 end
  o-16       110   0  4.8903E-02   400.0 end
 zr-90       210   0  2.1891E-02   400.0 end
 zr-91       210   0  4.7740E-03   400.0 end
 zr-92       210   0  7.2971E-03   400.0 end
 zr-94       210   0  7.3950E-03   400.0 end
 zr-96       210   0  1.1914E-03   400.0 end
```

```
sn-112      210   0  4.6807E-06   400.0 end
sn-114      210   0  3.1365E-06   400.0 end
sn-115      210   0  1.7372E-06   400.0 end
sn-116      210   0  7.0113E-05   400.0 end
sn-117      210   0  3.7059E-05   400.0 end
sn-118      210   0  1.1687E-04   400.0 end
sn-119      210   0  4.1402E-05   400.0 end
sn-120      210   0  1.5726E-04   400.0 end
sn-122      210   0  2.2342E-05   400.0 end
sn-124      210   0  2.7939E-05   400.0 end
fe-54       210   0  5.6347E-06   400.0 end
fe-56       210   0  8.7595E-05   400.0 end
fe-57       210   0  2.0056E-06   400.0 end
fe-58       210   0  2.6741E-07   400.0 end
cr-50       210   0  3.3012E-06   400.0 end
cr-52       210   0  6.3662E-05   400.0 end
cr-53       210   0  7.2179E-06   400.0 end
cr-54       210   0  1.7969E-06   400.0 end
ni-58       210   0  2.5275E-05   400.0 end
ni-60       210   0  9.6629E-06   400.0 end
ni-61       210   0  4.1836E-07   400.0 end
ni-62       210   0  1.3291E-06   400.0 end
ni-64       210   0  3.3691E-07   400.0 end
hf-174      210   0  3.5856E-09   400.0 end
hf-176      210   0  1.1523E-07   400.0 end
hf-177      210   0  4.1182E-07   400.0 end
hf-178      210   0  6.0418E-07   400.0 end
hf-179      210   0  3.0166E-07   400.0 end
hf-180      210   0  7.7688E-07   400.0 end
o-16        310   0  3.3376E-02   400.0 end
h-1         310   0  6.6751E-02   400.0 end
'Node[11][01]    major actinides + principal fission products
 u-234      111   0  4.8455E-06   400.0 end
 u-235      111   0  5.5189E-04   400.0 end
 u-238      111   0  2.2979E-02   400.0 end
np-237      111   0  3.9271E-06   400.0 end
pu-238      111   0  8.4223E-07   400.0 end
pu-239      111   0  1.3088E-04   400.0 end
pu-240      111   0  2.7784E-05   400.0 end
pu-241      111   0  1.0475E-05   400.0 end
pu-242      111   0  2.2416E-06   400.0 end
am-241      111   0  4.0253E-06   400.0 end
am-243      111   0  2.3816E-07   400.0 end
tc-99       111   0  1.7637E-05   400.0 end
cs-133      111   0  2.9383E-05   400.0 end
nd-143      111   0  2.3689E-05   400.0 end
nd-145      111   0  1.7591E-05   400.0 end
sm-147      111   0  5.4407E-06   400.0 end
sm-150      111   0  3.8913E-06   400.0 end
sm-151      111   0  2.4783E-07   400.0 end
```

```
 eu-151      111   0  2.0746E-08   400.0 end
 sm-152      111   0  2.3003E-06   400.0 end
 eu-153      111   0  1.2786E-06   400.0 end
 gd-155      111   0  3.2771E-08   400.0 end
  o-16       111   0  4.8903E-02   400.0 end
 zr-90       211   0  2.1891E-02   400.0 end
 zr-91       211   0  4.7740E-03   400.0 end
 zr-92       211   0  7.2971E-03   400.0 end
 zr-94       211   0  7.3950E-03   400.0 end
 zr-96       211   0  1.1914E-03   400.0 end
 sn-112      211   0  4.6807E-06   400.0 end
 sn-114      211   0  3.1365E-06   400.0 end
 sn-115      211   0  1.7372E-06   400.0 end
 sn-116      211   0  7.0113E-05   400.0 end
 sn-117      211   0  3.7059E-05   400.0 end
 sn-118      211   0  1.1687E-04   400.0 end
 sn-119      211   0  4.1402E-05   400.0 end
 sn-120      211   0  1.5726E-04   400.0 end
 sn-122      211   0  2.2342E-05   400.0 end
 sn-124      211   0  2.7939E-05   400.0 end
 fe-54       211   0  5.6347E-06   400.0 end
 fe-56       211   0  8.7595E-05   400.0 end
 fe-57       211   0  2.0056E-06   400.0 end
 fe-58       211   0  2.6741E-07   400.0 end
 cr-50       211   0  3.3012E-06   400.0 end
 cr-52       211   0  6.3662E-05   400.0 end
 cr-53       211   0  7.2179E-06   400.0 end
 cr-54       211   0  1.7969E-06   400.0 end
 ni-58       211   0  2.5275E-05   400.0 end
 ni-60       211   0  9.6629E-06   400.0 end
 ni-61       211   0  4.1836E-07   400.0 end
 ni-62       211   0  1.3291E-06   400.0 end
 ni-64       211   0  3.3691E-07   400.0 end
 hf-174      211   0  3.5856E-09   400.0 end
 hf-176      211   0  1.1523E-07   400.0 end
 hf-177      211   0  4.1182E-07   400.0 end
 hf-178      211   0  6.0418E-07   400.0 end
 hf-179      211   0  3.0166E-07   400.0 end
 hf-180      211   0  7.7688E-07   400.0 end
 o-16        311   0  3.3376E-02   400.0 end
 h-1         311   0  6.6751E-02   400.0 end
'Node[12][01]    major actinides + principal fission products
  u-234      112   0  4.8509E-06   400.0 end
  u-235      112   0  5.5348E-04   400.0 end
  u-238      112   0  2.2981E-02   400.0 end
 np-237      112   0  3.9039E-06   400.0 end
 pu-238      112   0  8.3369E-07   400.0 end
 pu-239      112   0  1.3066E-04   400.0 end
 pu-240      112   0  2.7647E-05   400.0 end
 pu-241      112   0  1.0407E-05   400.0 end
```

pu-242 112 0 2.2158E-06 400.0 end
am-241 112 0 3.9995E-06 400.0 end
am-243 112 0 2.3432E-07 400.0 end
tc-99 112 0 1.7568E-05 400.0 end
cs-133 112 0 2.9270E-05 400.0 end
nd-143 112 0 2.3611E-05 400.0 end
nd-145 112 0 1.7525E-05 400.0 end
sm-147 112 0 5.4260E-06 400.0 end
sm-150 112 0 3.8727E-06 400.0 end
sm-151 112 0 2.4745E-07 400.0 end
eu-151 112 0 2.0718E-08 400.0 end
sm-152 112 0 2.2909E-06 400.0 end
eu-153 112 0 1.2707E-06 400.0 end
gd-155 112 0 3.2564E-08 400.0 end
o-16 112 0 4.8903E-02 400.0 end
zr-90 212 0 2.1891E-02 400.0 end
zr-91 212 0 4.7740E-03 400.0 end
zr-92 212 0 7.2971E-03 400.0 end
zr-94 212 0 7.3950E-03 400.0 end
zr-96 212 0 1.1914E-03 400.0 end
sn-112 212 0 4.6807E-06 400.0 end
sn-114 212 0 3.1365E-06 400.0 end
sn-115 212 0 1.7372E-06 400.0 end
sn-116 212 0 7.0113E-05 400.0 end
sn-117 212 0 3.7059E-05 400.0 end
sn-118 212 0 1.1687E-04 400.0 end
sn-119 212 0 4.1402E-05 400.0 end
sn-120 212 0 1.5726E-04 400.0 end
sn-122 212 0 2.2342E-05 400.0 end
sn-124 212 0 2.7939E-05 400.0 end
fe-54 212 0 5.6347E-06 400.0 end
fe-56 212 0 8.7595E-05 400.0 end
fe-57 212 0 2.0056E-06 400.0 end
fe-58 212 0 2.6741E-07 400.0 end
cr-50 212 0 3.3012E-06 400.0 end
cr-52 212 0 6.3662E-05 400.0 end
cr-53 212 0 7.2179E-06 400.0 end
cr-54 212 0 1.7969E-06 400.0 end
ni-58 212 0 2.5275E-05 400.0 end
ni-60 212 0 9.6629E-06 400.0 end
ni-61 212 0 4.1836E-07 400.0 end
ni-62 212 0 1.3291E-06 400.0 end
ni-64 212 0 3.3691E-07 400.0 end
hf-174 212 0 3.5856E-09 400.0 end
hf-176 212 0 1.1523E-07 400.0 end
hf-177 212 0 4.1182E-07 400.0 end
hf-178 212 0 6.0418E-07 400.0 end
hf-179 212 0 3.0166E-07 400.0 end
hf-180 212 0 7.7688E-07 400.0 end
o-16 312 0 3.3376E-02 400.0 end

```
 h-1         312   0  6.6751E-02    400.0 end
'Node[13][01]    major actinides + principal  fission  products
  u-234       113   0  4.8875E-06    400.0 end
  u-235       113   0  5.6436E-04    400.0 end
  u-238       113   0  2.2990E-02    400.0 end
 np-237       113   0  3.7467E-06    400.0 end
 pu-238       113   0  7.7689E-07    400.0 end
 pu-239       113   0  1.2911E-04    400.0 end
 pu-240       113   0  2.6710E-05    400.0 end
 pu-241       113   0  9.9482E-06    400.0 end
 pu-242       113   0  2.0447E-06    400.0 end
 am-241       113   0  3.8240E-06    400.0 end
 am-243       113   0  2.0928E-07    400.0 end
 tc-99        113   0  1.7100E-05    400.0 end
 cs-133       113   0  2.8498E-05    400.0 end
 nd-143       113   0  2.3076E-05    400.0 end
 nd-145       113   0  1.7079E-05    400.0 end
 sm-147       113   0  5.3245E-06    400.0 end
 sm-150       113   0  3.7464E-06    400.0 end
 sm-151       113   0  2.4484E-07    400.0 end
 eu-151       113   0  2.0524E-08    400.0 end
 sm-152       113   0  2.2269E-06    400.0 end
 eu-153       113   0  1.2175E-06    400.0 end
 gd-155       113   0  3.1176E-08    400.0 end
  o-16        113   0  4.8903E-02    400.0 end
 zr-90        213   0  2.1891E-02    400.0 end
 zr-91        213   0  4.7740E-03    400.0 end
 zr-92        213   0  7.2971E-03    400.0 end
 zr-94        213   0  7.3950E-03    400.0 end
 zr-96        213   0  1.1914E-03    400.0 end
 sn-112       213   0  4.6807E-06    400.0 end
 sn-114       213   0  3.1365E-06    400.0 end
 sn-115       213   0  1.7372E-06    400.0 end
 sn-116       213   0  7.0113E-05    400.0 end
 sn-117       213   0  3.7059E-05    400.0 end
 sn-118       213   0  1.1687E-04    400.0 end
 sn-119       213   0  4.1402E-05    400.0 end
 sn-120       213   0  1.5726E-04    400.0 end
 sn-122       213   0  2.2342E-05    400.0 end
 sn-124       213   0  2.7939E-05    400.0 end
 fe-54        213   0  5.6347E-06    400.0 end
 fe-56        213   0  8.7595E-05    400.0 end
 fe-57        213   0  2.0056E-06    400.0 end
 fe-58        213   0  2.6741E-07    400.0 end
 cr-50        213   0  3.3012E-06    400.0 end
 cr-52        213   0  6.3662E-05    400.0 end
 cr-53        213   0  7.2179E-06    400.0 end
 cr-54        213   0  1.7969E-06    400.0 end
 ni-58        213   0  2.5275E-05    400.0 end
 ni-60        213   0  9.6629E-06    400.0 end
```

```
ni-61       213   0  4.1836E-07    400.0 end
ni-62       213   0  1.3291E-06    400.0 end
ni-64       213   0  3.3691E-07    400.0 end
hf-174      213   0  3.5856E-09    400.0 end
hf-176      213   0  1.1523E-07    400.0 end
hf-177      213   0  4.1182E-07    400.0 end
hf-178      213   0  6.0418E-07    400.0 end
hf-179      213   0  3.0166E-07    400.0 end
hf-180      213   0  7.7688E-07    400.0 end
o-16        313   0  3.3376E-02    400.0 end
h-1         313   0  6.6751E-02    400.0 end
'Node[14][01]    major actinides + principal fission products
 u-234      114   0  5.0343E-06    400.0 end
 u-235      114   0  6.0889E-04    400.0 end
 u-238      114   0  2.3028E-02    400.0 end
np-237      114   0  3.1442E-06    400.0 end
pu-238      114   0  5.7558E-07    400.0 end
pu-239      114   0  1.2230E-04    400.0 end
pu-240      114   0  2.2995E-05    400.0 end
pu-241      114   0  8.1502E-06    400.0 end
pu-242      114   0  1.4454E-06    400.0 end
am-241      114   0  3.1355E-06    400.0 end
am-243      114   0  1.2880E-07    400.0 end
tc-99       114   0  1.5236E-05    400.0 end
cs-133      114   0  2.5418E-05    400.0 end
nd-143      114   0  2.0893E-05    400.0 end
nd-145      114   0  1.5291E-05    400.0 end
sm-147      114   0  4.8982E-06    400.0 end
sm-150      114   0  3.2570E-06    400.0 end
sm-151      114   0  2.3436E-07    400.0 end
eu-151      114   0  1.9749E-08    400.0 end
sm-152      114   0  1.9703E-06    400.0 end
eu-153      114   0  1.0150E-06    400.0 end
gd-155      114   0  2.6085E-08    400.0 end
 o-16       114   0  4.8903E-02    400.0 end
zr-90       214   0  2.1891E-02    400.0 end
zr-91       214   0  4.7740E-03    400.0 end
zr-92       214   0  7.2971E-03    400.0 end
zr-94       214   0  7.3950E-03    400.0 end
zr-96       214   0  1.1914E-03    400.0 end
sn-112      214   0  4.6807E-06    400.0 end
sn-114      214   0  3.1365E-06    400.0 end
sn-115      214   0  1.7372E-06    400.0 end
sn-116      214   0  7.0113E-05    400.0 end
sn-117      214   0  3.7059E-05    400.0 end
sn-118      214   0  1.1687E-04    400.0 end
sn-119      214   0  4.1402E-05    400.0 end
sn-120      214   0  1.5726E-04    400.0 end
sn-122      214   0  2.2342E-05    400.0 end
sn-124      214   0  2.7939E-05    400.0 end
```

```
 fe-54       214   0  5.6347E-06   400.0 end
 fe-56       214   0  8.7595E-05   400.0 end
 fe-57       214   0  2.0056E-06   400.0 end
 fe-58       214   0  2.6741E-07   400.0 end
 cr-50       214   0  3.3012E-06   400.0 end
 cr-52       214   0  6.3662E-05   400.0 end
 cr-53       214   0  7.2179E-06   400.0 end
 cr-54       214   0  1.7969E-06   400.0 end
 ni-58       214   0  2.5275E-05   400.0 end
 ni-60       214   0  9.6629E-06   400.0 end
 ni-61       214   0  4.1836E-07   400.0 end
 ni-62       214   0  1.3291E-06   400.0 end
 ni-64       214   0  3.3691E-07   400.0 end
 hf-174      214   0  3.5856E-09   400.0 end
 hf-176      214   0  1.1523E-07   400.0 end
 hf-177      214   0  4.1182E-07   400.0 end
 hf-178      214   0  6.0418E-07   400.0 end
 hf-179      214   0  3.0166E-07   400.0 end
 hf-180      214   0  7.7688E-07   400.0 end
 o-16        314   0  3.3376E-02   400.0 end
 h-1         314   0  6.6751E-02   400.0 end
'Node[15][01]    major actinides + principal fission products
  u-234      115   0  5.3405E-06   400.0 end
  u-235      115   0  7.0489E-04   400.0 end
  u-238      115   0  2.3100E-02   400.0 end
 np-237      115   0  2.0366E-06   400.0 end
 pu-238      115   0  2.7477E-07   400.0 end
 pu-239      115   0  1.0458E-04   400.0 end
 pu-240      115   0  1.5568E-05   400.0 end
 pu-241      115   0  4.7373E-06   400.0 end
 pu-242      115   0  5.9022E-07   400.0 end
 am-241      115   0  1.8241E-06   400.0 end
 am-243      115   0  3.7386E-08   400.0 end
 tc-99       115   0  1.1445E-05   400.0 end
 cs-133      115   0  1.9127E-05   400.0 end
 nd-143      115   0  1.6199E-05   400.0 end
 nd-145      115   0  1.1602E-05   400.0 end
 sm-147      115   0  3.9209E-06   400.0 end
 sm-150      115   0  2.3253E-06   400.0 end
 sm-151      115   0  2.1128E-07   400.0 end
 eu-151      115   0  1.8053E-08   400.0 end
 sm-152      115   0  1.4388E-06   400.0 end
 eu-153      115   0  6.5227E-07   400.0 end
 gd-155      115   0  1.7743E-08   400.0 end
  o-16       115   0  4.8904E-02   400.0 end
 zr-90       215   0  2.1891E-02   400.0 end
 zr-91       215   0  4.7740E-03   400.0 end
 zr-92       215   0  7.2971E-03   400.0 end
 zr-94       215   0  7.3950E-03   400.0 end
 zr-96       215   0  1.1914E-03   400.0 end
```

```
sn-112      215   0  4.6807E-06   400.0 end
sn-114      215   0  3.1365E-06   400.0 end
sn-115      215   0  1.7372E-06   400.0 end
sn-116      215   0  7.0113E-05   400.0 end
sn-117      215   0  3.7059E-05   400.0 end
sn-118      215   0  1.1687E-04   400.0 end
sn-119      215   0  4.1402E-05   400.0 end
sn-120      215   0  1.5726E-04   400.0 end
sn-122      215   0  2.2342E-05   400.0 end
sn-124      215   0  2.7939E-05   400.0 end
fe-54       215   0  5.6347E-06   400.0 end
fe-56       215   0  8.7595E-05   400.0 end
fe-57       215   0  2.0056E-06   400.0 end
fe-58       215   0  2.6741E-07   400.0 end
cr-50       215   0  3.3012E-06   400.0 end
cr-52       215   0  6.3662E-05   400.0 end
cr-53       215   0  7.2179E-06   400.0 end
cr-54       215   0  1.7969E-06   400.0 end
ni-58       215   0  2.5275E-05   400.0 end
ni-60       215   0  9.6629E-06   400.0 end
ni-61       215   0  4.1836E-07   400.0 end
ni-62       215   0  1.3291E-06   400.0 end
ni-64       215   0  3.3691E-07   400.0 end
hf-174      215   0  3.5856E-09   400.0 end
hf-176      215   0  1.1523E-07   400.0 end
hf-177      215   0  4.1182E-07   400.0 end
hf-178      215   0  6.0418E-07   400.0 end
hf-179      215   0  3.0166E-07   400.0 end
hf-180      215   0  7.7688E-07   400.0 end
o-16        315   0  3.3376E-02   400.0 end
h-1         315   0  6.6751E-02   400.0 end
'Node[16][01]    major actinides + principal fission products
 u-234      116   0  5.5122E-06   400.0 end
 u-235      116   0  7.6061E-04   400.0 end
 u-238      116   0  2.3137E-02   400.0 end
np-237      116   0  1.5073E-06   400.0 end
pu-238      116   0  1.6482E-07   400.0 end
pu-239      116   0  9.2219E-05   400.0 end
pu-240      116   0  1.1673E-05   400.0 end
pu-241      116   0  3.1225E-06   400.0 end
pu-242      116   0  3.0651E-07   400.0 end
am-241      116   0  1.2021E-06   400.0 end
am-243      116   0  1.5345E-08   400.0 end
tc-99       116   0  9.3706E-06   400.0 end
cs-133      116   0  1.5674E-05   400.0 end
nd-143      116   0  1.3491E-05   400.0 end
nd-145      116   0  9.5554E-06   400.0 end
sm-147      116   0  3.3222E-06   400.0 end
sm-150      116   0  1.8499E-06   400.0 end
sm-151      116   0  1.9647E-07   400.0 end
```

```
 eu-151      116   0  1.6956E-08    400.0 end
 sm-152      116   0  1.1444E-06    400.0 end
 eu-153      116   0  4.8384E-07    400.0 end
 gd-155      116   0  1.4223E-08    400.0 end
  o-16       116   0  4.8904E-02    400.0 end
 zr-90       216   0  2.1891E-02    400.0 end
 zr-91       216   0  4.7740E-03    400.0 end
 zr-92       216   0  7.2971E-03    400.0 end
 zr-94       216   0  7.3950E-03    400.0 end
 zr-96       216   0  1.1914E-03    400.0 end
 sn-112      216   0  4.6807E-06    400.0 end
 sn-114      216   0  3.1365E-06    400.0 end
 sn-115      216   0  1.7372E-06    400.0 end
 sn-116      216   0  7.0113E-05    400.0 end
 sn-117      216   0  3.7059E-05    400.0 end
 sn-118      216   0  1.1687E-04    400.0 end
 sn-119      216   0  4.1402E-05    400.0 end
 sn-120      216   0  1.5726E-04    400.0 end
 sn-122      216   0  2.2342E-05    400.0 end
 sn-124      216   0  2.7939E-05    400.0 end
 fe-54       216   0  5.6347E-06    400.0 end
 fe-56       216   0  8.7595E-05    400.0 end
 fe-57       216   0  2.0056E-06    400.0 end
 fe-58       216   0  2.6741E-07    400.0 end
 cr-50       216   0  3.3012E-06    400.0 end
 cr-52       216   0  6.3662E-05    400.0 end
 cr-53       216   0  7.2179E-06    400.0 end
 cr-54       216   0  1.7969E-06    400.0 end
 ni-58       216   0  2.5275E-05    400.0 end
 ni-60       216   0  9.6629E-06    400.0 end
 ni-61       216   0  4.1836E-07    400.0 end
 ni-62       216   0  1.3291E-06    400.0 end
 ni-64       216   0  3.3691E-07    400.0 end
 hf-174      216   0  3.5856E-09    400.0 end
 hf-176      216   0  1.1523E-07    400.0 end
 hf-177      216   0  4.1182E-07    400.0 end
 hf-178      216   0  6.0418E-07    400.0 end
 hf-179      216   0  3.0166E-07    400.0 end
 hf-180      216   0  7.7688E-07    400.0 end
 o-16        316   0  3.3376E-02    400.0 end
 h-1         316   0  6.6751E-02    400.0 end
'Node[17][01]    major actinides + principal fission products
  u-234      117   0  5.6780E-06    400.0 end
  u-235      117   0  8.1595E-04    400.0 end
  u-238      117   0  2.3171E-02    400.0 end
 np-237      117   0  1.0613E-06    400.0 end
 pu-238      117   0  9.0859E-08    400.0 end
 pu-239      117   0  7.8315E-05    400.0 end
 pu-240      117   0  8.1711E-06    400.0 end
 pu-241      117   0  1.8401E-06    400.0 end
```

```
pu-242      117   0  1.3730E-07   400.0 end
am-241      117   0  7.0804E-07   400.0 end
am-243      117   0  5.2279E-09   400.0 end
tc-99       117   0  7.3966E-06   400.0 end
cs-133      117   0  1.2381E-05   400.0 end
nd-143      117   0  1.0824E-05   400.0 end
nd-145      117   0  7.5870E-06   400.0 end
sm-147      117   0  2.7085E-06   400.0 end
sm-150      117   0  1.4189E-06   400.0 end
sm-151      117   0  1.7922E-07   400.0 end
eu-151      117   0  1.5649E-08   400.0 end
sm-152      117   0  8.6490E-07   400.0 end
eu-153      117   0  3.4435E-07   400.0 end
gd-155      117   0  1.1462E-08   400.0 end
 o-16       117   0  4.8904E-02   400.0 end
zr-90       217   0  2.1891E-02   400.0 end
zr-91       217   0  4.7740E-03   400.0 end
zr-92       217   0  7.2971E-03   400.0 end
zr-94       217   0  7.3950E-03   400.0 end
zr-96       217   0  1.1914E-03   400.0 end
sn-112      217   0  4.6807E-06   400.0 end
sn-114      217   0  3.1365E-06   400.0 end
sn-115      217   0  1.7372E-06   400.0 end
sn-116      217   0  7.0113E-05   400.0 end
sn-117      217   0  3.7059E-05   400.0 end
sn-118      217   0  1.1687E-04   400.0 end
sn-119      217   0  4.1402E-05   400.0 end
sn-120      217   0  1.5726E-04   400.0 end
sn-122      217   0  2.2342E-05   400.0 end
sn-124      217   0  2.7939E-05   400.0 end
fe-54       217   0  5.6347E-06   400.0 end
fe-56       217   0  8.7595E-05   400.0 end
fe-57       217   0  2.0056E-06   400.0 end
fe-58       217   0  2.6741E-07   400.0 end
cr-50       217   0  3.3012E-06   400.0 end
cr-52       217   0  6.3662E-05   400.0 end
cr-53       217   0  7.2179E-06   400.0 end
cr-54       217   0  1.7969E-06   400.0 end
ni-58       217   0  2.5275E-05   400.0 end
ni-60       217   0  9.6629E-06   400.0 end
ni-61       217   0  4.1836E-07   400.0 end
ni-62       217   0  1.3291E-06   400.0 end
ni-64       217   0  3.3691E-07   400.0 end
hf-174      217   0  3.5856E-09   400.0 end
hf-176      217   0  1.1523E-07   400.0 end
hf-177      217   0  4.1182E-07   400.0 end
hf-178      217   0  6.0418E-07   400.0 end
hf-179      217   0  3.0166E-07   400.0 end
hf-180      217   0  7.7688E-07   400.0 end
o-16        317   0  3.3376E-02   400.0 end
```

```
 h-1         317   0  6.6751E-02   400.0 end
'Node[18][01]    major actinides + principal fission products
  u-234      118   0  5.9319E-06   400.0 end
  u-235      118   0  9.0420E-04   400.0 end
  u-238      118   0  2.3221E-02   400.0 end
 np-237      118   0  5.0931E-07   400.0 end
 pu-238      118   0  2.5971E-08   400.0 end
 pu-239      118   0  5.2572E-05   400.0 end
 pu-240      118   0  3.5577E-06   400.0 end
 pu-241      118   0  5.2069E-07   400.0 end
 pu-242      118   0  2.1875E-08   400.0 end
 am-241      118   0  2.0002E-07   400.0 end
 am-243      118   0  4.6814E-10   400.0 end
 tc-99       118   0  4.4162E-06   400.0 end
 cs-133      118   0  7.3988E-06   400.0 end
 nd-143      118   0  6.6254E-06   400.0 end
 nd-145      118   0  4.5737E-06   400.0 end
 sm-147      118   0  1.6973E-06   400.0 end
 sm-150      118   0  8.0381E-07   400.0 end
 sm-151      118   0  1.4074E-07   400.0 end
 eu-151      118   0  1.2562E-08   400.0 end
 sm-152      118   0  4.5775E-07   400.0 end
 eu-153      118   0  1.7315E-07   400.0 end
 gd-155      118   0  8.0829E-09   400.0 end
  o-16       118   0  4.8905E-02   400.0 end
 zr-90       218   0  2.1891E-02   400.0 end
 zr-91       218   0  4.7740E-03   400.0 end
 zr-92       218   0  7.2971E-03   400.0 end
 zr-94       218   0  7.3950E-03   400.0 end
 zr-96       218   0  1.1914E-03   400.0 end
 sn-112      218   0  4.6807E-06   400.0 end
 sn-114      218   0  3.1365E-06   400.0 end
 sn-115      218   0  1.7372E-06   400.0 end
 sn-116      218   0  7.0113E-05   400.0 end
 sn-117      218   0  3.7059E-05   400.0 end
 sn-118      218   0  1.1687E-04   400.0 end
 sn-119      218   0  4.1402E-05   400.0 end
 sn-120      218   0  1.5726E-04   400.0 end
 sn-122      218   0  2.2342E-05   400.0 end
 sn-124      218   0  2.7939E-05   400.0 end
 fe-54       218   0  5.6347E-06   400.0 end
 fe-56       218   0  8.7595E-05   400.0 end
 fe-57       218   0  2.0056E-06   400.0 end
 fe-58       218   0  2.6741E-07   400.0 end
 cr-50       218   0  3.3012E-06   400.0 end
 cr-52       218   0  6.3662E-05   400.0 end
 cr-53       218   0  7.2179E-06   400.0 end
 cr-54       218   0  1.7969E-06   400.0 end
 ni-58       218   0  2.5275E-05   400.0 end
 ni-60       218   0  9.6629E-06   400.0 end
```

```
ni-61       218   0  4.1836E-07    400.0 end
ni-62       218   0  1.3291E-06    400.0 end
ni-64       218   0  3.3691E-07    400.0 end
hf-174      218   0  3.5856E-09    400.0 end
hf-176      218   0  1.1523E-07    400.0 end
hf-177      218   0  4.1182E-07    400.0 end
hf-178      218   0  6.0418E-07    400.0 end
hf-179      218   0  3.0166E-07    400.0 end
hf-180      218   0  7.7688E-07    400.0 end
o-16        318   0  3.3376E-02    400.0 end
h-1         318   0  6.6751E-02    400.0 end
```

APPENDIX 4: SENSITIVITY COEFFICIENTS FOR MAJOR ACTINIDES

Appendix 4_Table 1: Sensitivity and Uncertainty of Major Actinides (20 GWD/MTU & ^{235}U=3.9 wt%)

		20 GWD/MTU & ^{235}U=3.9 wt%					
	Decay(yrs)	1		5		10	
		Sensitivity(total)	σ(±)	Sensitivity(total)	σ(±)	Sensitivity(total)	σ(±)
Major Actinides	^{234}U	-4.97E-04	5.95E-08	-4.52E-04	9.38E-08	-4.52E-04	9.38E-08
	^{235}U	1.06E-01	1.46E-05	7.82E-02	1.44E-05	7.82E-02	1.44E-05
	^{238}U	-3.88E-02	5.91E-06	-2.99E-02	9.45E-06	-2.99E-02	9.45E-06
	^{238}Pu	-5.66E-06	3.56E-10	-3.65E-06	3.33E-10	-3.65E-06	3.33E-10
	^{239}Pu	1.17E-02	1.81E-06	9.06E-03	2.11E-06	9.06E-03	2.11E-06
	^{240}Pu	-2.39E-03	2.84E-07	-2.54E-03	4.21E-07	-2.54E-03	4.21E-07
	^{241}Pu	1.98E-04	1.99E-08	1.53E-04	2.08E-08	1.53E-04	2.08E-08
	^{242}Pu	-2.28E-06	4.77E-10	-2.68E-06	7.71E-10	-2.68E-06	7.71E-10
	^{241}Am	-9.64E-05	4.27E-09	-8.31E-05	5.34E-09	-8.31E-05	5.34E-09

Appendix 4_Table 2: Sensitivity and Uncertainty of Major Actinides (40 GWD/MTU & ^{235}U=3.9 wt%)

		40 GWD/MTU & ^{235}U=3.9 wt%					
	Decay(yrs)	1		5		10	
		Sensitivity(total)	σ(±)	Sensitivity(total)	σ(±)	Sensitivity(total)	σ(±)
Major Actinides	^{234}U	-4.52E-04	9.38E-08	-4.52E-04	9.38E-08	-4.52E-04	9.38E-08
	^{235}U	7.82E-02	1.44E-05	7.82E-02	1.44E-05	7.82E-02	1.44E-05
	^{238}U	-2.99E-02	9.45E-06	-2.99E-02	9.45E-06	-2.99E-02	9.45E-06
	^{238}Pu	-3.65E-06	3.33E-10	-3.65E-06	3.33E-10	-3.65E-06	3.33E-10
	^{239}Pu	9.06E-03	2.11E-06	9.06E-03	2.11E-06	9.06E-03	2.11E-06
	^{240}Pu	-2.54E-03	4.21E-07	-2.54E-03	4.21E-07	-2.54E-03	4.21E-07
	^{241}Pu	1.53E-04	2.08E-08	1.53E-04	2.08E-08	1.53E-04	2.08E-08
	^{242}Pu	-2.68E-06	7.71E-10	-2.68E-06	7.71E-10	-2.68E-06	7.71E-10
	^{241}Am	-8.31E-05	5.34E-09	-8.31E-05	5.34E-09	-8.31E-05	5.34E-09

Appendix 4_Table 3: Sensitivity and Uncertainty of Major Actinides (60 GWD/MTU & ^{235}U=3.9 wt%)

		60 GWD/MTU & ^{235}U=3.9 wt%					
	Decay(yrs)	1		5		10	
		Sensitivity(total)	σ(±)	Sensitivity(total)	σ(±)	Sensitivity(total)	σ(±)
Major Actinides	^{234}U	-4.5222E-04	9.3805E-08	-4.5222E-04	9.38E-08	-4.52E-04	9.38E-08
	^{235}U	7.82E-02	1.44E-05	7.82E-02	1.44E-05	7.82E-02	1.44E-05
	^{238}U	-2.99E-02	9.45E-06	-2.99E-02	9.45E-06	-2.99E-02	9.45E-06
	^{238}Pu	-3.65E-06	3.33E-10	-3.65E-06	3.33E-10	-3.65E-06	3.33E-10
	^{239}Pu	9.06E-03	2.11E-06	9.06E-03	2.11E-06	9.06E-03	2.11E-06
	^{240}Pu	-2.54E-03	4.21E-07	-2.54E-03	4.21E-07	-2.54E-03	4.21E-07
	^{241}Pu	1.53E-04	2.08E-08	1.53E-04	2.08E-08	1.53E-04	2.08E-08
	^{242}Pu	-2.68E-06	7.71E-10	-2.68E-06	7.71E-10	-2.68E-06	7.71E-10
	^{241}Am	-8.31E-05	5.34E-09	-8.31E-05	5.34E-09	-8.31E-05	5.34E-09

APPENDIX 5: GRAPHICAL REPRESENTATION OF YIELD OF ACTINIDES AS A FUNCTION OF BURNUP

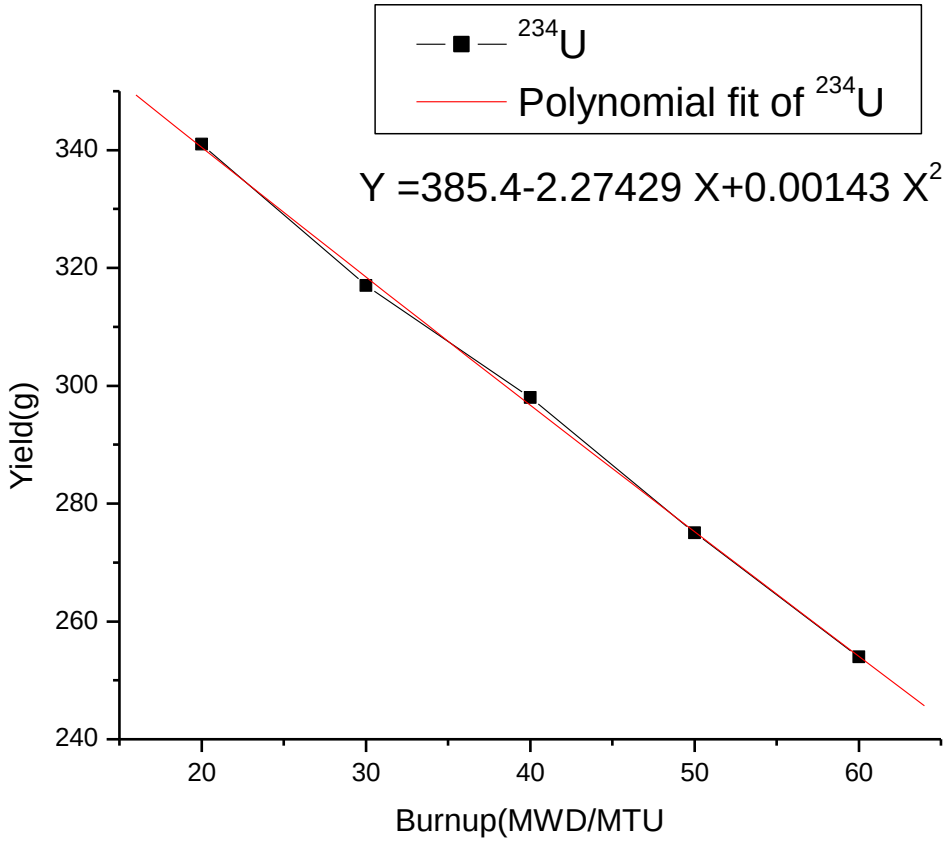

Appendix5:Figure 1: Depletion of ^{234}U

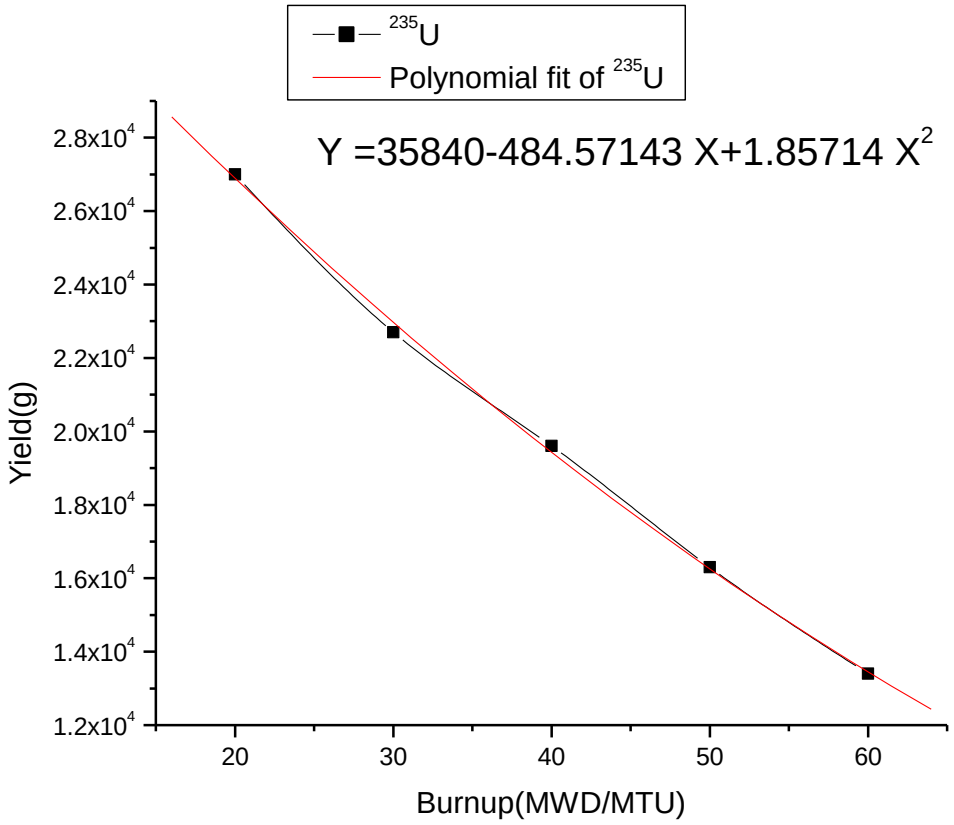

Appendix5:Figure 2: Depletion of ^{235}U

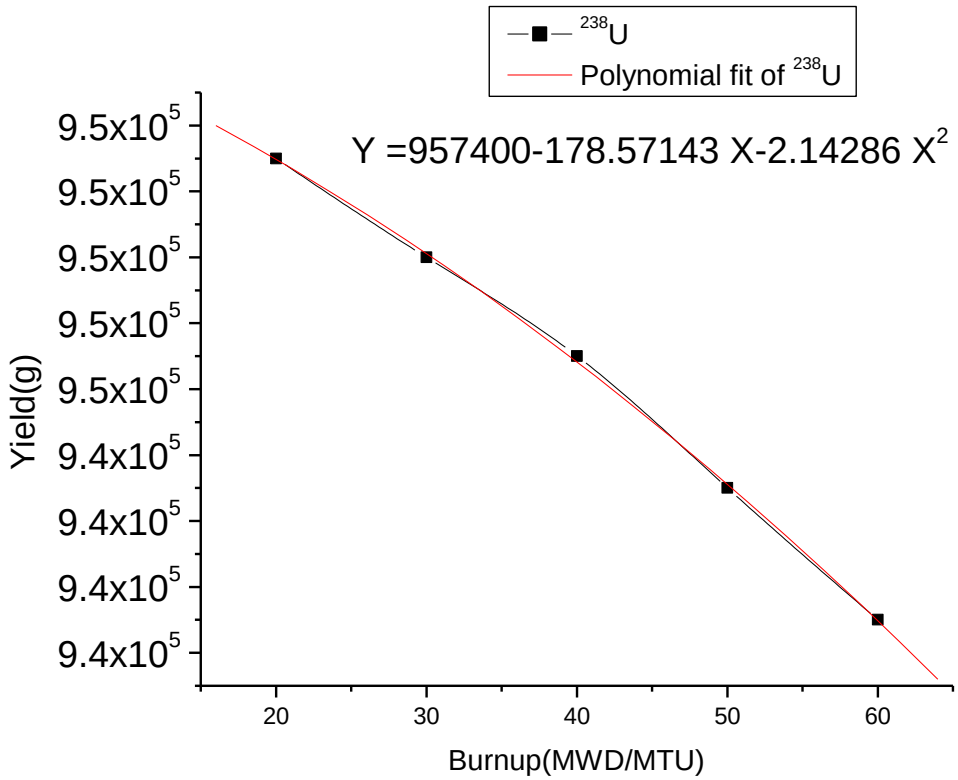

Appendix5:Figure 3: Depletion of ^{238}U

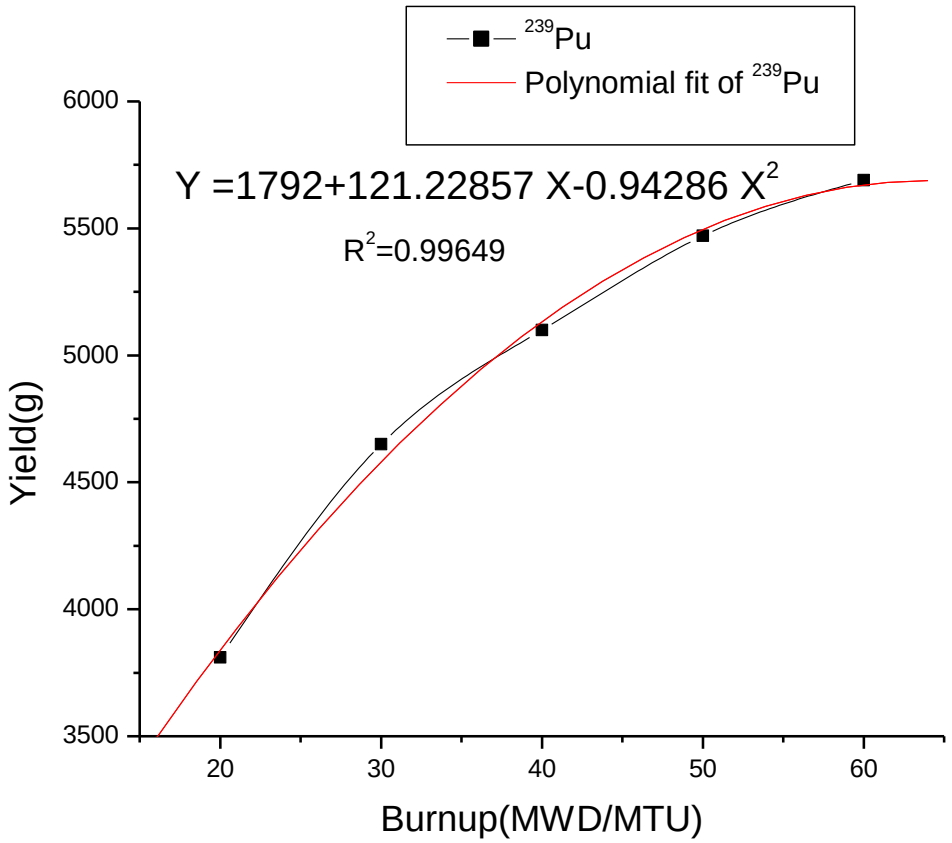

Appendix5:Figure 4: Yield of ^{239}Pu

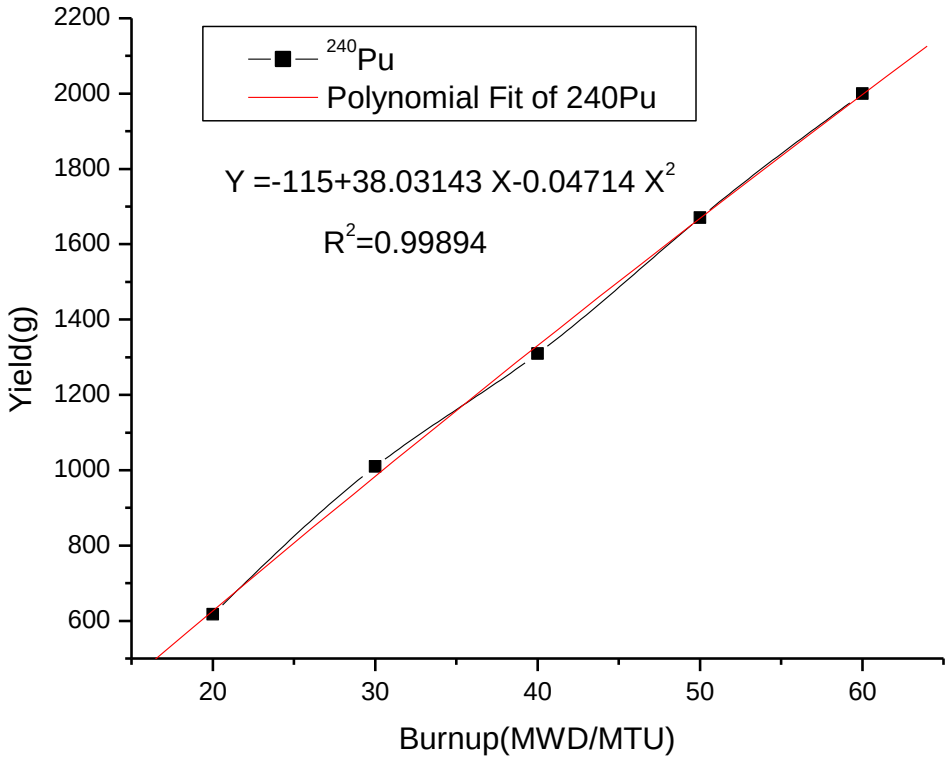

Appendix5:Figure 5: Yield of ^{240}Pu

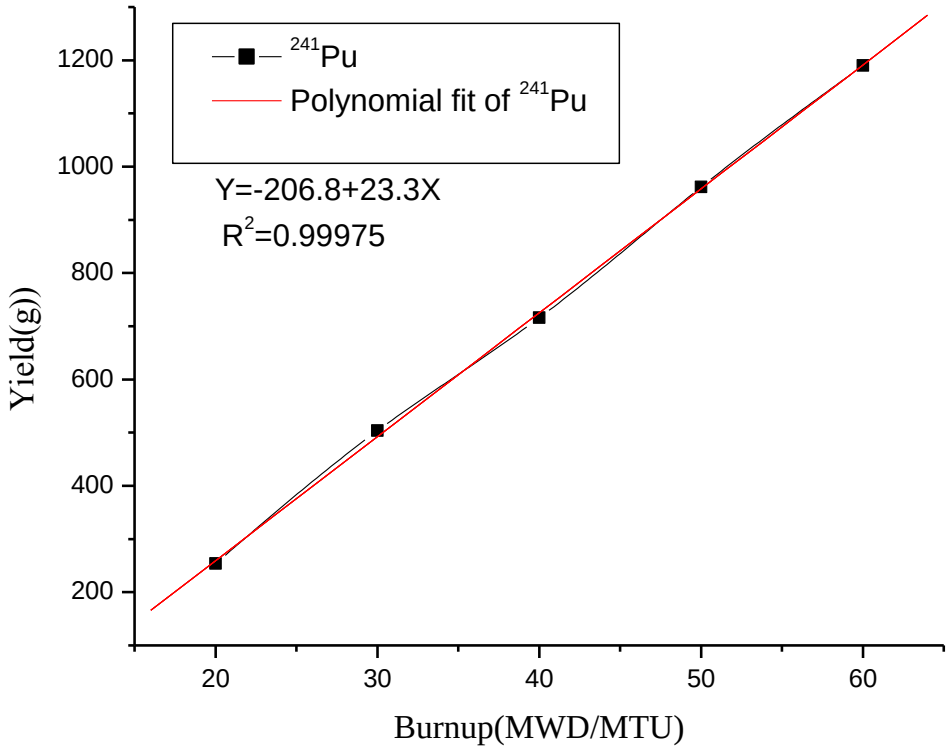

Appendix5:Figure 6: Yield of ^{241}Pu

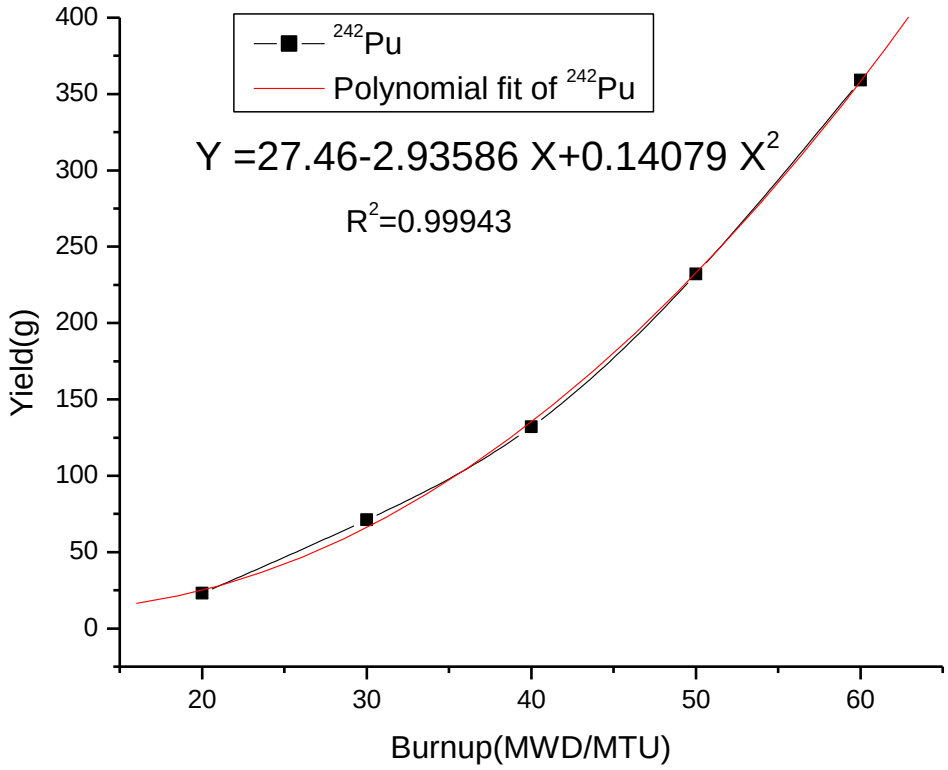

Appendix5:Figure 7: Yield of ^{242}Pu

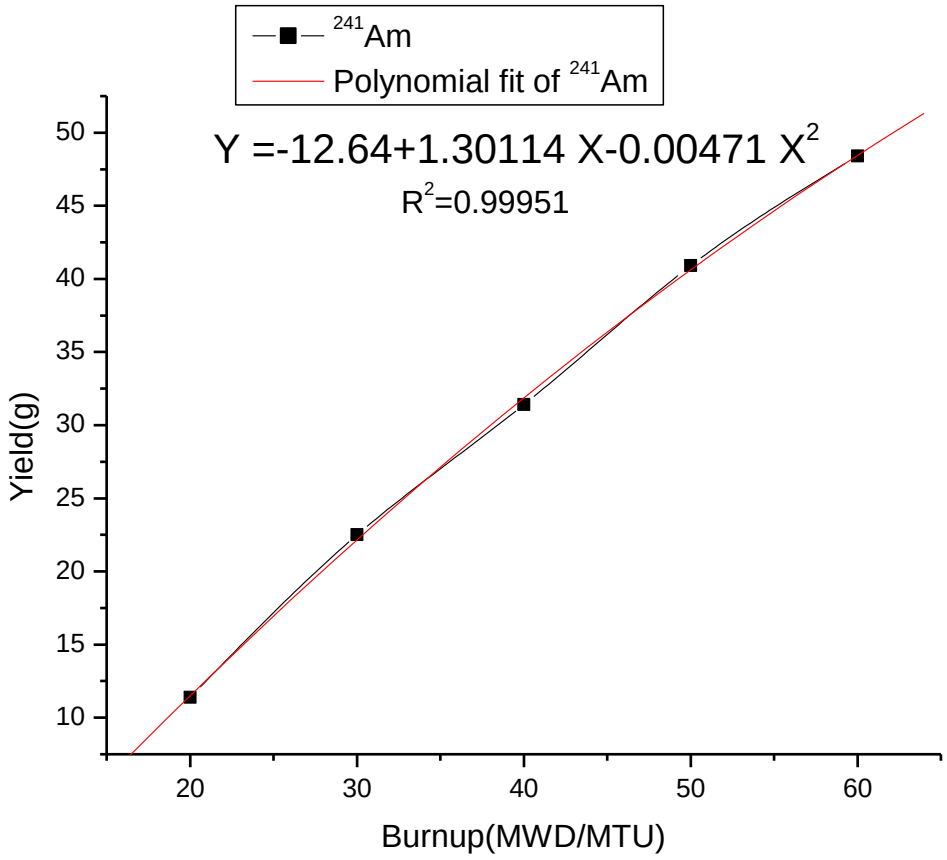

Appendix5:Figure 8: Yield of ^{241}Am

APPENDIX 6: GRAPHICAL REPRESENTATION OF THE YIELD OF FISSION PRODUCTS AS A FUNCTION OF BURNUP

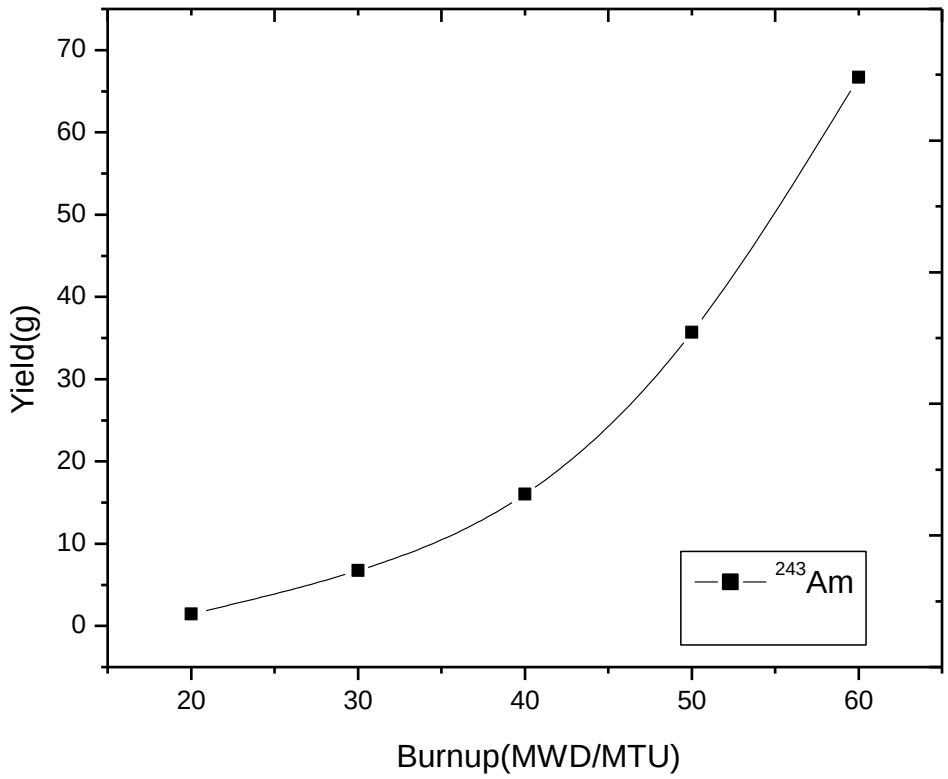

Appendix6_Fig. 1: Growth of ^{243}Am with increase in burnup

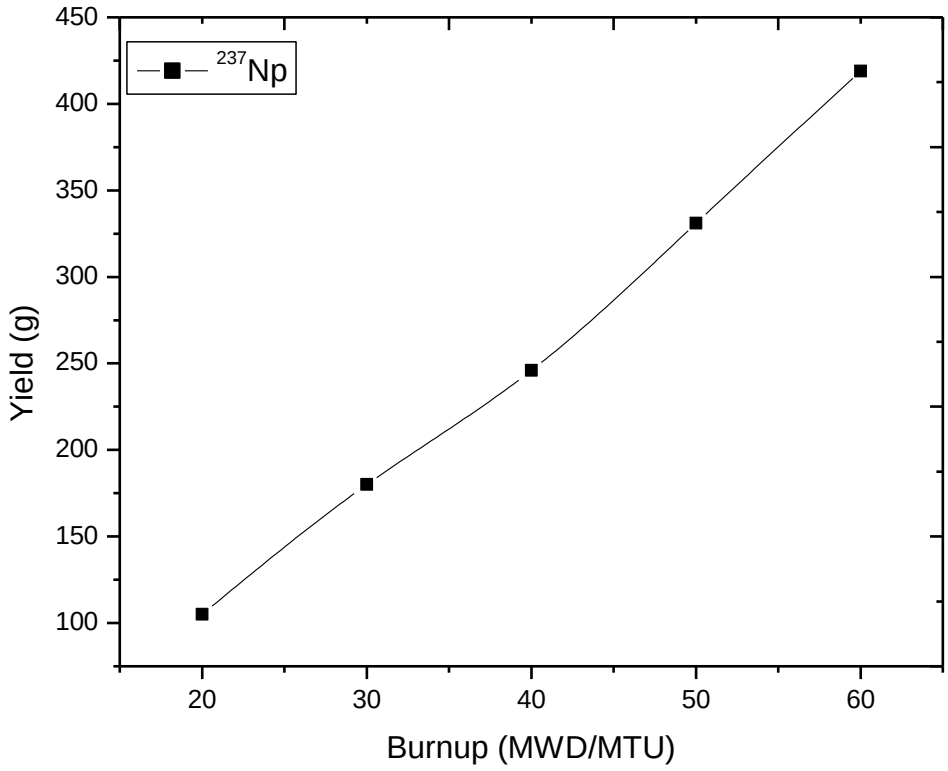

Appendix6_Fig. 2 : Growth of ^{237}Np with increase in Burnup

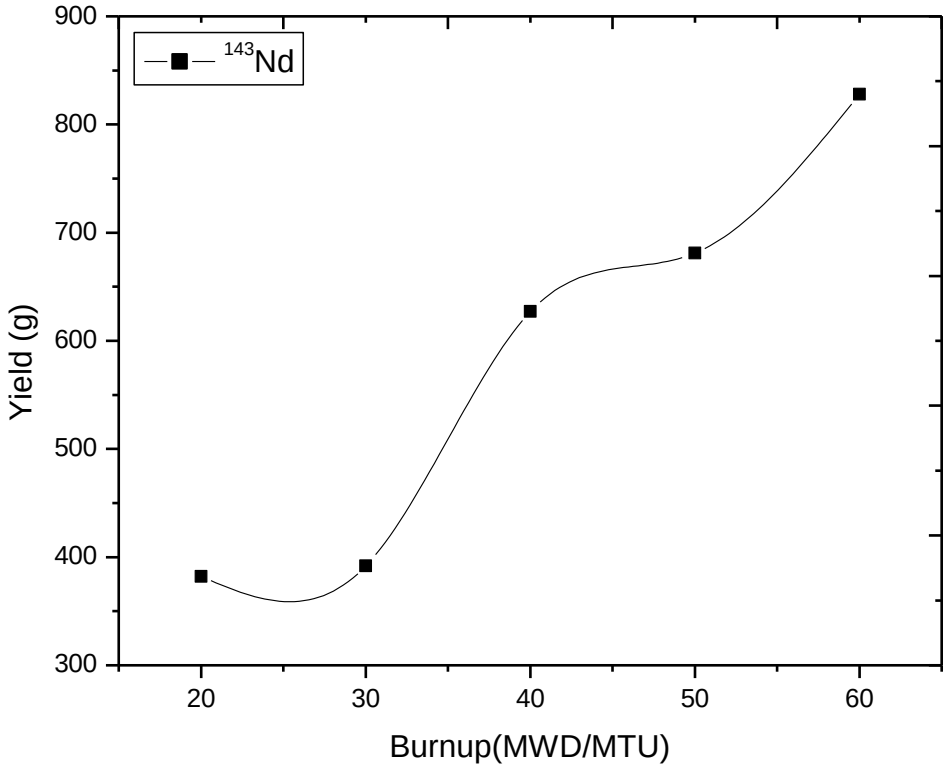

Appendix6_Fig. 3: Growth of ^{143}Nd with increase in Burnup

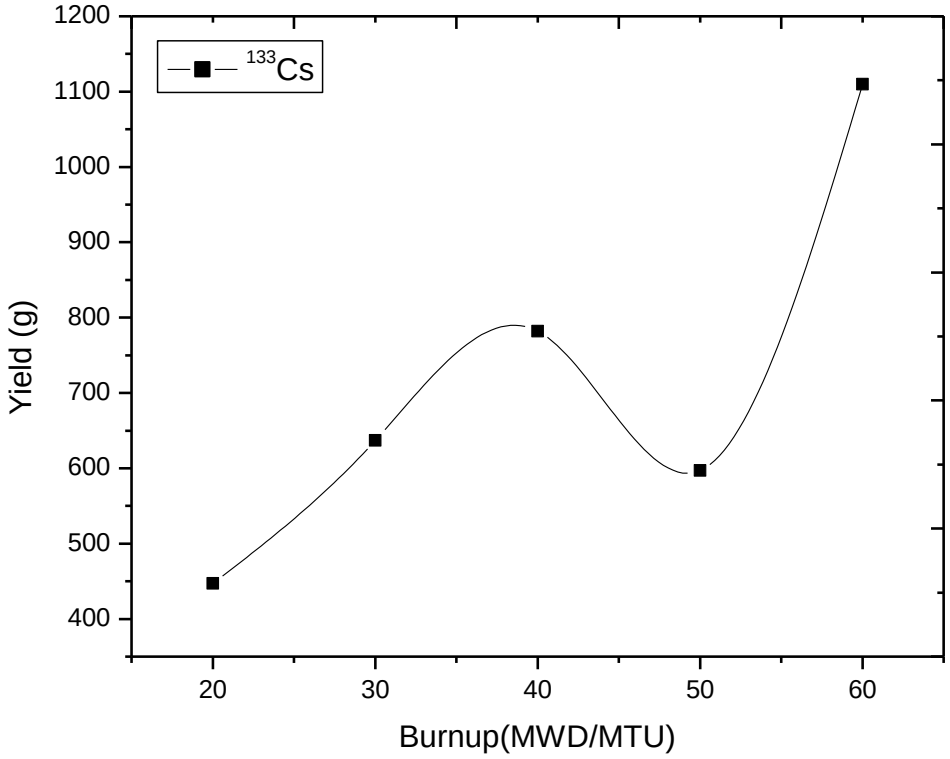

Appendix6_Fig. 4: Growth of ^{133}Cs with increase in Burnup

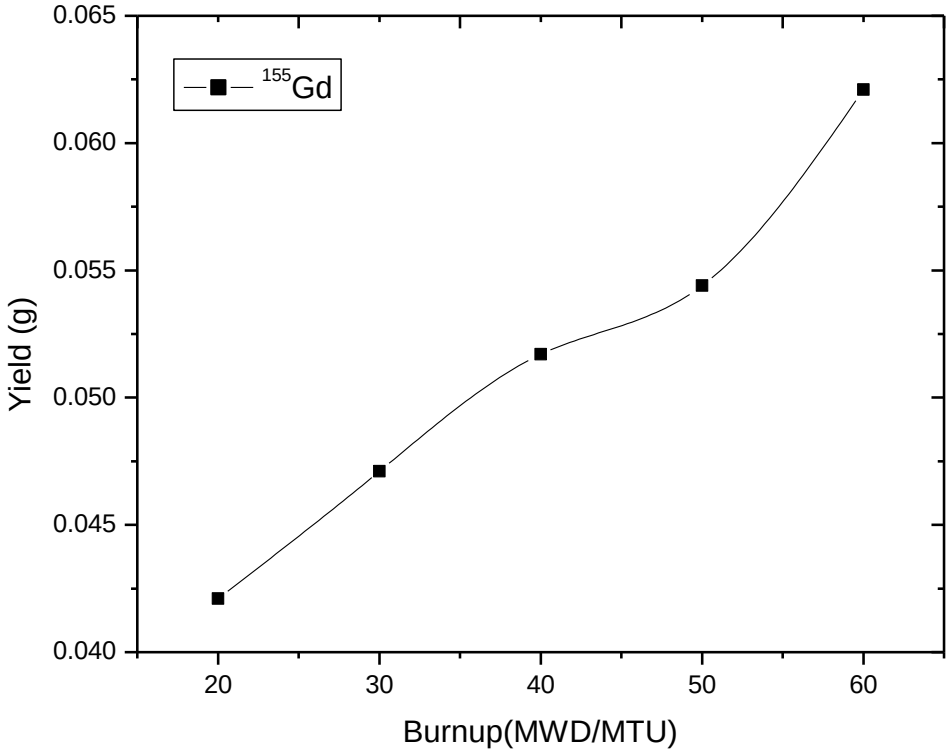

Appendix6_Fig. 5: Growth of ^{155}Gd with increase in Burnup

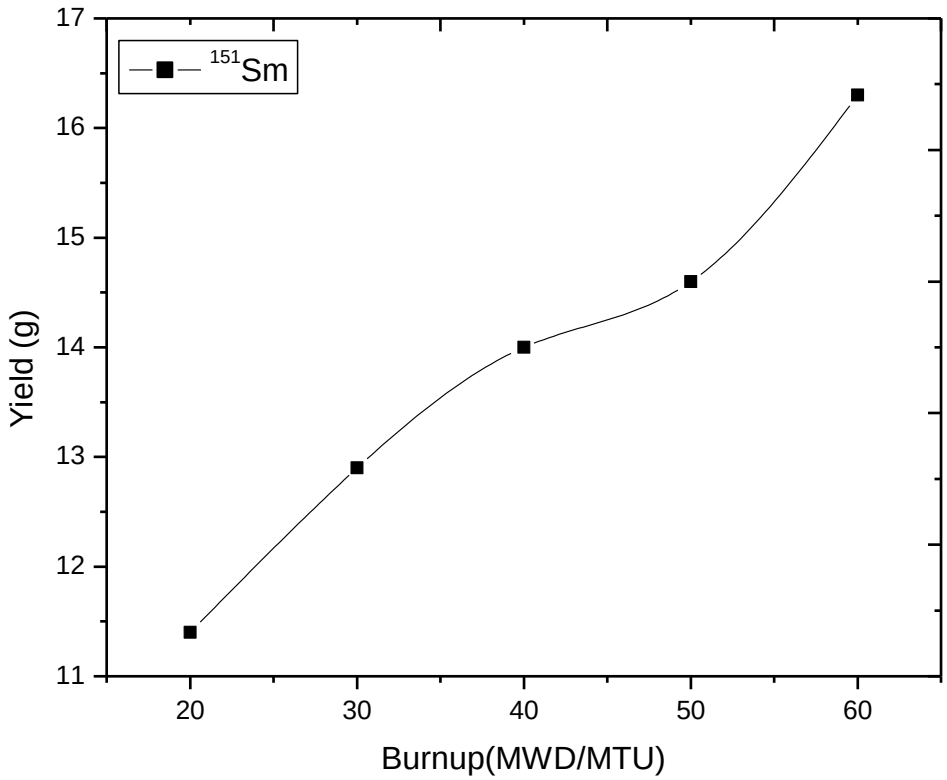

Appendix6_Fig. 6: Growth of ^{151}Sm with increase in Burnup

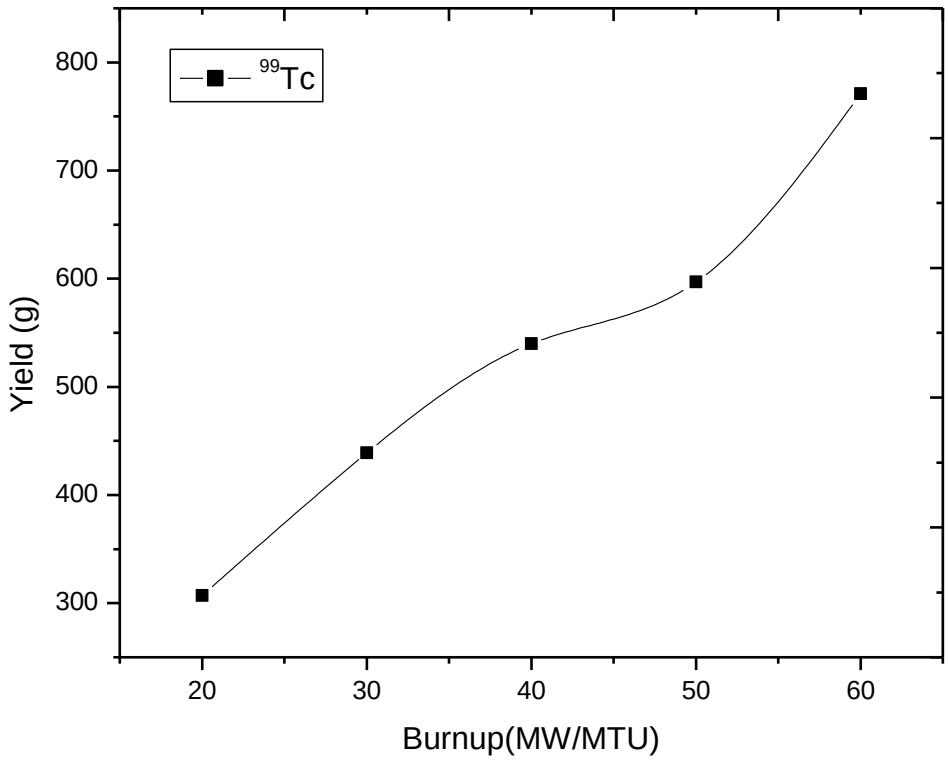

Appendix6_Fig. 7: Growth of ^{99}Tc as a function of burnup

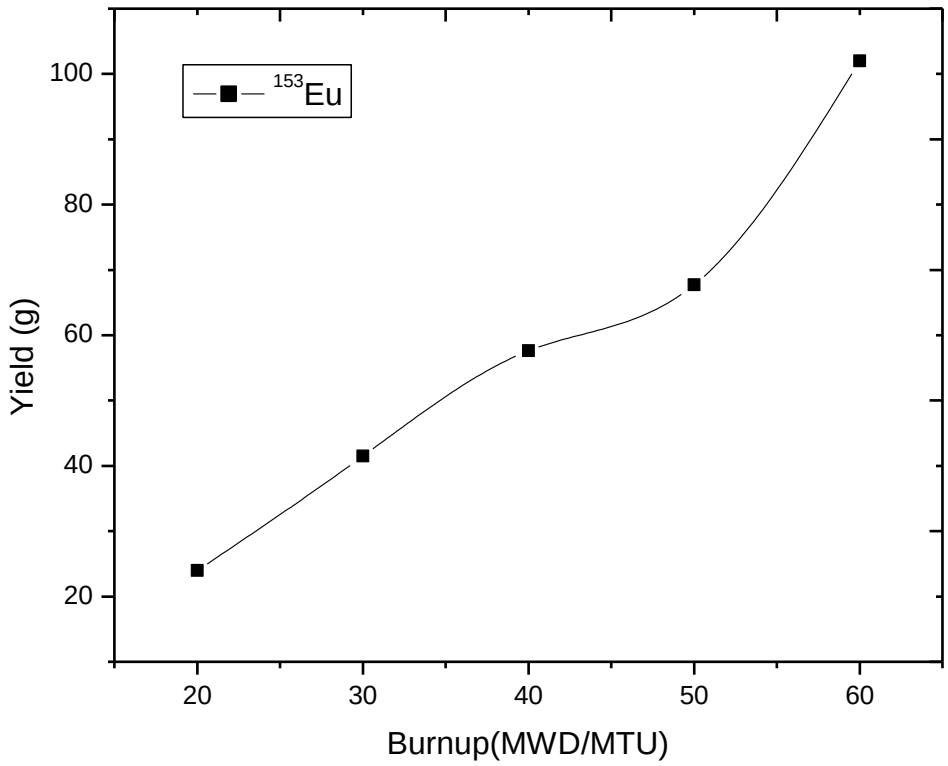

Appendix6_Fig. 8: Growth of ^{153}Eu as a function of Burnup

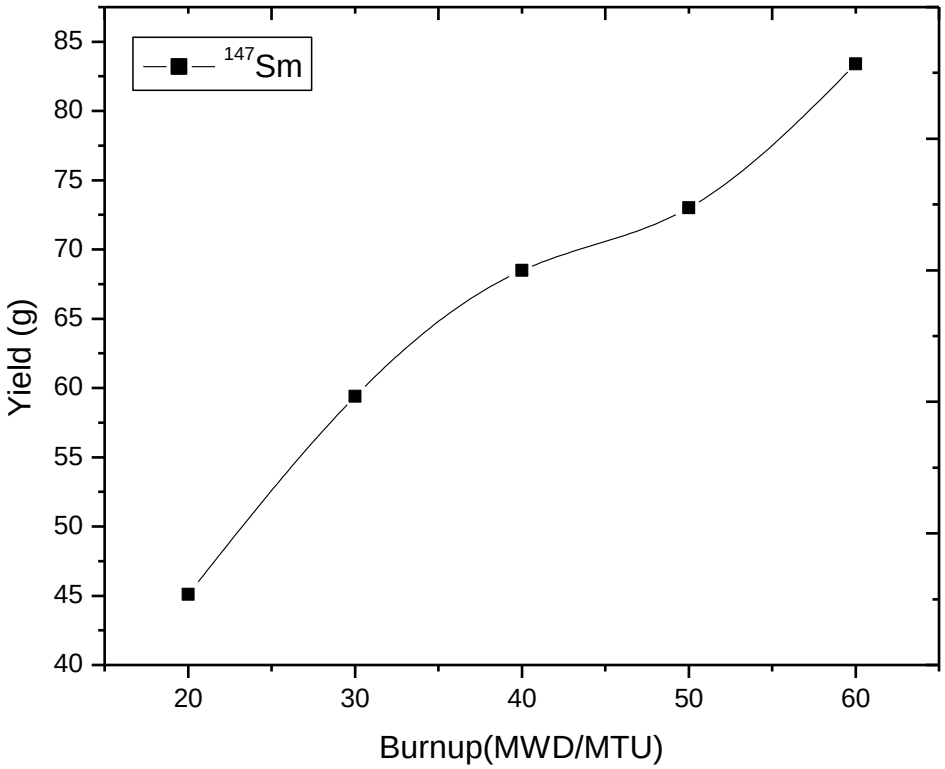

Appendix6_Fig. 9: Growth of ^{147}Sm as a function of Burnup

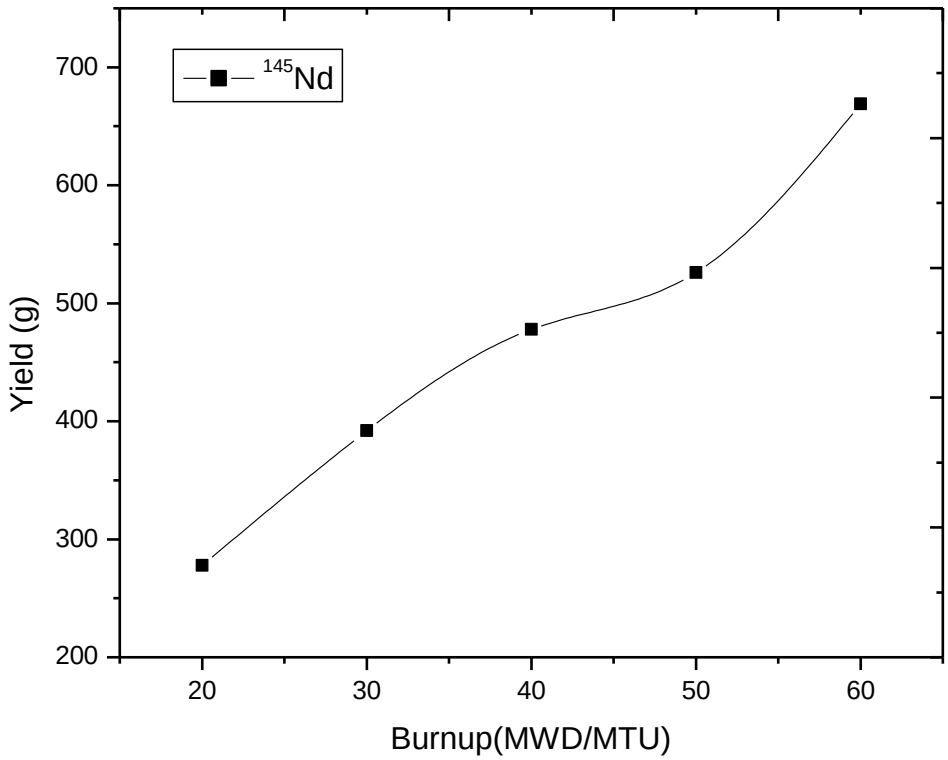

Appendix6_Fig. 10: Growth of ^{145}Nd as a function of Burnup.

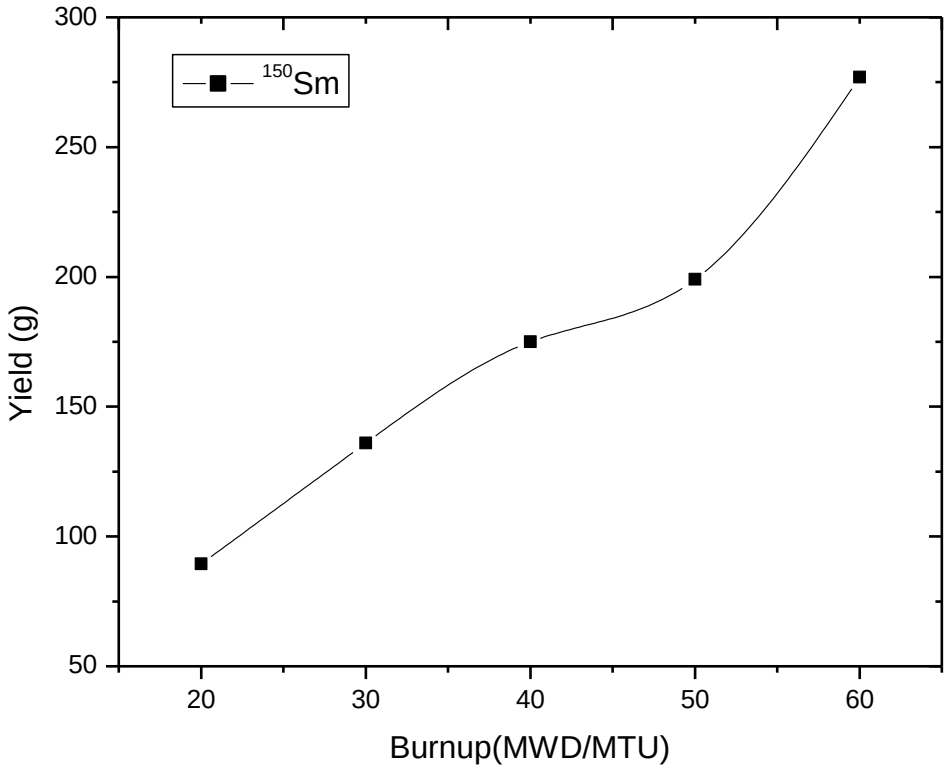

Appendix6_Fig. 11: Growth of ^{150}Sm as a function of Burnup

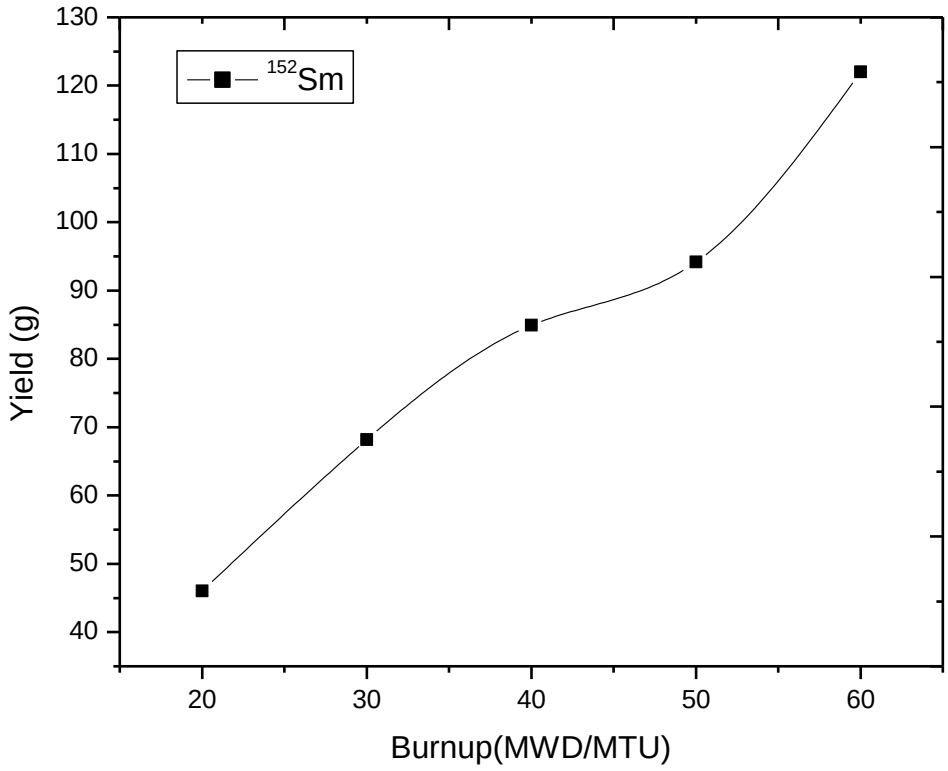

Appendix6_Fig. 12: Growth of ^{152}Sm as a function of Burnup

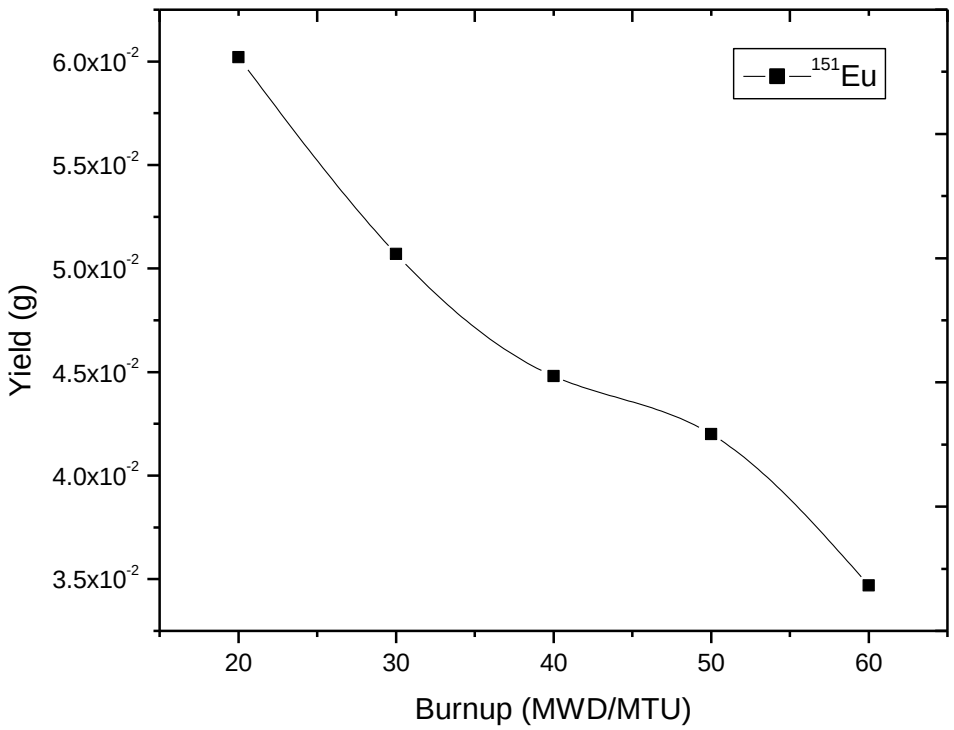

1Appendix6_Fig. 13: Decay of ^{151}Eu as a function of Burnup

APPENDIX 7: INPUT FILE WITH THE MISLOADED FUEL ASSEMBLY

```
'Input generated by GeeWiz SCALE 6.1.3 Compiled  on Tue Sep  6 15:23:32  2011
=csas6
major  actinides
v7-238
read composition
 zr-90       2 0 0.021891  400    end
 zr-91       2 0 0.0047739  400   end
 zr-92       2 0 0.007297  400    end
 zr-94       2 0 0.0073949  400   end
 zr-96       2 0 0.0011913  400   end
 sn-112      2 0 4.6807e-06 400    end
 sn-114      2 0 3.1848e-06 400    end
 sn-115      2 0 1.6406e-06 400    end
 sn-116      2 0 7.0162e-05 400    end
 sn-117      2 0 3.7059e-05 400    end
 sn-118      2 0 0.00011687  400   end
 sn-119      2 0 4.145e-05 400   end
 sn-120      2 0 0.00015721  400   end
 sn-122      2 0 2.2342e-05 400    end
 sn-124      2 0 2.7939e-05 400    end
 fe-54       2 0 5.582e-06 400    end
 fe-56       2 0 8.7625e-05  400    end
 fe-57       2 0 2.0236e-06  400    end
 fe-58       2 0 2.6931e-07  400    end
 cr-50       2 0 3.3012e-06  400    end
 cr-52       2 0 6.3661e-05  400    end
 cr-53       2 0 7.2186e-06  400    end
 cr-54       2 0 1.7969e-06  400    end
 ni-58       2 0 2.5202e-05  400    end
 ni-60       2 0 9.7076e-06  400    end
 ni-61       2 0 4.2198e-07  400    end
 ni-62       2 0 1.3455e-06  400    end
 ni-64       2 0 3.4265e-07  400    end
 hf-174      2 0 3.5414e-09 400    end
 hf-176      2 0 1.1642e-07 400    end
 hf-177      2 0 4.1169e-07 400    end
 hf-178      2 0 6.0381e-07 400    end
 hf-179      2 0 3.0146e-07 400    end
 hf-180      2 0 7.7645e-07 400    end
 o-16        3 0 0.033377  400    end
 h-1         3 0 0.066753  400    end
 co-59       3 0 1e-20 400    end
 o-16        4 0 0.064742  400    end
 b-10        4 0 0.00040445  400   end
 b-11        4 0 0.001628  400    end
 c           4 0 0.0005081  400   end
```

```
al-27       4 0 0.043162  400   end
fe-54       5 0 0.0034542  400   end
fe-56       5 0 0.053698  400   end
fe-57       5 0 0.0012295  400   end
fe-58       5 0 0.00016393  400   end
cr-50       5 0 0.00075918  400   end
cr-52       5 0 0.01464  400   end
cr-53       5 0 0.0016599  400   end
cr-54       5 0 0.00041322  400   end
ni-58       5 0 0.0052842  400   end
ni-60       5 0 0.0020202  400   end
ni-61       5 0 8.7463e-05  400   end
ni-62       5 0 0.00027787  400   end
ni-64       5 0 7.0435e-05  400   end
c          5 0 0.00031849  400   end
si-28       5 0  0.0015701  400   end
si-29       5 0  7.9763e-05 400   end
si-30       5 0  5.2642e-05 400   end
p-31        5 0  6.9469e-05 400   end
mn-55       5 0 0.0017407  400   end
fe-54       6 0 0.0032989  400   end
fe-56       6 0 0.051785  400   end
fe-57       6 0 0.001196  400   end
fe-58       6 0 0.00015916  400   end
cr-50       6 0 0.017869  400   end
ni-58       6 0 0.0054482  400   end
ni-60       6 0 0.0020987  400   end
ni-61       6 0 9.1227e-05  400   end
ni-62       6 0 0.00029087  400   end
ni-64       6 0 7.4076e-05  400   end
b-10        6 0 0.00077817  400   end
b-11        6 0  0.0031322  400   end
si-28       6 0  0.0015424  400   end
si-29       6 0  7.8356e-05 400   end
si-30       6 0  5.1713e-05 400   end
mn-55       6 0 0.00171  400   end
al-27       7 0 0.0602  400   end
o-16        8 0 0.033377  400   end
h-1        8 0 0.066753  400   end
c          9 0 0.0395  400   end
h-poly      9 0 0.078999  400   end
fe-54       10 0 0.004122  400   end
fe-56       10 0 0.064706  400   end
fe-57       10 0 0.0014944  400   end
fe-58       10 0 0.00019887  400   end
ni-58       10 0 0.00064601  400   end
ni-60       10 0 0.00024884  400   end
ni-61       10 0 1.0817e-05 400   end
ni-62       10 0 3.4489e-05 400   end
ni-64       10 0 8.7834e-06 400   end
```

```
si-28       10 0 0.0027363  400   end
si-29       10 0 0.00013901  400   end
si-30       10 0 9.1742e-05  400   end
mn-55       10 0 0.00046434  400   end
c-graphite  10 0 0.012399  400   end
fe-54       11 0 0.0034169  400   end
fe-56       11 0 0.053638  400   end
fe-57       11 0 0.0012387  400   end
fe-58       11 0 0.00016485  400   end
cr-50       11 0 0.00070654  400   end
cr-52       11 0 0.013625  400   end
cr-53       11 0 0.001545  400   end
cr-54       11 0 0.00038457  400   end
ni-58       11 0 0.0057207  400   end
ni-60       11 0 0.0022036  400   end
ni-61       11 0 9.5788e-05  400   end
ni-62       11 0 0.00030542  400   end
ni-64       11 0 7.778e-05  400   end
mn-55       11 0 0.00171  400   end
zr-90       12 0 0.021591  400   end
zr-91       12 0 0.0047086  400   end
zr-92       12 0 0.0071971  400   end
zr-94       12 0 0.0072937  400   end
zr-96       12 0 0.001175  400   end
sn-112      12 0 3.1985e-06  400   end
sn-114      12 0 2.1763e-06  400   end
sn-115      12 0 1.1211e-06  400   end
sn-116      12 0 4.7945e-05  400   end
sn-117      12 0 2.5324e-05  400   end
sn-118      12 0 7.9864e-05  400   end
sn-119      12 0 2.8325e-05  400   end
sn-120      12 0 0.00010743  400   end
sn-122      12 0 1.5267e-05  400   end
sn-124      12 0 1.9092e-05  400   end
fe-54       12 0 8.194e-06  400   end
fe-56       12 0 0.00012863  400   end
fe-57       12 0 2.9706e-06  400   end
fe-58       12 0 3.9533e-07  400   end
nb-93       12 0 0.00042133  400   end
uo2         21 den=10.958  1 400
                        92234  0.04
                        92235  2.4
                        92236  0.02
                        92238  97.54   end
zirc2       22 1 400   end
h2o         23 1 400   end
co-59       23 0 1e-20 400   end
u-234       101 0 5.5772e-06  400   end
u-235       101 0 0.00045861  400   end
u-238       101 0 0.023521  400   end
```

pu-238 101 0 9.6828e-08 400 end
pu-239 101 0 7.8376e-05 400 end
pu-240 101 0 1.0574e-05 400 end
pu-241 101 0 2.3831e-06 400 end
pu-242 101 0 2.4207e-07 400 end
am-241 101 0 8.8245e-07 400 end
o-16 101 0 0.048887 400 end
u-234 102 0 5.1698e-06 400 end
u-235 102 0 0.00037295 400 end
u-238 102 0 0.023438 400 end
pu-238 102 0 2.9704e-07 400 end
pu-239 102 0 0.00010208 400 end
pu-240 102 0 1.9955e-05 400 end
pu-241 102 0 5.8852e-06 400 end
pu-242 102 0 1.0223e-06 400 end
am-241 102 0 2.1794e-06 400 end
o-16 102 0 0.048887 400 end
u-234 103 0 5.0092e-06 400 end
u-235 103 0 0.00034186 400 end
u-238 103 0 0.023402 400 end
pu-238 103 0 4.1838e-07 400 end
pu-239 103 0 0.0001091 400 end
pu-240 103 0 2.3846e-05 400 end
pu-241 103 0 7.4937e-06 400 end
pu-242 103 0 1.5413e-06 400 end
am-241 103 0 2.7738e-06 400 end
o-16 103 0 0.048886 400 end
u-234 104 0 5.0025e-06 400 end
u-235 104 0 0.00034058 400 end
u-238 104 0 0.023401 400 end
pu-238 104 0 4.2408e-07 400 end
pu-239 104 0 0.00010937 400 end
pu-240 104 0 2.4011e-05 400 end
pu-241 104 0 7.563e-06 400 end
pu-242 104 0 1.5661e-06 400 end
am-241 104 0 2.7993e-06 400 end
o-16 104 0 0.048886 400 end
u-234 105 0 5.0034e-06 400 end
u-235 105 0 0.00034076 400 end
u-238 105 0 0.023401 400 end
pu-238 105 0 4.2326e-07 400 end
pu-239 105 0 0.00010933 400 end
pu-240 105 0 2.3987e-05 400 end
pu-241 105 0 7.5531e-06 400 end
pu-242 105 0 1.5625e-06 400 end
am-241 105 0 2.7957e-06 400 end
o-16 105 0 0.048886 400 end
u-234 106 0 5.0092e-06 400 end
u-235 106 0 0.00034186 400 end
u-238 106 0 0.023402 400 end

pu-238 106 0 4.1838e-07 400 end
pu-239 106 0 0.0001091 400 end
pu-240 106 0 2.3846e-05 400 end
pu-241 106 0 7.4937e-06 400 end
pu-242 106 0 1.5413e-06 400 end
am-241 106 0 2.7738e-06 400 end
o-16 106 0 0.048886 400 end
u-234 107 0 5.0198e-06 400 end
u-235 107 0 0.00034387 400 end
u-238 107 0 0.023405 400 end
pu-238 107 0 4.0953e-07 400 end
pu-239 107 0 0.00010867 400 end
pu-240 107 0 2.3587e-05 400 end
pu-241 107 0 7.385e-06 400 end
pu-242 107 0 1.5028e-06 400 end
am-241 107 0 2.7336e-06 400 end
o-16 107 0 0.048886 400 end
u-234 108 0 5.0276e-06 400 end
u-235 108 0 0.00034534 400 end
u-238 108 0 0.023406 400 end
pu-238 108 0 4.0315e-07 400 end
pu-239 108 0 0.00010835 400 end
pu-240 108 0 2.3399e-05 400 end
pu-241 108 0 7.306e-06 400 end
pu-242 108 0 1.4752e-06 400 end
am-241 108 0 2.7045e-06 400 end
o-16 108 0 0.048886 400 end
u-234 109 0 5.0285e-06 400 end
u-235 109 0 0.00034552 400 end
u-238 109 0 0.023406 400 end
pu-238 109 0 4.0236e-07 400 end
pu-239 109 0 0.00010831 400 end
pu-240 109 0 2.3375e-05 400 end
pu-241 109 0 7.2961e-06 400 end
pu-242 109 0 1.4718e-06 400 end
am-241 109 0 2.7008e-06 400 end
o-16 109 0 0.048886 400 end
u-234 110 0 5.0247e-06 400 end
u-235 110 0 0.00034479 400 end
u-238 110 0 0.023406 400 end
pu-238 110 0 4.0554e-07 400 end
pu-239 110 0 0.00010847 400 end
pu-240 110 0 2.3469e-05 400 end
pu-241 110 0 7.3356e-06 400 end
pu-242 110 0 1.4855e-06 400 end
am-241 110 0 2.7154e-06 400 end
o-16 110 0 0.048886 400 end
u-234 111 0 5.0218e-06 400 end
u-235 111 0 0.00034424 400 end
u-238 111 0 0.023405 400 end

pu-238 111 0 4.0793e-07 400 end
pu-239 111 0 0.00010859 400 end
pu-240 111 0 2.354e-05 400 end
pu-241 111 0 7.3652e-06 400 end
pu-242 111 0 1.4959e-06 400 end
am-241 111 0 2.7263e-06 400 end
o-16 111 0 0.048886 400 end
u-234 112 0 5.0266e-06 400 end
u-235 112 0 0.00034515 400 end
u-238 112 0 0.023406 400 end
pu-238 112 0 4.0395e-07 400 end
pu-239 112 0 0.00010839 400 end
pu-240 112 0 2.3422e-05 400 end
pu-241 112 0 7.3158e-06 400 end
pu-242 112 0 1.4786e-06 400 end
am-241 112 0 2.7081e-06 400 end
o-16 112 0 0.048886 400 end
u-234 113 0 5.0596e-06 400 end
u-235 113 0 0.00035146 400 end
u-238 113 0 0.023413 400 end
pu-238 113 0 3.7742e-07 400 end
pu-239 113 0 0.00010701 400 end
pu-240 113 0 2.2619e-05 400 end
pu-241 113 0 6.9803e-06 400 end
pu-242 113 0 1.3641e-06 400 end
am-241 113 0 2.5842e-06 400 end
o-16 113 0 0.048886 400 end
u-234 114 0 5.1918e-06 400 end
u-235 114 0 0.00037731 400 end
u-238 114 0 0.023442 400 end
pu-238 114 0 2.8251e-07 400 end
pu-239 114 0 0.00010103 400 end
pu-240 114 0 1.9429e-05 400 end
pu-241 114 0 5.6728e-06 400 end
pu-242 114 0 9.6155e-07 400 end
am-241 114 0 2.1009e-06 400 end
o-16 114 0 0.048887 400 end
u-234 115 0 5.464e-06 400 end
u-235 115 0 0.00043377 400 end
u-238 115 0 0.023498 400 end
pu-238 115 0 1.3867e-07 400 end
pu-239 115 0 8.5945e-05 400 end
pu-240 115 0 1.308e-05 400 end
pu-241 115 0 3.2442e-06 400 end
pu-242 115 0 3.9068e-07 400 end
am-241 115 0 1.2016e-06 400 end
o-16 115 0 0.048887 400 end
u-234 116 0 5.6148e-06 400 end
u-235 116 0 0.00046703 400 end
u-238 116 0 0.023528 400 end

```
pu-238      116 0 8.5025e-08  400   end
pu-239      116 0 7.5675e-05  400   end
pu-240      116 0 9.7693e-06  400   end
pu-241      116 0 2.1218e-06  400   end
pu-242      116 0 2.0272e-07  400   end
am-241      116 0 7.8562e-07 400   end
o-16        116 0 0.048887  400   end
u-234       117 0 5.7595e-06  400   end
u-235       117 0 0.00050041  400   end
u-238       117 0 0.023555  400   end
pu-238      117 0 4.8166e-08  400   end
pu-239      117 0 6.4251e-05  400   end
pu-240      117 0 6.812e-06 400   end
pu-241      117 0 1.2422e-06  400   end
pu-242      117 0 9.0889e-08  400   end
am-241      117 0 4.5964e-07 400   end
o-16        117 0 0.048887  400   end
u-234       118 0 5.9805e-06  400   end
u-235       118 0 0.0005544  400   end
u-238       118 0 0.023594  400   end
pu-238      118 0 1.4542e-08  400   end
pu-239      118 0 4.3165e-05  400   end
pu-240      118 0 2.9395e-06  400   end
pu-241      118 0 3.4814e-07  400   end
pu-242      118 0 1.4468e-08  400   end
am-241      118 0 1.2858e-07 400   end
o-16        118 0 0.048888  400   end
zr-90       202 0 0.021891  400   end
zr-91       202 0 0.0047739  400   end
zr-92       202 0 0.007297  400   end
zr-94       202 0 0.0073949  400   end
zr-96       202 0 0.0011913  400   end
sn-112      202 0 4.6807e-06 400   end
sn-114      202 0 3.1848e-06 400   end
sn-115      202 0 1.6406e-06 400   end
sn-116      202 0 7.0162e-05 400   end
sn-117      202 0 3.7059e-05 400   end
sn-118      202 0 0.00011687  400   end
sn-119      202 0 4.145e-05 400   end
sn-120      202 0 0.00015721  400   end
sn-122      202 0 2.2342e-05 400   end
sn-124      202 0 2.7939e-05 400   end
fe-54       202 0 5.582e-06 400   end
fe-56       202 0 8.7625e-05  400   end
fe-57       202 0 2.0236e-06  400   end
fe-58       202 0 2.6931e-07  400   end
cr-50       202 0 3.3012e-06  400   end
cr-52       202 0 6.3661e-05  400   end
cr-53       202 0 7.2186e-06  400   end
cr-54       202 0 1.7969e-06  400   end
```

ni-58 202 0 2.5202e-05 400 end
ni-60 202 0 9.7076e-06 400 end
ni-61 202 0 4.2198e-07 400 end
ni-62 202 0 1.3455e-06 400 end
ni-64 202 0 3.4265e-07 400 end
hf-174 202 0 3.5414e-09 400 end
hf-176 202 0 1.1642e-07 400 end
hf-177 202 0 4.1169e-07 400 end
hf-178 202 0 6.0381e-07 400 end
hf-179 202 0 3.0146e-07 400 end
hf-180 202 0 7.7645e-07 400 end
zr-90 203 0 0.021891 400 end
zr-91 203 0 0.0047739 400 end
zr-92 203 0 0.007297 400 end
zr-94 203 0 0.0073949 400 end
zr-96 203 0 0.0011913 400 end
sn-112 203 0 4.6807e-06 400 end
sn-114 203 0 3.1848e-06 400 end
sn-115 203 0 1.6406e-06 400 end
sn-116 203 0 7.0162e-05 400 end
sn-117 203 0 3.7059e-05 400 end
sn-118 203 0 0.00011687 400 end
sn-119 203 0 4.145e-05 400 end
sn-120 203 0 0.00015721 400 end
sn-122 203 0 2.2342e-05 400 end
sn-124 203 0 2.7939e-05 400 end
fe-54 203 0 5.582e-06 400 end
fe-56 203 0 8.7625e-05 400 end
fe-57 203 0 2.0236e-06 400 end
fe-58 203 0 2.6931e-07 400 end
cr-50 203 0 3.3012e-06 400 end
cr-52 203 0 6.3661e-05 400 end
cr-53 203 0 7.2186e-06 400 end
cr-54 203 0 1.7969e-06 400 end
ni-58 203 0 2.5202e-05 400 end
ni-60 203 0 9.7076e-06 400 end
ni-61 203 0 4.2198e-07 400 end
ni-62 203 0 1.3455e-06 400 end
ni-64 203 0 3.4265e-07 400 end
hf-174 203 0 3.5414e-09 400 end
hf-176 203 0 1.1642e-07 400 end
hf-177 203 0 4.1169e-07 400 end
hf-178 203 0 6.0381e-07 400 end
hf-179 203 0 3.0146e-07 400 end
hf-180 203 0 7.7645e-07 400 end
zr-90 204 0 0.021891 400 end
zr-91 204 0 0.0047739 400 end
zr-92 204 0 0.007297 400 end
zr-94 204 0 0.0073949 400 end
zr-96 204 0 0.0011913 400 end

sn-112 204 0 4.6807e-06 400 end
sn-114 204 0 3.1848e-06 400 end
sn-115 204 0 1.6406e-06 400 end
sn-116 204 0 7.0162e-05 400 end
sn-117 204 0 3.7059e-05 400 end
sn-118 204 0 0.00011687 400 end
sn-119 204 0 4.145e-05 400 end
sn-120 204 0 0.00015721 400 end
sn-122 204 0 2.2342e-05 400 end
sn-124 204 0 2.7939e-05 400 end
fe-54 204 0 5.582e-06 400 end
fe-56 204 0 8.7625e-05 400 end
fe-57 204 0 2.0236e-06 400 end
fe-58 204 0 2.6931e-07 400 end
cr-50 204 0 3.3012e-06 400 end
cr-52 204 0 6.3661e-05 400 end
cr-53 204 0 7.2186e-06 400 end
cr-54 204 0 1.7969e-06 400 end
ni-58 204 0 2.5202e-05 400 end
ni-60 204 0 9.7076e-06 400 end
ni-61 204 0 4.2198e-07 400 end
ni-62 204 0 1.3455e-06 400 end
ni-64 204 0 3.4265e-07 400 end
hf-174 204 0 3.5414e-09 400 end
hf-176 204 0 1.1642e-07 400 end
hf-177 204 0 4.1169e-07 400 end
hf-178 204 0 6.0381e-07 400 end
hf-179 204 0 3.0146e-07 400 end
hf-180 204 0 7.7645e-07 400 end
zr-90 205 0 0.021891 400 end
zr-91 205 0 0.0047739 400 end
zr-92 205 0 0.007297 400 end
zr-94 205 0 0.0073949 400 end
zr-96 205 0 0.0011913 400 end
sn-112 205 0 4.6807e-06 400 end
sn-114 205 0 3.1848e-06 400 end
sn-115 205 0 1.6406e-06 400 end
sn-116 205 0 7.0162e-05 400 end
sn-117 205 0 3.7059e-05 400 end
sn-118 205 0 0.00011687 400 end
sn-119 205 0 4.145e-05 400 end
sn-120 205 0 0.00015721 400 end
sn-122 205 0 2.2342e-05 400 end
sn-124 205 0 2.7939e-05 400 end
fe-54 205 0 5.582e-06 400 end
fe-56 205 0 8.7625e-05 400 end
fe-57 205 0 2.0236e-06 400 end
fe-58 205 0 2.6931e-07 400 end
cr-50 205 0 3.3012e-06 400 end
cr-52 205 0 6.3661e-05 400 end

cr-53 205 0 7.2186e-06 400 end
cr-54 205 0 1.7969e-06 400 end
ni-58 205 0 2.5202e-05 400 end
ni-60 205 0 9.7076e-06 400 end
ni-61 205 0 4.2198e-07 400 end
ni-62 205 0 1.3455e-06 400 end
ni-64 205 0 3.4265e-07 400 end
hf-174 205 0 3.5414e-09 400 end
hf-176 205 0 1.1642e-07 400 end
hf-177 205 0 4.1169e-07 400 end
hf-178 205 0 6.0381e-07 400 end
hf-179 205 0 3.0146e-07 400 end
hf-180 205 0 7.7645e-07 400 end
zr-90 206 0 0.021891 400 end
zr-91 206 0 0.0047739 400 end
zr-92 206 0 0.007297 400 end
zr-94 206 0 0.0073949 400 end
zr-96 206 0 0.0011913 400 end
sn-112 206 0 4.6807e-06 400 end
sn-114 206 0 3.1848e-06 400 end
sn-115 206 0 1.6406e-06 400 end
sn-116 206 0 7.0162e-05 400 end
sn-117 206 0 3.7059e-05 400 end
sn-118 206 0 0.00011687 400 end
sn-119 206 0 4.145e-05 400 end
sn-120 206 0 0.00015721 400 end
sn-122 206 0 2.2342e-05 400 end
sn-124 206 0 2.7939e-05 400 end
fe-54 206 0 5.582e-06 400 end
fe-56 206 0 8.7625e-05 400 end
fe-57 206 0 2.0236e-06 400 end
fe-58 206 0 2.6931e-07 400 end
cr-50 206 0 3.3012e-06 400 end
cr-52 206 0 6.3661e-05 400 end
cr-53 206 0 7.2186e-06 400 end
cr-54 206 0 1.7969e-06 400 end
ni-58 206 0 2.5202e-05 400 end
ni-60 206 0 9.7076e-06 400 end
ni-61 206 0 4.2198e-07 400 end
ni-62 206 0 1.3455e-06 400 end
ni-64 206 0 3.4265e-07 400 end
hf-174 206 0 3.5414e-09 400 end
hf-176 206 0 1.1642e-07 400 end
hf-177 206 0 4.1169e-07 400 end
hf-178 206 0 6.0381e-07 400 end
hf-179 206 0 3.0146e-07 400 end
hf-180 206 0 7.7645e-07 400 end
zr-90 207 0 0.021891 400 end
zr-91 207 0 0.0047739 400 end
zr-92 207 0 0.007297 400 end

zr-94 207 0 0.0073949 400 end
zr-96 207 0 0.0011913 400 end
sn-112 207 0 4.6807e-06 400 end
sn-114 207 0 3.1848e-06 400 end
sn-115 207 0 1.6406e-06 400 end
sn-116 207 0 7.0162e-05 400 end
sn-117 207 0 3.7059e-05 400 end
sn-118 207 0 0.00011687 400 end
sn-119 207 0 4.145e-05 400 end
sn-120 207 0 0.00015721 400 end
sn-122 207 0 2.2342e-05 400 end
sn-124 207 0 2.7939e-05 400 end
fe-54 207 0 5.582e-06 400 end
fe-56 207 0 8.7625e-05 400 end
fe-57 207 0 2.0236e-06 400 end
fe-58 207 0 2.6931e-07 400 end
cr-50 207 0 3.3012e-06 400 end
cr-52 207 0 6.3661e-05 400 end
cr-53 207 0 7.2186e-06 400 end
cr-54 207 0 1.7969e-06 400 end
ni-58 207 0 2.5202e-05 400 end
ni-60 207 0 9.7076e-06 400 end
ni-61 207 0 4.2198e-07 400 end
ni-62 207 0 1.3455e-06 400 end
ni-64 207 0 3.4265e-07 400 end
hf-174 207 0 3.5414e-09 400 end
hf-176 207 0 1.1642e-07 400 end
hf-177 207 0 4.1169e-07 400 end
hf-178 207 0 6.0381e-07 400 end
hf-179 207 0 3.0146e-07 400 end
hf-180 207 0 7.7645e-07 400 end
zr-90 208 0 0.021891 400 end
zr-91 208 0 0.0047739 400 end
zr-92 208 0 0.007297 400 end
zr-94 208 0 0.0073949 400 end
zr-96 208 0 0.0011913 400 end
sn-112 208 0 4.6807e-06 400 end
sn-114 208 0 3.1848e-06 400 end
sn-115 208 0 1.6406e-06 400 end
sn-116 208 0 7.0162e-05 400 end
sn-117 208 0 3.7059e-05 400 end
sn-118 208 0 0.00011687 400 end
sn-119 208 0 4.145e-05 400 end
sn-120 208 0 0.00015721 400 end
sn-122 208 0 2.2342e-05 400 end
sn-124 208 0 2.7939e-05 400 end
fe-54 208 0 5.582e-06 400 end
fe-56 208 0 8.7625e-05 400 end
fe-57 208 0 2.0236e-06 400 end
fe-58 208 0 2.6931e-07 400 end

```
cr-50      208 0 3.3012e-06 400   end
cr-52      208 0 6.3661e-05 400   end
cr-53      208 0 7.2186e-06 400   end
cr-54      208 0 1.7969e-06 400   end
ni-58      208 0 2.5202e-05 400   end
ni-60      208 0 9.7076e-06 400   end
ni-61      208 0 4.2198e-07 400   end
ni-62      208 0 1.3455e-06 400   end
ni-64      208 0 3.4265e-07 400   end
hf-174     208 0 3.5414e-09 400   end
hf-176     208 0 1.1642e-07 400   end
hf-177     208 0 4.1169e-07 400   end
hf-178     208 0 6.0381e-07 400   end
hf-179     208 0 3.0146e-07 400   end
hf-180     208 0 7.7645e-07 400   end
zr-90      209 0 0.021891 400   end
zr-91      209 0 0.0047739 400   end
zr-92      209 0 0.007297 400   end
zr-94      209 0 0.0073949 400   end
zr-96      209 0 0.0011913 400   end
sn-112     209 0 4.6807e-06 400   end
sn-114     209 0 3.1848e-06 400   end
sn-115     209 0 1.6406e-06 400   end
sn-116     209 0 7.0162e-05 400   end
sn-117     209 0 3.7059e-05 400   end
sn-118     209 0 0.00011687 400   end
sn-119     209 0 4.145e-05 400   end
sn-120     209 0 0.00015721 400   end
sn-122     209 0 2.2342e-05 400   end
sn-124     209 0 2.7939e-05 400   end
fe-54      209 0 5.582e-06 400   end
fe-56      209 0 8.7625e-05 400   end
fe-57      209 0 2.0236e-06 400   end
fe-58      209 0 2.6931e-07 400   end
cr-50      209 0 3.3012e-06 400   end
cr-52      209 0 6.3661e-05 400   end
cr-53      209 0 7.2186e-06 400   end
cr-54      209 0 1.7969e-06 400   end
ni-58      209 0 2.5202e-05 400   end
ni-60      209 0 9.7076e-06 400   end
ni-61      209 0 4.2198e-07 400   end
ni-62      209 0 1.3455e-06 400   end
ni-64      209 0 3.4265e-07 400   end
hf-174     209 0 3.5414e-09 400   end
hf-176     209 0 1.1642e-07 400   end
hf-177     209 0 4.1169e-07 400   end
hf-178     209 0 6.0381e-07 400   end
hf-179     209 0 3.0146e-07 400   end
hf-180     209 0 7.7645e-07 400   end
zr-90      210 0 0.021891 400   end
```

zr-91 210 0 0.0047739 400 end
zr-92 210 0 0.007297 400 end
zr-94 210 0 0.0073949 400 end
zr-96 210 0 0.0011913 400 end
sn-112 210 0 4.6807e-06 400 end
sn-114 210 0 3.1848e-06 400 end
sn-115 210 0 1.6406e-06 400 end
sn-116 210 0 7.0162e-05 400 end
sn-117 210 0 3.7059e-05 400 end
sn-118 210 0 0.00011687 400 end
sn-119 210 0 4.145e-05 400 end
sn-120 210 0 0.00015721 400 end
sn-122 210 0 2.2342e-05 400 end
sn-124 210 0 2.7939e-05 400 end
fe-54 210 0 5.582e-06 400 end
fe-56 210 0 8.7625e-05 400 end
fe-57 210 0 2.0236e-06 400 end
fe-58 210 0 2.6931e-07 400 end
cr-50 210 0 3.3012e-06 400 end
cr-52 210 0 6.3661e-05 400 end
cr-53 210 0 7.2186e-06 400 end
cr-54 210 0 1.7969e-06 400 end
ni-58 210 0 2.5202e-05 400 end
ni-60 210 0 9.7076e-06 400 end
ni-61 210 0 4.2198e-07 400 end
ni-62 210 0 1.3455e-06 400 end
ni-64 210 0 3.4265e-07 400 end
hf-174 210 0 3.5414e-09 400 end
hf-176 210 0 1.1642e-07 400 end
hf-177 210 0 4.1169e-07 400 end
hf-178 210 0 6.0381e-07 400 end
hf-179 210 0 3.0146e-07 400 end
hf-180 210 0 7.7645e-07 400 end
zr-90 211 0 0.021891 400 end
zr-91 211 0 0.0047739 400 end
zr-92 211 0 0.007297 400 end
zr-94 211 0 0.0073949 400 end
zr-96 211 0 0.0011913 400 end
sn-112 211 0 4.6807e-06 400 end
sn-114 211 0 3.1848e-06 400 end
sn-115 211 0 1.6406e-06 400 end
sn-116 211 0 7.0162e-05 400 end
sn-117 211 0 3.7059e-05 400 end
sn-118 211 0 0.00011687 400 end
sn-119 211 0 4.145e-05 400 end
sn-120 211 0 0.00015721 400 end
sn-122 211 0 2.2342e-05 400 end
sn-124 211 0 2.7939e-05 400 end
fe-54 211 0 5.582e-06 400 end
fe-56 211 0 8.7625e-05 400 end

```
fe-57      211 0 2.0236e-06  400   end
fe-58      211 0 2.6931e-07  400   end
cr-50      211 0 3.3012e-06  400   end
cr-52      211 0 6.3661e-05  400   end
cr-53      211 0 7.2186e-06  400   end
cr-54      211 0 1.7969e-06  400   end
ni-58      211 0 2.5202e-05  400   end
ni-60      211 0 9.7076e-06  400   end
ni-61      211 0 4.2198e-07  400   end
ni-62      211 0 1.3455e-06  400   end
ni-64      211 0 3.4265e-07  400   end
hf-174     211 0 3.5414e-09 400   end
hf-176     211 0 1.1642e-07 400   end
hf-177     211 0 4.1169e-07 400   end
hf-178     211 0 6.0381e-07 400   end
hf-179     211 0 3.0146e-07 400   end
hf-180     211 0 7.7645e-07 400   end
zr-90      212 0 0.021891  400   end
zr-91      212 0 0.0047739  400   end
zr-92      212 0 0.007297  400   end
zr-94      212 0 0.0073949  400   end
zr-96      212 0 0.0011913  400   end
sn-112     212 0 4.6807e-06 400   end
sn-114     212 0 3.1848e-06 400   end
sn-115     212 0 1.6406e-06 400   end
sn-116     212 0 7.0162e-05 400   end
sn-117     212 0 3.7059e-05 400   end
sn-118     212 0 0.00011687  400   end
sn-119     212 0 4.145e-05 400   end
sn-120     212 0 0.00015721  400   end
sn-122     212 0 2.2342e-05 400   end
sn-124     212 0 2.7939e-05 400   end
fe-54      212 0 5.582e-06 400   end
fe-56      212 0 8.7625e-05  400   end
fe-57      212 0 2.0236e-06  400   end
fe-58      212 0 2.6931e-07  400   end
cr-50      212 0 3.3012e-06  400   end
cr-52      212 0 6.3661e-05  400   end
cr-53      212 0 7.2186e-06  400   end
cr-54      212 0 1.7969e-06  400   end
ni-58      212 0 2.5202e-05  400   end
ni-60      212 0 9.7076e-06  400   end
ni-61      212 0 4.2198e-07  400   end
ni-62      212 0 1.3455e-06  400   end
ni-64      212 0 3.4265e-07  400   end
hf-174     212 0 3.5414e-09 400   end
hf-176     212 0 1.1642e-07 400   end
hf-177     212 0 4.1169e-07 400   end
hf-178     212 0 6.0381e-07 400   end
hf-179     212 0 3.0146e-07 400   end
```

hf-180 212 0 7.7645e-07 400 end
zr-90 213 0 0.021891 400 end
zr-91 213 0 0.0047739 400 end
zr-92 213 0 0.007297 400 end
zr-94 213 0 0.0073949 400 end
zr-96 213 0 0.0011913 400 end
sn-112 213 0 4.6807e-06 400 end
sn-114 213 0 3.1848e-06 400 end
sn-115 213 0 1.6406e-06 400 end
sn-116 213 0 7.0162e-05 400 end
sn-117 213 0 3.7059e-05 400 end
sn-118 213 0 0.00011687 400 end
sn-119 213 0 4.145e-05 400 end
sn-120 213 0 0.00015721 400 end
sn-122 213 0 2.2342e-05 400 end
sn-124 213 0 2.7939e-05 400 end
fe-54 213 0 5.582e-06 400 end
fe-56 213 0 8.7625e-05 400 end
fe-57 213 0 2.0236e-06 400 end
fe-58 213 0 2.6931e-07 400 end
cr-50 213 0 3.3012e-06 400 end
cr-52 213 0 6.3661e-05 400 end
cr-53 213 0 7.2186e-06 400 end
cr-54 213 0 1.7969e-06 400 end
ni-58 213 0 2.5202e-05 400 end
ni-60 213 0 9.7076e-06 400 end
ni-61 213 0 4.2198e-07 400 end
ni-62 213 0 1.3455e-06 400 end
ni-64 213 0 3.4265e-07 400 end
hf-174 213 0 3.5414e-09 400 end
hf-176 213 0 1.1642e-07 400 end
hf-177 213 0 4.1169e-07 400 end
hf-178 213 0 6.0381e-07 400 end
hf-179 213 0 3.0146e-07 400 end
hf-180 213 0 7.7645e-07 400 end
zr-90 214 0 0.021891 400 end
zr-91 214 0 0.0047739 400 end
zr-92 214 0 0.007297 400 end
zr-94 214 0 0.0073949 400 end
zr-96 214 0 0.0011913 400 end
sn-112 214 0 4.6807e-06 400 end
sn-114 214 0 3.1848e-06 400 end
sn-115 214 0 1.6406e-06 400 end
sn-116 214 0 7.0162e-05 400 end
sn-117 214 0 3.7059e-05 400 end
sn-118 214 0 0.00011687 400 end
sn-119 214 0 4.145e-05 400 end
sn-120 214 0 0.00015721 400 end
sn-122 214 0 2.2342e-05 400 end
sn-124 214 0 2.7939e-05 400 end

fe-54 214 0 5.582e-06 400 end
fe-56 214 0 8.7625e-05 400 end
fe-57 214 0 2.0236e-06 400 end
fe-58 214 0 2.6931e-07 400 end
cr-50 214 0 3.3012e-06 400 end
cr-52 214 0 6.3661e-05 400 end
cr-53 214 0 7.2186e-06 400 end
cr-54 214 0 1.7969e-06 400 end
ni-58 214 0 2.5202e-05 400 end
ni-60 214 0 9.7076e-06 400 end
ni-61 214 0 4.2198e-07 400 end
ni-62 214 0 1.3455e-06 400 end
ni-64 214 0 3.4265e-07 400 end
hf-174 214 0 3.5414e-09 400 end
hf-176 214 0 1.1642e-07 400 end
hf-177 214 0 4.1169e-07 400 end
hf-178 214 0 6.0381e-07 400 end
hf-179 214 0 3.0146e-07 400 end
hf-180 214 0 7.7645e-07 400 end
zr-90 215 0 0.021891 400 end
zr-91 215 0 0.0047739 400 end
zr-92 215 0 0.007297 400 end
zr-94 215 0 0.0073949 400 end
zr-96 215 0 0.0011913 400 end
sn-112 215 0 4.6807e-06 400 end
sn-114 215 0 3.1848e-06 400 end
sn-115 215 0 1.6406e-06 400 end
sn-116 215 0 7.0162e-05 400 end
sn-117 215 0 3.7059e-05 400 end
sn-118 215 0 0.00011687 400 end
sn-119 215 0 4.145e-05 400 end
sn-120 215 0 0.00015721 400 end
sn-122 215 0 2.2342e-05 400 end
sn-124 215 0 2.7939e-05 400 end
fe-54 215 0 5.582e-06 400 end
fe-56 215 0 8.7625e-05 400 end
fe-57 215 0 2.0236e-06 400 end
fe-58 215 0 2.6931e-07 400 end
cr-50 215 0 3.3012e-06 400 end
cr-52 215 0 6.3661e-05 400 end
cr-53 215 0 7.2186e-06 400 end
cr-54 215 0 1.7969e-06 400 end
ni-58 215 0 2.5202e-05 400 end
ni-60 215 0 9.7076e-06 400 end
ni-61 215 0 4.2198e-07 400 end
ni-62 215 0 1.3455e-06 400 end
ni-64 215 0 3.4265e-07 400 end
hf-174 215 0 3.5414e-09 400 end
hf-176 215 0 1.1642e-07 400 end
hf-177 215 0 4.1169e-07 400 end

hf-178 215 0 6.0381e-07 400 end
hf-179 215 0 3.0146e-07 400 end
hf-180 215 0 7.7645e-07 400 end
zr-90 216 0 0.021891 400 end
zr-91 216 0 0.0047739 400 end
zr-92 216 0 0.007297 400 end
zr-94 216 0 0.0073949 400 end
zr-96 216 0 0.0011913 400 end
sn-112 216 0 4.6807e-06 400 end
sn-114 216 0 3.1848e-06 400 end
sn-115 216 0 1.6406e-06 400 end
sn-116 216 0 7.0162e-05 400 end
sn-117 216 0 3.7059e-05 400 end
sn-118 216 0 0.00011687 400 end
sn-119 216 0 4.145e-05 400 end
sn-120 216 0 0.00015721 400 end
sn-122 216 0 2.2342e-05 400 end
sn-124 216 0 2.7939e-05 400 end
fe-54 216 0 5.582e-06 400 end
fe-56 216 0 8.7625e-05 400 end
fe-57 216 0 2.0236e-06 400 end
fe-58 216 0 2.6931e-07 400 end
cr-50 216 0 3.3012e-06 400 end
cr-52 216 0 6.3661e-05 400 end
cr-53 216 0 7.2186e-06 400 end
cr-54 216 0 1.7969e-06 400 end
ni-58 216 0 2.5202e-05 400 end
ni-60 216 0 9.7076e-06 400 end
ni-61 216 0 4.2198e-07 400 end
ni-62 216 0 1.3455e-06 400 end
ni-64 216 0 3.4265e-07 400 end
hf-174 216 0 3.5414e-09 400 end
hf-176 216 0 1.1642e-07 400 end
hf-177 216 0 4.1169e-07 400 end
hf-178 216 0 6.0381e-07 400 end
hf-179 216 0 3.0146e-07 400 end
hf-180 216 0 7.7645e-07 400 end
zr-90 217 0 0.021891 400 end
zr-91 217 0 0.0047739 400 end
zr-92 217 0 0.007297 400 end
zr-94 217 0 0.0073949 400 end
zr-96 217 0 0.0011913 400 end
sn-112 217 0 4.6807e-06 400 end
sn-114 217 0 3.1848e-06 400 end
sn-115 217 0 1.6406e-06 400 end
sn-116 217 0 7.0162e-05 400 end
sn-117 217 0 3.7059e-05 400 end
sn-118 217 0 0.00011687 400 end
sn-119 217 0 4.145e-05 400 end
sn-120 217 0 0.00015721 400 end

sn-122 217 0 2.2342e-05 400 end
sn-124 217 0 2.7939e-05 400 end
fe-54 217 0 5.582e-06 400 end
fe-56 217 0 8.7625e-05 400 end
fe-57 217 0 2.0236e-06 400 end
fe-58 217 0 2.6931e-07 400 end
cr-50 217 0 3.3012e-06 400 end
cr-52 217 0 6.3661e-05 400 end
cr-53 217 0 7.2186e-06 400 end
cr-54 217 0 1.7969e-06 400 end
ni-58 217 0 2.5202e-05 400 end
ni-60 217 0 9.7076e-06 400 end
ni-61 217 0 4.2198e-07 400 end
ni-62 217 0 1.3455e-06 400 end
ni-64 217 0 3.4265e-07 400 end
hf-174 217 0 3.5414e-09 400 end
hf-176 217 0 1.1642e-07 400 end
hf-177 217 0 4.1169e-07 400 end
hf-178 217 0 6.0381e-07 400 end
hf-179 217 0 3.0146e-07 400 end
hf-180 217 0 7.7645e-07 400 end
zr-90 218 0 0.021891 400 end
zr-91 218 0 0.0047739 400 end
zr-92 218 0 0.007297 400 end
zr-94 218 0 0.0073949 400 end
zr-96 218 0 0.0011913 400 end
sn-112 218 0 4.6807e-06 400 end
sn-114 218 0 3.1848e-06 400 end
sn-115 218 0 1.6406e-06 400 end
sn-116 218 0 7.0162e-05 400 end
sn-117 218 0 3.7059e-05 400 end
sn-118 218 0 0.00011687 400 end
sn-119 218 0 4.145e-05 400 end
sn-120 218 0 0.00015721 400 end
sn-122 218 0 2.2342e-05 400 end
sn-124 218 0 2.7939e-05 400 end
fe-54 218 0 5.582e-06 400 end
fe-56 218 0 8.7625e-05 400 end
fe-57 218 0 2.0236e-06 400 end
fe-58 218 0 2.6931e-07 400 end
cr-50 218 0 3.3012e-06 400 end
cr-52 218 0 6.3661e-05 400 end
cr-53 218 0 7.2186e-06 400 end
cr-54 218 0 1.7969e-06 400 end
ni-58 218 0 2.5202e-05 400 end
ni-60 218 0 9.7076e-06 400 end
ni-61 218 0 4.2198e-07 400 end
ni-62 218 0 1.3455e-06 400 end
ni-64 218 0 3.4265e-07 400 end
hf-174 218 0 3.5414e-09 400 end

```
hf-176     218 0 1.1642e-07 400   end
hf-177     218 0 4.1169e-07 400   end
hf-178     218 0 6.0381e-07 400   end
hf-179     218 0 3.0146e-07 400   end
hf-180     218 0 7.7645e-07 400   end
o-16      302 0 0.033377 400   end
h-1       302 0 0.066753 400   end
co-59      302 0 1e-20 400   end
o-16      303 0 0.033377 400   end
h-1       303 0 0.066753 400   end
co-59      303 0 1e-20 400   end
o-16      304 0 0.033377 400   end
h-1       304 0 0.066753 400   end
co-59      304 0 1e-20 400   end
o-16      305 0 0.033377 400   end
h-1       305 0 0.066753 400   end
co-59      305 0 1e-20 400   end
o-16      306 0 0.033377 400   end
h-1       306 0 0.066753 400   end
co-59      306 0 1e-20 400   end
o-16      307 0 0.033377 400   end
h-1       307 0 0.066753 400   end
co-59      307 0 1e-20 400   end
o-16      308 0 0.033377 400   end
h-1       308 0 0.066753 400   end
co-59      308 0 1e-20 400   end
o-16      309 0 0.033377 400   end
h-1       309 0 0.066753 400   end
co-59      309 0 1e-20 400   end
o-16      310 0 0.033377 400   end
h-1       310 0 0.066753 400   end
co-59      310 0 1e-20 400   end
o-16      311 0 0.033377 400   end
h-1       311 0 0.066753 400   end
co-59      311 0 1e-20 400   end
o-16      312 0 0.033377 400   end
h-1       312 0 0.066753 400   end
co-59      312 0 1e-20 400   end
o-16      313 0 0.033377 400   end
h-1       313 0 0.066753 400   end
co-59      313 0 1e-20 400   end
o-16      314 0 0.033377 400   end
h-1       314 0 0.066753 400   end
co-59      314 0 1e-20 400   end
o-16      315 0 0.033377 400   end
h-1       315 0 0.066753 400   end
co-59      315 0 1e-20 400   end
o-16      316 0 0.033377 400   end
h-1       316 0 0.066753 400   end
co-59      316 0 1e-20 400   end
```

```
 o-16       317 0 0.033377  400   end
 h-1        317  0 0.066753  400   end
 co-59       317 0 1e-20 400   end
 o-16       318 0 0.033377  400   end
 h-1        318  0 0.066753  400   end
 co-59       318 0 1e-20 400   end
end composition
read celldata
  latticecell squarepitch fuelr=0.4096  21 gapr=0.418  0 cladr=0.475  22 hpitch=0.63  23 end
  latticecell squarepitch fuelr=0.4096  101 gapr=0.418  0 cladr=0.475  2 hpitch=0.63  3 end
  latticecell squarepitch fuelr=0.4096  102 gapr=0.418  0 cladr=0.475  202 hpitch=0.63  302 end
  latticecell squarepitch fuelr=0.4096  103 gapr=0.418  0 cladr=0.475  203 hpitch=0.63  303 end
  latticecell squarepitch fuelr=0.4096  104 gapr=0.418  0 cladr=0.475  204 hpitch=0.63  304 end
  latticecell squarepitch fuelr=0.4096  105 gapr=0.418  0 cladr=0.475  205 hpitch=0.63  305 end
  latticecell squarepitch fuelr=0.4096  106 gapr=0.418  0 cladr=0.475  206 hpitch=0.63  306 end
  latticecell squarepitch fuelr=0.4096  107 gapr=0.418  0 cladr=0.475  207 hpitch=0.63  307 end
  latticecell squarepitch fuelr=0.4096  108 gapr=0.418  0 cladr=0.475  208 hpitch=0.63  308 end
  latticecell squarepitch fuelr=0.4096  109 gapr=0.418  0 cladr=0.475  209 hpitch=0.63  309 end
  latticecell squarepitch fuelr=0.4096  110 gapr=0.418  0 cladr=0.475  210 hpitch=0.63  310 end
  latticecell squarepitch fuelr=0.4096  111 gapr=0.418  0 cladr=0.475  211 hpitch=0.63  311 end
  latticecell squarepitch fuelr=0.4096  112 gapr=0.418  0 cladr=0.475  212 hpitch=0.63  312 end
  latticecell squarepitch fuelr=0.4096  113 gapr=0.418  0 cladr=0.475  213 hpitch=0.63  313 end
  latticecell squarepitch fuelr=0.4096  114 gapr=0.418  0 cladr=0.475  214 hpitch=0.63  314 end
  latticecell squarepitch fuelr=0.4096  115 gapr=0.418  0 cladr=0.475  215 hpitch=0.63  315 end
  latticecell squarepitch fuelr=0.4096  116 gapr=0.418  0 cladr=0.475  216 hpitch=0.63  316 end
  latticecell squarepitch fuelr=0.4096  117 gapr=0.418  0 cladr=0.475  217 hpitch=0.63  317 end
  latticecell squarepitch fuelr=0.4096  118 gapr=0.418  0 cladr=0.475  218 hpitch=0.63  318 end
end celldata
read parameter
 gen=10000
 nsk=1000
 flx=yes
 htm=yes
 far=yes
 gas=yes
 mfp=yes
 cfx=yes
end parameter
read geometry
unit 21
com="fresh fuel rod cell"
 cylinder 1   0.4095    182.88   -182.88
 cylinder 2    0.418    200.97   -185.68
 cylinder 3    0.475    200.97   -185.68
 cylinder 4    0.475    200.97   -185.71
 cuboid 5     0.63    -0.63     0.63    -0.63    201.1   -185.81
 media 21 1 1
 media 0 1 2 -1
 media 22 1 3 -2
 media 11 1 4 -3
```

```
 media 23 1 5 -4
 boundary 5
unit 1
com="fuel rod cell"
 cylinder 2    0.418   200.97  -185.68
 cylinder 3    0.475   200.97  -185.68
 cylinder 4    0.475   200.97  -185.71
 cuboid 5     0.63    -0.63     0.63    -0.63    201.1  -185.81
 cylinder 101   0.4095  -162.53  -182.88
 cylinder 102   0.4095  -142.22  -182.88
 cylinder 103   0.4095   -121.9  -182.88
 cylinder 104   0.4095  -101.58  -182.88
 cylinder 105   0.4095   -81.27  -182.88
 cylinder 106   0.4095   -60.95  -182.88
 cylinder 107   0.4095   -40.63  -182.88
 cylinder 108   0.4095   -20.32  -182.88
 cylinder 109   0.4095        0  -182.88
 cylinder 110   0.4095    20.32  -182.88
 cylinder 111   0.4095    40.63  -182.88
 cylinder 112   0.4095    60.95  -182.88
 cylinder 113   0.4095    81.27  -182.88
 cylinder 114   0.4095   101.58  -182.88
 cylinder 115   0.4095    121.9  -182.88
 cylinder 116   0.4095   142.22  -182.88
 cylinder 117   0.4095   162.53  -182.88
 cylinder 118   0.4095   182.88  -182.88
 media 101 1 101 vol=77342.68
 media 102 1 102 -101 vol=77342.68
 media 103 1 103 -102 vol=77342.68
 media 104 1 104 -103 vol=77342.68
 media 105 1 105 -104 vol=77342.68
 media 106 1 106 -105 vol=77342.68
 media 107 1 107 -106 vol=77342.68
 media 108 1 108 -107 vol=77342.68
 media 109 1 109 -108 vol=77342.68
 media 110 1 110 -109 vol=77342.68
 media 111 1 111 -110 vol=77342.68
 media 112 1 112 -111 vol=77342.68
 media 113 1 113 -112 vol=77342.68
 media 114 1 114 -113 vol=77342.68
 media 115 1 115 -114 vol=77342.68
 media 116 1 116 -115 vol=77342.68
 media 117 1 117 -116 vol=77342.68
 media 118 1 118 -117 vol=77342.68
 media 8 1 2 -118 vol=81085.74
 media 2 1 3 -2 vol=418253.7
 media 11 1 4 -3 vol=152.7673
 media 8 1 5 -4 vol=2195419
 boundary 5
unit 2
```

```
com="burnable  poison rod"
 cylinder 1   0.4095    147.08   -147.08
 cylinder 2   0.4095    200.97   -184.38
 cylinder 3    0.418    200.97   -184.41
 cuboid 4     0.63    -0.63     0.63    -0.63    201.1   -185.81
 media 4 1 1 vol=104138.3
 media 8 1 2 -1 vol=27411.72
 media 2 1 3 -2 vol=5528.919
 media 8 1 4 -3 vol=259390.2
 boundary 4
unit 3
com="instrumentation  tube"
 cylinder 1   0.4095    182.88   -182.88
 cylinder 2    0.418    185.68   -185.68
 cuboid 3     0.63    -0.63     0.63    -0.63    201.1   -185.81
 media 8 1 1 vol=5395.254
 media 2 1 2 -1 vol=312.3727
 media 8 1 3 -2 vol=10811.92
 boundary 3
unit 24
com="complete  fresh fuel assembly"
 cuboid 1    10.55   -10.55    10.55   -10.55   185.81  -185.81
 cuboid 2    10.66   -10.66    10.66   -10.66   185.81  -185.81
 cuboid 3    11.66   -11.66    11.66   -11.66   185.81  -185.81
 array 2 1  place 9 9 1 0 0 0
 cuboid 4     14.5    -14.5     14.5    -14.5    201.1   -185.81
 media 11 1 2 -1 vol=126717.8
 media 8 1 3 -2 vol=783422.8
 media 6 1 4 -3 vol=2522055
 boundary 4
unit 4
com="complete  fuel assembly"
 cuboid 1    10.55   -10.55    10.55   -10.55   185.81  -185.81
 cuboid 2    10.66   -10.66    10.66   -10.66   185.81  -185.81
 cuboid 3    11.66   -11.66    11.66   -11.66   185.81  -185.81
 array 1 1  place 9 9 1 0 0 0
 cuboid 4     14.5    -14.5     14.5    -14.5    201.1   -185.81
 media 11 1 2 -1 vol=126717.8
 media 8 1 3 -2 vol=783422.8
 media 6 1 4 -3 vol=2522055
 boundary 4
unit 5
com="section  1: inner cylinder  enclosing  the first 12 fuel assemblies"
 cuboid 1    62.25   -62.25     0.75    -0.75    201.1  -185.81
 hole 6
 hole 7
 cylinder 2     72.5    211.8   -211.8
 hole 24   origin   x=16.25 y=16.25 z=0
 hole 4   origin   x=46.95 y=16.25 z=0
 hole 4   origin   x=16.25 y=46.95 z=0
```

```
 hole 4   origin   x=-16.25  y=-16.25  z=0
 hole 4   origin   x=-16.25  y=-46.95  z=0
 hole 4   origin   x=-46.95  y=-16.25  z=0
 hole 4   origin   x=16.25  y=-16.25  z=0
 hole 4   origin   x=46.95  y=-16.25  z=0
 hole 4   origin   x=16.25  y=-46.95  z=0
 hole 4   origin   x=-16.25  y=16.25  z=0
 hole 4   origin   x=-16.25  y=46.95  z=0
 hole 4   origin   x=-46.95  y=16.25  z=0
 media 6 1 1 vol=69400.04
 media 11 1 2 -1 vol=2496562
 boundary 2
unit 6
com="vertical  top part of boral panel"
 cuboid 1     0.75    -0.75    62.25     0.75    185.81   -185.81
 media 6 1 1 vol=34281.95
 boundary 1
unit 7
com="vertical  bottom part of boral panel"
 cuboid 1     0.75    -0.75    -0.75   -62.25    185.81   -185.81
 media 6 1 1 vol=34281.95
 boundary 1
unit 8
com="section  2: steel basket"
 cylinder 1     76.1    211.8   -211.8
 hole 5
 media 11 1 1 vol=177350.3
 boundary 1
unit 9
com="section  3: air"
 cylinder 1     78.1    211.8   -211.8
 hole 8
 media 8 1 1 vol=2277099
 boundary 1
unit 10
com="section  4: steel basket"
 cylinder 1     80.1    211.8   -211.8
 hole 9
 media 11 1 1 vol=439157
 boundary 1
unit 11
com="section  5:outer source circle"
 cylinder 1    112.3    211.8   -211.8
 hole 10
 hole 4   origin   x=94.9 y=0 z=0
 hole 4   origin   x=0 y=94.9 z=0
 hole 4   origin   x=87.676  y=36.316  z=0   rotate  a1=20 a2=0 a3=0
 hole 4   origin   x=36.316  y=87.676  z=0   rotate  a1=-20 a2=0 a3=0
 hole 4   origin   x=67.105  y=67.105  z=0   rotate  a1=-45 a2=0 a3=0
 hole 4   origin   x=-94.9 y=0 z=0
```

```
 hole 4   origin   x=-87.676  y=36.316  z=0    rotate  a1=-20 a2=0 a3=0
 hole 4   origin   x=-67.105  y=67.105  z=0    rotate  a1=45 a2=0 a3=0
 hole 4   origin   x=-36.316  y=87.676  z=0    rotate  a1=20 a2=0 a3=0
 hole 4   origin   x=-87.676  y=-36.316  z=0    rotate  a1=20 a2=0 a3=0
 hole 4   origin   x=-67.105  y=-67.105  z=0    rotate  a1=45 a2=0 a3=0
 hole 4   origin   x=-36.316  y=-87.676  z=0    rotate  a1=-20 a2=0 a3=0
 hole 4   origin   x=88.6 y=-36.699  z=0    rotate  a1=-20 a2=0 a3=0
 hole 4   origin   x=67.105  y=-67.105  z=0    rotate  a1=45 a2=0 a3=0
 hole 4   origin   x=36.316  y=-87.676  z=0    rotate  a1=20 a2=0 a3=0
 hole 4   origin   x=0  y=-94.9  z=0
 media 11 1 1
 boundary 1
unit 12
com="section  6: steel basket"
 cylinder 1    120.4    211.8    -211.8
 hole 11
 media 11 1 1 vol=2431279
 boundary 1
global unit 13
com="section  7:cast iron"
 cylinder 1    144.3    211.8    -211.8
 hole 12
 hole 14   origin   x=132  y=0 z=0
 hole 14   origin   x=132.0662  y=11.8863  z=0
 hole 14   origin   x=130.469  y=23.6768  z=0
 hole 14   origin   x=127.8214  y=35.2768  z=0
 hole 14   origin   x=124.1446  y=46.5927  z=0
 hole 14   origin   x=119.4683  y=57.5334  z=0
 hole 14   origin   x=113.83  y=68.011  z=0
 hole 14   origin   x=107.2752  y=77.9409  z=0
 hole 14   origin   x=99.8568  y=87.2433  z=0
 hole 14   origin   x=91.6343  y=95.8432  z=0
 hole 14   origin   x=82.674  y=103.6715  z=0
 hole 14   origin   x=73.048  y=110.665  z=0
 hole 14   origin   x=62.8339  y=116.7675  z=0
 hole 14   origin   x=52.1139  y=121.9299  z=0
 hole 14   origin   x=40.9743  y=126.1105  z=0
 hole 14   origin   x=29.5048  y=129.2758  z=0
 hole 14   origin   x=17.7978  y=131.4002  z=0
 hole 14   origin   x=5.9474  y=132.4666  z=0
 hole 14   origin   x=-5.9509  y=132.4664  z=0
 hole 14   origin   x=-17.8012  y=131.3997  z=0
 hole 14   origin   x=-29.5082  y=129.275  z=0
 hole 14   origin   x=-40.9776  y=126.1095  z=0
 hole 14   origin   x=-52.1171  y=121.9285  z=0
 hole 14   origin   x=-62.837  y=116.7659  z=0
 hole 14   origin   x=-73.0509  y=110.6631  z=0
 hole 14   origin   x=-82.6767  y=103.6693  z=0
 hole 14   origin   x=-91.6368  y=95.8408  z=0
 hole 14   origin   x=-99.859  y=87.2407  z=0
```

```
 hole 14   origin  x=-107.2773  y=77.9381  z=0
 hole 14   origin  x=-113.8318  y=68.008  z=0
 hole 14   origin  x=-119.4698  y=57.5303  z=0
 hole 14   origin  x=-124.1458  y=46.5894  z=0
 hole 14   origin  x=-127.8223  y=35.2734  z=0
 hole 14   origin  x=-130.4696  y=23.6734  z=0
 hole 14   origin  x=-132.0665  y=11.8828  z=0
 hole 14   origin  x=-132.6 y=-0.0035  z=0
 hole 14   origin  x=-132.0659  y=-11.8897  z=0
 hole 14   origin  x=-130.4684  y=-23.6803  z=0
 hole 14   origin  x=-127.8205  y=-35.2801  z=0
 hole 14   origin  x=-124.1434  y=-46.5959  z=0
 hole 14   origin  x=-119.4668  y=-57.5366  z=0
 hole 14   origin  x=-113.8282  y=-68.0139  z=0
 hole 14   origin  x=-107.2732  y=-77.9437  z=0
 hole 14   origin  x=-99.8545  y=-87.2459  z=0
 hole 14   origin  x=-91.6318  y=-95.8456  z=0
 hole 14   origin  x=-82.6713  y=-103.6736  z=0
 hole 14   origin  x=-73.0451  y=-110.6669  z=0
 hole 14   origin  x=-62.8309  y=-116.7692  z=0
 hole 14   origin  x=-52.1107  y=-121.9313  z=0
 hole 14   origin  x=-40.971  y=-126.1116  z=0
 hole 14   origin  x=-29.5014  y=-129.2765  z=0
 hole 14   origin  x=-17.7943  y=-131.4006  z=0
 hole 14   origin  x=-5.9439  y=-132.4667  z=0
 hole 14   origin  x=5.9543  y=-132.4662  z=0
 hole 14   origin  x=17.8046  y=-131.3992  z=0
 hole 14   origin  x=29.5116  y=-129.2742  z=0
 hole 14   origin  x=40.9809  y=-126.1084  z=0
 hole 14   origin  x=52.1203  y=-121.9272  z=0
 hole 14   origin  x=62.8401  y=-116.7642  z=0
 hole 14   origin  x=73.0538  y=-110.6612  z=0
 hole 14   origin  x=82.6794  y=-103.6671  z=0
 hole 14   origin  x=91.6393  y=-95.8384  z=0
 hole 14   origin  x=99.8613  y=-87.238  z=0
 hole 14   origin  x=107.2793  y=-77.9353  z=0
 hole 14   origin  x=113.8336  y=-68.005  z=0
 hole 14   origin  x=119.4713  y=-57.5272  z=0
 hole 14   origin  x=124.147  y=-46.5862  z=0
 hole 14   origin  x=127.8232  y=-35.2701  z=0
 hole 14   origin  x=130.4703  y=-23.67 z=0
 hole 14   origin  x=132.0668  y=-11.8794  z=0
 media 10 1 1 vol=1924719
 boundary 1
unit 14
com="polyethylene  rods"
 cylinder 1     3.5    201.1    -168.9
 media 9 1 1
 boundary 1
end geometry
```

```
read array
ara=1 nux=17  nuy=17 nuz=1  typ=square
 com='fuel assembly matrix'
 fill
   1   1   1   1   1   1   1   1   1   1   1   1   1   1   1   1   1
   1   1   1   1   1   1   1   1   1   1   1   1   1   1   1   1   1
   1   1   1   1   1   2   1   1   2   1   1   2   1   1   1   1   1
   1   1   1   2   1   1   1   1   1   1   1   1   1   2   1   1   1
   1   1   1   1   1   1   1   1   1   1   1   1   1   1   1   1   1
   1   1   2   1   1   2   1   1   2   1   1   2   1   1   2   1   1
   1   1   1   1   1   1   1   1   1   1   1   1   1   1   1   1   1
   1   1   1   1   1   1   1   1   1   1   1   1   1   1   1   1   1
   1   1   2   1   1   2   1   1   3   1   1   2   1   1   2   1   1
   1   1   1   1   1   1   1   1   1   1   1   1   1   1   1   1   1
   1   1   1   1   1   1   1   1   1   1   1   1   1   1   1   1   1
   1   1   2   1   1   2   1   1   2   1   1   2   1   1   2   1   1
   1   1   1   1   1   1   1   1   1   1   1   1   1   1   1   1   1
   1   1   1   2   1   1   1   1   1   1   1   1   1   2   1   1   1
   1   1   1   1   1   2   1   1   2   1   1   2   1   1   1   1   1
   1   1   1   1   1   1   1   1   1   1   1   1   1   1   1   1   1
   1   1   1   1   1   1   1   1   1   1   1   1   1   1   1   1   1  end fill
ara=2 nux=17  nuy=17 nuz=1  typ=square
 com='fuel assembly matrix'
 fill
  21  21  21  21  21  21  21  21  21  21  21  21  21  21  21  21  21  21
  21  21  21  21  21  21  21  21  21  21  21  21  21  21  21  21  21  21
  21  21  21  21  21   2  21  21   2  21  21   2  21  21  21  21  21
  21  21  21   2  21  21  21  21  21  21  21  21  21  21   2  21  21  21
  21  21  21  21  21  21  21  21  21  21  21  21  21  21  21  21  21  21
  21  21   2  21  21   2  21  21   2  21  21   2  21  21   2  21  21
  21  21  21  21  21  21  21  21  21  21  21  21  21  21  21  21  21  21
  21  21  21  21  21  21  21  21  21  21  21  21  21  21  21  21  21  21
  21  21   2  21  21   2  21  21   3  21  21   2  21  21   2  21  21
  21  21  21  21  21  21  21  21  21  21  21  21  21  21  21  21  21  21
  21  21  21  21  21  21  21  21  21  21  21  21  21  21  21  21  21  21
  21  21   2  21  21   2  21  21   2  21  21   2  21  21   2  21  21
  21  21  21  21  21  21  21  21  21  21  21  21  21  21  21  21  21  21
  21  21  21   2  21  21  21  21  21  21  21  21  21   2  21  21  21
  21  21  21  21  21   2  21  21   2  21  21   2  21  21  21  21  21
  21  21  21  21  21  21  21  21  21  21  21  21  21  21  21  21  21  21
  21  21  21  21  21  21  21  21  21  21  21  21  21  21  21  21  21  21  end fill
end array
end data
end
```

APPENDIX 8: k_{eff} of various neutron absorber insets

	BASKET									END-EFFECT						CENTRAL INSTRUMENTATION TUBE					
	BASKET COMPOSITION CHANGED			INSIDE THE BASKET			OUTSIDE THE BASKET			Region4:H_2O			Region4:Borated Steel			SANDWICH			PIN/CORD DESIGN		
	k_{eff}	σ	$(\Delta k/k_{ref})$ %	k_{eff}	σ	$(\Delta k/k_{ref})$ %	k_{eff}	σ	$(\Delta k/k_{ref})$ %	k_{eff}	σ	$(\Delta k/k_{ref})$ %	k_{eff}	σ	$(\Delta k/k_{ref})$ %	k_{eff}	σ	$(\Delta k/k_{ref})$ %	k_{eff}	σ	$(\Delta k/k_{ref})$ %
BORAFLEX_fe	0.599	0.001	16.691	0.663	0.001	7.710	0.635	0.001	11.591	0.725	0.001	-0.842	0.675	0.001	6.062	0.717	0.001	0.241	0.715	0.001	0.482
BORAFLEX_Si	0.599	0.001	16.635	0.667	0.001	7.157	0.637	0.001	11.362	0.726	0.001	-0.967	0.677	0.001	5.755	0.717	0.001	0.149	0.716	0.001	0.399
AA1100_fe	0.643	0.001	10.491	0.664	0.001	7.544	0.646	0.001	10.081	0.725	0.001	-0.912	0.676	0.001	5.984	0.714	0.001	0.572	0.715	0.001	0.505
AA1100_Si	0.616	0.001	14.319	0.666	0.001	7.331	0.646	0.001	10.165	0.724	0.001	-0.814	0.676	0.001	5.927	0.716	0.001	0.306	0.715	0.001	0.504
ALCAN_Fe	0.616	0.001	14.272	0.666	0.0	7.35	0.648	0.001	9.756	0.7	0.0	-1.02	0.6	0.0	6.26	0.7	0.0	0.43	0.7	0.0	0.42

					01	0				26	01	3	74	01	5	15	01	7	15	01	7
ALCANfeB4C14	0.619	0.001	13.853	0.659	0.001	8.268	0.651	0.001	9.335	0.726	0.001	-1.001	0.678	0.001	5.702	0.715	0.001	0.561	0.701	0.001	2.409
ALCANfeB4C15	0.620	0.001	13.742	0.658	0.001	8.443	0.649	0.001	9.697	0.726	0.001	-1.027	0.677	0.001	5.734	0.716	0.001	0.292	0.701	0.001	2.451
ALCAN_Si	0.616	0.001	14.294	0.666	0.001	7.323	0.646	0.001	10.035	0.725	0.001	-0.870	0.676	0.001	5.912	0.716	0.001	0.344	0.715	0.001	0.447
ALCAN_SiB4C14	0.621	0.001	13.568	0.658	0.001	8.389	0.650	0.001	9.516	0.726	0.001	-0.985	0.679	0.001	5.535	0.716	0.001	0.316	0.702	0.001	2.367
ALCAN_SiB4C15	0.618	0.001	13.970	0.660	0.001	8.161	0.650	0.001	9.532	0.727	0.001	-1.130	0.680	0.001	5.410	0.714	0.001	0.636	0.702	0.001	2.246
Bounding (H_2O) Ref std	0.719	0.001																			

APPENDIX 9: INPUTFILE OF KENOVI FOR 4 VERTICAL CASKS IN A SQUARE MATRIX

```
'Input generated by GeeWiz SCALE 6.0.2 Compiled on January 30, 2009

=csas6

Cask Storage

v7-238

read composition

 uo2         1 1 296
                          92234 0.04
                          92235 3.9
                          92236 0.02
                          92238 96.04    end
 zirc2       2 1 296    end
 h2o         3 1 296    end
 co-59        3 0 1e-20 296    end
 b4c         4 0.0126 296    end
 atomal2o3        4 3.7 2
                          13027 2
                          8016 3
```

0.9874 296 end

ss304 5 1 296 end

wtptboratedsteel 6 7.8 6

5000 0.9

14000 1

25055 2

24050 19

26000 67.1

28000 10

1 296 end

al 7 0 0.0602 296 end

h2o 8 1 296 end

polyethylene 9 1 296 end

wtptcast-iron 10 7.06 5

25055 0.6

14000 1.96

26000 92.63

```
                    6312  3.5
                    28000  1.31
                1 296   end
 wtptgnbsteel    11   7.8  4
                    25055  2
                    26000  69.5
                    28000  10.5
                    24000  18
                1 296   end
end composition
read parameter
 gen=1010
 nsk=10
 flx=yes
 htm=yes
 fdn=yes
 far=yes
```

```
 gas=yes
end parameter
read geometry
unit 1
com='fuel rod cell'
 cylinder 1   0.4095    182.88   -182.88
 cylinder 2    0.418    200.97   -185.68
 cylinder 3    0.475    200.97   -185.68
 cylinder 4    0.475    200.97   -185.71
 cuboid 5     0.63    -0.63     0.63    -0.63    201.1   -185.81
 media 1 1 1 vol=1392378
 media 0 1 2 -1 vol=81085.74
 media 2 1 3 -2 vol=418253.7
 media 5 1 4 -3 vol=152.7673
 media 8 1 5 -4 vol=2195419
 boundary 5
unit 2
```

```
com='burnable  poison  rod'
 cylinder  1   0.4095    147.08   -147.08
 cylinder  2   0.4095    200.97   -184.38
 cylinder  3    0.418    200.97   -184.41
 cuboid  4     0.63    -0.63     0.63    -0.63    201.1   -185.81
 media  4 1  1 vol=104138.3
 media  0 1  2 -1 vol=27411.72
 media  2 1  3 -2 vol=5528.919
 media  8 1  4 -3 vol=259390.2
 boundary  4
unit  3
com='instrumentation   tube'
 cylinder  1   0.4095    182.88   -182.88
 cylinder  2    0.418    185.68   -185.68
 cuboid  3     0.63    -0.63     0.63    -0.63    201.1   -185.81
 media  8 1  1 vol=5395.254
 media  2 1  2 -1 vol=312.3727
```

```
 media 8 1 3 -2 vol=10811.92
 boundary 3
unit 4
com='complete fuel assembly'
 cuboid 1    10.55   -10.55    10.55   -10.55   185.81  -185.81
 cuboid 2    10.66   -10.66    10.66   -10.66   185.81  -185.81
 cuboid 3    11.66   -11.66    11.66   -11.66   185.81  -185.81
 array 1 1  place 9 9 1 0 0 0
 cuboid 4     14.5    -14.5     14.5    -14.5    201.1  -185.81
 media 5 1 2 -1 vol=126717.8
 media 0 1 3 -2 vol=783422.8
 media 6 1 4 -3 vol=2522055
 boundary 4
unit 5
com='section 1: inner cylinder enclosing the first 12 fuel assemblies'
 cuboid 1    62.25   -62.25     0.75    -0.75    201.1  -185.81
 hole 6
```

```
hole 7
cylinder 2    72.5    211.8   -211.8
hole 4   origin   x=16.25  y=16.25 z=0
hole 4   origin   x=46.95  y=16.25 z=0
hole 4   origin   x=16.25  y=46.95 z=0
hole 4   origin   x=-16.25  y=-16.25 z=0
hole 4   origin   x=-16.25  y=-46.95 z=0
hole 4   origin   x=-46.95  y=-16.25 z=0
hole 4   origin   x=16.25  y=-16.25 z=0
hole 4   origin   x=46.95  y=-16.25 z=0
hole 4   origin   x=16.25  y=-46.95 z=0
hole 4   origin   x=-16.25  y=16.25 z=0
hole 4   origin   x=-16.25  y=46.95 z=0
hole 4   origin   x=-46.95  y=16.25 z=0
media 6 1 1 vol=69400.04
media 5 1 2 -1 vol=2496562
boundary 2
```

```
unit 6
com='vertical top part of boral panel'
 cuboid 1     0.75    -0.75    62.25     0.75   185.81   -185.81
 media 6 1 1 vol=34281.95
 boundary 1
unit 7
com='vertical bottom part of boral panel'
 cuboid 1     0.75    -0.75    -0.75   -62.25   185.81   -185.81
 media 6 1 1 vol=34281.95
 boundary 1
unit 8
com='section 2: steel basket'
 cylinder 1     76.1    211.8   -211.8
 hole 5
 media 5 1 1 vol=177350.3
 boundary 1
unit 9
```

```
com='section 3: air'
 cylinder 1     78.1    211.8   -211.8
 hole 8
 media 0 1 1 vol=2277099
 boundary 1
unit 10
com='section 4: steel basket'
 cylinder 1     80.1    211.8   -211.8
 hole 9
 media 5 1 1 vol=439157
 boundary 1
unit 11
com='section 5:outer source circle'
 cylinder 1    112.3    211.8   -211.8
 hole 10
 hole 4   origin   x=94.9 y=0 z=0
 hole 4   origin   x=0 y=94.9 z=0
```

```
hole 4  origin  x=87.676 y=36.316 z=0   rotate  a1=20 a2=0 a3=0
hole 4  origin  x=36.316 y=87.676 z=0   rotate  a1=-20 a2=0 a3=0
hole 4  origin  x=67.105 y=67.105 z=0   rotate  a1=-45 a2=0 a3=0
hole 4  origin  x=-94.9 y=0 z=0
hole 4  origin  x=-87.676 y=36.316 z=0   rotate  a1=-20 a2=0 a3=0
hole 4  origin  x=-67.105 y=67.105 z=0   rotate  a1=45 a2=0 a3=0
hole 4  origin  x=-36.316 y=87.676 z=0   rotate  a1=20 a2=0 a3=0
hole 4  origin  x=-87.676 y=-36.316 z=0   rotate  a1=20 a2=0 a3=0
hole 4  origin  x=-67.105 y=-67.105 z=0   rotate  a1=45 a2=0 a3=0
hole 4  origin  x=-36.316 y=-87.676 z=0   rotate  a1=-20 a2=0 a3=0
hole 4  origin  x=88.6 y=-36.699 z=0   rotate  a1=-20 a2=0 a3=0
hole 4  origin  x=67.105 y=-67.105 z=0   rotate  a1=45 a2=0 a3=0
hole 4  origin  x=36.316 y=-87.676 z=0   rotate  a1=20 a2=0 a3=0
hole 4  origin  x=0 y=-94.9 z=0
media 5 1 1
boundary 1
unit 12
```

```
com='section 6: steel basket'
 cylinder 1    120.4    211.8    -211.8
 hole 11
 media 5 1 1 vol=2431279
 boundary 1
unit 13
com='section 7:cast iron'
 cylinder 1    144.3    211.8    -211.8
 hole 12
 hole 14    origin   x=132 y=0 z=0
 hole 14    origin   x=132.0662 y=11.8863 z=0
 hole 14    origin   x=130.469 y=23.6768 z=0
 hole 14    origin   x=127.8214 y=35.2768 z=0
 hole 14    origin   x=124.1446 y=46.5927 z=0
 hole 14    origin   x=119.4683 y=57.5334 z=0
 hole 14    origin   x=113.83 y=68.011 z=0
 hole 14    origin   x=107.2752 y=77.9409 z=0
```

hole 14 origin x=99.8568 y=87.2433 z=0

hole 14 origin x=91.6343 y=95.8432 z=0

hole 14 origin x=82.674 y=103.6715 z=0

hole 14 origin x=73.048 y=110.665 z=0

hole 14 origin x=62.8339 y=116.7675 z=0

hole 14 origin x=52.1139 y=121.9299 z=0

hole 14 origin x=40.9743 y=126.1105 z=0

hole 14 origin x=29.5048 y=129.2758 z=0

hole 14 origin x=17.7978 y=131.4002 z=0

hole 14 origin x=5.9474 y=132.4666 z=0

hole 14 origin x=-5.9509 y=132.4664 z=0

hole 14 origin x=-17.8012 y=131.3997 z=0

hole 14 origin x=-29.5082 y=129.275 z=0

hole 14 origin x=-40.9776 y=126.1095 z=0

hole 14 origin x=-52.1171 y=121.9285 z=0

hole 14 origin x=-62.837 y=116.7659 z=0

hole 14 origin x=-73.0509 y=110.6631 z=0

hole 14 origin x=-82.6767 y=103.6693 z=0

hole 14 origin x=-91.6368 y=95.8408 z=0

hole 14 origin x=-99.859 y=87.2407 z=0

hole 14 origin x=-107.2773 y=77.9381 z=0

hole 14 origin x=-113.8318 y=68.008 z=0

hole 14 origin x=-119.4698 y=57.5303 z=0

hole 14 origin x=-124.1458 y=46.5894 z=0

hole 14 origin x=-127.8223 y=35.2734 z=0

hole 14 origin x=-130.4696 y=23.6734 z=0

hole 14 origin x=-132.0665 y=11.8828 z=0

hole 14 origin x=-132.6 y=-0.0035 z=0

hole 14 origin x=-132.0659 y=-11.8897 z=0

hole 14 origin x=-130.4684 y=-23.6803 z=0

hole 14 origin x=-127.8205 y=-35.2801 z=0

hole 14 origin x=-124.1434 y=-46.5959 z=0

hole 14 origin x=-119.4668 y=-57.5366 z=0

hole 14 origin x=-113.8282 y=-68.0139 z=0

hole 14 origin x=-107.2732 y=-77.9437 z=0

hole 14 origin x=-99.8545 y=-87.2459 z=0

hole 14 origin x=-91.6318 y=-95.8456 z=0

hole 14 origin x=-82.6713 y=-103.6736 z=0

hole 14 origin x=-73.0451 y=-110.6669 z=0

hole 14 origin x=-62.8309 y=-116.7692 z=0

hole 14 origin x=-52.1107 y=-121.9313 z=0

hole 14 origin x=-40.971 y=-126.1116 z=0

hole 14 origin x=-29.5014 y=-129.2765 z=0

hole 14 origin x=-17.7943 y=-131.4006 z=0

hole 14 origin x=-5.9439 y=-132.4667 z=0

hole 14 origin x=5.9543 y=-132.4662 z=0

hole 14 origin x=17.8046 y=-131.3992 z=0

hole 14 origin x=29.5116 y=-129.2742 z=0

hole 14 origin x=40.9809 y=-126.1084 z=0

hole 14 origin x=52.1203 y=-121.9272 z=0

hole 14 origin x=62.8401 y=-116.7642 z=0

```
 hole 14   origin   x=73.0538  y=-110.6612  z=0
 hole 14   origin   x=82.6794  y=-103.6671  z=0
 hole 14   origin   x=91.6393  y=-95.8384  z=0
 hole 14   origin   x=99.8613  y=-87.238  z=0
 hole 14   origin   x=107.2793  y=-77.9353  z=0
 hole 14   origin   x=113.8336  y=-68.005  z=0
 hole 14   origin   x=119.4713  y=-57.5272  z=0
 hole 14   origin   x=124.147  y=-46.5862  z=0
 hole 14   origin   x=127.8232  y=-35.2701  z=0
 hole 14   origin   x=130.4703  y=-23.67  z=0
 hole 14   origin   x=132.0668  y=-11.8794  z=0
 media 10 1 1 vol=1924719
 boundary 1
unit 14
com='polyethylene  rods'
 cylinder 1      3.5    201.1    -168.9
 media 9 1 1
```

```
 boundary 1
global unit 15
com='cask storage building'
 cuboid 1     3000    -3000     1175    -1175    448.5   -448.5
 hole 13
 hole 13   origin   x=325 y=0 z=0
 hole 13   origin   x=0 y=325 z=0
 hole 13   origin   x=325 y=325 z=0
 media 0 1 1
 boundary 1
end geometry
read array
ara=1 nux=17 nuy=17 nuz=1 typ=square
 com='fuel assembly matrix'
 fill
   1   1   1   1   1   1   1   1   1   1   1   1   1   1   1   1   1
   1   1   1   1   1   1   1   1   1   1   1   1   1   1   1   1   1
```

1 1 1 1 1 2 1 1 2 1 1 2 1 1 1 1 1

1 1 1 2 1 1 1 1 1 1 1 1 1 2 1 1 1

1 1 1 1 1 1 1 1 1 1 1 1 1 1 1 1 1

1 1 2 1 1 2 1 1 2 1 1 2 1 1 2 1 1

1 1 1 1 1 1 1 1 1 1 1 1 1 1 1 1 1

1 1 1 1 1 1 1 1 1 1 1 1 1 1 1 1 1

1 1 2 1 1 2 1 1 3 1 1 2 1 1 2 1 1

1 1 1 1 1 1 1 1 1 1 1 1 1 1 1 1 1

1 1 1 1 1 1 1 1 1 1 1 1 1 1 1 1 1

1 1 2 1 1 2 1 1 2 1 1 2 1 1 2 1 1

1 1 1 1 1 1 1 1 1 1 1 1 1 1 1 1 1

1 1 1 2 1 1 1 1 1 1 1 1 1 2 1 1 1

1 1 1 1 1 2 1 1 2 1 1 2 1 1 1 1 1

1 1 1 1 1 1 1 1 1 1 1 1 1 1 1 1 1

1 1 1 1 1 1 1 1 1 1 1 1 1 1 1 1 1

end fill

end array

```
end data

end
```

REFERENCES

[Online] // http://www.engineeringtoolbox.com/air-composition-d_212.html. - The Engineering toolbox. - 22 04 2012. - http://www.engineeringtoolbox.com/air-composition-d_212.html.

Abbey DC and Dowson F Citicality Of Interacting Arrays Of Fissile Material-II [Journal]. - Risely, Lancs UK : Journal of Nuclear Energy Parts A/B, Pergamon Press, 1962 йил. - II : Vol. 17 pp 7 to 13.

ANL Reactor Physics Constants [Book]. - Chicago : United States Aomic Commission, 1963. - Vol. II.

Barbaras Sean A. and Knight Travis W. Transuranic Transmutation and Criticality Calculations Sensitivity to Heterogeneous Lattice Effects [Conference] // WM2012 Conference. - Phoenix : [s.n.], 2012.

Becker B. On the influence of resonance scattering Treatment In Monte Carlo Codes On High Temperature Reactor Characteristics [Report]. - [s.l.] : Universitat Stuttgard, 2010.

Bertulani CA and Danielewicz P Introduction to nuclear reactions [Book]. - Bristol : Institute of Physics, 2004.

Blakeman E.D. [et al.] PWR Facility Modelling Using MCNP5 and the CADIS/ADVANTG Variance Reduction Methodology. [Report]. - Oak Ridge. : Oak Ridge National Laboratory, 2007.

Bledsoe J.A Favorite and K.C Eigen value sensitivity to system dimensions [Journal]. - Los Almos : Annals of nuclear energy, 2010 йил. - Vols. 37 (2010)522-528.

Borgonovi G.M. [et al.] Crystal Binding Effects on Doppler Broadening of Neutron Absorption Resonances [Journal]. - San Diego : Physical Review, 1969. - C : Vol. 1(6).

Bowman R.D and Busch S.M. KENO V.a Primer: A Primer for Criticality Calculations with SCALE/KENO V.a using GeeWiz [Report]. - Oak Ridge : Oak Ridge National Laboratory, 2005.

Bowman S.M KENO-VI Primer: A Primer for Criticality Calculations with SCALE/KENO-VI Using GeeWiz [Report]. - Oak Ridge : Oak Ridge National Laboratory, 2008. - ORNL/TM-2008/069.

Bowman S.M. Keno-vi primer: A Primer for criticality calculations with Scale/Keno-vi using Geewiz [Report]. - Oak Ridge : Oak Ridge National Laboratory, 2008.

Broadhead B.L [et al.] Investigation of Nuclide Importance to Functional Requirements Related to Transport and Long-Term Storage of LWR Spent Fuel [Report]. - Oak Ridge : Oak Ridge National Laboratory, 1995.

Broadhead B.L [et al.] Sensitivity and Uncertainty-based Criticality Safety Validation Techniques [Journal]. - Oak Ridge : Nuclear Science and Engineering, 2004. - 340-366 : Vol. 146.

Broadhead B.L and Gauld I.C Rankings of Nuclide Importance in Spent Fuel for Shielding application [Conference] // ANS2000 Radiation Protection and Shielding Division Topical Conference, Radiation Protection for our National Priorities: Medicine, the Environment and the Legacy. - Spokane, Washington : American Nuclear Society, 2000.

Broadhead B.L Verification and Validation Plan for the SCALE CODE system. [Report]. - Oak Ridge : Oak Ridge National Laboratory, 1996.

Broadhead BL [et al.] Sensitivity and Uncertainty-based Criticality Validation Techniques [Journal]. - Oak Ridge : Nuclear Science and Engineering, 2004. - Vol. 146.

Buchillier T, Aroua A and Bochud FO Neutron measurements around storage casks containing spent fuel and vitrified high-level radioactive waste at Zwilag [Journal]. - Lausanne : Oxford University Pres, 2007. - 4 : Vol. 124.

Buchillier T, Aroua A and Buchad F.O Neutron measurements around storage casks containing spent fuel and vitrified high-level radioactive waste at Zwilag [Journal]. - Lausanne : Oxford university press, 2007. - 4 : Vol. 124.

Butland A.T.D A note on crystalline binding in uranium dioxide and its effects on the Doppler broadening of uranium resonances [Journal]. - Dorset : Annals of Nuclear Sciences and Engineering, 1974. - Vol. 1.

Caruso S. [et al.] Validation of 134Cs, 137Cs and 154Eu single ratios as burnup monitors for ultra-high burnup UO2 fuel [Journal]. - Lausanne, Switzerland : Annals of Nuclear Energy 34 (2007) 28–35, 2006. - Vol. 34.

Chochran Robert G and Tsoulfanidis Nicholas The nuclea Fuel Cycle: Analysis and Management [Book]. - La Grange Park, Illinois : American Nuclear Society, 1999. - Vol. II.

Christoforou S A Zero-variance based scheme for Monte Carlo Criticality simulation [Report]. - Delft, The Netherlands : Delft University of Technology, 2010.

Cousinou P [et al.] Taking burnup credit into account in criticality studies:the situation as it is now and the prospect for future [Journal]. - Cedex, France : Journal of Nuclear Engineering and design, 2001 йил. - Vols. 208 (2001)205-214.

Cullen D.E. Program SIGMA1(version 79-1):Doppler broaden evaluated cross section in the evaluated nuclear data file/version B (ENDF/B) format [Report]. - [s.l.] : Lawrence Livermore Laboratory, 1979.

Dean VF and Blackwood LG ICSBEP Guide to the expression of uncertainty [Report]. - Idaho : Idaho National Laboratory, 2007.

DME Nuclear Energy Policy And Strategy for The Republic of South Africa [Report] / Department of Minerals and Energy. - Pretoria : Department of Minerals and Energy, 2007. - Draft for Public Comment.

DoE Integrated Resource Plan for electricity 2010-2030, revision II [Report]. - Pretoria : Department of Energy (DoE), 2011.

Down A Full Linear Theory [Report]. - 2006.

Dowson D.C Criticality Of Interacting Arrays of Fissile Material-I, General Theory [Journal]. - Risley, UK : Jounal of Nuclear Energy Parts A/B, Pergamon Press, 1962 йил. - I : Vols. 17, pp 1 to 6.

Duderstadt James J. and Hamilton Louis J Nuclear Reactor Analysis [Book]. - Ann Arbor : John Wiley & Sons, 1976. - ISBN 0-471-22363-8.

Duderstadt JJ and Hamilton LJ Nuclear Reactor Analysis [Book]. - Michigan : John Willey & Sons, 2010. - Vols. ISBN 0-471-22363-8.

Dupree SA and Fraley SK A Monte Carlo Primer: A Practical Approach to Radiation Transport [Book]. - New Mexico : Kluwer Accademic/Plenum Publishers, 2002.

EFFECTS OF THE LOCATION OF A MISLOADED FUEL ASSEMBLY ON THE NEUTRON MULTIPLICATION FACTOR OF CASTOR X/28 F SPENT FUEL CASK [Journal]. - Johnnesburg : International Nuclear Safety Journal, 2015.

EPRI An assessment of Boraflex performance in Spent Nuclear Fuel Storage Racks [Report]. - New York : Northeast Technology Corporation, 1988.

EPRI CAFTA, Software manual, EPRI, Palo Alto, CA:2007, Software Product ID#1015515 [Report]. - CA : EPRI, 2007.

EPRI Criticality Risks during transportation of spent nuclear fuel:Revision 1. [Report]. - CA : EPRI, Palo Alto CA:2002.1016635, 2008.

EPRI Dry Cask Storage Probabilistic Risk Assessment Scoping study [Report]. - CA : EPRI, Palo Alto,CA 1003011, 2002.

Finney R.L and Thomas G.B Calculus [Book]. - Massachusetts : Addison-Wesley Publishing company, 1990.

Finney Ross L. and George B Thomas Jr Calculus [Book]. - Massachusetts : Addison-Wesley, 1990. - ISBN 0-201-52579-8.

Framatome AFA 3GA 17X17 UO2 Fuel Assembly Koeberg FMS 3.9% [Report]. - Lyon : Framatome Nuclear Fuel, 2000.

Frohner FH and Larson DC Cross-section fluctuations and self-shielding effects in the unresolved resonance region [Report]. - Paris : Nuclear Energy Agency, 2000.

Gabrielli Fabrizio Models for transient analyses in advanced test reactors [Report]. - Stuttgart : Intitut fur kernenergetik und energiessysteme der universitat Stuttgart, 2011.

Gabrielli Fabrizio Models for transient analyses in advanced test reactors [Report]. - Stuttgart : Intitut fur kernenergetik und energiessysteme der universitat Stuttgart, 2011.

Garland J Core Composition Changes [Book]. - Ontario : University of McMaster, Ontario, Canada, 2005.

Garland Wm J Reactor Physics: Multigroup Diffusion [Book]. - Hamilton, Ontarion : University of McMasterm Hamilton, Ontarion, Canada, 2005.

Garrick B.J. Lessons learned from 21 nuclear plant probabilistic Risk Assessment [Journal]. - Newport Port Beach : Nuclear Safety, 1988.

Gauld I.C. and Mueller D.E Evaluation of cross-section sensitivities in computing burnup credit fission product concentration [Report]. - Oak Ridge : Oak Ridge National Laboratory, 2005.

Gauld I.C. Strategies for application of Isotopic Uncertainties in Burnup Credit [Report]. - Oak Ridge : Oak Ridge National Laboratory, 2003. - Nureg/CR-6811.

Gauld I.C. Strategies for Application of Isotopic Uncertainties in Burnup Credit [Report]. - Oak Ridge : Oak Ridge National Laboratory, 2003. - NUREG/CR-6811.

Gauld I.C., Bowman S.M. and Leal J.E. Horwedel and L.C. ORIGEN-ARP: Automated Rapid Processor For Spent Fuel Depletion, Decay, and Source-term Analysi [Report]. - Oak Ridge : US NRC, 2004.

Gauld IC and Ryman JC Nuclide Importance to Criticality Safety, Decay Heating and Source Terms Related To Transport and Interim Storage of High-Burnup LWR Fuel [Journal]. - Oak Ridge : Oak Ridge National Laboratory, 2000. - NUREG/CR-6700.

Gauld IC and Ryman JC Nuclide importance to criticality safety,Decay Heating and Source Term related to Transport and Interim Storage of Hig- Burnup LWR Fuel [Report]. - Oak Ridge : Oak Ridge National Laboratory, 2000. - Nureg/CR-6700.

Gauld IC and Sanders CE Development and applications of prototypic SCALE control module for automated burnup credits [Report]. - Oak Ridge : American nuclear society, 2001. - 35238.

Gauld IC, Bowman SM and Parks CV SCALE: A Modular System for Performing Standardized Computer Analysis for Licensing And Evaluations [Report]. - Tennessee : Radiation Safety Information Computational Centre, 2000.

Gautreau R and Savin W Theory and Problems of Modern Physics [Book]. - Schaum's Outline Series : McGraw-Hill, 1978.

Giancoli D.C Physics for Scientists and Engineers [Book]. - London : Prentice-Hall, 1988. - Vol. 2nd edition.

GM Borgonovi DH Houston, JU Koppel, EL Slaggie Crystal Binding Effects on Doppler Broadening of Neutron Absorption Resonances [Journal]. - San Diego : Physical Review, 1969. - C : Vol. 1(6).

Griesmeyer JM and Ghoniem GM The response of fission gas bubbles to the dynamic behaviour of point defects [Journal]. - Los Angeles : North-Holland, 1978. - Vols. 80(1979)88-101.

Hahn BD Essential MATLAB for Scientists and Engineers [Book]. - Cape Town : Maskew Miller, 2007. - Vol. 3rd Edition.

Hayes SL Basics of Nuclear Fuels [Report]. - Idaho : Idaho National Laboratory, 2010.

Hollenbach DF [et al.] Keno-VI: A General Quadratic Version ofthe Keno Program [Report]. - Oak Ridge : Oak Ridge National Laboratory, 2009.

Hollenbach DF and Bucholz JA Theoreriucal Background for Calculational Methods in SCALE [Report]. - Oak Ridge : ORNL, 2005.

Hollenbach DF and Petrie LM CSAS6: Control Module for Enhanced Criticality Safety Analysis with KENO-VI [Report]. - Oak Ridge : Oak Ridge National Laboratory, 2004.

http://www.nap.edu/openbook.php?record_id=11263&page=24 [Online] // Safety and Security of commercial spent nuclear fuel storage. - National Academies Press, 2006. - 16 10 2014. - http://www.nap.edu/openbook.php?record_id=11263&page=24.

IAEA Criticality Safety in the Handling of Fissile Material-SPECIFIC SAFETY GUIDE [Report]. - Vienna, Austria : International Atomic Energy Agency, 2014.

IAEA Dispersion of Radioactive Material in Air and Water And consideration of population distribution in site evaluation for nuclear power plants [Journal]. - Vienna : IAEA, 2002 йил. - Vols. IAEA Safety Guide No. NS-G-3.2.

IAEA Integrity of Reactor Pressure Vessel in Nuclear Power Plants: Assessment of Irradiation Embrittlement Effects in Reactor Pressure Vessel Steel [Report]. - Vienna : International Atomic Energy Agency, 2009.

IAEA Multipurpose container technologies for spent fuel management [Report] = IAEA-Tecdoc 1192 / Nuclear Fuel Cycle and Materials Section ; International Atomic Energy Agency. - Vienna : International Atomic Energy Agency, 2000. - ISSN 1011-4289.

IAEA Operation and Maintenance of spent fuel storage and transportation Casks/containers [Report]. - Vienna : International Atomic Energy Agency, 2007.

IAEA Optimization strategies for cask design and container loading in long term spent fuel storage [Report]. - Vienna : International Atomic Energy Agency, 2006. - IAEA-TECDOC-1523.

IAEA Optimization Strategies for Cask Design and container loading in long term spent fuel storage [Book]. - Vienna : International Atomic Energy Agency, 2006. - Vols. IAEA-TECDOC 1523. - ISBN 92-0-112706-5.

International Atomic Energy Agency Technical and Economic limits for fuel burnup extention [Report]. - San Carlos de Bariloche, Argentina : International Atomic Energy Agency, 1999. - IAEA-Tecdoc 1299.

Iqbal M, Khan J and Mirza SM Design of a modular dry storage facility for typical PWR spent fuel [Journal]. - Islamabad : Journal of nuclear energy, 2006 йил. - Vols. 48(2006)487-494.

J.C.Wagner, DeHart M.D. and Park C.V. Recommendations for adressing axial burnup in PWR burnup credit analyses [Report]. - Oak Ridge : Oak Ridge National Laboratory, 2003.

Jackson KA Kinetic Processes: Crystal growth, diffusion and phase transition in Material [Book]. - Darmstadt : Wiley, 2004.

James J Duderstad Louis J Hamilton Nuclear Reactor Analysis [Book]. - Ann Arbor, Michigan : John Wiley & Sons, 1976. - ISBN0-471-22363-8.

Japanese Atomic Energy Agency Cross section Table (26-Fe-56) [Online]. - Japanese Atomic Energy Agency. - 9 May 2012. - http://wwwndc.jaea.go.jp/cgi-bin/Tab80WWW.cgi?lib=J33&iso=Fe056.

Japanese Atomic Energy Agency Cross section Table(26-Fe-27) [Online]. - Japanese Atomic Energy Agency. - 9 May 2012. - http://wwwndc.jaea.go.jp/cgi-bin/Tab80WWW.cgi?lib=J33&iso=Fe057.

JJ Duderstadt LJ Hamilton Nuclear Reactor Analysis [Book]. - Michigan : John Wiley and Sons, 1976. - Vols. ISBN 0-471-22363-8.

Johnson R.S Singular Perturbation Theory: Mathematical and Analytical Techniques with Application to engineering [Book]. - Boston : Springer, 2005.

Kadotani Hiroyuki Crystal Binding Effects of OU2 on the Effective Resonance Intergral [Journal]. - [s.l.] : Journal of Nuclear Sciences and Technology, 1970. - Vol. 7(3).

Kawaguchi A [et al.] Irradiation-Induced Phase Transition of Paraffins [Journal]. - Kyoto : Kyoto University, 1981. - Vols. 59, No 44.

Kawaguchi A [et al.] Some aspects of the lattice Destruction of Polyethylene due to Electron Irradiation. [Journal]. - Kyoto : Kyoto University, 1982. - Vol. 60 No 1.

Kittel C Quantum Theory of Soliids [Book]. - Carlifonia : John Wiley & Sons, 1987. - Vol. 2nd.

Knief R.A Nuclear Criticality Safety-Theory and Practice [Book]. - La Grange Park, Illinois : American Nuclear Society, 2000. - Vol. VII.

Knudsen JK Commercial Spent Nuclear Fuel Waste Package Misload Analysis [Report]. - 2003.

Kononen Mattias Temperature induced stress in reactor containment building // Master of Science thesis. - Stocholm, Sweden : KTH, 2012. - A Case study of Forsmark F1.

Kralik M, Kulich V and Studeny J Neutron spectroscopy at the interim storage facility for spent nuclear fuel [Journal]. - Prague : Elsevier, 2002. - Vol. 476.

Kulikowska T Reactor lattice Transport [Report]. - Swierk, Poland : Institute of Atomic Energy, , 2000.

Labuschagne A [et al.] An introduction to numerical analysis [Book]. - Pretoria : Celtis, 2007. - Vol. 5th edition.

Lamarsh J.R. Introduction to nuclear reactor theor [Book]. - [s.l.] : Amercan Nuclear Society, 2002.

Lamarsh JR Introduction to nuclear reactor theor [Book]. - [s.l.] : Amercan Nuclear Society, 2002.

Landau DP and Binder K A Guide to Monte Carlo Simulation in Statistical Physics [Book]. - Cambridge : Cambridge University Press, 2005.

Lee SH, Ahn JG and HRHwang Conceptual Cask Design with Burnup Credit [Report]. - Daejon, Korea : Korean Power Engineering Company, 2002.

Lee SH, Ahn JG and Hwang HR Conceptual Cask Design with Burnup Credit [Report]. - Daejeon, Korea : Korea Power Engineering Company.

Leotlela M.J [et al.] The effects of storage patterns on the neutron multiplication factor of spent nuclear fuel casks [Journal]. - Johannesburg : International Nuclear Safety Journal, 2012. - 1 : Vol. 1. - ISSN 2285-8717.

Leotlela M.J and I. Malgas I. Petr Effects of the location of a misloaded fuel assembly on the neutron multpication factor of Castor X/28F spent fuel cask [Journal]. - Johannesburg : International Nuclear Safety Journal, 2015. - 1 : Vol. 4. - ISSN 2285-8717.

Leotlela M.J. [et al.] Ranking Of Aluminium Composite Materials For Use As Neutron Absorber Inserts In Spent Fuel Pools [Report]. - Johannesburg : International Nuclear Safety Journal, 2015. - pp. 24-38.

Leotlela M.J., Malgas I and Taviv E Sensitivity analysis of parameters important to nuclear criticality safety of Castor X/28F spent fuel cask [Journal] / ed. Barnby Alexa. - Munchen : Kerntechnik, 2015. - 5 : Vol. 80.

Leotlela MJ [et al.] The effects of storage patters on the neutron multiplication factor of spent nuclear fuel casks [Journal]. - Johannesburg : International Nuclear Safety Journal, 2012. - 1 : Vol. 1.

Leotlela MJ Investigation of the release of gaseous fission products from Pebbled Bed Modular Reactor's TRISO coated Fuel Particle during the HFR-K5 fuell Irradiation [Report] : A Research Report submitted to the Faculty of Science, University of the Witwatersrand, Johannesburg, in partial fulfillment of the requirements for the degree of Master of Science / School of Physics ; University of the Witwatersrand,. - Johannesburg : University of the Witwatersrand,, 2010.

Lewins J A derivative of the time-dependent adjoint equation for neutron importance in the transport,continuous slowing-down and diffusion model. [Journal]. - Osnabruck, Germany : Pergamon Press, 1960. - Vol. 13 pp 1 to 5.

Lewins J Importance: The adjoint function [Journal]. - Oxford : Pergamon Press, 1965.

Lewins JD Construction of Adjoint Equations and their Adjoint Operations-Terminology? [Journal]. - Cambridge : Pergamon Press, 1984. - Vol. 11 No 6 pp 311.

Lewins JD Importance: The adjoint function; The Physical Basis of Variational and Pertubation Theory in Transport and Diffusion Problems [Book]. - London : Pergamon Press, 1965.

Lewis E.E Fundamentals of Nuclear Reactor Physics [Book]. - London : Academic press, 2008. - ISBN: 978-0-12-370631-7.

Lewis EE Fundermentals of Nuclear Reactor Physisc [Book]. - Sandiego Califonia : Elsevier, 2008. - ISBN 978-0-12-370631-3.

Likhanskii VV and Zborovskii VG On the stability of spatial distribution of crystal structure defects in irradiated high burnup UO2 fuel [Journal]. - Moscow : Elvier, 2005. - Vol. 350.

Lindquist K. [et al.] Guideline for Boraflex Use in Spent-fuel Storage Racks [Report]. - Kingston, New York : EPRI, 1993. - TR-103300.

Matzke Hj and Spino J Formation of the rim structure in high burnup fuel. [Journal]. - Karlsruhe : Elsevier, 1997. - Vol. 248(1997).

Matzke Hj and Spino J Formation of the rim structure in high burnup fuels [Journal]. - Karlsruhe : Journal of Nuclear Materials, 1997. - Vols. 248(170-179).

Matzke Hj On the rim effect in high burnup UO2 LWR fuels [Journal]. - Karlsruhe : Journal of nuclear materials, 1992. - Vols. 189(141-148).

Matzke Hj On the rim effect in high burnup UO2 LWR fuels [Journal]. - Karlsruhe : Journal of nuclear materials, 1992.

Matzke Hj Radiation damage in nuclear fuel materials: The "rim" effect in UO2 and damages in inert matrices for transmutation of actinides [Journal]. - Karlsruhe : Elsevier, 1996. - Vol. B 116.

Matzke Hj Radiation damage in nuclear fuel materials:the "rim" effect in UO2 and damage in inert matrices for transmutation of actinides [Journal]. - Karsruhe : Journal of Nuclear Instruments and Methods in Physical Research , 1996. - Vols. B 116(121-125).

Matzke Hj Radiation Damage in nuclear materials [Journal]. - Karlsruhe : North-Holland, 1992.

Mayne A.J. Storage of fissile Material [Journal]. - Didcot : Nuclear Energy, 1955. - pp 77 to 84 : Vol. 2.

McCartin. BJ Rayleigh-Schrodinger Pertubation Theory: Pseudoinverse Formulation [Report]. - [s.l.] : Kettering University, 2009.

McConnel Paul Transportation issues And Resolutions-Compilation of Laboratory Transportation Work Package Report [Report] / US DOE. - [s.l.] : Sandia National Laboratory, 2012. - FCRD-UFD-2012-000342.

McConnell Paul Transportation Issues and Resolusion-Compilataion of Laboratory Transportation Worm Packages Report [Report]. - [s.l.] : Sandia National Laboratory, 2012.

MCNP_X5_Team MCNP-A General Monte Carlo N-Particle Transport Code, Version 5 [Report]. - [s.l.] : Los Alamos National Laboratory, 2003.

Merzbacher E Quantum Mechanics [Book]. - Denver : John Wiley & Sons,INC, 1998. - Vol. 3rd edition.

Moro J and Dopico FM First Order Eigenvalue Perturbation Theory and the newtonian Diagram [Report]. - Madrid : Universidad Carlos III de Madrid, 2000.

Mosebetsi J Leotlela Isaac Malgas, E Taviv SENSITIVITY ANALYSIS OF PARAMETERS IMPORTANT TO NUCLEAR CRITICALITY SAFETY OF CASTOR X/28F [Journal]. - [s.l.] : KERNTECHNIK, 2015. - Vol. 80.

Mueller D.E Interpretation of Sensitivity Coefficients [Report]. - [s.l.] : Personnal correspondence, 2015.

Mueller D.E personal communication. - 2015.

Mueller DE and Gauld IC Evaluation of Cross-Section Sensitivity in Computing Burnup Credit Fission Product Concentration [Report]. - Oak Ridge : Oak Ridge National Laboratory, 2005a. - ORNL/TM-2005/48.

Mueller DE and Rearden BT Sensitivity coefficient generation for a burnup credit cask model using Tsunami-3D [Journal]. - Knoxville : American Nuclear Society, 2005c.

Mueller DE and Rearden BT Sensitivity Coefficient Generation for A Burnup Credit Cask Model Using TSUNAMI-3D [Conference] // Integrating Criticality Safety into Resurgence of Nuclear Power. - Knoxville : American Nuclear Society, 2005.

Mueller DE and Waner JC Application of Sensitivity/Uncertainty Methods to the Burnup Credit Validation [Conference] // International Atomic Energy Agency Technical Committee Meeting on Advances in Applications of Burnup Credit to Enhance Spent Fuel Transportation. - London : IAEA Conference, 2006.

Mueller DE lmp error // Personal email. - January 2013d.

Mueller DE Misloading // personal correspondence (email). - Oak Ridge : [s.n.], 2013b.

Mueller DE Precursor of Major Actinides // Personal correspondence. - 14 1 2013a.

Mueller DE RE: S/U of keff to Polyethylene temp // Personal Communication (email). - 2013.

Mueller DE Relative Sensitivity Coefficients of Major Actinides // Personal correspondence(email). - 2013c.

Mueller DE, Rearden BT and Hollenbach DF Application of SCALE TSUNAMI Tools for the validation of Criticality Safety Calculations involving U-233 [Report]. - Oak Ridge : Oak Ridge National Laboratory, 2009.

Mueller Donald E. and Rearden Bradley T. Sensitivity coefficient generation for a Burnup Credit Cask Model using TSUNAMI-3D [Journal]. - Knoxville, Tennessee : American Nuclear Society, LaGrange Park, IL, 2005.

National Nuclear Regulator Regulatory Documents [Online] // http://www.nnr.co.za/regulatory-documents/. - 11 February 2015. - http://www.nnr.co.za/regulatory-documents/.

Nichols A.L Nuclear Data Requirements for decay heat calculations [Report]. - Vienna : International Atomic Energy Agency, 2002.

Nicolaou G and Tsagas N Criticality Safety of spent nuclear fuel assemblies from the transmutation of minor actinides in fast reactors [Journal]. - Xanthi, Greece : Annals of Nuclear Energy, 2006 йил. - Vols. 33(2006) 305-309.

Northeast Technology Corp Material Qualification of ALCAN composite for spent fuel storage [Report]. - Kingston, NY : Northeast Technology Corp, 2008. - NET-259-03.

O'Dell R D Nuclear Criticality Safety [Conference] // Proceedings of a Short Course held at D.H Lawrence Ranch, New Mexico, 7-11 May 1973. - New Mexico : Technical Information Centre, Office of Information Services, United States Atomic Energy Commission, 1973. - Vols. TID-26286.

O'Dell RD Nuclear Criticality Safety [Conference] // Proceeding of a shortcourse held at D.H Lawrence Ranch, May 7-11 1973. - New Maxico : Technical Information Centre, Office of Information Services, United States Atomic Energy Commission, 1974.

O'Leary Patrick M, Lambert Ray W and Ozer Odelli RackSaver Neutron Absorbing Insert Development and Testing [Report]. - Richland, Washington : EPRI, 1996.

ORNL Presentation on Direct Perturbation Calculations. - [s.l.] : Oak Ridge, 2011.

Parks C.V [et al.] U.S. Regulatory Research Program for Implementation in Transport Cask [Conference] // International Symposium on Packaging and Transportation of Radioactive Material (PATRAM2001). - Chicago : PATRAM2001, 2001.

Parks C.V and Meuller J.C wagner and D.E Full burnup credit in transport and storage casks:Benefits and Implementations [Report]. - Las Vegas : Oak Ridge National laboratory, 2006.

Parks C.V. and Meuller J.C. Wagner and D.E. Full burnup credit in transport and storage casks:Benefits and Implementations [Report]. - Las Vegas : Oak Ridge National laboratory, 2006.

Patterson C, Garzarolli F and Adamson R Processes going on in Nonfailed Rod during Normal Operation [Report]. - Molnlycke : Advanced Nuclear Technology International, 2010.

Peplow D.E and Wagner J.C Automated Variance Reduction for SCALE Shielding Calculations [Journal]. - Carlsbad, New Mexico : American Nuclear Society's 14th Biennial Topical Meeting of Radiation Protection and Shielding, 2006.

Pesic M.J. and Milosevic M.P An analysis of burnup reactivity credit for reactor RA spent fuel storage [Journal]. - Belgrade, Yugoslavia : Journal of Nuclear Engineering and Design, 1997 йил. - Vols. 180(1998) 29-35.

Petrie L.M. and B.T.Rearden McDancoff Data Guide [Report]. - Oak Ridge : Oak Ridge National Laboratory, 2011. - ORNL/TM-2005/39.

Pidwirny Michael and Jones Scott 'Physical and Chemical Characteristics of Seawater' [Online] // Fundamentals of Physical Geography,. - University of British Columbia, 2006. - 18 October 2011. - http://www.physicalgeography.net/fundamentals/8p.html.

Rabenstein WD Fuel Assembly Mechanical Design Report For The supply of 17X17 Westingouse 374 Robust Fuel Assemblies [Report]. - [s.l.] : Westinghouse Electric, 1999.

Radulescu G and Gauld IC STARBUCS: A Scale Control Module For Automated Criticality Safety Analyses Using Burnup Credit [Report] / Nuclear Science and Technology ; Oak Ridge National Laboratory. - Knoxville : Oak Ridge National Laboratory, 2009. - ORNL/TM-2005/39.

Radulescu G, Mueller D.E and Wagner J.C Sensitivity and Uncertainty Analysis of Commercial Reactor Criticals for Burnup Credit. [Report]. - Oak Ridge : Oak Ridge National Laboratory, 2008.

Radulescu G, Mueller DE and Wagner JC Sensitivity and Uncertainty Analysis of Commercial Reactor Criticals for Burnup Credit [Report]. - Oak Ridge : Oak Ridge National Laboratory, 2008.

Radulescu G. and Gauld I.C. Enhancements to the burnup credit criticality safety sequence in Scale [Report]. - Oak Ridge : Oak Ridge National Laboratory, 2006.

Radulescu G. and Gauld I.C. STARBUCS: A Scale control module for automated criticality safety analyses using burnup credit [Report]. - Oak Ridge : Oak Ridge National Laboratory, 2011.

Radulescu G. and Gauld I.C. STARBUCS: A SCALE control module for automated criticality safety analyses using burnup credit [Report]. - Oak Ridge, Tennessee : Oak Ridge National Laboratory, 2009. - ORNL/TM-2005/39.

Rearden B SCALE 6 Criticality Safety Course: KENO-Va and KENO-VI [Report]. - Oak Ridge : Oak Ridge National Laboratory, 2011.

Rearden B.T. and Mueller D.E. Recent use of Covariance Data for Criticality Safety Assessment [Journal]. - Oak Ridge : Elevier, 2008 йил. - Vols. Nuclear Data sheets 109 (2008) 2739-2744.

Rearden BT Pertubation Theory Eigenvalues Sensitivity Analysis with Monte Carlo Techniques [Journal] // Nuclear Science and Engineering. - 2004. - pp. 367-382.

Rest J and Hoffman GL Dynamics of irradiation induced grain subdivision and swelling in U3Si2 and UO2 [Journal]. - Argone : Journal of nuclear material, 1994. - Vol. 210.

Rest J and Hoffman GL Dynamics of irradiation-induced grain subdivision and swelling in U3Si2 and UO2 [Journal]. - Argonne : Journal of nuclear material, 1994. - Vol. 210.

Rimpler A Bonner sphere neutron spectrometry at spent fuel casks [Journal]. - Berlin : Elsevier, 2002. - Vol. 476.

Rimpler A Bonner sphere neutron spectrometry at spent fuel casks [Journal]. - Berlin : Elsevier, 2002. - Vol. 476.

Rimpler A, Borst M and Seifarth D Neutron measurements around TN85-type storage cask with high-active waste. [Journal]. - Gorleben : Elsevier, 2010. - Vol. 45.

Rodel R, Krietsch T and Zesiler P Current Type B Package approval procedure in Germany: Selected Topics from Safety Assessment [Report]. - [s.l.] : PATRAM CONFERENCE, 1998.

Saegusa T, Yagawa G and Aritomi M Topics of research and development on concrete cask storage of spent nuclear fuel [Journal]. - Tokyo : Journal of nuclear engineering and design, 2007 йил. - Vols. 238(2008)1168-1174.

Sanchez Richard, Mao Li and Santandrea Simone Treatment of Boundary Conditions in Trajectory-Based Deterministic Transport Methods [Journal]. - Saclay, France : Nuclear Science and Engineering, 2001. - Vol. 140.

Sanders C.E and Wagner J.C. Parametric Study of the Effect of Control Rods for PWR Burnup Credit [Report]. - Oak Ridge : Oak Ridge National Laboratory, 2002. - NUREG/CR-6759.

Sanders Charlotta [et al.] Transportation Cask Receipt/Return Facility Criticality Safety Evaluation [Report] = Licensing Calculations. - 2005. - 140-00C-HCR0-00300-000-00A.

Seidel K. [et al.] The influence of atomic, molecular and solid state effects on the neutron resonance cross section. [Report]. - Vienna : International Atomic Energey Agency, 1989.

Sitenko A.G. Theory of nuclear reactions [Book]. - Kiev : World Scientific Publishing Co, 1990.

Sitenko AG Theory of nuclear reactions [Book]. - Kiev : World Scientific Publishing Co, 1990.

Sitenko AG Theory of nuclear reactions [Book] / trans. Kocherga OD. - London : World Scientific Publishing Co. Pte.Ltd, 1990. - ISBN 9971-50-481-2.

Spanier J and Gelbard EM Monte Carlo Principles and Neutron Transport Problems [Book]. - New York : Dover Publications, 2008.

Sprung J.L. [et al.] Reexamination of Spent Fuel Shipment Risk Estimates [Report]. - Albuquerque, NM 87185-0744 : Sandia National Laboratories, 2000.

Stacey WM Nuclear Reactor Physics [Book]. - New York : John Wiley and Sons, Inc, 2001.

Stamatelatos M.G. Cross section space shielding in doubly heterogeneous HTGR systems [Report]. - New Mexico : Los Almos Scientific Laboratory, 1975.

Stamatelatos MG Cross section space shielding in doubly heterogeneous HTGR systems [Report]. - New Mexico : Los Almos Scientific Laboratory, 1975.

Suyama K, Murazaka M and Okuda Y Decreasing in neutron multiplication factors in spent fuel storage facilities by changing fuel assembly position in axial direction [Journal]. - Ibaraki, Japan : Annals of Nuclear Energy, 2007 йил. - Vols. 34 (2007) 417-423.

Suyama K. [et al.] Active reduction of the end-effect by local installation of neutron absorbers [Journal]. - Ibaraki, Japan : Annals of Nuclear Energy, 2008 йил. - Vols. 35 (2008) 1628-1635.

Tang J.T Thomas and J.S Some effects of packaging Material on Critical Arrays of Fissile Materials [Conference] // Computer Science Division, Oak Ridge National Laboratory, Union Carbide Corporation, Nuclear Division. - San Francisco : Computer Science Division, Oak Ridge National Laboratory, Union Carbide Corporation, Nuclear Division, 1977.

Taviv E. personal correspondence. - Centurion : [s.n.], 2013.

Thomas Topical Safety Analysis Report for the Transport and Storage Casks for 28 PWR Fuel Assemblies-Castor X/28 F- [Report] : Safety Analysis Report / GNB Gessellscchaft fur Nuklear-Behalte mbH,Essen ; GNB. - Essen, Germany : GNB, 1992. - GNB B 276/92E.

Trkov A From Basic Nuclear Data to Applications [Report]. - Trieste : Lecture given at the Workshop on Nuclear Data and Nuclear Reactors: Physics, Design and Safety, 2000.

Tsao Cheng Si and Pan Lung Kwang Reevaluation of the Burnup of Spent Fuel Pins by the Activity Ratio of 134Cs/137Cs [Journal]. - Taoyuan,Taiwan : Appl. Radiar. Iso, 1993. - 7 : Vol. 44.

Turos A, Matzke Hj and Meyer O Lattice location of fission product in UO2 single crystals [Journal]. - Karlsruhe : Nuclear Instrument and Methods In Physics Reserach, 1992.

US NRC Onsite Spent Fuel Criticalitys Analyses NRR Action Plan [Report]. - [s.l.] : US Nuclear Regulatory Commission, 2010.

USNRC Standard Review Plan for Spent Fuel Dry Storage System at a General Licence Facility [Report] = NUREG-1536, Revision 1. - Washington : NRC, 2010.

Veshchnov MS and Shestak VE Model for crystal defects in UO2 under irradiation up to high burnups [Journal]. - Moscow : Journal of Nuclear Material, 2009. - Vols. 384(2009)12-18.

Veshchunov M.S and Shestak V.E Model for evolution of crystal defects in UO2 under irradiation up to high burnups [Journal]. - Moscow : Journal of nuclear materials, 2009. - Vol. 384.

Wagner J.C Computational Benchmark for estimation of reactivity margin from fission products and minor actinides in PWR burnup credit [Report]. - Oak Ridge : Oak Ridge National Laboratory, 2001. - NUREG/CR-6747.

Wagner J.C. and DeHart M.D. Review of axial burnup distribution considerations for Burnup Credit Calculation [Report]. - Oak Ridge : Oak Ridge National Laboratory, 2000. - ORNL/TM-1999/246.

Wagner J.C. and Sander C.E. Assessment of reactivity margins and loading curves for PWR Burnup Credit Cask design [Report]. - Oak Ridge : Oak Ridge National Laboratory, 2003. - NUREG/CR-6800.

Wagner J.C. and Sanders C.E. Parametric Study of the Effect of Control Rods for PWR Burnup Credit [Report]. - Oak Ridge : Oak Ridge National Laboratory, 2002. - NUREG/CR-6759.

Wagner J.C. and Sanders E. Assessment of reactivity margin and loading curves for PWR burnup credit cask designs [Report]. - Oak Ridge : Oak Ridge National Laboratory, 2003. - NUREG/CR-6800.

Wagner J.C., Douglas D.E. and Mosher S.W. FW-CADIS for Global and Regional Variance Reduction of Monte Carlo Radiation Transport calculations [Journal]. - Oak Ridge : Nuclear Science and Engineering, 2013. - Vol. 176.

Wagner JC Computational benchmark for estimation of reactivity margin from Fission Products and Minor Actinides in PWR Burn-up Creduts [Report]. - Washington : Nuclear regulatory Commission, 2001.

Wagner JC Criticality Analysis of Assembly Misload in a PWR burnup Credit Cask [Report]. - Oak Ridge : Oak Ridge National Laboratory, 2008.

Wagner John C Evaluation of Burnup Credit for Accommodating PWR Spent Nuclear Fuel in High-Capacity cask design [Report]. - Oak Ridge : Oak Ridge National Laborator, 2006.

Was Gary S Fundamentall of Radiation Material Science: Metals and alloys [Book]. - Berlin : Springer-Verlag, 2007. - ISBN 978-3-540-49471-3.

Was GS Fundamental of Radiation Material Science [Book]. - Michigan : Springer-Verlag, 2007.

Weber WJ [et al.] Irradiation-induced crystaline-to-amorphous phase transition in alpha-SiC [Journal]. - Mecico : Elsevier, 1996. - 116(1996) 322-326.

Wei J and Martin WR Application of the chord method to obtain analytical expressions for Dancoff Factors in Stochastic media [Journal]. - New York : Journal of Nuclear Science and Engineering, 2011. - Vol. 169.

Withee D.E. and Carlson C.J. Spent fuel burnup credit in casks: An NRC Perspective [Conference] // Proceeding of the 27th Water Reactor Safety Information meeting held in Bethesda Mariott Hotell, Bethesda, Maryland. - Maryland : US Nuclear Regulatory Commission, 2000. - Vols. pp 419-436.

WNTI Nuclear Fuel Cycle Transport:The IAEA Regulations and their Relevance to Severe Accidents [Report]. - London : World Nuclear Transport Institute, 2010.

Young Hugh D Statistical Treatment of Experimental data [Book]. - londond : Mc Graw-Hill, 1962.